ASL-CR-82-0122-1

AD

Reports Control Symbol
OSD - 1366

AD A117663

ANALYSIS OF MULTIPLE SOURCE OBSCURANTS ON THE REALISTIC BATTLEFIELD (AMSORB)

VOLUME I - MATHEMATICAL MODELS AND COMPUTER PROGRAM DESCRIPTION

MAY 1982

By

Richard K. Dumbauld
Steven F. Saterlie
Craig S. Cheney

H. E. Cramer Company, Inc.
Salt Lake City, Utah

Under Contract DAAD07-79-C-0122

CONTRACT MONITOR: John T. Marrs

DTIC FILE COPY

DTIC
ELECTE
JUL 30 1982
S D
D

Approved for public release; distribution unlimited.

US Army Electronics Research and Development Command
Atmospheric Sciences Laboratory
White Sands Missile Range, NM 88002

82 07 19

NOTICES

Disclaimers

The findings in this report are not to be construed as an official Department of the Army position, unless so designated by other authorized documents.

The citation of trade names and names of manufacturers in this report is not to be construed as official Government indorsement or approval of commercial products or services referenced herein.

Disposition

Destroy this report when it is no longer needed. Do not return it to the originator.

SECURITY CLASSIFICATION OF THIS PAGE (When Data Entered)

REPORT DOCUMENTATION PAGE		READ INSTRUCTIONS BEFORE COMPLETING FORM
1. REPORT NUMBER ASL-CR-82-0122-1	2. GOVT ACCESSION NO.	3. RECIPIENT'S CATALOG NUMBER
4. TITLE (and Subtitle) ANALYSIS OF MULTIPLE SOURCE OBSCURANTS ON THE REALISTIC BATTLEFIELD (AMSORB) VOLUME I - MATHEMATICAL MODELS AND COMPUTER PROGRAM DESCRIPTION		5. TYPE OF REPORT & PERIOD COVERED Final Report 6. PERFORMING ORG. REPORT NUMBER
7. AUTHOR(s) Richard K. Dumbauld, Steven F. Saterlie, and Craig S. Cheney		8. CONTRACT OR GRANT NUMBER(s) DAAD07-79-C-0122
9. PERFORMING ORGANIZATION NAME AND ADDRESS H. E. Cramer Company, Inc. Salt Lake City, Utah		10. PROGRAM ELEMENT, PROJECT, TASK AREA & WORK UNIT NUMBERS DA Task 1L162111AH71
11. CONTROLLING OFFICE NAME AND ADDRESS US Army Electronics Research and Development Command Adelphi, MD 20783		12. REPORT DATE May 1982 13. NUMBER OF PAGES 213
14. MONITORING AGENCY NAME & ADDRESS(if different from Controlling Office) US Army Atmospheric Sciences Laboratory White Sands Missile Range, NM 88002		15. SECURITY CLASS. (of this report) UNCLASSIFIED 15a. DECLASSIFICATION/DOWNGRADING SCHEDULE

16. DISTRIBUTION STATEMENT (of this Report)

Approved for public release; distribution unlimited

17. DISTRIBUTION STATEMENT (of the abstract entered in Block 20, if different from Report)

18. SUPPLEMENTARY NOTES

Contract Monitor: John T. Marrs

19. KEY WORDS (Continue on reverse side if necessary and identify by block number)

Dispersion model	Battlefield environment	WP smoke
Mesoscale prediction model	Probability of detection	HC smoke
Smoke model	Obscuration model	Cloud brightness
Transmittance	Smoke munitions	Smoke obscurations
Line of sight integrated concentration (CL)		Obscurants

20. ABSTRACT (Continue on reverse side if necessary and identify by block number)

The Analysis of Multiple Source Obscurants on the Realistic Battlefield (AMSORB) computer program is designed to calculate line of sight integrated concentrations, transmittance and probability of detection in a polluted battlefield environment. Provision is made in the program for treatment of pollutants from smoke munitions, explosive munitions, moving vehicles, muzzle blasts, burning vegetation, vehicles, and buildings. The program calculates wind fields in complex terrain and uses this information to calculate cloud trajectories of the pollutants and the line of sight integrated

DD FORM 1 JAN 73 1473 EDITION OF 1 NOV 65 IS OBSOLETE

SECURITY CLASSIFICATION OF THIS PAGE (When Data Entered)

20. ABSTRACT (cont)

concentrations, transmittance and probability of detection between user-specified points (observer and target). Volume I of the report describes: the wind field, trajectory/transport and dispersion models; the source characteristics used in the program; the AMSORB model routines; and the general structure of the program. Volume II is a user's manual for the program and Volume III contains a computer listing of the program.

FOREWORD

This final report under Contract No. DAAD07-79-C-0122 with Atmospheric Sciences Laboratory (ASL) at the White Sands Missile Range describes computerized techniques for the automatic calculation of line-of-sight integrated concentrations, transmittance and probability of detection in a polluted battlefield environment. Specific provision has been made for automated treatment of atmospheric contaminant sources typically present in the battlefield. The program incorporates many features of the Smoke Obscuration Routine and EPAMS programs developed by the H. E. Cramer Company under previous contracts with ASL and relies on source description material and source models contained in the E-O SAEL programs compiled by ASL. This report consists of three volumes. Volume I describes the various model components, the mathematical relationships used in the program, and the procedures used to relate the various program components. Volume II contains users' instructions for operating the program. Volume III contains a listing of the program.

Mr. Robert Umstead, who served as COR for ASL under the contract until the spring of 1980 and his replacement, Mr. John Marrs, provided valuable technical guidance in specifying Army requirements and valuable assistance in assembling the requisite source description data and source models used in the program.

Accession For
NTIS GRA&I
DTIC TAB
Unannounced
Justification
By
Distribution/
Availability Codes
Dist | Avail and/or Special
A

DTIC COPY INSPECTED

TABLE OF CONTENTS

Section	Title	Page No.
	FOREWORD	i
1	INTRODUCTION	1
	1.1 Background	1
	1.2 Purpose	3
	1.3 The AMSORB Program	3
	1.4 Organization of the Report	5
2	MESOSCALE WIND-FIELD MODEL, TRAJECTORY/TRANSPORT ROUTINE, AND DISPERSION MODELS	7
	2.1 Mesoscale Wind-Field Model	7
	2.2 Trajectory/Transport Routine	10
	2.3 Dispersion Models	13
	2.4 Obscuration Model Routine	53
3	BATTLEFIELD ENVIRONMENT SOURCE CHARACTERISTICS	69
	3.1 Smoke Munition Source Characteristics	69
	3.2 Explosive Munition Source Characteristics	72
	3.3 Moving Vehicle Source Characteristics	83
	3.4 Muzzle Blast Source Characteristics	86
	3.5 Burning Brush/Vegetation Source Characteristics	90
	3.6 Burning Building Source Characteristics	96
	3.7 Source Characteristics for Burning Vehicle	98
	3.8 User-Specified Source Models and Inputs	98
4	AMSORB MODEL ROUTINES	102
	4.1 Mixing-Layer Analysis Routine	102
	4.2 Battlefield Source Characteristics Routine	118
	4.3 Dispersion Model Routines and Meteorological Parameters Required by the Dispersion Models	121
	4.4 Obscuration Model Routine and Model Parameters	136
	4.5 Battlefield Environment Routine	154
5	STRUCTURE OF THE COMPUTER PROGRAM: ANALYSIS, DATA PROCESSOR, APPLICATION AND GRAPHICS PHASES OF AMSORB	168
	5.1 Analysis Phase of AMSORB	171
	5.2 Data Processor Phase of AMSORB	177
	5.3 Application Phase of AMSORB	178
	5.4 Graphics Phase of AMSORB	186

TABLE OF CONTENTS (Continued)

Section	Title	Page No.
6	EXAMPLE CALCULATIONS	190
	6.1 Example Battlefield Scenario	192
	6.2 Battlefield Environment Routine (BEC) Calculations	199
	REFERENCES	209

VOLUME II

TABLE OF CONTENTS

Section	Title
A	USERS' INSTRUCTIONS FOR THE ANALYSIS, DATA PROCESSOR, APPLICATION AND GRAPHICS PHASES OF AMSORB

VOLUME III

TABLE OF CONTENTS

Title
COMPLETE FORTRAN LISTING OF THE AMSORB PROGRAM

SECTION I
INTRODUCTION

1.1 BACKGROUND

The Atmospheric Sciences Laboratory (ASL), White Sands Missile Range (WSMR), New Mexico, has been directed to develop plans and operational techniques for determining atmospheric effects on electro-optical/millimeter systems operating in a battlefield environment. The atmosphere of the battlefield is polluted by smoke, gasses and particles from artillery shell and bomb bursts, smoke munitions, vehicle traffic and other battlefield activities. The effectiveness of electro-optical and near-millimeter wavelength devices can be severely affected by the presence of these pollutants. The effects of obscurants on sensing devices are related to the type of obscurant, the integrated line-of-sight concentration (CL), the response of the sensor to attenuation in the sensor wavelength and other optical effects. In turn, CL is directly related to the amount of obscurant released to the atmosphere and the dispersion and transport of the obscurant in the atmosphere.

ASL has been conducting and sponsoring major efforts in the development of appropriate meteorological inputs to dispersion and transport models and improved methods for accurately and realistically describing the transport and dispersion of natural and battle-induced contaminants. These efforts include the implementation of automated procedures for estimating cloud trajectories and dispersion characteristics downwind from sources of contaminate material in regions of complex terrain. The EPAMS program (Dumbauld and Bjorklund, 1977) previously developed for ASL contains the following features that are retained in the program described in this report:

- Diagnostic analysis routines for calculating the depth of the atmospheric surface mixing layer and

the wind velocity within this layer from routine meteorological measurements

- A diagnostic Mesoscale Wind-Field Model that uses this information to calculate the wind field and mixing-layer depth contours above regions of complex terrain

- Diagnostic application routines which use the output from the mesoscale model routines with input source characteristics and dispersion models to calculate dosages and concentrations of contaminate material

- Graphics routines to produce displays of the wind-field solutions, mixing-layer depth contours and dosage and concentration isopleths as overlays on the complex terrain contours

Under Contract No. DAEA-18-77-C-0060, the H. E. Cramer Company added the MS3 smoke obscuration routine to the EPAMS program (Dumbauld, Saterlie and Cheney, 1979). The MS3 Routine allows the program user to calculate line-of-sight concentrations, transmittance and probability of detection downwind from standard chemical smoke sources employed by the U. S. Army. It is coupled with the EPAMS program in that the diagnostic analysis routines and diagnostic Mesoscale Wind-Field Model are used to calculate meteorological inputs representative of the specific battlefield area of interest for use in the smoke dispersion models. Many of the routines used in the MS3 are also used in the new program. As explained below, the technical objectives of the work described in this report are a logical continuation of the overall ASL efforts to describe atmospheric effects on EO systems.

1.2 PURPOSE

The primary purpose of the work described in this report is to provide a working prototype computerized model for estimating the dispersion and downwind transport of contaminants introduced into the lower atmosphere by the multiplicity of sources typically present in the battlefield area (dust and smoke from exploding munitions, moving vehicles, muzzle blasts; smoke from burning vegetation). Further, the computer program is to provide a means of estimating the line-of-sight (LOS) concentration, transmittance and probability of detection as affected by the transport and dispersion of the contaminants. The program is to perform these functions with limited meteorological input data and a minimum of user specification of the source characteristics required by the computer program.

1.3 THE AMSORB PROGRAM

The AMSORB (Analysis of Multiple Source Obscurants on the Realistic Battlefield) prototype computer program has been developed in response to the purposes stated in Section 1.2 above. Figure 1-1 is a simplified diagram showing the functional elements of the AMSORB program, which is based on the previously-developed EPAMS program functional concepts. The Analysis Phase is called by the AMSORB Executive as a result of a standing request for a routine analysis of meteorological conditions in the battlefield surface mixing layer. The Analysis Phase extracts available upper-air and surface meteorological data from the Data Base. As shown in Figure 1-1, the Analysis Phase is comprised of two major elements. The Mixing-Layer Analysis Routine calculates initialization parameters for the Mesoscale Wind-Field Model, as well as some meteorological inputs for direct use in the Applicatio Phase, using Data Base inputs. The Mesoscale Wind-Field Model calculates wind-velocity patterns and mixing heights for use in the trajectory/transport subelement of the Applications Phase. The Analysis Phase does not communicate

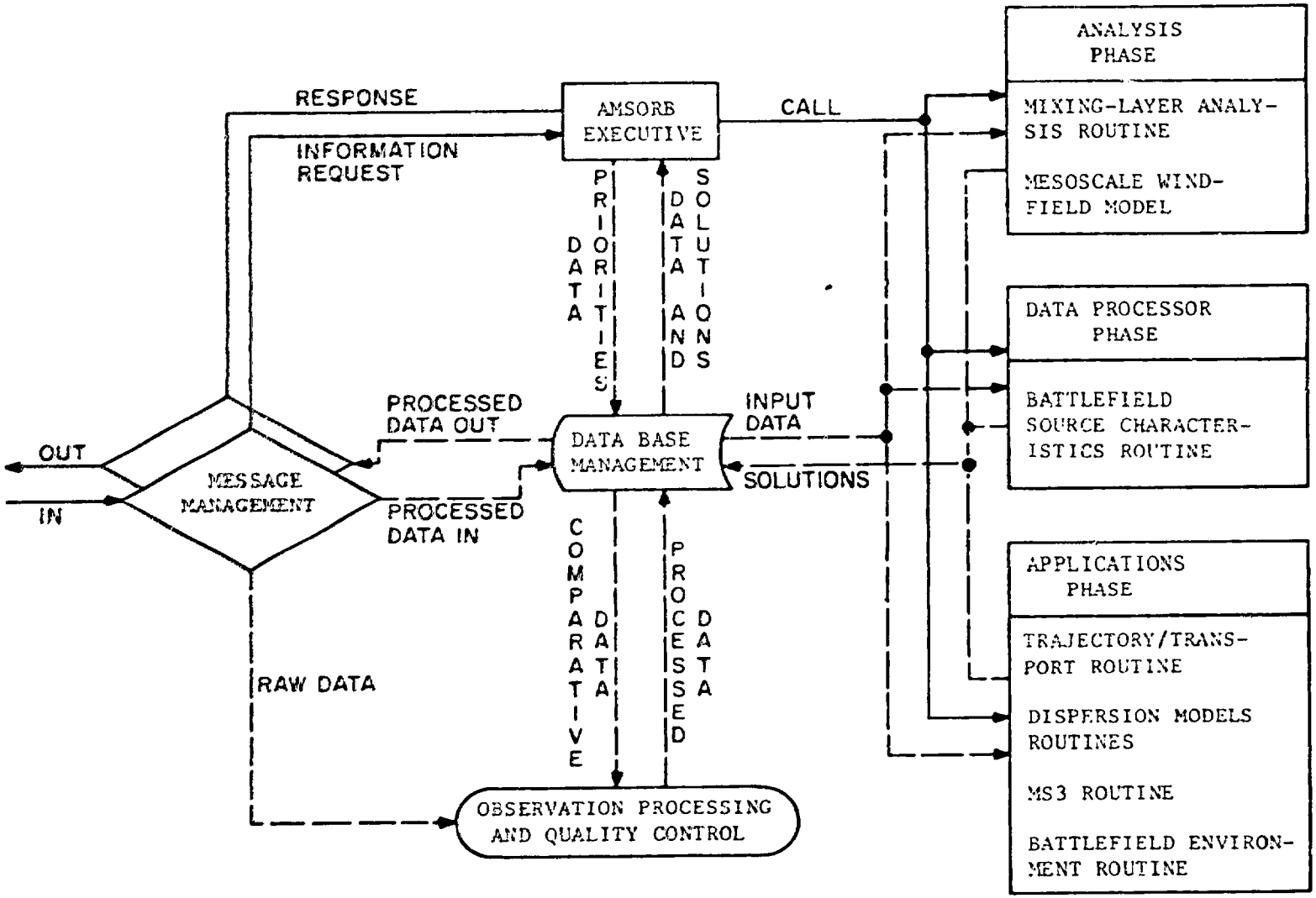

FIGURE 1-1. Schematic diagram of the AMSORB (Analysis of Multiple Source Obscurants on the Realistic Battlefield) Functional Elements.

directly with the Applications Phase, but supplies solutions to the Data Base for subsequent use. The Applications Phase is called by the AMSORB Executive as a result of a request for information routed through the AMSORB Executive. The Trajectory/Transport Routine, Dispersion Model Routine and the MS3 Routine in the Application Phase are identical to the corresponding routines previously included in the EPAMS program and can be called and used in the same manner. The Battlefield Environment Routine is the new addition to the program for accomplishing the calculation of LOS concentrations, transmittance and probability of detection when all types of sources are present on the battlefield. The Battlefield Environment Routine cannot be called by the user unless the user has first requested, through the AMSORB Executive, source characteristics for the battlefield scenario from the Data Processor Phase. The Battlefield Source Characteristics Routine automatically passes the requisite source characteristics to the Data Base depending on the types of sources the user specifies. The source characteristics routine has been placed as a separate routine in the AMSORB program to facilitate updating as new information on source characteristics becomes available.

1.4 ORGANIZATION OF THE REPORT

Many of the automated operations of the AMSORB Program are based on elements of the EPAMS program described in the report by Dumbauld and Bjorklund (1977) and the Smoke Obscuration Routine for EPAMS described by Dumbauld, Saterlie and Cheney (1979). To provide the background information required to understand the concepts of the AMSORB program, we have abstracted or reproduced in this report some of the original reports. Section 2 of Volume I below contains a description of the Mesoscale Wind-Field Model, the transport and dispersion models, and the obscuration (visibility and probability of detection) models used in the AMSORB Program. The models and procedures used to develop source characteristics for the Battlefield Environment Routine are described

in Section 3. Section 4 describes the various model routines in the AMSORB Program and the analysis routines and other procedures used to develop model input parameters for these routines. The computer program structure of AMSORB is outlined in Section 5. Section 6 describes the results of example calculations made using the AMSORB program.

SECTION 2

MESOSCALE WIND-FIELD MODEL, TRAJECTORY/TRANSPORT ROUTINE, AND DISPERSION MODELS

2.1 MESOSCALE WIND-FIELD MODEL

The Analysis Phase of AMSORB uses a numerical modeling technique developed for ASL by Tingle and Bjorklund (1973) to calculate details of the mesoscale wind-field and depth of the surface-mixing layer above complex terrain. This modeling technique is used in AMSORB for the same purpose. A brief description of the technique, abstracted from the report by Dumbauld and Bjorklund (1977), follows.

The computer algorithm, based on the shallow - fluid equations of oceanography, describes the motion of fluid in two dimensions by the expressions:

$$\frac{\partial u}{\partial t} + u\frac{\partial u}{\partial x} + v\frac{\partial u}{\partial y} + g'\frac{\partial}{\partial x}(H_m + z_T) = 0 \qquad (2\text{-}1)$$

$$\frac{\partial u}{\partial t} + u\frac{\partial v}{\partial x} + v\frac{\partial v}{\partial y} + g'\frac{\partial}{\partial y}(H_m + z_T) = 0 \qquad (2\text{-}2)$$

$$\frac{\partial H_m}{\partial t} + \frac{\partial (uH_m)}{\partial x} + \frac{\partial (vH_m)}{\partial y} = 0 \qquad (2\text{-}3)$$

where

u, v = x,y components of the fluid velocity in the layer next to the terrain

H_m = depth of the surface mixing layer

z_T = height of the terrain

g' = reduced acceleration of gravity

$= g\left(1 - \frac{\rho_1}{\rho_o}\right)$

g = acceleration of gravity

ρ_0 = fluid density in the surface mixing layer

ρ_1 = fluid density in the passive layer above the surface mixing layer

These equations describe mesoscale wind-patterns above complex terrain when the atmosphere above the terrain can be distinctively divided into two layers of different densities. This condition typically exists when the mixing layer above the terrain is capped by an elevated inversion. The interaction of the upper layer with the lower layer is limited to reducing the speed of gravity waves in the lower layer. Equations (2-1) (2-2) and (2-3) are written in their momentum form. Mesoscale wind patterns are generated by impulsively accelerating the momentum in the lower layer to a constant value and, after an empirically-determined model time (see Section 5.1) in which the flow in the region of interest is assumed to become stabilized, using the steady-state solution thus obtained.

The computer algorithm contains an explicit Lax-Wendroff finite-differencing procedure using nine grid points and one time level in combination with a nine-point low-pass filter. The finite differences are centered to preserve high-order accuracy. The grid arrangement and finite-differencing form of the equations are described in the report by Tingle and Bjorklund (1973). High-frequency oscillations generated in critical flow situations near regions where hydraulic jumps occur are removed by the filtering technique, which is based on a suggestion by Shapiro (1970) and has the advantage that its smoothing effect is easily determined from its response function. In the Analysis Phase, the filter is applied every seventh time step. It is well known that the length of the time step Δt used in obtaining the solution

also affects the stability of the finite difference solution. The time step is altered automatically in this algorithm in accordance with the expression

$$\Delta t = \frac{\lambda_s}{\sqrt{2}} \frac{\Delta x_{min}}{\left[\sqrt{u^2 + v^2} + \sqrt{g\, H_m}\right]_{max}} \qquad (2\text{-}4)$$

where the stability parameter λ_s is dependent on the grid spacing Δx and varies between zero and one. For the present application which uses a minimum spacing $\left(\Delta x_{min}\right)$ of 5 kilometers, the stability parameter has been set equal to 0.4. Because the entire solution grid must be searched to determine the maximum wave speed in the denominator of Equation (2-4), the value of Δt is calculated every second time step rather than every time step to save computation time.

A sensitivity analysis of the two-layer Mesoscale Wind-Field Model indicated that model instability can frequently occur in localized terrain regions where the inversion height H_m is initialized, or is adjusted by the model to a few tens of meters above the higher terrain elevations. The momentum conservation properties of the computational scheme are such that wind velocities in these localized regions may become unreasonably large as the depth of the lower layer approaches a minimum value. In order to prevent this type of solution instability, the u- and v-components of the solution at any given time step are automatically set to zero and the layer depth set equal to a minimum depth of 30 meters if the calculated depth for a grid point is less than 30 meters. Limited experience in the application of this feature of the mesoscale model indicates that computational stability is preserved without significant loss of momentum over the entire grid and with the result that wind fields in the immediate vicinity of higher elevations under these conditions appear to be reasonable.

The computerized algorithm uses an expanding grid in the boundary area beyond the terrain region of interest to damp outgoing waves and eliminate incoming waves based on the technique suggested by Lavoie (1972). Grid points in the boundary region are placed at distances of 10, 20, 40, 80 and 160 kilometers from all four sides of the interior grid. The terrain heights at all points in the boundary region are set equal to the minimum elevation within the interior grid. The initial momentum is set equal to the momentum used in initializing parameters in the interior grid.

The form of the finite-differenced equations and other details on which the mesoscale wind-field computer algorithm is based are contained in the paper by Tingle and Bjorklund (1973).

2.2 TRAJECTORY/TRANSPORT ROUTINE

The Trajectory/Transport Routine in the Applications Phase of AMSORB shown in Figure 1-1 has been abstracted from the EPAMS program (Dumbauld and Bjorklund, 1977). This routine is designed to calculate:

(1) Cloud trajectories and mean-layer winds and mixing-layer depths at fixed intervals along the trajectories for use in the intermediate- and long-range dispersion models described in Section 2.3.1 below

(2) The mean wind direction, mean wind speed and mixing-layer depth at the location of sources located near the lines-of-sight for use in the obscuration-dispersion models described in Sections 2.3.2 and 2.3.3 below

In both calculations, the Trajectory/Transport Routine uses the wind vector and mixing-layer depth values given by the Mesoscale Wind-Field Model at the solution grid points.

The cloud trajectory from a release at any point within the mesoscale model solution grid is calculated using a simple Euler predictor-corrector scheme and nine-point interpolation procedure. The computer program uses wind vector data from the Mesoscale Wind-Field Model solution at nine grid points surrounding the point of release and, through the interpolation procedure, calculates the u- and v-components of the wind at the point of release. If the smoke-dispersion models described in Section 2.3.2 are to be used in the ensuing calculations, these components are resolved and the mean wind direction and speed are made available to the smoke dispersion model. In calculating cloud trajectories, the first point on the trajectory is determined by resolving the components and placing a point at a fixed distance interval along the resultant vector. The fixed distance interval is set at one-tenth the grid spacing used in the mesoscale wind-field solution matrix (in the present program a fixed interval of 500 meters is used). Wind-velocity components at this point are also estimated from the nine-point interpolation procedure. The new u- and v-components are then averaged with the previously-determined components at the starting point. The final estimate of the first point on the trajectory is then calculated by resolving the averaged components and moving a fixed interval along the resultant vector. This final estimate of the first point on the trajectory is then treated in the same manner as the initial starting point (source) and the interpolation and iteration scheme repeated to find the second point on the trajectory. This procedure is repeated until the trajectory passes outside the grid area containing wind-vector data or the number of iterations exceeds a predetermined limit.

The interpolation method is based on an evaluation of a truncated two-dimensional Taylor's expansion formula (Carnahan, Luther and Wilkes, 1969, p. 430) given by

$$f(x,y) = f_{i,j} + hf_x + kf_y + \frac{h^2}{2} f_{xx} + hkf_{xy} + \frac{k^2}{2} f_{yy} \qquad (2\text{-}5)$$

where

$$h = x - x_i$$

$$k = y - y_j$$

and $f_{i,j}$ is either the u-or v-component at x_i, y_j, the nearest grid point to the point of interpolation (x,y). The partial derivatives f_x, f_y, f_{xx}, f_{xy} and f_{yy} are estimated by divided differences.

The depth of the mixing layer at fixed intervals along the trajectory and at the release point or smoke source location is also interpolated from data provided by the Mesoscale Wind-Field Model using a four-point bivariate interpolation formula given by

$$H_m(x,y) = (1 - p)\,(1 - q)\,H_{m_{i,j}} + p\,(1-q)\,H_{m_{i+1,j}} + q\,(1 - p)\,H_{m_{i,j+1}} + pq\,H_{m_{i+j,j+1}} \qquad (2\text{-}6)$$

where

$$p = (x - x_i) / (x_{i+1} - x_i)$$

$$q = (y - y_j) / (y_{j+1} - y_j)$$

and $H_{m_{i,j}}$, $H_{m_{i+1,j}}$, $H_{m_{i,j+1}}$, and $H_{m_{i+1,j+1}}$ are the mixing layer depths at the four surrounding grid points.

2.3 DISPERSION MODELS

The AMSORB program retains the Dispersion Models Routine and the MS3 Routine previously used in the Application Phase of the EPAMS program described by Dumbauld, Saterlie and Cheney (1979). The volume-source dispersion models for instantaneous and continuous sources and models for predicting the buoyant rise of continuous stack emissions contained in the Dispersion Models Routine are used to calculate isopleths of dosage and concentration, with or without cloud depletion due to decay, gravitational settling and precipitation scavenging, along the cloud trajectory predicted by the Trajectory/Transport Routine. The models are specifically formulated to account for changes in mean wind-speed and depth of the surface mixing-layer along the predicted trajectory while conserving mass continuity. The Dispersion Models Routine in AMSORB can be selected by the program user as a "stand-alone" dispersion routine for predicting dispersion at intermediate-and long-travel distances from instantaneous and continuous volume sources.

The MS3 Routine, added to EPAMS under Contract No. DAEA18-77-C-0060 with ASL, is primarily for use in predicting line-of-sight integrated concentration (CL) and dosage (CLID) downwind from quasi-continuous and instantaneous obscurant sources. The model has no specific means of accounting for changes in the mean wind-speed and depth of the surface mixing layer along a trajectory, and is thus intended for use over shorter distances where these meteorological parameters can be considered constant in time and space.

The Battlefield Environment Routine in the Applications Phase of AMSORB incorporates features of both the Dispersion Models and MS3 Routines to calculate CL and CLID along user specified lines of sight. The techniques used to calculate the cloud dimensions σ_x, σ_y and σ_z in the Dispersion Models Routine are used in the Battlefield Environment Routine to define cloud dimensions along the trajectory from the source

to a distance of about one mesoscale model grid spacing from the lines-of-sight. The dimensions of the cloud at this point become the initial source dimensions for use in, for example, the quasi-continuous obscurant source model to calculate CL and CLID along the lines-of-sight. Dispersion models have been added to the Battlefield Environment Routine for an obscurant released by traveling vehicles. The dispersion models used in the routines are described in more detail in the following paragraphs.

2.3.1 Dispersion Models Routine

The volume- and continuous-source models in the Dispersion Models Routine of AMSORB are similar to models described by Cramer, et al., (1972).

Instantaneous Volume-Source Model

The concentration for an instantaneous volume-source can be expressed as the product of four terms:

$$\chi_n = \{\text{Peak Term}\}\ \{\text{Lateral Term}\}\ \{\text{Vertical Term}\}\ \{\text{Depletion Term}\} \quad (2\text{-}7)$$

The Peak Term describes the concentration at the cloud centerline and is given by the expression

$$\text{Peak Term} = \frac{Q}{(2\pi)^{3/2}\ \sigma_{xn}\ \sigma_{yn}\ \sigma_{zn}} \quad (2\text{-}8)$$

where

Q = total source strength

σ_{xn} = standard deviation of the concentration distribution in the alongwind direction at the nth distance along the cloud trajectory

σ_{yn} = standard deviation of the concentration distribution in the crosswind direction at the nth distance along the cloud trajectory

σ_{zn} = standard deviation of the concentration distribution in the vertical at the nth distance along the cloud trajectory

The Vertical Term describes the vertical distribuiton of material at the nth distance along the cloud trajectory as modified by reflections of material at the top of the surface mixing layer and at the earth's surface and by gravitational settling of particulates. The expression for the Vertical Term is

$$\text{Vertical Term} = \sum_{a=0}^{\omega} \left\{ r^{a} \exp\left[-\frac{1}{2} \left(\frac{2a\,H_{m,n} - H' + z + V_s \sum_{n=1}^{N} \frac{\Delta x_n}{\bar{u}_n}}{\sigma_{zn}} \right)^2 \right] + r^{a+1} \exp\left[-\frac{1}{2} \left(\frac{2a\,H_{m,n} + H' + z - V_s \sum_{n=1}^{N} \frac{\Delta x_n}{\bar{u}_n}}{\sigma_{zn}} \right)^2 \right] \right\}$$

$$+ \sum_{a=1}^{\omega} \left\{ r^{a} \exp\left[-\frac{1}{2} \left(\frac{2a\,H_{m,n} + H' - z - V_s \sum_{n=1}^{N} \frac{\Delta x_n}{\bar{u}_n}}{\sigma_{zn}} \right)^2 \right] + r^{a-1} \exp\left[-\frac{1}{2} \left(\frac{2a\,H_{m,n} - H' - z + V_s \sum_{n=1}^{N} \frac{\Delta x_n}{\bar{u}_n}}{\sigma_{zn}} \right)^2 \right] \right\} \quad (2\text{-}9)$$

where, for convenience in writing the Vertical Term, 0^0 (zero to the zeroeth power) is set equal to unity and

H' = effective release height (see Equation (2-21))

z = calculation height

$H_{m,n}$ = mixing layer depth from mesoscale model for n^{th} distance along the trajectory

r = fraction of material reflected at the surface (1 for complete reflection and 0 for no reflection)

V_s = settling velocity for material in a given size category

Δx_n = incremental distance along the cloud trajectory

$\bar{u}_n$ = mean wind speed in the layer containing the cloud at the nth point along the trajectory (see Equation (2-18) below)

The Lateral Term is given by

$$\text{Lateral Term} = \exp\left[-\frac{1}{2}\left(\frac{y}{\sigma_{yn}}\right)^2\right] \qquad (2\text{-}10)$$

where

y = crosswind distance from the centerline of the cloud trajectory

The Depletion Term refers to the loss of material by simple decay processes and by precipitation scavenging. The form of the Depletion Term for each of these processes is:

$$\text{(Decay)} \qquad \exp\left[-k \sum_{n=1}^{N} \frac{\Delta x_n}{\bar{u}_n}\right] \tag{2-11}$$

$$\text{(Precipitation Scavenging)} \qquad \exp\left[-\Lambda \sum_{n=1}^{N} \frac{\Delta x_n}{\bar{u}_n}\right] \tag{2-12}$$

where

k = decay coefficient or fraction of material lost per unit time

Λ = washout coefficient or fraction of material removed by scavenging per unit time

The subset of equations describing the standard deviations of the alongwind σ_{xn}, crosswind σ_{yn} and vertical σ_{zn} concentration distributions is:

$$\sigma_{xn} = \left[\left(\frac{L\,(x_n)}{4.3}\right)^2 + \left(\sigma_{x(n-1)}\right)^2\right]^{1/2} = \left[\left(\frac{0.6\,\Delta\bar{u}_n}{4.3\,\bar{u}_n}\,\Delta x_n\right)^2 + \left(\sigma_{x(n-1)}\right)^2\right]^{1/2} \tag{2-13}$$

where

$L\,(x_n)$ = alongwind dimension of the cloud

$\Delta\bar{u}_n$ = wind speed shear at the nth point along the trajectory

$$= \frac{\bar{u}_{5,n}}{5^{p_n}} \left(z_{T,n}^{p_n} - z_{B,n}^{p_n} \right) \tag{2-14}$$

$\bar{u}_{5,n}$ = wind speed at a height of five meters at the nth point along the trajectory

p_n = wind power-law coefficient at the nth point along the trajectory

$z_{T,n}$ = top of the cloud at the nth point

$$= \begin{cases} H' + 2.15\,\sigma_{zn}; & z_{T,n} < H_{m,n} \\ H_{m,n} \quad ; & z_{T,n} \geq H_{m,n} \end{cases} \tag{2-15}$$

$z_{B,n}$ = base of the cloud at the nth point

$$= \begin{cases} H' - 2.15\,\sigma_{zn} \; ; & z_{B,n} > 0 \\ 0 \quad ; & z_{B,n} \leq 0 \end{cases} \tag{2-16}$$

$$\bar{u}_{5,n} = \frac{\bar{\bar{u}}_n \left(H_{m,n} - 5 \right) 5^{p_n} \left(1 + p_n \right)}{H_{m,n}^{(1+p_n)} - 5^{(1+p_n)}} \tag{2-17}$$

$\bar{\bar{u}}_n$ = mean layer wind speed from mesoscale model at n^{th} point

$\bar{u}_n$ = mean wind speed in the layer containing the cloud

$$= \frac{\bar{u}_{5,n} \left(z_{T,n}^{(1+p_n)} - z_{B,n}^{(1+p_n)} \right)}{(1+p)\ (5)^{p_n} \left(z_{T,n} - z_{B,n} \right)} \tag{2-18}$$

Δx_n = incremental distance between the n points (equal to 500 meters)

$$\sigma_{yn} = \sigma'_{A,n}\left[\Delta x_n + \left(\frac{\sigma_{y,n-1}}{\sigma'_{A,n}}\right)^{1/\alpha}\right]^{\alpha} \qquad (2\text{-}19)$$

where

$\sigma'_{A,n}$ = standard deviation of the wind azimuth angle at the nth point

$$= \sigma_{A,n}\left(\frac{\pi}{180}\right)\left(\frac{H'}{5}\right)^{m}\left(\frac{\tau}{600}\right)^{0.2} \qquad (2\text{-}20)$$

m = power-law exponent for variation of σ_A with height above ground

$$H' = \begin{cases} H ; & H \geq 5 \\ 5 ; & H < 5 \end{cases} \qquad (2\text{-}21)$$

τ = source function time =2.5 seconds for instantaneous sources

$\sigma'_{A,n}$ = ten-minute standard deviation of the wind azimuth angle

$$\sigma_{zn} = \sigma'_{E,n}\left[\Delta x_n + \left(\frac{\sigma_{z,n-1}}{\sigma_{E,n}}\right)^{1/\beta}\right]^{\beta} \qquad (2\text{-}22)$$

where

$$\sigma'_{E,n} = \sigma_{E,n}\,(\pi/180)\,(H'/5)^{q} \qquad (2\text{-}23)$$

q = power-law exponent for variation of σ_E with height above ground

$\sigma_{E,n}$ = standard deviation of the wind elevation angle

The cloud expansion coefficients α (lateral) and β (vertical) in the above equations are set to unity for instantaneous sources.

The concentration χ_n is calculated under the additional restriction that $\chi_n \leq \chi_{n-1}$. If $\chi_n > \chi_{n-1}$, the values of σ_{yn} and σ_{xn} are increased proportionately so that $\chi_n = \chi_{n-1}$ and the calculations continued.

Dosage for an instantaneous source is obtained from the expression

$$D_n = \frac{\chi_n \sqrt{2\pi}\, \sigma_{xn}}{\bar{u}_{z,n}} \tag{2-24}$$

where

$\bar{u}_{z,n}$ = mean wind speed at the calculation height z and n^{th} point on the trajectory

$$= \begin{cases} \bar{u}_{5,n} \left(\frac{z}{5}\right)^{p_n}; & z > 1 \\ \bar{u}_{5,n} \left(\frac{1}{5}\right)^{p_n}; & z \leq 1 \end{cases} \tag{2-25}$$

Continuous-Source Model

The Continuous-Source Model used in AMSORB is a modified version of the Gaussian model for continuous sources described by Pasquill (1962) in which the concentration is also expressed as the product of four terms:

$$\chi_{c,n} = \{\text{Peak Term}\}\{\text{Lateral Term}\}\{\text{Vertical Term}\}\{\text{Depletion Term}\} \quad (2\text{-}26)$$

The Peak Term of the continuous-source concentration model is given by the expression

$$\text{Peak Term} = \frac{Q'}{2\pi\, \sigma_{zn}\, \sigma'_{yn}\, \bar{u}_n} \quad (2\text{-}27)$$

where

Q' = source strength expressed as a rate

σ'_{yn} = standard deviation of the concentration distribution in the crosswind direction for a continuous source at the nth distance along the plume trajectory

and $\bar{u}_n$ and σ_{zn} are respectively defined by Equations (2-18) and (2-22). The Vertical, Depletion and Lateral Terms (with σ_{yn} replaced by σ'_{yn} where appropriate) are identical to the similar terms described for the instantaneous volume source. The subset of equations describing σ'_{yn} is:

$$\sigma'_{yn} = \sigma'_{Ac,n}\left[\Delta x_n + \left(\frac{\sigma'_{y,n-1}}{\sigma'_{Ac,n}}\right)^{1/\alpha}\right]^{\alpha} \quad (2\text{-}28)$$

where

$$\sigma'_{Ac,n} = \sigma_{A,n} \frac{\pi}{180} \left(\frac{H'}{5}\right)^m \qquad (2\text{-}29)$$

and the remaining parameters have been defined previously. The default values of α and β used in the program for continuous sources are $\alpha = 0.9$ and $\beta = 1$.

Plume-Rise Models for Continuous Stack Emissions

The effective height H of a buoyant plume is given by the sum of the physical stack height h and the buoyant rise Δh. For a neutral or unstable atmosphere, the effective stack height is given by (after Briggs, 1971; 1972)

$$H = h + t \left\{ \frac{15.98}{\bar{u}(h)} \left[r_s^2 \, w \left(1 - \frac{T_s}{T_c} \right) \right]^{1/3} h^{2/3} \right\} \qquad (2\text{-}30)$$

where

r_s = the inner radius of the stack at the exit (m)

w = the stack exit velocity ($m\ s^{-1}$)

T_c = the stack exit temperature (^oK) for the continuous source

T_s = ambient air temperature (^oK)

f = empirical correction factor

h = actual stack height (m)

$\bar{u}(h)$ = mean wind speed at stack height (m s^{-1})

$$= \bar{u}_{5,n=1}\left(\frac{h}{5}\right)^{p_{n=1}} \tag{2-31}$$

The factor f, which limits the plume rise as $\bar{u}(h)$ approaches the stack exit velocity w, is defined by

$$f = \left\{ \begin{array}{ll} 1 & ; \ \bar{u}(h) \leq w/1.5 \\ \left(\frac{3w - 3\bar{u}(h)}{w}\right) & ; \ w/1.5 < \bar{u}(h) < w \\ 0 & ; \ \bar{u}(h) \geq w \end{array} \right\} \tag{2-32}$$

Equation (2-30) is used when the net radiation index equals or exceeds 2, $\bar{u}(h)$ equals or exceeds 5 meters per second, or the potential temperature lapse rate $\bar{\Phi}$ is equal to or less than 0. When these conditions are not met, the program uses the corresponding Briggs (1972) rise formula for a stable atmosphere given by

$$H = \left\{ \begin{array}{ll} h + 2.397\ f\left[\frac{wr_s^2 T_s}{\bar{u}(h)\ \bar{\Phi}}\left(1 - \frac{T_s}{T_c}\right)\right]^{1/3} & ; \ \frac{\pi\ \bar{u}(h)}{10\ S^{1/2}} < h \\ h + 1.903\ f\left\{\frac{wr_s^2 T_s}{\bar{u}(h)\ \bar{\Phi}}\left[1 - \cos\left(\frac{10\ S^{1/2}\ h}{\bar{u}(h)}\right)\right]\right\}^{1/3} & ; \ \frac{\pi\ \bar{u}(h)}{10\ S^{1/2}} \geq h \end{array} \right\} \tag{2-33}$$

where

S = stability parameter

$$= \frac{9.8}{T_s} \bar{\phi} \tag{2-34}$$

$\bar{\phi}$ = height-weighted mean potential temperature lapse rate over an approximately 200-meter interval above h

$$= \frac{\sum_{z=h}^{z=h+200} \phi_z \Delta Z_z}{\sum_{z=h}^{z=h+200} \Delta Z_z} \tag{2-35}$$

$$\phi_z = \frac{T_{A,z+1} - T_{A,z}}{\Delta Z_z} \tag{2-36}$$

$$\Delta Z_z = Z_{z+1} - Z_z \tag{2-37}$$

$T_{A,z}$ = potential temperature at height Z_z

$T_{Z,z+1}$ = potential temperature at height Z_{z+1}

2.3.2 MS3 Routine

The obscurant dispersion models in the MS3 Routine calculate CL and CLID downwind from quasi-continuous and instantaneous sources.

Quasi-Continuous Obscurant Source Model

According to experiments conducted at Dugway Proving Ground (Salomon, et al, 1978 and Petersen, 1978), the amount of aerosolized smoke, $M_x(t)$, at any given time from quasi-continuous smoke munitions is given by the expression

$$M_x(t) = M_o \cdot MYF \cdot YF \left[A\left(\frac{t}{t_B}\right) + B\left(\frac{t}{t_B}\right)^2 + C\left(\frac{t}{t_B}\right)^3 + D\left(\frac{t}{t_B}\right)^4 \right] \qquad (2\text{-}38)$$

where

M_o = total mass in grams before ignition

MYF = munition yield fraction

YF = yield factor accounting for the effects of moisture in the air

t_B = total burn time in minutes

t = time in minutes

A,B,C,D = experimentally-derived coefficients

The amount of smoke produced by the munition as a function of time is, therefore,

$$Q(t) = \frac{d}{dt} M_x(t)$$

or

$$Q(t) = M_o \cdot MYF \cdot YF \left(\frac{A}{t_B} + \frac{2Bt}{t_B^2} + \frac{3Ct^2}{t_B^3} + \frac{4Dt^3}{t_B^4} \right) \qquad (2\text{-}39)$$

This expression is used to characterize the smoke munition source strength in the dispersion model. It should be noted that Equation (2-39) is an extremely important factor in determining the shape and magnitude of the CL time profile at short distances downwind from a quasi-continuous

source. The smoke dispersion model performance has been compared with smoke munition trial data by Carter, Dumbauld and Rafferty (1979).

Quasi-Continuous Source Obscurant Dispersion Model

The concentration at time t in seconds at a point x,y,z downwind from a quasi-continuous volume source emitting smoke over a time t_B is given by the expression

$$\chi_v = \int_0^{t_B} \frac{Q(\tau)}{(2\pi)^{3/2}\,\sigma_x\,\sigma_y\,\sigma_z} \left\{ \exp\left[-\frac{1}{2}\left(\frac{x-\bar{u}(t-\tau)}{\sigma_x} \right)^2 \right] \right\} \left\{ \exp\left[-\frac{1}{2}\left(\frac{y}{\sigma_y} \right)^2 \right] \right\} \left\{ \exp\left[-\frac{1}{2}\left(\frac{H(t)-z}{\sigma_z} \right)^2 \right] \right.$$

$$\left. + \exp\left[-\frac{1}{2}\left(\frac{H(t)+z}{\sigma_z} \right)^2 \right] + \sum_{i=1}^{\infty} \left\{ \exp\left[-\frac{1}{2}\left(\frac{2iH_m - H(t)-z}{\sigma_z} \right)^2 \right] \right. \right. \qquad (2\text{-}40)$$

$$\left. + \exp\left[-\frac{1}{2}\left(\frac{2iH_m - H(t)+z}{\sigma_z} \right)^2 \right] + \exp\left[-\frac{1}{2}\left(\frac{2iH_m + H(t)-z}{\sigma_z} \right)^2 \right] \right.$$

$$\left. \left. + \exp\left[-\frac{1}{2}\left(\frac{2iH_m + H(t)+z}{\sigma_z} \right)^2 \right] \right\} \right\} d\tau$$

where

$Q\{t\}$ = source emission rate (see Equation (2-39))

σ_x = standard deviation of the alongwind concentration distribution (m)

σ_y = standard deviation of the crosswind concentration distribution (m)

σ_z = standard deviation of the vertical concentration distribution (m)

$\bar{u}$ = mean cloud transport speed ($m\ s^{-1}$)

$H\{t\}$ = effective height of the cloud centroid at time t (m)

H_m = depth of the surface mixing layer (m)

If we perform the integration over the variable τ, the solution for time t is

$$\chi_v = \frac{J}{2\pi\ \sigma_y\ \sigma_z}\ \{\xi_5\} \qquad (2\text{-}41)$$

where

ξ_5 = the lateral and vertical terms following the first set of closed brackets

and

$$J = \frac{YF \cdot M_o \cdot MYF}{\sqrt{2\pi}\,\bar{u}} \left\{ \left[\left(\xi_4 a_1 + \xi_3 \right) a_1 + \left(\xi_2 + 2\xi_4 \right) \right] \right.$$

$$\left[\exp\left(\frac{-a_1^2}{2} \right) \right] - \left[\left(\xi_4 a_2 + \xi_3 \right) a_2 + \left(\xi_2 + 2\xi_4 \right) \right] \qquad (2\text{-}42)$$

$$\left[\exp\left(-\frac{a_2^2}{2} \right) \right] + \sqrt{\frac{\pi}{2}} \left(\xi_1 + \xi_3 \right)$$

$$\left. \left[\operatorname{erf}\left(\frac{a_2}{\sqrt{2}} \right) - \operatorname{erf}\left(\frac{a_1}{\sqrt{2}} \right) \right] \right\}$$

$$\xi_1 = \frac{1}{60t_B} \left[A + \frac{2B}{60t_B} \left(\frac{\bar{u}t - x}{\bar{u}} \right) + \frac{3C}{(60t_B)^2} \left(\frac{\bar{u}t - x}{\bar{u}} \right)^2 \right. \qquad (2\text{-}43)$$

$$\left. + \frac{4D}{(60t_B)^3} \left(\frac{\bar{u}t - x}{\bar{u}} \right)^3 \right]$$

$$\xi_2 = \frac{\sigma_x}{(60t_B)^2\,\bar{u}} \left[2B + \frac{6C}{60t_B} \left(\frac{\bar{u}t - x}{\bar{u}} \right) + \frac{12D}{(60t_B)^2} \left(\frac{\bar{u}t - x}{\bar{u}} \right)^2 \right] \qquad (2\text{-}44)$$

$$\xi_3 = \frac{\sigma_x^2}{(60t_B)^3\,\bar{u}^2}\left[3C + \frac{12D}{60t_B}\left(\frac{\bar{u}t-x}{\bar{u}}\right)\right] \tag{2-45}$$

$$\xi_4 = \frac{4D\,\sigma_x^3}{(60t_B)^4\,\bar{u}^3} \tag{2-46}$$

$$a_1 = \frac{x - \bar{u}t}{\sigma_x} \tag{2-47}$$

$$a_2 = \frac{x - \bar{u}(t-\tau_s)}{\sigma_x} \tag{2-48}$$

$$\tau_s = \begin{cases} t, & t_B \geq t \\ t_B, & t_B < t \end{cases} \tag{2-49}$$

The standard deviation of the alongwind concentration distribution used in the smoke dispersion model is

$$\sigma_x = \left[\left(\frac{L(\bar{x})}{4.3}\right)^2 + \sigma_{xo}^2\right]^{1/2} \tag{2-50}$$

where

$$L(\bar{x}) = \begin{cases} \left(\frac{0.6\,\Delta\bar{u}}{\bar{u}}\right)\bar{x} & ;\ \Delta\bar{u} > 0 \\ 0 & ;\ \Delta\bar{u} \leq 0 \end{cases} \tag{2-51}$$

$$\bar{x} = \left\{ \begin{array}{lll} \bar{u}\,t & ; & t < \dfrac{x}{\bar{u}} \\ x & ; & \dfrac{x}{\bar{u}} \leq t \leq \dfrac{x}{\bar{u}} + 60t_B \\ \bar{u}(t-60t_B) & ; & \dfrac{x}{\bar{u}} + 60t_B < t \end{array} \right\} \qquad (2\text{-}52)$$

σ_{xo} = standard deviation of the alongwind concentration distribution at the source

$\Delta\bar{u}$ = vertical wind-speed shear in the layer containing the cloud

$$= \frac{\bar{u}_5}{5^p}\left[z_2^{\,p} - z_1^{\,p}\right] \qquad (2\text{-}53)$$

$\bar{u}_5$ = Mean wind speed at the reference height of 5 meters (see Equation (2-17))

z_2 = effective upper bound of the cloud

$$= \left\{ \begin{array}{ll} H(t) + 2.15\,\bar{\sigma}_z & ; \quad z_2 < H_m \\ H_m & ; \quad z_2 \geq H_m \end{array} \right\} \qquad (2\text{-}54)$$

z_1 = effective lower bound of the cloud

$$= \left\{ \begin{array}{ll} H(t) - 2.15\,\bar{\sigma}_z & ; \quad z_1 > 2 \text{ meters} \\ 2 \text{ meters} & ; \quad z_1 \leq 2 \text{ meters} \end{array} \right\} \qquad (2\text{-}55)$$

$\bar{\sigma}_z$ = average standard deviation of the vertical concentration distribution along the line-of-sight

$$= \frac{1}{(x_2-x_1)} \int_{x_1}^{x_2} \sigma_z \, dx \qquad (2\text{-}56)$$

x_1, x_2 = downwind distance coordinates of the line-of-sight

$$\bar{u} = \left\{ \begin{array}{ll} \dfrac{\bar{u}_5 \left[z_2^{1+p} - z_1^{1+p} \right]}{(z_2-z_1)\ 5^p\ (1+p)} & ;\ \bar{u} > \bar{u}(2 \text{ meters}) \\ \bar{u}(2 \text{ meters}) & ;\ \bar{u} \leq \bar{u}(2 \text{ meters}) \end{array} \right\} \qquad (2\text{-}57)$$

The standard deviation of the crosswind concentration distribution is

$$\sigma_y = \left[\left(\sigma'_A(t_s)\ x_{ry} \left(\frac{\bar{x}+x_y-x_{ry}(1-a)}{a\ x_{ry}} \right)^a \right)^2 + \left(\frac{\Delta\theta'}{4.3} \bar{x} \right)^2 \right]^{1/2} \qquad (2\text{-}58)$$

where

$\sigma'_A(t_s)$ = standard deviation of the azimuth wind angle in radians measured over the time t_s

$$= \sigma'_A(t_o) \left(\frac{t_s}{t_o} \right)^{1/5} \qquad (2\text{-}59)$$

$\sigma'_A(\tau_o)$ = standard deviation of the azimuth wind angle in radians measured over the reference time τ_o

x_{ry} = distance over which rectilinear crosswind cloud expansion occurs downwind from a virtual point source

x_y = crosswind virtual distance

$$= \begin{cases} \dfrac{\sigma_{yR}}{\sigma'_A(\tau_s)} - x_{Ry} & ; \ \sigma_{yR} \le \sigma'_A(\tau_s)\, x_{ry} \\ \alpha x_{ry} \left(\dfrac{\sigma_{yR}}{\sigma'_A(\tau_s)\, x_{ry}} \right)^{1/\alpha} - x_{Ry} + x_{ry}(1-\alpha); & \sigma_{yR} > \sigma'_A(\tau_s)\, x_{ry} \end{cases} \quad (2\text{-}60)$$

σ_{yR} = standard deviation of the crosswind concentration distribution at a reference distance x_{Ry} downwind from the source

$\Delta\theta'$ = azimuth wind direction shear in radians within the layer containing the cloud

$$= \frac{\Delta\theta}{\Delta z} \cdot \left(\frac{\pi}{180} \right) (z_2 - z_1) \quad (2\text{-}61)$$

$\frac{\Delta\theta}{\Delta z}$ = change of wind direction in degrees with height in the surface mixing layer

The standard deviation of the vertical concentration distribution used in the smoke dispersion model is

$$\sigma_z = \sigma'_E \bar{x}_{rz} \left[\frac{\bar{x} + x_z - x_{rz}(1-\beta)}{\beta x_{rz}} \right]^{\beta} \qquad (2\text{-}62)$$

where

σ'_E = standard deviation of the elevation wind angle in radians

x_{rz} = distance over which rectilinear vertical cloud expansion occurs downwind from a virtual point source

x_z = vertical virtual distance

$$= \begin{cases} \dfrac{\sigma_{zR}}{\sigma'_E} - x_{Rz} & \sigma_{zR} \le \sigma'_E x_{rz} \\ \beta x_{rz} \left(\dfrac{\sigma_{zR}}{\sigma'_E x_{rz}} \right)^{1/\beta} - x_{Rz} + x_{rz}(1-\beta); & \sigma_{zR} > \sigma'_E x_{rz} \end{cases} \qquad (2\text{-}63)$$

σ_{zR} = standard deviation of the vertical concentration distribution at a reference distance x_{Rz} downwind from the source

Equation (2-43) yields concentration as a function of time at a specific point (x, y, z). In the computer program, the line-of-sight integrated concentration is obtained by numerically integrating Equation

(2-41) over the line-of-sight using a Gauss-Legendre technique (Abramowitz and Stegun, 1964, Equation 25.4.30, page 887) with 24 arbitrary points in the interval containing the cloud.

Instantaneous Source Obscurant Model

The line-of-sight integrated concentration for an instantaneous source can be obtained from Equation (2-40) by setting $Q(\tau)$ equal to the total source strength Q and integrating over the line-of-sight rather than time. The result of integrating between the end-points (x_1, y_1, z_1) and (x_2, y_2, z_2) of the line-of-sight is given by the expression

$$
\begin{aligned}
CL_I = \Bigg\{ & \frac{\sqrt{\pi}\, S}{2\sqrt{a}} \exp\left(\frac{b^2 - 4ac}{4a}\right)\left[\operatorname{erf}\left(\sqrt{av} + \frac{b}{2\sqrt{a}}\right) - \operatorname{erf}\left(\frac{b}{2\sqrt{a}}\right)\right] \\
& + \exp\left(\frac{e^2 - 4af}{4a}\right)\left[\operatorname{erf}\left(\sqrt{av} + \frac{e}{2\sqrt{a}}\right) - \operatorname{erf}\left(\frac{e}{2\sqrt{a}}\right)\right] \\
& + \sum_{i=1}^{\infty} \Bigg\{ \exp\left(\frac{g_i^2 - 4ah_i}{4a}\right)\left[\operatorname{erf}\left(\sqrt{av} + \frac{g_i}{2\sqrt{a}}\right) - \operatorname{erf}\left(\frac{g_i}{2\sqrt{a}}\right)\right] \\
& + \exp\left(\frac{k_i^2 - 4al_i}{4a}\right)\left[\operatorname{erf}\left(\sqrt{av} + \frac{k_i}{2\sqrt{a}}\right) - \operatorname{erf}\left(\frac{k_i}{2\sqrt{a}}\right)\right] \\
& + \exp\left(\frac{m_i^2 - 4ap_i}{4a}\right)\left[\operatorname{erf}\left(\sqrt{av} + \frac{m_i}{2\sqrt{a}}\right) - \operatorname{erf}\left(\frac{m_i}{2\sqrt{a}}\right)\right]
\end{aligned}
\qquad (2\text{-}64)
$$

(Equation (2-64) is continued)

$$+ \exp\left(\frac{q_i^2 - 4ar_i}{4a}\right)\left[\operatorname{erf}\left(\sqrt{av} + \frac{q_i}{2\sqrt{a}}\right) - \operatorname{erf}\left(\frac{q_i}{2\sqrt{a}}\right)\right]\Bigg\}\Bigg\} \quad (2\text{-}64)\ (\text{Cont.})$$

where

$$S = \frac{KQ}{(2\pi)^{3/2}\,\sigma_x\,\sigma_y\,\sigma_z} \quad (2\text{-}65)$$

Q = total source strength

$$a = \frac{\sigma_y^2\,\sigma_z^2\cos^2\delta + \sigma_x^2\,\sigma_z^2\cos^2\varepsilon + \sigma_x^2\,\sigma_y^2\cos^2\xi}{2\sigma_x^2\,\sigma_y^2\,\sigma_z^2} \quad (2\text{-}66)$$

$$b = \frac{\sigma_y^2\,\sigma_z^2(x_1 - \bar{u}t)\cos\delta + \sigma_x^2\,\sigma_z^2\,y_1\cos\varepsilon - \sigma_x^2\,\sigma_y^2(H\{t\} - z_1)\cos\xi}{\sigma_x^2\,\sigma_y^2\,\sigma_z^2} \quad (2\text{-}67)$$

$$c = \frac{\sigma_y^2\,\sigma_z^2(x_1 - \bar{u}t)^2 + \sigma_x^2\,\sigma_z^2\,y_1^2 + \sigma_x^2\,\sigma_y^2(H\{t\} - z_1)^2}{2\sigma_x^2\,\sigma_y^2\,\sigma_z^2} \quad (2\text{-}68)$$

$$e = \frac{\sigma_y^2\,\sigma_z^2(x_1 - \bar{u}t)\cos\delta + \sigma_x^2\,\sigma_z^2\,y_1\cos\varepsilon + \sigma_x^2\,\sigma_y^2(H\{t\} + z_1)\cos\xi}{\sigma_x^2\,\sigma_y^2\,\sigma_z^2} \quad (2\text{-}69)$$

$$f = \frac{\sigma_y^2 \sigma_z^2 \left(x_1 - \bar{u}t\right)^2 + \sigma_x^2 \sigma_z^2 y_1^2 + \sigma_x^2 \sigma_y^2 \left(H\{t\} + z_1\right)^2}{2 \sigma_x^2 \sigma_y^2 \sigma_z^2} \tag{2-70}$$

$$g_i = \frac{1}{\sigma_x^2 \sigma_y^2 \sigma_z^2} \left[\sigma_y^2 \sigma_z^2 \left(x_1 - \bar{u}t\right) \cos \delta + \sigma_x^2 \sigma_z^2 y_1 \cos \varepsilon \right. \tag{2-71}$$

$$\left. - \sigma_x^2 \sigma_y^2 \left(2iH_m - H\{t\} - z_1\right) \cos \xi \right]$$

$$h_i = \frac{1}{2\sigma_x^2 \sigma_y^2 \sigma_z^2} \left[\sigma_y^2 \sigma_z^2 \left(x_1 - \bar{u}t\right)^2 + \sigma_x^2 \sigma_z^2 y_1^2 \right. \tag{2-72}$$

$$\left. + \sigma_x^2 \sigma_y^2 \left(2iH_m - H\{t\} - z_1\right)^2 \right]$$

$$k_i = \frac{1}{\sigma_x^2 \sigma_y^2 \sigma_z^2} \left[\sigma_y^2 \sigma_z^2 \left(x_1 - \bar{u}t\right) \cos \delta + \sigma_x^2 \sigma_z^2 y_1 \cos \varepsilon \right. \tag{2-73}$$

$$\left. + \sigma_x^2 \sigma_y^2 \left(2iH_m - H\{t\} + z_1\right) \cos \xi \right]$$

$$l_i = \frac{1}{2\sigma_x^2 \sigma_y^2 \sigma_z^2} \left[\sigma_y^2 \sigma_z^2 \left(x_1 - \bar{u}t\right)^2 + \sigma_x^2 \sigma_z^2 y_1^2 \right. \tag{2-74}$$

(Equation (2-74) is continued)

$$+ \sigma_x^2 \sigma_y^2 \left(2iH_m - H\{t\} + z_1\right)^2 \Big] \qquad (2\text{-}74)\ (\text{Cont.})$$

$$m_i = \frac{1}{\sigma_x^2 \sigma_y^2 \sigma_z^2} \Big[\sigma_y^2 \sigma_z^2 \left(x_i - \bar{u}t\right) \cos \delta + \sigma_x^2 \sigma_z^2 y_1 \cos \varepsilon$$

$$- \sigma_x^2 \sigma_y^2 \left(2iH_m + H\{t\} - z_1\right) \cos \xi \Big] \qquad (2\text{-}75)$$

$$p_i = \frac{1}{2\sigma_x^2 \sigma_y^2 \sigma_z^2} \Big[\sigma_y^2 \sigma_z^2 \left(x_1 - \bar{u}t\right)^2 + \sigma_x^2 \sigma_z^2 y_1^2$$

$$+ \sigma_x^2 \sigma_y^2 \left(2iH_m + H\{t\} - z_1\right)^2 \Big] \qquad (2\text{-}76)$$

$$q_i = \frac{1}{\sigma_x^2 \sigma_y^2 \sigma_z^2} \Big[\sigma_y^2 \sigma_z^2 \left(x_1 - \bar{u}t\right) \cos \delta + \sigma_x^2 \sigma_z^2 y_1 \cos \varepsilon$$

$$+ \sigma_x^2 \sigma_y^2 \left(2iH_m + H\{t\} + z_1\right) \cos \xi \Big] \qquad (2\text{-}77)$$

$$r_i = \frac{1}{2\sigma_x^2 \sigma_y^2 \sigma_z^2} \Big[\sigma_y^2 \sigma_z^2 \left(x_1 - \bar{u}t\right)^2 + \sigma_x^2 \sigma_z^2 y_1^2 \qquad (2\text{-}78)$$

(Equation (2-78) is continued)

$$+ \sigma_x^2 \sigma_y^2 \left(2iH_m + H(t) + z_1\right)^2\Big] \qquad \begin{matrix}(2\text{-}78)\\(\text{Cont.})\end{matrix}$$

$$\delta = \cos^{-1}\left(\frac{x_2 - x_1}{\sqrt{v}}\right) \qquad (2\text{-}79)$$

$$\varepsilon = \cos^{-1}\left(\frac{y_2 - y_1}{\sqrt{v}}\right) \qquad (2\text{-}80)$$

$$\xi = \cos^{-1}\left(\frac{z_2 - z_1}{\sqrt{v}}\right) \qquad (2\text{-}81)$$

$$v = \left(x_2 - x_1\right)^2 + \left(y_2 - y_1\right)^2 + \left(z_2 - z_1\right)^2 \qquad (2\text{-}82)$$

The remaining parameters in Equations (2-64) through (2-82) have been defined under the discussion of quasi-continuous sources above, except that $\bar{x}$ for all instantaneous sources is defined by

$$\bar{x} = \bar{u}\, t \qquad (2\text{-}83)$$

Cloud-Rise Models For Buoyant Instantaneous and Quasi-Continuous Obscurant Sources

The MS3 Routine incorporates cloud-rise models for instantaneous and quasi-continuous smoke sources which release appreciable heat during the smoke emission phase. The models given below are

primarily based on material contained in a preprint of a paper by G. A. Briggs (1971) presented at the Second International Clean Air Congress. The rise models given by Briggs for stable atmospheres are specified. Experience in using these models for predicting the rise of ground clouds from rocket launches and of plumes from stacks indicates the stable formulas predict nearly the same rise as that given by the Briggs models for adiabatic atmospheres, if the vertical gradient of potential temperature is arbitrarily set to a small value (3.322×10^{-4} degrees meter^{-1}) when the atmospheric lapse rate is adiabatic or unstable.

The effective height of the cloud centroid downwind from an instantaneous source is given by

$$H(t) = \begin{cases} h + \left[\dfrac{4\ F_I}{\gamma_I^3\ s}\ \left(1 - \cos\left(s^{1/2}\ t\right)\right)\right]^{1/4} ; & t < \pi/s^{1/2} \\ h + \left[\dfrac{8\ F_I}{\gamma_I^3\ s}\right]^{1/4} ; & t \geq \pi/s^{1/2} \end{cases} \qquad (2\text{-}84)$$

where

h = source height (m)

$$F_I = \frac{g Q_I'}{4\ c_p \rho \pi\ T} \qquad (2\text{-}85)$$

g = acceleration due to gravity (9.8 m s^{-2})

Q_I' = heat released (cal)

c_p = specific heat of air at constant pressure (0.24 cal g^{-1} $^oK^{-1}$)

ρ = density of the ambient air (g m^{-3})

T = ambient air temperature (^oK)

γ_I = entrainment coefficient for an instantaneous source (~0.6)

$$s = \frac{g}{T}\frac{\Delta\Phi}{\Delta z} \tag{2-86}$$

$\frac{\Delta\Phi}{\Delta z}$ = height weighted mean potential temperature lapse rate over a height interval of about 50 meters above the surface

$$= \frac{\sum_{z=0}^{z\cong 50m} \Phi_z \Delta Z_z}{\sum_{z=0}^{z\cong 50m} \Delta Z_z} \tag{2-87}$$

$$\Phi_z = \frac{T_{A,z+1} - T_{A,z}}{\Delta Z_z} \tag{2-88}$$

$$Z_z = Z_{z+1} - Z_z \tag{2-89}$$

$T_{A,z}$ = potential temperature at height Z_z

$T_{A,z+1}$ = potential temperature at height Z_{z+1}

The effective height of the cloud centroid downwind from a quasi-continuous source is given by the expression

$$H\{t\} = \begin{cases} h + \left[\dfrac{3\,F_c}{\bar{u}\,\gamma_c^2\,s}\left(1 - \cos\left(s^{1/2}\,t\right)\right)\right]^{1/3} & ;\ t < \pi/s^{1/2} \\ h + \left[\dfrac{6\,F_c}{\bar{u}\,\gamma_c^2\,s}\right]^{1/3} & ;\ t \geq \pi/s^{1/2} \end{cases} \qquad (2\text{-}90)$$

where

$$F_c = \frac{gQ_c'}{\pi\,\rho\,c_p\,T} \qquad (2\text{-}91)$$

Q_c' = effective rate of heat release in calories per second

γ_c = entrainment coefficient for a continuous source (~0.66)

t = time after munition is ignited

Equation (2-84) for instantaneous sources and Equation (2-90) for quasi-continuous sources are automatically used to calculate the effective height $H\{t\}$ when values of either Q_I' or Q_c' are specified in the lookup data tables for specific obscurant sources.

2.3.3 Battlefield Environment Routine Dispersion Models

As noted in the Introduction to Section 2.3, the Battlefield Environment Routine incorporates the same models described in Sections 2.3.1 and 2.3.2 above. When the Battlefield Environment Routine is selected by the user, the program automatically selects the proper model for use in calculating CL and CLID along the lines-of-sight specified by the user depending on the source category and the distance of the source from the lines-of-sight. For example, suppose the user has identified an explosive munition source (see Section 3.2 below for a description of explosive munition sources handled by the program) functioned at 7 kilometers from the line-of-sight. Further assume that the program has used the Mesoscale Wind-Field Model and Trajectory/Transport Routine to determine that the source contributes to the obscurant concentration along the line-of-sight at the time of interest and the mesoscale grid solution is based on a 2.5-kilometer spacing. The program would then use the techniques described in Section 2.3.1 for calculating the concentration and cloud dimensions along the cloud trajectory until the cloud trajectory intersects the boundaries of the grid square containing the intersection of the cloud trajectory and the line-of-sight. The cloud dimensions σ_{xn}, σ_{yn} and σ_{zn} determined to exist at this boundary from application of the Instantaneous Volume Source Model described in Section 2.3.1 and the initial source strength Q are then used to define the initial conditions for the application of the Instantaneous Source Obscurant Model described in Section 2.3.2 above. The Instantaneous Source Obscurant Model uses the meteorological parameters for the grid square containing the line-of-sight in the calculation of CL and CLID along the line-of-sight. The probability of detecting a target is then calculated, if the user desires, using the Obscuration Model Routine described in Section 2.4 below. If the source had been determined by the program to be within the same grid square as the line of sight, then the program would have used the source parameters from the explosive munition source characteristics model and the meteorological inputs for the grid square directly in the Instantaneous Source Obscurant Model.

A similar procedure is followed when the user defined source category is for a quasi-continuous obscurant source, except the Battlefield Environment Routine uses the Continuous-Source Model described in Section 2.3.1 and the Quasi-Continuous Source Obscurant Model described in Section 2.3.2. It should be noted that the primary purpose for using the Dispersion Models Routine described in Section 2.3.1 in the Battlefield Environment Routine is to simply account for the effects of changes in wind speed and depth of the surface mixing layer along cloud trajectories that exceed the mesoscale grid spacing while preserving mass continuity. When the trajectory between the source and line of sight is contained within a grid square or enters the grid square containing the line of sight, the resolution of the mesoscale model is such that wind speed and depth of the surface mixing layer are assumed constant along the trajectory.

Mobile Line Source Dispersion Model

A Mobile Line Source Model routine has been added to the battlefield environment routine, which is not available for use in the MS3 Routine. The line source geometry is shown in Figure 2-1. The vehicle is assumed to move from 0 to point A at a constant speed V_T. The concentration at point $r(\alpha,\beta,z)$ from an instantaneous source generated at point S by the moving vehicle is given by

$$\chi(\alpha,\beta,z,t) = \frac{Q_E\, V_T\, dt'}{(2\pi)^{3/2}\, \sigma_x\, \sigma_y\, \sigma_z} \left\{ \sum_{a=0}^{\infty} \left[\exp\left[-\frac{1}{2}\left(\frac{2a\, H_m - H + z + V_s(t-t')}{\sigma_z} \right)^2 \right] \right.\right.$$

$$\left.\left. + \exp\left[-\frac{1}{2}\left(\frac{2a\, H_m + H + z - V_s(t-t')}{\sigma_z} \right)^2 \right] \right] \qquad (2\text{-}92)$$

$$+ \sum_{a=1}^{\infty} \left[\exp\left[-\frac{1}{2}\left(\frac{2a\, H_m + H - z - V_s(t-t')}{\sigma_z} \right)^2 \right] \right.$$

(Equation (2-92) is continued)

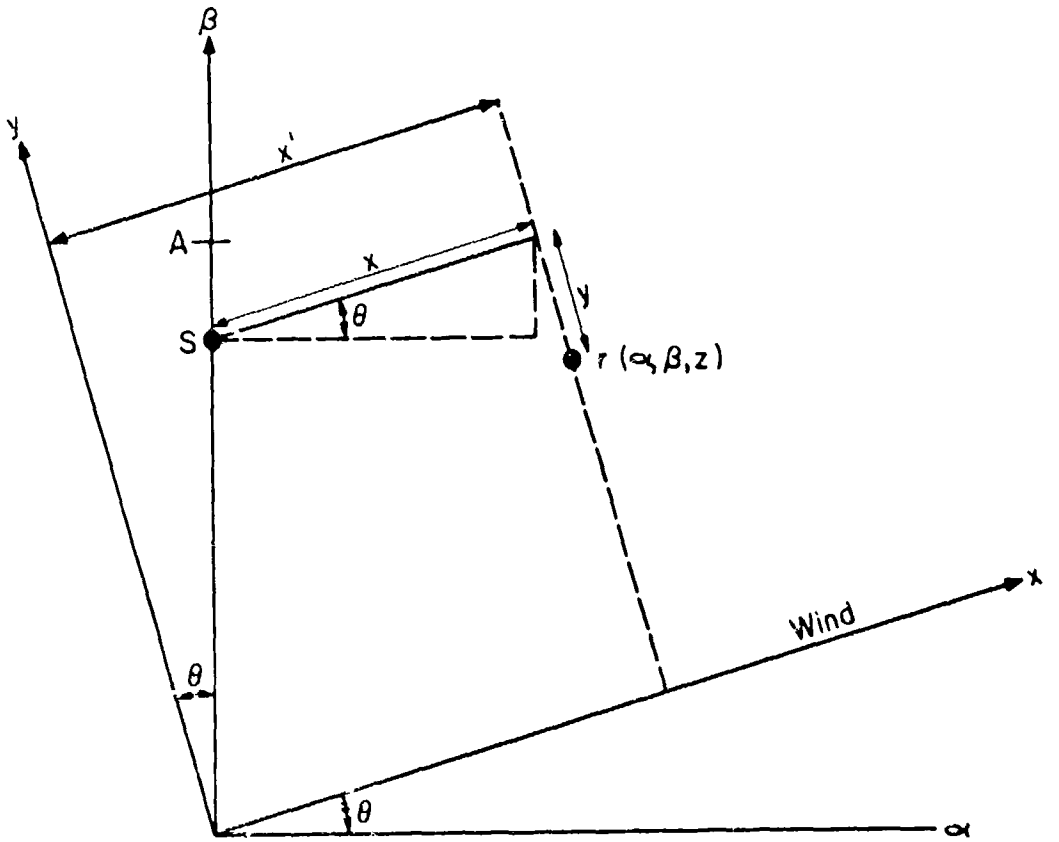

FIGURE 2-1. Plan view of the mobile line source geometry.

$$+ \exp\left[-\frac{1}{2}\left(\frac{2a\ H_m - H - z + V_s(t-t')}{\sigma_z}\right)^2\right]\Bigg]$$

$$\left\{\exp\left[-\frac{1}{2}\left(\frac{V_T t'\cos\theta + x'\tan\theta - (\beta/\cos\theta)}{\sigma_x}\right)^2\right]\right\} \qquad \text{(2-92) (Continuation)}$$

$$\left\{\exp\left[-\frac{1}{2}\left(\frac{x' - V_T t'\sin\theta - \bar{u}(t-t')}{\sigma_x}\right)^2\right]\right\}$$

where

Q_E = constant emission rate (g m^{-1})

V_T = vehicle speed (m s^{-1})

dt' = instant the source is generated at point S

t = time concentration is calculated

t' = travel time of the vehicle

and the parameters H_m, H, z, V_s, σ_x, σ_y and σ_z have their usual meaning. If we start the vehicle at times t' equal 0 and t equal 0, the concentration at point $r(\alpha,\beta,z)$ from all the instantaneous point sources comprising the line source generated by the vehicle traveling over a time t_1 can be calculated by integrating Equation (2-92) over the interval t_1. Note that the limit of integration t_1 must be equal to t for times t less than or equal to t_1 and equal to t_1 for times t greater than t_1. The integration can be analytically performed only if the standard deviations σ_x, σ_y and σ_z have a similar functional dependence on the time t'. We have performed the integration under the assumptions that:

$$\sigma_z = \frac{\sigma'_A\{\tau=2.5\}}{k}\left[\bar{u}(t-t') + x_v\right] \tag{2-93}$$

$$\sigma_y = \sigma'_A\{\tau=2.5\}\left[\bar{u}(t-t') + x_v\right] \tag{2-94}$$

$$\sigma_x = T''\left[\bar{u}(t-t') + x_v\right] \tag{2-95}$$

$$k = \frac{\sigma'_A\{\tau=2.5\}}{\sigma'_E} \tag{2-96}$$

$$x_v = \frac{\sigma_o}{\sigma'_A\{\tau=2.5\}} \tag{2-97}$$

$$x' = \alpha\cos\theta + \beta\sin\theta \tag{2-98}$$

and where T" is determined such that σ_x given by Equation (2-95) will approximate the value that would have been obtained if Equation (2-50) had been used to calculate σ_x. The results of integrating Equation (2-92) are given by the expression

$$\chi_v(\alpha,\beta,z,t) = S\left\{\sum_{a=0}^{\infty}\left[\exp\left(\frac{T^2}{4N} - A\right)\right]\frac{1}{2N}\left[\exp\left(-N\left(\frac{1}{b_1} + \frac{T}{2N}\right)^2\right)\right.\right. \tag{2-99}$$

$$\left.\left. - \exp\left(-N\left(\frac{1}{b_2} + \frac{T}{2N}\right)^2\right)\right] + \frac{T\sqrt{\pi}}{4N^{3/2}}\left[\operatorname{erf}\left(\sqrt{N}\left(\frac{1}{b_1} + \frac{T}{2N}\right)\right)\right.\right.$$

(Equation (2-99) is continued)

$$- \operatorname{erf}\left(\sqrt{N}\left(\frac{1}{b_2} + \frac{T}{2N}\right)\right)\Bigg]\Bigg\}$$

$$+ \exp\left(\frac{U^2}{4P} - A\right)\Bigg\{\frac{1}{2P}\left[\exp\left(-P\left(\frac{1}{b_1} + \frac{U}{2P}\right)^2\right) - \exp\left(-P\left(\frac{1}{b_2} + \frac{U}{2P}\right)^2\right)\right]$$

$$+ \frac{U\sqrt{\pi}}{4P^{3/2}}\left[\operatorname{erf}\left(\sqrt{P}\left(\frac{1}{b_1} + \frac{U}{2P}\right)\right) - \operatorname{erf}\left(\sqrt{P}\left(\frac{1}{b_2} + \frac{U}{2P}\right)\right)\right]\Bigg\}\Bigg] \qquad (2\text{-}99)$$

(Continued)

$$+ \sum_{a=1}^{\infty}\Bigg[\exp\left(\frac{V^2}{4Q} - A\right)\Bigg\{\frac{1}{2Q}\left[\exp\left(-Q\left(\frac{1}{b_1} + \frac{V}{2Q}\right)^2\right) - \exp\left(-Q\left(\frac{1}{b_2} + \frac{V}{2Q}\right)^2\right)\right]$$

$$+ \frac{V\sqrt{\pi}}{4Q^{3/2}}\left[\operatorname{erf}\left(\sqrt{Q}\left(\frac{1}{b_1} + \frac{V}{2Q}\right)\right) - \operatorname{erf}\left(\sqrt{Q}\left(\frac{1}{b_2} + \frac{V}{2Q}\right)\right)\right]\Bigg\}$$

$$+ \exp\left(\frac{W^2}{4R} - A\right)\Bigg\{\frac{1}{2R}\left[\exp\left(-R\left(\frac{1}{b_1} + \frac{W}{2R}\right)^2\right) - \exp\left(-R\left(\frac{1}{b_2} + \frac{W}{2R}\right)^2\right)\right]$$

$$+ \frac{W\sqrt{\pi}}{4R^{3/2}}\left[\operatorname{erf}\left(\sqrt{R}\left(\frac{1}{b_1} + \frac{W}{2R}\right)\right) - \operatorname{erf}\left(\sqrt{R}\left(\frac{1}{b_2} + \frac{W}{2R}\right)\right)\right]\Bigg\}\Bigg]\Bigg\}$$

where

$$N = B^2 + F^2 + G^2 \qquad (2\text{-}100)$$

$$P = C^2 + F^2 + G^2 \qquad (2\text{-}101)$$

$$Q = D^2 + F^2 + G^2 \tag{2-102}$$

$$R = E^2 + F^2 + G^2 \tag{2-103}$$

$$T = 2(BJ - FL + GM) \tag{2-104}$$

$$U = 2(GM - FL - CJ) \tag{2-105}$$

$$V = 2(GM - FL - DJ) \tag{2-106}$$

$$W = 2(EJ - FL + GM) \tag{2-107}$$

$$A = M^2 + L^2 + J^2 \tag{2-108}$$

$$B = kT''\left(2a\ H_m - H + z - (V_s\ x_v/\bar{u})\right. \tag{2-109}$$

$$C = kT''\left(2a\ H_m + H + z + (V_s\ x_v/\bar{u})\right) \tag{2-110}$$

$$D = kT''\left(?a\ H_m + H - z + (V_s\ x_v/\bar{u})\right) \tag{2-111}$$

$$E = kT''\left(2a\ H_m - H - z - (V_s\ x_v/\bar{u})\right) \tag{2-112}$$

$$F = T''\left[x'\tan\theta - (\beta/\cos\theta) + V_T\left(t+(x_v/\bar{u})\right)\cos\theta\right] \tag{2-113}$$

$$G = \sigma'_A\{\tau=2.5\}\left[x' + x_v - V_T\sin\theta\left(t + (x_v/\bar{u})\right)\right] \tag{2-114}$$

$$J = k\ V_s/(\sqrt{2}\ \sigma'_A\{\tau=2.5\}\ \bar{u}) \tag{2-115}$$

$$L = V_T\cos\theta/(\sqrt{2}\ \sigma'_A\{\tau=2.5\}\bar{u}) \tag{2-116}$$

$$M = (V_T\sin\theta - \bar{u})/(\sqrt{2}\ T''\ \bar{u}) \tag{2-117}$$

$$S = Q_E\ V_T\ k\ T''/(\pi^{3/2}\sqrt{2}\ \bar{u}) \tag{2-118}$$

$$b_1 = \sqrt{2}\ T''\ \sigma'_A\{\tau=2.5\}\left[\bar{u}t + x_v\right] \tag{2-119}$$

$$b_2 = \begin{cases} \sqrt{2}\ T''\ \sigma'_A\{\tau=2.5\}\left[\bar{u}(t-t_1) + x_v\right]; & t > t_1 \\ \sqrt{2}\ T''\ \sigma'_A\{\tau=2.5\}\ x_v \quad ; & t \leq t_1 \end{cases} \tag{2-120}$$

The purpose of the parameter T'', as noted above, is to approximate Equation (2-50) using Equation (2-95) in a manner that, after the integration of Equation (2-92) over the time t' is performed, yields the average value of σ_x from all the instantaneous sources affecting the concentration at the point r{α,β,z}. To obtain the appropriate value of T'', we first determine the portion of the line source contributing to the concentration at the point r at time t. This is accomplished by calculating the origin of clouds from instantaneous sources comprising the line source which lie within approximately 5 σ_y in any direction from the point r at time t. We then calculate a value of T'' by setting Equations (2-50) and (2-95) equal to one another and solving for T'', resulting in the following expression for T'':

$$T'' = k' \left\{ \frac{x\left[x^2+(\sigma_o/k')^2\right]^{1/2} + (\sigma_o/k')^2\ \ell n\left\{ x + \left[x^2+(\sigma_o/k')^2\right]^{1/2} \right\} \Big|_{x=x_1}^{x=x_2}}{x_2^{\,2} - x_1^{\,2} + 2x_v(x_2-x_1)} \right\} \tag{2-121}$$

where the symbolic notation $\Big|_{x=x_1}^{x=x_2}$ means that the numerator is evaluated at x equal x_1 and x_2.

The values of x_1 and x_2 are determined from the coordinate transformation matrix

$$\left.\begin{aligned}\begin{pmatrix} x_1 \\ y_1 \end{pmatrix} &= \begin{pmatrix} x_1' \\ 0 \end{pmatrix}\begin{pmatrix} \cos(\xi-\theta) & -\sin(\xi-\theta) \\ \sin(\xi-\theta) & \cos(\xi-\theta) \end{pmatrix} \\ \begin{pmatrix} x_2 \\ y_2 \end{pmatrix} &= \begin{pmatrix} x_2' \\ 0 \end{pmatrix}\begin{pmatrix} \cos(\xi-\theta) & -\sin(\xi-\theta) \\ \sin(\xi-\theta) & \cos(\xi-\theta) \end{pmatrix}\end{aligned}\right\} \tag{2-122}$$

where

$$x_1' = (\alpha_i'^2 - R)/\cos^2\left(\tan^{-1}(5\sigma_A'\{\tau=2.5\})\right) \tag{2-123}$$

$$x_2' = (\alpha_i'^2 + R)/\cos^2\left(\tan^{-1}(5\sigma_A'\{\tau=2.5\})\right) \tag{2-124}$$

$$R = \left[\alpha_i'^2 - (\alpha_i'^2 + \beta_i'^2)\cos^2\left(\tan^{-1}(5\sigma_A'\{\tau=2.5\})\right)\right]^{1/2} \tag{2-125}$$

$$\begin{pmatrix} \alpha_i' \\ \beta_i' \end{pmatrix} = \begin{pmatrix} \alpha_i \\ \beta_i \end{pmatrix}\begin{pmatrix} \cos(\theta-\xi) & -\sin(\theta-\xi) \\ \sin(\theta-\xi) & \cos(\theta-\xi) \end{pmatrix} \tag{2-126}$$

$$\alpha_i = \alpha - V_T\, t \cos(90 - \theta) \tag{2-127}$$

$$\beta_i = \beta - V_T\, t \sin(90 - \theta) \tag{2-128}$$

$$\xi = \tan^{-1}\left[(\bar{u}\sin\theta)/(\bar{u}\cos\theta - V_T)\right] \tag{2-129}$$

$$k' = \frac{0.6\,\overline{\Delta\bar{u}}}{4.3\,\bar{u}} \tag{2-130}$$

The angle ξ in Equation (2-129) is the angle between the mean wind direction and the locus of points of the instantaneous clouds generated by the moving vehicle prior to the calculation time t. Inspection of Equation (2-129) shows the angle is dependent on the wind speed $\bar{u}$ and, as shown by Equation (2-57), the wind speed in turn is dependent on cloud dimensions. For this reason, the program performs an iteration to define the appropriate value of $\bar{u}$ and the angle ξ for the portion of the line source generated cloud which may be in the vicinity of the calculation point at time t. This value of $\bar{u}$ determined in the iteration is then used in the dispersion model (Equation (2-99) and following equations). The parameters $\bar{\bar{u}}$ and $\Delta\bar{\bar{u}}$ are, respectively, the values of the mean wind speed and wind speed sheer required to equate Equations (2-50) and (2-95). When the cloud is fully mixed in the surface mixing layer, e.g.

$$x_1 \geq x^* = \frac{H_m}{2.15\ \sigma'_E} - x_v \quad , \tag{2-131}$$

the program calculates $\bar{u}$ and $\overline{\Delta\bar{u}}$ from the expressions:

$$\bar{\bar{u}} = \frac{\bar{u}_R}{(1+p)\ z_R^{\,p}\ (H_m-2)} \left(H_m^{\,1+p} - 2^{1+p} \right) \tag{2-132}$$

$$\overline{\Delta\bar{u}} = \frac{\bar{u}_R}{z_R^{\,p}} \left(H_m^{\,p} - 2^p \right) \tag{2-133}$$

However, when $x_1 < x^*$, they are evaluated from the following expressions:

$$\bar{\bar{u}} = \frac{\bar{u}_R}{(x_2-x_1)(1+p)\ z_R^{\,p}} \left\{ \frac{(2.15\ \sigma'_E)^p}{(1+p)} \left[\left(x^{**} + \frac{x_v}{\sigma'_E} \right)^{1+p} - \left(x_1 + \frac{x_v}{\sigma'_E} \right)^{1+p} \right] \right.$$

$$\left. + \frac{(x_2-x^{**})}{(H_m-2)} \left[H_m^{\,1+p} - 2^{1+p} \right] \right\} \qquad (2\text{-}134)$$

$$\overline{\Delta\bar{u}} = \frac{\bar{u}_R}{(x_2-x_1)\ z_R^{\,p}} \left\{ \frac{(2.15\ \sigma'_E)^p}{(1+p)} \left[\left(x^{**} + \frac{x_v}{\sigma'_E} \right)^{1+p} - \left(x_1 - \frac{x_v}{\sigma'_E} \right)^{1+p} \right] \right.$$

$$\left. + (x_2 - x^{**})\ H_m^{\,p} - (x_2 - x_1)\ 2^p \right\} \qquad (2\text{-}135)$$

where

$$x^{**} = \left\{ \begin{array}{ll} x^* & ;\ x^* > x_2 \\ x_2 & ;\ x_1 < x^* \leq x_2 \end{array} \right\} \qquad (2\text{-}136)$$

2.4 OBSCURATION MODEL ROUTINE

2.4.1 Obscuration Model

The Obscuration Model of AMSORB is a modified version of a model developed by Gomez and Duncan (1978) for use in the ASL Smoke Obscuration Model (ASLSOM). The ASLSOM routines were based on an obscuration model contained in the SOMI obscuration program (Johnson, et al., 1972) developed for the JTCG/ME. The Obscuration Model calculates target, background brightness and cloud brightness, light transmission through an obscuring cloud, scattering of light by aerosols, and target-background contrasts. When the model routine is used in conjunction with dispersion-model routines described in Section 2.3.2 and 2.3.3, the primary output is the probability of detecting a target. The probability of detection depends on the amount and type of obscurant present, general lighting conditions, relative contrast of the target and background, and the amount and type of natural obscurants which may affect detection.

The ASLSOM visibility model contains options for calculating the probability of detection for visible, infrared, laser and electro-optical (EO) sensors. These options and the option to consider the effects of adverse weather (rain, fog, etc.) contained in ASLSOM have been retained in the Obscuration Model used in AMSORB, although only the option for calculating the probability of detection in the visible region of the spectrum has been verified. The Obscuration Model and the modifications made in the ALSOM smoke visibility-model routine for application in AMSORB are described in Section 2.4.2 below.

The probability of detecting a target is calculated from the relationship (Johnson, et al., 1972)

$$PD = 0.5 \left\{ \text{erf} \left[1.462 \left((C/C_B) - 1 \right) \right] + 1 \right\} \qquad (2\text{-}137)$$

where

C = contrast

$$= \frac{2M}{2 - M} \tag{2-138}$$

M = modulation contrast

$$= \frac{2(B_t - B_b)}{B_t + B_b} \tag{2-139}$$

B_t = target brightness as seen by the observer

B_b = background brightness as seen by the observer

C_B = threshold constrast for a 50 percent probability of detection (visible spectrum)

Values of C_B determined by Blackwell (1946) for various target illuminations and sizes are used in the AMSORB program (see Section 4.4). Equation (2-137) shows that the constrast C must be greater than the threshold constrast C_B to have a probability of detection of greater than 50 percent.

The target brightness seen by the observer is

$$B_t = B_{t_o} \tau_t + B_c \tag{2-140}$$

where

B_{t_o} = brightness at the target location of a target with reflectivity R_t

τ_t = transmission factor from the target to observer

B_c = cloud brightness with respect to the target due to light scattered into the line-of-sight between the target and observer

The subset of equations defining B_{t_o} and τ_t is

$$B_{t_o} = R_t \sum_{i=1}^{N} B_{o_i} \tau_i \cos (180 - \phi_i) \tag{2-141}$$

where the summation extends over only those light sources where ϕ_i is greater than or equal to 90°, since light sources behind the target do not contribute to its brightness, and where

B_{o_i} = brightness of the ith light source (sky, sun, terrain)

ϕ_i = scattering angle for the ith light source (see Figure 4-5 in Section 4.4)

τ_i = fraction of light reaching the target from the ith light source

$$= \prod_{\ell} \exp \left[- \alpha_\ell\{\lambda\} \int_{x_t,y_t,z_t}^{x_i,y_i,z_i} \chi_{v;\ell}\{x,y,z,t\} \, d\ell \right] \tag{2-142}$$

$$= \exp \left\{ - \sum_{\ell=1}^{P} \left[\alpha_\ell\{\lambda\} \int_{x_t,y_t,z_t}^{x_i,y_i,z_i} \chi_{v;\ell}\{x,y,z,t\} \, d\ell \right] \right\} \tag{2-143}$$

$\alpha_\ell\{\lambda\}$ = attenuation coefficient for light of wavelength λ and the obscurant from the ℓth source

$\chi_{v;\ell}\{x,y,z,t\}$ = concentration at time t at the point (x,y,z) given by Equation (2-41) for the obscurant from the ℓth source

In Equation (2-142), for example, ℓ=1 might be a smoke source, ℓ=2 might be a dust source and so forth for the total of P different sources. The quantity $d\ell$ in Equation (2-142) is oriented along the line-of-sight between the target at (x_t,y_t,z_t) and the light source at (x_i,y_i,z_i). Since each light source or sky segment is an infinite distance from the target, the position (x_i,y_i,z_i) is specified by multiplying the direction vectors to the light source by a large number (Johnson, et al., 1972). In Equation (2-140) the fraction of light transmitted from the target to the observer τ_t is given by:

$$\tau_t = \prod_{\ell} \exp\left(-\alpha_\ell\{\lambda\} CL_\ell\right) \tag{2-144}$$

where

CL_ℓ = line-of-sight integrated concentration between the target and observer for the obscurant from the ℓth source

$$= \int_{x_o,y_o,z_o}^{x_t,y_t,z_t} \chi_{v;\ell}\{x,y,z,t\}\, d\ell \tag{2-145}$$

where the observer is located at the coordinate (x_o,y_o,z_o) and $d\ell$ is oriented along the line-of-sight between the target and observer.

The cloud brightness B_c is defined by the expression

$$B_c = \sum_{j=1}^{M} \left\{ \tau_{jo} \sum_{\ell=1}^{P} \left[C_{j\ell} \sum_{i=1}^{N} (B_{oi} F_{i\ell} \tau_{ij}) \right] \right\} d\ell \qquad (2\text{-}146)$$

where

τ_{jo} = fraction of light from the jth incremental cloud volume along the line-of-sight reaching the observer

$$= \prod_{\ell} \exp \left[- \alpha_\ell(\lambda) \int_{x_o,y_o,z_o}^{x_j,y_j,z_j} \chi_{v;\ell}\{x,y,z,t\} \; d\ell \right] \qquad (2\text{-}147)$$

$C_{j\ell}$ = concentration due to the ℓth obscurant source in the jth cloud element, assumed constant within the element and equal to $\chi_{v;\ell}\{x_j,y_j,z_j,t\}$

τ_{ij} = fraction of light reaching the jth cloud element from the ith light source

$$= \prod_{\ell} \exp \left[- \alpha_\ell(\lambda) \int_{x_j,y_j,z_j}^{x_i,y_i,z_i} \chi_{v;\ell}\{x,y,z,t\} \; d\ell \right] \qquad (2\text{-}148)$$

$F_{i\ell}$ = fraction per unit concentration (due to the ℓth obscurant) of the light intensity which is scattered through an angle ϕ_i into the observer's line of sight

$$= \frac{F_\ell\{\phi_i,\lambda\}}{k^2} \qquad (2\text{-}149)$$

k = propagation constant

$= 2\pi/\lambda$

and the scattering function ($F_\ell\{\phi_i,\lambda\}$) is a complex function of the type of particle, the particle-size distribution, the refractive index of the aerosols, the wavelength of light and the scattering angle. The computer program uses tabular values of this function which have been precalculated for several types of smokes using a Mie scattering program (see Section 4.4). No Mie fractions for obscurants other than WP or HC smoke have as yet been calculated and thus only these values are currently used in the program regardless of the obscurant specified. When more than one type of obscurant is present, the summation over N light sources and M cloud elements indicated in Equation (2-145) is performed for each type of obscurant and summed over the P sources to obtain the total cloud brightness.

The brightness B_b of a background of reflectivity R_b is determined in the same manner as the target brightness in Equations (2-140) through (2-148) by replacing the end point of integration (x_t,y_t,z_t) with the end point (x_b,y_b,z_b) and R_t by R_b. If the target and background are coincident, the only difference in brightness between them is due to the difference in their reflectivities.

Detailed explanations of the theoretical background of the obscuration model described above are given by Johnson, et al. (1972) and by Gomez and Duncan (1978).

2.4.2 Revisions of the ASLSOM Smoke Visibility Computer Code

Revisions in the ASLSOM smoke visibility computer code were necessary to make the code compatible with the concentration models described in Sections 2.3.2 and 2.3.3, with AMSORB, to improve the computational efficiency of the combined programs and to allow consideration of multiple obscurants. The significant revisions made in the code were:

- Modification of the input routines
- Automation of the threshold contrast calculation
- Addition of a test to determine if any obscurant is required to obscure the target
- Replacement of the routine determining whether and when the obscurant cloud intersects the line-of-sight
- Addition of a routine to divide the line-of-sight into a specified number of cloud elements
- Addition of coding to allow simultaneous calculations for different types of obscurants
- Modification of the sky-partitioning routine
- Modification of the test for large obscurant concentrations
- Modification of the test for small obscurant concentrations
- Replacement of the output routine

Each of these changes is discussed below.

Modifications of the Input Routine

The input routines of the ASLSOM visibility program were modified to automate the probability-of-detection calculation. In most cases, the data required to perform the calculations are included in the program in the form of "look-up" tables, are calculated under various assumptions, or are supplied to the obscuration model from other portions of the program. Details concerning the tables, and input calculation procedures are given in Section 4.4 below. For calculating the probability of detecting targets in the visual spectrum (visible scenarios), the only input required is the position of the target and observer and a code specifying target and background characteristics. The target is defined to be the object being viewed by the observer. For infrared, laser and other wavelengths outside the visible spectrum, the current version of the program requires that all inputs needed by the original code be supplied.

AMSORB uses the tabular values of threshold contrast described in Section 4.4 to calculate the probability of detection, where the ASLSOM and SOMI codes required the user to input appropriate values. The use of "look-up" tables incorporated within the program structure has the advantage in that the threshold contrast can be determined after the target and background brightness calculations have been performed. This allows the program to choose a value based on whether the target actually appears brighter or darker than the background, rather than basing the value only on a comparison of the two reflectivities. A target that is brighter than its background under conditions when no obscurant is present may appear darker than its background due to obscurant above the target attenuating the light which illuminates it. For a target and background which are coincident, this is not a problem and a comparison of reflectivities can be used.

Addition of a Test To Determine If Any Obscurant is Required to Obscure the Target

In some cases the target and background reflectivities may be nearly identical so that, under the assumptions made in the Obscuration Model that contrast is the only factor affecting detection, no obscurant is required to obscure the target. The test incorporated in the modified code compares the reflectivities of the target R_t and background R_b and defines the contrast as

$$C = \left| \frac{R_t - R_b}{R_b} \right| \tag{2-150}$$

The value of C is compared to the threshold contrast C_B from Blackwell's (1946) data for a given illumination and target size, using the tabular values described in Section 4.4. If C is less than C_B, the probability of detection is calculated from Equation (2-137) with the value of C given by Equation (2-150). For a probability of detection less than or equal to 5 percent, the calculations are stopped and a solution is printed stating that no obscurant is required to obscure the target. If the probability of detection is greater than 5 percent, the complete calculations using Equations (2-138) through (2-149) are performed to find the actual value of the contrast C.

Replacement of the Routine Determining Whether and When the Obscurant Cloud Intersects the Line-of-Sight

The modified obscuration routine in AMSORB does not require the user to specify times when the probability-of-detection or line-of-sight concentrations are to be calculated as in the ASLSOM code. Instead, the program automatically determines whether the obscurant cloud intersects the line-of-sight and the time interval required for the obscurant cloud to pass through the line-of-sight. The cloud arrival time at the

line-of-sight t_a and cloud passage time t_p for obscurants from each source (munition or submunition in the case of smoke sources) is given by

$$t_a = \frac{x_{min} - 3.04\,\sigma_x}{\bar{u}} \tag{2-151}$$

and

$$t_p = 60t_B + \frac{x_{max} + 3.04\,\sigma_x}{\bar{u}} \tag{2-152}$$

where

x_{min} = minimum alongwind separation distance between the source and any point on the line-of-sight

x_{max} = maximum alongwind separation distance between the source and any point on the line-of-sight

t_B = total source emission time (burn time for quasi-continuous smoke sources) in minutes

σ_x = see Equation (2-50)

$\bar{u}$ = see Equation (2-57)

The maximum time interval from the smallest value of t_a greater than zero, calculated for all sources, to the largest value of t_p for all sources, is subdivided into the number of times the user specifies that probability-of-detection calculations are to be made. The probability of detection is then calculated for this number of times during the time interval required for the obscurant from all sources to pass through the line-of-sight.

The obscurant for any specific source is not considered in the calculation for a specific time t_i within the maximum time interval if the interval between t_a and t_p for that munition does not encompass t_i. It is also not considered if there is no point on the line-of-sight between the target and observer which is within $\pm 5\ \sigma_z$ (see Equation (2-62) for σ_z) of the effective height of the cloud $H(t_i)$ for that source. It should be noted that all obscurant sources are considered in the calculation of integrated concentrations between the ith light source and j^{th} cloud element for all values of t_i within the maximum time interval. If no obscurant from any source passes through the line-of-sight between the observer and target, no probability-of-detection calculation is made and a message stating this condition is printed.

Addition of a Routine Used to Divide the Line-of-Sight into Cloud Elements

The obscuration code in AMSORB contains an automated procedure for dividing the line-of-sight between the target and observer into elements for the cloud brightness calculations. The code uses portions of the transport and dispersion models to define the lateral and vertical boundaries of the obscurant cloud at any distance from the source as 5 standard deviations from the cloud centerline. The effective line source within these cloud boundaries is defined and divided into 20 equally-spaced cloud elements for each calculation time. If the line length of each element $d\ell$ is less than 1 meter at this point, the number of elements is decreased until the length $d\ell$ is 1 meter and this number of elements is used in the calculations of cloud brightness. If, on the other hand, $d\ell$ is greater than 1 meter, the trapezoidal rule of integration is used in combination with the dispersion model to calculate the integrated concentration along the effective cloud length. The number of cloud elements is then doubled to 40 and a similar procedure followed. If $d\ell$ is less than 1 meter, the number of elements is reduced until $d\ell$ equals 1 meter and this number of elements is used in the cloud brightness calculations. If $d\ell$ exceeds 1 meter for 40 elements, the integrated concentration

is calculated and compared with the integrated concentration calculated using 20 elements. If the change in integrated concentration is less than $1.5\text{x}10^{-3}$ percent, the number of elements is decreased until the change is $1.5\text{x}10^{-3}$ percent. The entire procedure of doubling the elements, checking the length of $d\ell$, and comparing the percentage change with the criteria of $1.5\text{x}10^{-3}$ percent is continued until either a 1-meter spacing or a spacing yielding less than a $1.5\text{x}10^{-3}$ percent change in the integrated concentration is achieved. For the trial calculations we have performed, the procedure has led to changes in the cloud brightness of less than 0.1 percent and even smaller changes in the calculated value of contrast C used in the probability-of-detection calculation.

Addition of Coding Permitting Simultaneous Calculations for Different Types of Obscurant Sources

The Obscuration Model code in AMSORB has the capability of performing probability-of-detection calculations when sources containing different types of obscurants are released at the same or different times. In the program, the line-of-sight integrated concentrations are calculated separately for each source, which allows the source characteristics and the time the source is released to be different for each type of source. The line-of-sight concentrations and elemental concentrations along the line-of-sight are summed for each source of the same type and the total attenuation calculated from the expression

$$t = \exp\left[-\sum_{\ell=1}^{P} \alpha_\ell \, \rangle_{v;\ell}\right] \qquad (2\text{-}153)$$

where there are P different types of obscurants and the attenuation coefficients α_ℓ are known for each type of obscurant. The cloud brightness

of the plume containing these multiple obscurants is calculated according to Equation (2-146) and takes into account the difference in scattering and attenuation properties of each type of obscurant.

Modification of the Sky-Partitioning Routine

The user must input the number and location of light sources to the ASLSOM and SOMI visibility codes. The number of light sources and their location are obtained by using a separate program. For use in the automated AMSORB program, we developed data tables in the mass storage file containing the location of sky segments based on their position with respect to a standard reference frame. For each data case, this standard reference frame is translated to a new reference frame that is oriented with respect to the line-of-sight between the target and observer. These data tables are based on the results of extensive target brightness calculations made with the SOMI routine using hundreds of sky partitions. The results obtained using the simplified procedure outlined below are generally more accurate than those obtained using the SOMI routine.

The procedure used to define the light source locations described in Section 4.4 is based on the division of the sky into either 6 partitions of equal solid angle when the sun is shining on the face of the target or 16 partitions when the sun is behind the target. In both cases, another partition of equal solid angle is formed whose centroid has the actual coordinates of the sun's position and has the sun's brightness. The sun's partition may overlap some of the other sky partitions, but this causes no problem in the calculations since each partition is handled independently. The sun is thus placed in its own partition, resulting in either a total of 7 or 17 partitions being used in the calculations. The sun's position in the sky is automatically obtained from a routine contained in the mesoscale model routine, which calculates the position as a function of date, time of day, and the longitude and latitude. The cloud cover is

also passed to the obscuration model from the mesoscale model routine. If the sky is overcast, the sun is not considered in the calculation and 16 partitions or segments are used in the calculations. The program will not currently handle nighttime scenarios and some changes will be required so the user can input the brightness and position of the moon or other light sources such as flares.

Modification of the Test for Large Obscurant Concentrations

The ASLSOM smoke visibility model contains a check to determine if the existing concentration of obscurants is sufficient to obscure the target without consideration of the cloud brightness, thus eliminating the necessity of performing the time-consuming cloud brightness calculations. We have changed the location of this test in AMSORB so that the line-integrated concentration between the observer and target is checked prior to any target and background brightness calculations. Computer runs using data from smoke trials also indicated that the critical level of concentration required to obscure the target without considering cloud brightness needed to be increased. Cloud brightness calculations are not considered necessary in AMSORB when the product of the line-integrated concentration and the coefficient of attenuation is equal to or greater than 11, rather than the value of 7 used in ASLSOM.

Modification of the Test for Small Obscurant Concentrations

The ASLSOM model also contains a check to determine if the amount of obscurant between the target and observer is so small that the probability of detection is at least 95 percent. The ASLSOM program first calculates the target brightness, reduced by the smoke cloud, and then calculates the attenuation of the target brightness due to the smoke between the target and observer without making the cloud brightness calculation. If the target brightness is reduced less than 5 percent by the smoke between the target and observer, the ASLSOM code concludes

that the probability of detection is greater than 95 percent and does not perform the cloud brightness calculation. In cases where the reflectivities of the target and background are similar, even a small amount of obscurant can cause a reduction in the probability of detection. For this reason, the Obscuration Model Routine in AMSORB, in addition to the above tests on transmission and brightness, computes the probability of detection given by Equation (2-137) with the cloud brightness B_c set to zero before the conclusion is reached that the probability of detection is greater than 95 percent and cloud brightness need not be calculated.

Replacement of the Output Routine

The output routine of ASLSOM was changed to reflect the types of calculations made in AMSORB, and the MS3 Routine includes options for selecting graphical output showing time profiles of line-of-sight integrated concentration, probability of detection and light transmittance.

2.4.3 Limitations of the MS3 Routine

The AMSORB routines have certain limitations. As mentioned above, the current version of the program does not contain sufficient data in the mass storage data files to perform completely automated calculations for nighttime scenarios, and for making probability-of-detection calculations for lasers and infrared scenarios. Thus, when such calculations are desired, the AMSORB program requires the user to specify the same inputs as those required by the ASLSOM code. Also, because of the lack of data, we have been unable to check completely the operation of these portions of the code. The adverse weather module of ASLSOM has been included in AMSORB, but also has not been checked.

The mass storage data files contain source data for various smoke munitions, munition produced dust, dust produced by moving vehicles, muzzle blast smoke and dust, burning vegetation, burning buildings, and burning vehicles. We have included data for only those smoke munitions

tested recently at Dugway Proving Ground. The mass storage files contain Mie scattering fractions for only WP smoke in the visible spectrum and HC smoke at the 10.6-micrometer wavelength in the infrared. Because of this limitation, Mie scattering fractions for WP smoke are currently used for all obscurants in the visible spectrum unless other values are input by the user. Attenuation coefficients for all obscurants at all wavelengths of interest are also not available, although values exist for visible light for all of the obscurants mentioned above.

Most, if not all, of these limitations are caused by the lack of suitable data for use in the program and will be removed when such data become available and are placed in the mass storage data file. Details of the data obscuration calculations now included in the mass storage data file are given in Section 4.4.

SECTION 3

BATTLEFIELD ENVIRONMENT SOURCE CHARACTERISTICS

The source characteristics of obscurant sources are required for use in the MS3 and Battlefield Environment (BEC) Routines of AMSORB. This section contains a description of the source characteristics and models used in developing source characteristics (SORDAT routine) for smoke munition sources, dust clouds produced from munition bursts and from moving vehicles, smoke and dust clouds from muzzle blasts, and smoke from burning vegetation, buildings and vehicles. In some cases, source characteristics models developed for the E-O SAEL program library (Duncan, et al, 1979) are included in the AMSORB program and are used to develop source inputs in the SORDAT routine of AMSORB.

3.1 SMOKE MUNITION SOURCE CHARACTERISTICS

Table 3-1 gives the source inputs required by the dispersion models to treat smoke munition sources. The user need only supply the source coordinates, the detonation time, the direction of travel with respect to grid north of the projectile prior to detonation, and the type of smoke munition being used when the munition is selected from one of the fifteen munitions or submunitions for which data are available in the AMSORB mass storage data file. Source input data for these smoke sources are shown in Table 3-2. The parameters for all sources, except the bulk white phosphorus (WP) sources were experimentally determined during wind-tunnel trials at Dugway Proving Ground (Peterson, 1978). The parameters for the bulk WP munitions (last four munitions in Table 3-2) approximate values obtained by using CL profiles measured at short distances from static-firings of the munitions in field trials (DPG, 1978b) to develop the emission characteristics. The orientation of the submunition patterns of the 155 mm hexacloroethane (HC) smoke projectile, and the 155 mm XM825 WP smoke projectile are dependent on the flight

TABLE 3-1

SMOKE SOURCE MODEL INPUTS

Parameter Symbol	Parameter Description	Program Default Value
x, y, z	Source coordinates (m)	
M_o	Total mass before ignition (g)	
MYF	Munition yield fraction	
YF	Yield factor accounting for the effects of moisture in the air	
t_o	Time of detonation (s)	
t_B	Total burn time (min)	
ICAT	Type of smoke	1
A, B, C, D	Coefficients of the source release rate expression	
σ_{xo}	Standard deviation of the alongwind concentration distribution at the source (m)	
σ_{yo}	Standard deviation of the crosswind concentration distribution at the source (m)	
σ_{zo}	Standard deviation of the vertical concentration distribution at the source (m)	
Q'_c	Effective rate of heat release from quasi-continuous sources (cal s^{-1})	0
DIR	Direction of the projectile flight with respect to grid north (degrees)	0
TYPSMK	Code specifying the type of smoke	0

TABLE 3-2

SUMMARY OF SMOKE SOURCE PARAMETERS CONTAINED IN THE DATA COMPONENT OF AMSORB

	Agent	M $(g)^o$	MYF	t_b (min)	BURN COEFFICIENTS A	B	C	D	Source Sigmas (m)	Heat Content (kcal s^{-1})
155mm HC M1 Canister	Zn	3455	0.12	2.3	.537	.238	1.593	-1.368	.35[a]	0
155mm HC M2 Canister	Zn	1989	0.19	1.3	.643	-.254	2.291	-1.662	.29[a]	0
105mm HC Canister	Zn	1178	0.16	2.0	.230	2.159	-.679	- .748	.17[a]	0
Six Inch WP Wick	P	206	0.67	6.5	1.808	-1.278	.961	- .502	.12[a]	0
Three Inch WP Wick	P	63	0.71	7.8	1.631	.399	-1.969	1.003	.17[a]	0
2.75 in. Rocket WP Wedge	P	210	0.66	4.3	.521	1.053	- .370	- .187	.12[a]	0
81mm Navy RP Wedge	P	58	0.53	4.3	.653	-1.568	5.103	-3.218	.12[a]	0
155mm Navy RP Wedge	P	39	0.64	3.6	1.047	-4.821	10.640	-5.873	.12[a]	0
81mm German RP Wedge	P	11	0.55	6.4	1.731	-1.426	1.447	- .777	.12[a]	0
155mm XM825 WP Wedge	P	b	0.77	11.5	3.137	-6.834	8.593	-3.926	c	0
155mm WP M110E2	P	7076	0.59	1.5	6.0257	-15.515	17.914	-7.4208	σ_{xo} = 1.86 σ_{yo} = 1.16 σ_{zo} = 2.33	452
105mm WP M60A2	P	1814	0.30	0.833	6.8429	-16.639	17.673	-6.8131	σ_{xo} = 0.93 σ_{yo} = 1.63 σ_{zo} = 1.86	208
81mm M375A2 Mortar	P	726	0.37	0.75	5.3723	-11.712	11.866	-4.4702	σ_{xo} = 1.63 σ_{yo} = 0.93 σ_{zo} = 1.40	93
4.2 in M328A1 Mortar	P	3692	0.59[d]	0.5233	5.2856	-11.702	11.859	-4.4702	σ_{xo} = 1.86 σ_{yo} = 2.09 σ_{zo} = 2.33	676

a $\sigma_{xo} = \sigma_{yo} = \sigma_{zo}$ for these munitions

b This munition is composed of 92 submunitions which have been modeled by 17 submunitions as shown in Table 3-3(b).

c The σ_{yo} chosen for each submunition is presented in Table 3-3(b). All submunitions have σ_{xo}=4.33 and σ_{zo}=0.12

d A best estimate was chosen for the yield fraction since the calculated data fit for this munition has not been completed.

direction of the projectile before impact. The characteristic submunition impact pattern for the 155 mm HC projectile, which contains 3-M1 and 1-M2 canisters, is shown in Table 3-3(a) and the characteristic pattern and other source characteristics for the 155 mm XM825 WP projectile are given in Table 3-3(b) (see Carter, Dumbauld and Rafferty, 1979 for the basis of these patterns). In the AMSORB program, the user specifies the ground impact centroid location of the submunition pattern and the direction of the projectile flight (measured clockwise from north). The program automatically calculates the coordinates of each submunition based on the angle ϕ in Table 3-3 that a line joining the submunition position and the centroid of the pattern makes with the direction of the projectile flight, using the distance between the impact centroid location and the submunition also given in Table 3-3.

The HC munition produces elemental zinc which, in contact with moisture in the air, produces the obscuring agent, hydrated zinc chloride. Similarly, the phosphorus emitted by WP and RP munitions produces phosphoric acid. In the program, the yield factor YF accounting for the production of these materials is linearly interpolated from the tabular values of YF as a function of relative humidity given in Table 3-4. The empirical values of the yield factors for WP and RP were obtained from a Dugway Proving Ground Report (DPG, 1978a) and those for HC munitions from the report by Petersen (1978). The relative humidity measured at the surface weather station nearest the source location is used in the calculation of YF.

3.2 EXPLOSIVE MUNITION SOURCE CHARACTERISTICS

The explosion of an artillery projectile or detonation of a mine produces dust clouds from the dust and debris lofted into the atmosphere by the force of the explosion. The amount of dust produced depends on the size and type of munition, the height of the detonation, the thickness of vegetative cover and the type of soil. A completely

TABLE 3-3

SUBMUNITION IMPACT PATTERNS

(a) Impact Pattern of submunitions for the 155mm HC Smoke Projectile

Canister/submunition	ϕ^a (degrees)	Distance to Pattern Centroid (m)
M1	348.1	36.41
M1	15.9	13.65
M2	180.0	5.62
M1	175.0	43.29

(b) Impact Pattern of submunitions, total mass of submunition before ignition (M_o) and source dimension (σ_o) for the 155mm XM825 WP Wedge

Submunition	M_o (g)	σ_o (m)	ϕ^a (degrees)	Distance to Pattern Centroid (m)
1	261	10.5	180.0	120.0
2	349	14.0	175.9	105.3
3	523	20.9	175.2	90.3
4	523	20.9	174.3	75.4
5	610	24.4	166.0	61.8
6	697	27.9	170.5	45.6
7	697	27.9	166.0	30.9
8	697	27.9	153.4	16.8
9	610	24.4	0.0	0.0
10	610	24.4	0.0	15.0
11	610	24.4	0.0	30.0
12	523	20.9	350.5	45.6
13	523	20.9	352.9	60.5
14	436	17.4	348.7	76.5
15	436	17.4	350.5	91.2
16	523	20.9	347.9	107.4
17	436	17.4	346.0	123.7

a ϕ is the angle that a line joining the submunition and centroid of the pattern makes with the direction of flight of the projectile.

TABLE 3-4

YIELD FACTORS FOR WP, RP AND HC SMOKE SOURCES
USED IN THE PROGRAM

Relative Humidity (percent)	WP and RP Sources	HC Sources
0	3.42	2.09
5	3.42	2.09
10	3.57	2.50
20	3.87	2.98
30	4.17	3.34
40	4.46	3.57
50	4.76	3.90
60	5.06	4.29
70	5.36	4.86
80	5.66	5.63
100	5.66	5.63

satisfactory theoretical description of all aspects of an exploding munition has not been developed. However, empirical relationships describing the initial dust cloud produced in an explosion have been developed principally by Ebersole, et al. (1979) and Zirkind (1979) from data measured during field trials at Dugway, Utah (DPG, 1978c), Fort Sill, Oklahoma (DPG, 1978d), White Sands, New Mexico (Lindberg, 1979) and Grafenwohr, Germany (Lundien, 1979). The inputs required to develop the source parameters for the dispersion model are described in Table 3-5. The only quantities the user needs to input, however, are the source coordinate, the time of detonation, the munition type, the soil type and the sod depth.

The amount of dust available for formation of a dust cloud is produced from the dust and debris propelled into the air by the explosion. The mass of dust lofted into the atmosphere and remaining airborne is given by

$$M_D = \eta \rho_s V_c \tag{3-1}$$

where ρ_s is the soil density and V_c is the crater volume. The term η in Equation (3-1) is an efficiency factor for soil suspension in the atmosphere and is considered by Ebersole, et. al.(1979) to be about 0.10 for common soils. The majority of the experimental evidence indicates the dust produced in the detonation is partitioned into a buoyant dust cloud and a nonbuoyant dust skirt. The amount of mass M_1, found in the buoyant cloud and the amount of mass M_2 in the nonbuoyant dust skirt are given by

$$M_i = \beta_i M_D \tag{3-2}$$

where the values of β_i were estimated by Zirkind (1979) to be

$$\beta_i = \begin{cases} 0.90 & i = 1; \text{ buoyant cloud} \\ 0.10 & i = 2; \text{ nonbuoyant dust skirt} \end{cases} \tag{3-3}$$

TABLE 3-5

SOURCE INPUTS FOR THE EXPLOSIVE MUNITION SOURCE MODEL

Parameter Symbol	Parameter Definition	Program Default Value
x, y	Source coordinates (m)	
t_o	Time of detonation (s)	
ITYPE	Type of explosive munition	5
W'	Equivalent charge weight of TNT (kg)	6.98
f	Fraction of energy available for crater formation	0.6
d_D	Detonation depth above or below the surface (m)	0
a_o, a_1, a_2, a_3,	Coefficients for determining the average scaled crater radius	0.503, -0.954 0.450, 1.19
b_o, b_1, b_2, b_3, b_4	Coefficients for determining the average scaled crater depth	0.251, -1.17, 0.494, 4.72, 3.34
ρ_s	Soil density (g cm^{-3})	1.5
d_s	Sod or vegetation cover depth (m)	0
ISOLTP	Soil type describing the soil texture and consistency	4

Studies by Ebersole, et al. (1979) showed that vegetative cover or sod depth d_s reduces the crater volume. They found that the crater volume for an explosive munition detonation could be expressed as

$$V_c = \frac{2\pi r_c^2 d_c}{3} \left\{ 1 - \frac{3}{2}\frac{d_s}{d_c}\left[1 - \frac{1}{3}\frac{d_s}{d_c} \right]^2 \right\} \tag{3-4}$$

where r_c is the crater radius and d_c is the crater depth. The crater radius and crater depth are given in terms of a scaled crater radius $\bar{r}_c$ and a scaled crater depth $\bar{d}_c$ according to

$$r_c = \bar{r}_c W^{1/3} \tag{3-5}$$

and

$$d_c = \bar{d}_c W^{0.3} \tag{3-6}$$

The effective energy W available for crater formation is found by reducing the available energy W' from the explosive charge in equivalent kilograms of TNT by some fraction f according to

$$W = fW' \tag{3-7}$$

A table of f values determined by Ebersole, et al. are given in Table 3-6 as a function of type of charge and detonation depth above or below the surface of the soil. A negative depth indicates the detonation occurred beneath the surface of the soil. The available energy W' in equivalent kilograms of TNT of the exploding munition required in Equation (3-7) is given in Table 3-7 for various munitions. The density of the soil is used in Equation (31) to determine the mass of airborne dust. The soil density depends on soil type and a table of various soil types and densities is given in Table 3-8. The scaled crater dimensions in Equations (3-5) and (3-6) also depend on soil type. The empirical

TABLE 3-6

FRACTION OF ENERGY AVAILABLE FOR CRATER FORMATION

Detonation type	Fraction of Energy Available for Crater Formation, f	Detonation Depth d_D (m)	Description
1	0.6	0	Live fire tilted at 30 degrees
2	0.6	0	Horizontal live fire
3	0.8	-0.3	Live fire tilted at 30 degrees
4	1.0	-0.6	Live fire tilted at 30 degrees
5	1.0	0	Static bare charge
6	1.0	-0.3	Static bare charge
7	0.6	0.3	Live fire
19	-	-	User entered bare charge
20	-	-	User entered artiliery projectile

TABLE 3-7

WEAPON TYPE AND EQUIVALENT WEIGHT OF TNT
(BASED ON INFORMATION CONTAINED IN DEPARTMENT OF THE ARMY FIELD MANUAL FM9-13)

Weapon Index	Weapon Description	Equivalent Charge Weight of TNT, W' (kg)
1	81 mm mortar	1.95
2	4.2 in mortar	3.70
3	120 mm tank gun	4.79
4	105 mm tank HEP	3.06
5	155 mm artillery	6.98
6	8 in artillery	16.63
20	User ertered type	--

TABLE 3-8

SOIL DENSITIES

Soil Category	Soil Density ($g\ cm^{-3}$)	Description
1	2.4	Rock
2	2.0	Clay or dry cohesive soils
3	0.7	Dry sandy soils
4	1.5	Loam, sandy soil and frozen ground
5	2.0	Soft rock
6	1.8	Wet sand, wet loam or ice
7	1.8	Wet cohesive soils (not saturated) and snow
10	-	User entered soil type

relationship developed by Ebersole, et al. (1979) from the field data for the scaled crater radius is

$$r_c = a_o + a_1 \lambda_c + a_2 \lambda_c^2 + a_3 \lambda_c^3 \tag{3-8}$$

and for the scaled crater depth is

$$\bar{d}_c = b_o + b_1 \lambda_c + b_2 \lambda_c^2 + b_3 \lambda_c^3 + b_4 \lambda_c^4 \tag{3-9}$$

where

$$\lambda_c = {}^{d_D}\!/_{W^{1/3}} \tag{3-10}$$

The term d_D in Equation (3-10) is the detonation depth in meters above or below the surface and can be obtained from Table 3-6 based on the detonation type. The polynomial coefficients used in Equations (3-8) and (3-9) are given in Table 3-9 for the soil categories in Table 3-8.

The dispersion models require the initial dimensions of the buoyant and nonbuoyant dust clouds produced by the explosion and also require the energy available for buoyant plume rise. The initial radius of the buoyant dust cloud at aerodynamic equilibrium (approximately 20-30 milliseconds after detonation) is used to determine initial source dimensions. This buoyant cloud radius in meters is given by (after Ebersole, et al., 1979)

$$R_o = 2.0\, W^{1/3} \left({}^{\rho_o}\!/_{\rho_A} \right)^{1/3} \tag{3-11}$$

where ρ_A is the air density in grams per cubic meter and ρ_o is 1225 g m^{-3}. The height of the centroid of the buoyant cloud depends

TABLE 3-9

COEFFICIENTS USED IN DETERMINING AVERAGE SCALED CRATER DIMENSIONS
(after Ebersole, et al, 1979)

(a) Coefficients for Average Scaled Crater Radius

Soil Category \ Coefficients	a_0	a_1	a_2	a_3
1, 2	0.271	-0.684	0.390	0.886
3	0.386	-0.849	0.367	0.993
4	0.503	-0.954	0.450	1.19
5, 6	0.629	-1.08	0.264	1.12
7	0.806	-1.28	-0.178	0.852

(b) Coefficients for Average Scaled Crater Depth

Soil Category \ Coefficients	b_0	b_1	b_2	b_3	b_4
1	0.112	-0.477	0.270	1.84	1.05
2	0.134	0.571	0.343	2.24	1.31
3, 5	0.189	-0.840	0.447	3.30	2.10
4	0.251	-1.17	0.494	4.72	3.34
6	0.331	-1.49	0.579	4.92	3.13
7	0.449	-1.82	0.322	4.11	2.02

on the type of charge used and is higher for bare charges than for artillery projectiles. Experimental observations by Ebersole, et al. (1979) of dust clouds produced by explosive munitions indicated that the initial height H of the cloud centroid is

$$H(t=0) = \begin{cases} 5R_o; & \text{bare charges detonated at the surface} \\ R_o; & \text{artillery projectiles.} \end{cases} \qquad (3\text{-}12)$$

where t equal to zero is the detonation time. For bare charges detonated beneath the surface, the height is given by R_o. The height of the centroid of the nonbuoyant dust cloud is assumed to be zero. The initial standard deviations of the two dust clouds are given in terms of the initial buoyant cloud radius as

$$\left.\begin{array}{l} \sigma_{xo} = \sigma_{yo} = \sigma_{zo} = R_o/2.15; \quad \text{buoyant cloud} \\ \left.\begin{array}{l} \sigma_{xo} = \sigma_{yo} = 1.155R_o \\ \sigma_{zo} = .93\,R_o \end{array}\right\} ; \quad \text{nonbuoyant dust skirt} \end{array}\right\} \qquad (3\text{-}13)$$

since the dust skirt is assumed to be a cylinder of height and radius equal to $2R_o$. Finally, the energy in calories available for plume rise is given as

$$Q_I' = kW \qquad (3\text{-}14)$$

where $k = 1.1 \times 10^6$ calories per kilogram of TNT.

3.3 MOVING VEHICLE SOURCE CHARACTERISTICS

A moving vehicle can generate dust through the interaction of the wheels or track with the ground. The dust produced is generally small particles less than 100 μm in diameter. The inputs required to develop the source parameters are listed in Table 3-10. The only quantities the user needs to input, however, are the vehicle location prior to moving (for example, the grid boundary for a vehicle entering the grid), the initial start time of vehicle movement, the total time of travel, a code specifying the vehicle type, a code specifying the soil type, the direction of travel of the vehicle with respect to grid north and the speed of travel.

Some work has been done by various agencies to determine the amount of dust produced by a moving vehicle. However, dust generation depends on a wide variety of factors which have not been accurately modeled. The source model in AMSORB is based on the currently approved EPA model developed by Midwest Research Institute, which gives the yearly average emission rate E in grams per vehicle meter as (Mann and Cowherd, 1977)

$$E = 0.2283 \; S_c \left(\frac{V_t}{13.41}\right)\left(\frac{N'}{4}\right)\left(\frac{365 - W_p}{365}\right) \qquad (3\text{-}15)$$

where S_c is the silt content of the surface soil in percent (percentage of the weight in particles whose diameters are less than 75 μm), V_t is the vehicle speed ($m\ s^{-1}$), N' is the number of wheels on the vehicle and W_p is the number of days during the year when precipitation exceeds 0.025 cm (0.01 in). Since the user of AMSORB is not interested in average emission rates, but requires current emission rates, we suggest W_p be set equal to 0 for dry soil and to 365 for wet soil.

The silt contents as a function of soil type are listed in Table 3-11 and were assigned based on work reported by Cowherd and

TABLE 3-10

SOURCE INPUTS FOR THE MOVING VEHICLE SOURCE MODEL

Parameter Symbol	Parameter Description	Program Default Value
x, y	Starting coordinates of the moving source (m)	
t_o	Start time of vehicle (s)	
t'	Vehicle travel time (s)	0
ITYPE	Code specifying the type of vehicle	1
N'	The number of wheels on the vehicle or a best estimate for track vehicles	4
ISOLTP	Code specifying soil type	4
S_c	Silt content (percent of the weight of particles in the surface soil which have diameters less than 75 μm)	25.7
θ_v	Direction of travel with respect to grid north (degrees)	0
V_t	Vehicle velocity ($m\ s^{-1}$)	13.41
V_s	Settling velocity of the soil particles ($m\ s^{-1}$)	0
W_p	Number of days during the year with .025 cm (.01 in) or more precipitation	0
σ_o	Standard deviation of the spherical distribution of the cloud at the source (m)	0.93

TABLE 3-11

SILT CONTENT OF SURFACE SOILS

Soil Category	S_c Silt Concent (%)	Description
1	0	Rock
2	95	Clay or dry cohesive soils
3	18	Dry sandy soils
4	25.7	Loam, sandy soil and frozen ground
5	12.0	Soft rock
6	0	Wet sand, wet loam or ice
7	0	Wet cohesive soils (not saturated) and snow
10	-	User entered soil type

Hendriks (1977) and Miller (1979). The emission rate depends on the number of wheels per vehicle. A table of the vehicle types and their number of wheels is given in Table 3-12. The number of wheels representing tracked vehicles were arbitrarily assigned. The dispersion model for moving vehicles is described in Section 2.3.3

3.4 MUZZLE BLAST SOURCE CHARACTERISTICS

The muzzle blast of a cannon or mortar can generate both dust and combustion product particles which act as obscurants on a battlefield. Particulates are generated from the combustion products of the propellant in the gun after the gases have emerged from the gun tube. This propellant cloud is largely water vapor formed by the oxidation of hydrogen in the cloud, but also contains smaller amounts of carbon particles as well as a few other gases. A dust cloud is also generated by the interaction of the muzzle blast shock wave with the ground. The ground is compressed and, as the rarefaction portion of the shock wave passes, the surface layer of dust is propelled into the air. The propellant cloud is formed almost instantly whereas the dust cloud requires about 6 seconds to form and reach the same height as the muzzle. The propellant and dust clouds combine very quickly and therefore we treat them as one cloud. Only the particulate yield of carbon from the propellant combustion will be considered in this model. For the visible wavelengths this is a fairly good approximation, but there is mounting evidence (Stuebing, et al.) that transmission in the infrared at 10.6 μm is affected to some extent by the NH_3 present in the cloud. This section describes the source model used to develop parameters describing the dust and smoke cloud formed by the muzzle blast of a cannon. The inputs needed for the source model are described in Table 3-13. However, only the location of the gun and height above ground of the muzzle, the time of firing, a weapon code specifying the type of gun being fired and a code specifying the soil type around the gun are required unless the

TABLE 3-12

VEHICLE TYPES MODELED IN THE VEHICLE MOVEMENT PRODUCED DUST SOURCE MODEL

Vehicle Code	Vehicle Description	Number of Wheels N'
1	1/4 ton Jeep	4
2	5/4 ton M880	4
3	2 1/2 ton truck	10
4	Dump truck	10
5	5 ton tractor	10
6	5 ton tractor with trailer	18
7	APC	16*
8	Tank	18*
20	User entered vehicle type	-

*Estimated values for track vehicles.

TABLE 3-13

SOURCE INPUTS FOR THE MUZZLE BLAST SOURCE MODEL

Parameter Symbol	Parameter Definition	Program Default Value
x, y	Source coordinates (m)	
h	Height of muzzle above ground (m)	2
t_o	Time of firing (s)	
ITYPE	Code specifying the weapon type	5
D_f	Muzzle blast flash diameter (m)	
σ_{xo}	Standard deviation of the alongwind concentration distribution at the source (m)	8.07
σ_{yo}	Standard deviation of the crosswind concentration distribution at the source (m)	2.03
σ_{zo}	Standard deviation of the vertical concentration distribution at the source (m)	2.03
M_c	Mass of combustion products formed in the combustion of the propellant charge in the gun (g)	
M_s	Mass of soil propelled into the air (g)	
ISOLTP	Code specifying the type of soil at the weapon location	4
ρ_s	Soil density ($g\ cm^{-3}$)	1.5

user wishes to use a type of weapon not considered in the input selection list.

The amount of smoke particulates and dust in the cloud can be determined from the expression

$$M_o = M_s + M_c \tag{3-17}$$

where M_s is the mass of soil propelled into the air and M_c is the mass of carbon particulates formed from the combustion products of the propellant in the gun. The mass of dust propelled into the air was calculated by using the assumption made by Gibson (1978) that the area of soil affected by the muzzle blast is determined by the area of ground intercepted by a spherical shock wave emanating from the muzzle and striking the ground at an incidence angle of 60 degrees. Gibson also assumes that only 10% of the first millimeter of soil in this area becomes airborne. Thus, the mass of soil injected into air by the shock wave is given by

$$M_s = 0.0001 \rho_g \left(\frac{h}{\tan(60^o)} \right)^2 \tag{3-18}$$

where ρ_g is the soil density (g m^{-3}) and h is the height of the muzzle bore hole above the ground (m). The soil density is given in Table 3-8 as a function of soil type.

The particulate mass M_c in Equation (3-17) is determined by assuming that the mass of carbon in the propellant is converted to particles and the rest of the constituents are emitted as vapors that do not coalesce on any particulates after emission. The grams of carbon formed in combustion of TNT (according to Thompson, 1979) is 328 grams of carbon per kilogram of TNT. The particulate mass for the different types of weapons was obtained by determining the amount of propellant

used as an average load in the gun from the U. S. Army Field Mannual FM9-13. The mass of propellants containing nitrocellulose or nitroglycerin was converted to equivalent mass of TNT using a scaling factor determined by comparing the energy available from the different types of propellant powder to that of TNT. A table of mass of carbon particulates by weapon type is given in Table 3-14. The size of the initial cloud can be determined from the dimension of the flash diameter D_f, according to Gibson (1978), by the following relationships:

$$\sigma_{yo} = \frac{1}{6} D_f$$

$$\sigma_{zo} = \sigma_{yo} \qquad (3\text{-}19)$$

$$\sigma_{xo} = 3\sigma_{yo}$$

If the dimensions of the flash in length L_f and width W_f are known, then the standard deviation of the concentration at the source can be determined from

$$\sigma_{yo} = \frac{1}{6} W_f$$

$$\sigma_{zo} = \sigma_{yo} \qquad (3\text{-}20)$$

$$\sigma_{xo} = \frac{1}{6} L_f$$

and these values can be input to the program instead of D_f.

3.5 BURNING BRUSH/VEGETATION SOURCE CHARACTERISTICS

Brush or vegetation can be ignited by explosions or incendiary munitions and the subsequent smoke produced in the combustion can sub-

TABLE 3-14

ESTIMATED PARTICULATE MASS PRODUCED FROM COMBUSTION OF PROPELLANT IN A WEAPON

Weapon Type	Description	Mass of Carbon Particulate, M_c (g)
1	81 mm mortar	14.8
2	4.2 in mortar	47.9
3	120 mm tankgun	1391
4	105 mm tank HEP	298.7
5	155 mm artillery	1468
6	8 in artillery	3080
20	User entered type	-

stantially degrade visibility. The particulates emitted from burning vegetation depend at a minimum on the amount and kind of vegetation present, the moisture content, local meteorological conditions and the availability of oxygen. Table 3-15 gives the inputs used in the AMSORB burning vegetation source model. However, only the location of the centroid of the burning brush, the time combustion starts, a code specifying the type of regional vegetation involved, and the area involved in the burning need to be specified for the model since the program will automatically assign values to other required parameters from data tables contained in the program.

The amount of particulate matter emitted by the fire over its entire burn time is given approximately by the following relationship used by the Environmental Protection Agency (Vatavuk and Yamate, 1975):

$$M_o = P \cdot \ell_f \cdot A \tag{3-22}$$

where A is the area of the fire, ℓ_f is the fuel loading of vegetation and P is the particulate yield. The particulate yield for most fires varies between 10 and 90 g/kg of fuel consumed according to Comez, et al. (1979) and Eccleston, et al. (1974). Thus, an average value for brush and grass fires of

$$P = 18 \text{ g/kg of fuel} \tag{3-23}$$

is used in the computer program. The average fuel loadings by regions of the country are presented in Table 3-16 and are the same as those used by Vatavuk and Yamate. The effective heat release rate Q_c' (cal s^{-1}) emitted by the fire is given as

$$Q_c' = H_E \cdot K_B \cdot \ell_f/60 \tag{3-24}$$

TABLE 3-15

SOURCE INPUTS FOR THE BURNING BRUSH/VEGETATION SOURCE MODEL

Parameter Symbol	Parameter Description	Program Default Value
x, y	Source coordinates of the centroid of the burning vegetation (m)	
t_o	Time combustion starts (s)	
MYF	Yield fraction indicating the amount of combustion mass which remains airborne as obscuring particles	1.0
t_B	Total burn time (min)	
A,B,C,D	Coefficients of the source release rate expression	1.0,0,0,0
σ_{xo}	Standard deviation of the alongwind concentration distribution at the source (m)	2.89
σ_{yo}	Standard deviation of the crosswind concentration distribution at the source (m)	2.89
σ_{zo}	Standard deviation of the vertical concentration distribution at the source (m)	2.89
ITYPRG	Code specifying the type of region and indicating the type of vegetation present	3
l_f	Estimated fuel loading (kg m^{-2})	6.7
$\bar{l}_f$	Average fuel loading corresponding to the burn rate $\bar{R}_B$ (kg m^{-2})	0.8
$\bar{R}_B$	Burn rate (m^2 min^{-1})	140
P	Pollutant yield from the fire/grams of particulate emitted per kilogram of fuel consumed	18
H_E	Heat released by the combusion of the particular fuel (cal kg^{-1})	3.9×10^6
A_T	Area of the burning vegetation for total burn (m^2)	100

TABLE 3-16

ESTIMATED AVERAGE FUEL LOADINGS
(after Vatavuk and Yamate, 19/5)

Code	Area or Region	Estimated Average Fuel Loading, ℓ_f ($kg\ m^{-2}$)
1	Rocky Mountain Group	8.3
2	Region 1: Northern	13.5
3	Region 2: Rocky Mountain	6.7
4	Region 3: Southwestern	2.2
5	Region 4: Intermountain	4.0
6	Pacific Group	4.3
7	Region 5: California	4.0
8	Region 6: Pacific Northwest	13.5
9	Region 10: Alaska	3.6
10	Coastal	13.5
11	Interior	2.5
12	Southern Group	2.0
13	Region 8: Southern	2.0
14	Eastern Group	2.5
15	North Central Group	2.5
16	Region 9: Conifers	2.2
17	Hardwoods	2.7
20	User entered type	-

where H_E is the heat emitted (cal kg^{-1}), R_B is the burn rate ($m^2 min^{-1}$), ℓ_f is the average fuel loading of the burning vegetation and the factor of 60 is included to convert to seconds. If the heat released is not input by the program user, the program uses a standard value for pine wood and dry grass given by Gomez, et al. (1979) as

$$H_E = 3.9 \times 10^6 \text{ cal/kg of fuel consumed} \tag{3-25}$$

The burn rate R_B in Equation (3-24) is determined from

$$R_B = \bar{R}_B \frac{\bar{\ell}_f}{\ell_f} \tag{3-26}$$

where $\bar{\ell}_f$ is an average fuel loading for the vegetation and $\bar{R}_B$ is the measured average burn rate for an average fuel loading $\bar{\ell}_f$. The AMSORB program uses values of $140 m^2$ min^{-1} and 0.8 kg m^{-2} respectively for $\bar{R}_B$ and $\bar{\ell}_f$ based on measurements reported by Daniels, et al., (1975). The burn time in minutes can be determined from the expression

$$t_B = A_T/R_B \tag{3-27}$$

where A_T is the total area of vegetation involved in the combustion. When the standard deviations of the alongwind, crosswind and vertical concentration distributions at the source are not input by the user, the program determines those values according to the following relationship

$$\sigma_{xo} = \sigma_{yo} = \sigma_{zo} = \sqrt{(A_T/12)} \tag{3-28}$$

assuming that a uniform distribution of vegetation exists over the entire burn area.

3.6 BURNING BUILDING SOURCE CHARACTERISTICS

The AMSORB program uses an approach to define source characteristics for burning buildings similar to the approach used for burning vegetation described in Section 3.5 above. Table 3-17 describes the inputs used in the burning building source model. However, only the location of the centroid of the burning building, the time combustion starts, the building height, the area of the building and the mass of combustibles involved need be input since the program will automatically assign values to the other parameters based on the data tables present in the program.

The amount of particulate matter emitted by the fire over its entire burn time is calculated using Equation (3-22). In this application for burning buildings, A_T is the area of the building, ℓ_f is the fuel loading in the building and P is the particulate yield. The effective heat release rate Q_c' in calories per second emitted by the fire is found using Equation (3-24). If the heat released is not input, the program uses the value for pine wood and dry grass (see Equation (3-25)). The burn rate used to determine the heat release rate as well as the burn time is given by Equation (3-26). The burn time for the building is given by Equation (3-27). The standard deviations of the alongwind, crosswind and vertical concentration distributions at the source can be input. If they are not, the program defines the alongwind and crosswind standard deviation from the expression

$$\sigma_{xo} = \sigma_{yo} = \left(\frac{A_T}{3\pi}\right)^{1/2} \qquad (3\text{-}29)$$

where A_T is the building area. The vertical standard deviation at the source for a building of height h_b is given by

$$\sigma_{zo} = \frac{2h_B}{\sqrt{12}} \qquad (3\text{-}30)$$

TABLE 3-17

SOURCE INPUTS FOR THE BURNING BUILDING SOURCE MODEL

Parameter Symbol	Parameter Description	Program Default Value
x, y	Source coordinates of the centroid of the building (m)	
MYF	Yield fraction indicating the amount of combustion mass which remains airborne as obscuring particles	1.0
h_B	Building height (m)	2.0
M_o	Mass of combustible material in the building (kg)	
A, B, C, D	Coefficients of the source release rate expression	1.0, 0, 0, 0
σ_{xo}	Standard deviation of the alongwind concentration distribution at the source (m)	0.631
σ_{yo}	Standard deviation of the crosswind concentration distribution at the source (m)	0.631
σ_{zo}	Standard deviation of the vertical concentration distribuation at the source (m)	1.15
l_f	Estimated fuel loading in the building ($kg\ m^{-2}$)	20.0
$\bar{l}_f$	Average fuel loading for the burn rate $\bar{R}_B$ ($kg\ m^{-2}$)	0.8
$\bar{R}_B$	Burn rate for the average fuel loading specified by $\bar{l}_f$ ($m^2\ min^{-1}$)	140
P	Pollutant yield from the fire (grams of particulate emitted per kilogram of fuel consumed	18.0
H_g	Heat released by the combustion of the particular fuel ($cal\ kg^{-1}$)	3.9×10^6
A_T	Area of the burning building (m^2)	3.75

3.7 SOURCE CHARACTERISTICS FOR BURNING VEHICLE

Table 3-18 lists the general source inputs required for a burning vehicle as well as the default parameter values entered in the computer program. The default values are based on data for a burning automobile obtained by Gomez, et al, (1979). The inputs in Table 3-18 are those required by the quasi-continuous source model because it is assumed that the total vehicle burn time is on the order of 10 minutes or longer. If the program user has source input parameter values for a burning vehicle that are more appropriate than the default values, they can be entered in the program and used in the diffusion model calculations.

The default values listed in Table 3-18 reflect the details of the data obtained by Gomez, et al. (1979) for a burning automobile. For example, the fraction MYF has been set equal to 1.0 because only the total airborne mass of particulates was measured. Also, the default values assigned to the coefficients of the expressions for the source release rate (A=1.0; B, C, D=0) reflect the assumption of a constant release rate for the total burn time of 45 minutes. The default value assigned to the standard deviations of the concentration distributions of the source were all set equal to 0.866 meters under the assumption that the horizontal and vertical cloud dimensions were 3 meters.

3.8 USER-SPECIFIED SOURCE MODELS AND INPUTS

Provision has been made in the SORDAT routine of AMSORB for user-specified source models which can be applied to both instantaneous and quasi-continuous sources. Table 3-19 lists the requisite source parameters which must be input by the user.

TABLE 3-18

SOURCE INPUTS FOR BURNING VEHICLE

Parameter Symbol	Parameter Definition	Program Default Value
x, y	Source coordinates (m)	
t_o	Time combustion starts (s)	
M_o	Total mass of particulates emitted by the burning vehicle (g)	900
MYF	Fraction of M_o which becomes airborne	1.0
t_R	Total burn time (min)	45
A,B,C,D	Coefficients of the source release rate expression	1.0, 0, 0, 0
xo	Standard deviation of the along-wind concentration distribution at the source (m)	0.866
yo	Standard deviation of the cross-wind concentration distribution at the source (m)	0.866
zo	Standard deviation of the vertical concentration distribution at the source (m)	0.866
Q'_c	Effective rate of heat release from the burning vehicle (cal s^{-1})	667

TABLE 3-19

INPUTS FOR USER SPECIFIED SOURCE MODELS

Parameter Symbol	Parameter Description
x, y, z	Source coordinates (m)
M_o	Total mass before ignition (g)
MYF	Source yield fraction
t_o	Initial source release time (s)
t_B	Total burn time (min)
A, B, C, D	Coefficients of the source release rate expression
σ_{xo}	Standard deviation of the alongwind concentration distribution at the source (m)
σ_{yo}	Standard deviation of the crosswind concentration distribution at the source (m)
σ_{zo}	Standard deviation of the vertical concentration distribution at the source (m)
Q'_I	Total heat released from instantaneous sources (cal)
Q'_c	Effective rate of heat release from quasi-continuous sources (cal s^{-1})
TYPSMK	Code identifying type of obscurant (1, 2, 3)

Obscuration calculations require attenuation coefficients and Mie scattering coefficients which depend on the type of obscurant. The user must therefore enter a parameter value for the type of obscurant, denoted by the code identification TYPSMK, in the program. A value of 1 for TYPSMK refers to HC smoke and a value of 2 refers to WP smoke. The program data base contains values of attenuation coefficients, Mie scattering fractions and the yield fractions YF for each of these obscurants. A value of 3 entered for TYPSMK specifies a user-specified obscurant and the user must input appropriate attenuation coefficients and Mie scattering fractions. Because no relative humidity yield fractions can be entered in the program for user-specified obscurants, the program assumes that the yield factor YF, accounting for the effects of moisture, is unity.

SECTION 4
AMSORB MODEL ROUTINES

The computer program AMSORB consists of a number of separate routines, each of which contributes directly or indirectly to a battlefield environment solution. This section describes these routines and defines the basic model parameters contained in the routines. Section 4.1 describes the Mixing-Layer Analysis Routine (MIXLYR) that utilizes rawinsonde, USAF-GWC wind and temperature data, and surface meteorological data contained in mass storage data base files to calculate initialization parameters required by the Mesoscale Wind-Field Model. The Battlefield Source Characteristics Routine (SORDAT), described in Section 4.2, processes user-provided battlefield source input data to generate a data base file containing source locations and source characteristics. The input parameters required by the various dispersion models are discussed in Section 4.3. The dispersion routines use surface meteorological data and mixing-layer parameters provided by the Mesoscale Wind-Field Model as direct inputs, and source data from user-provided inputs. Section 4.4 discusses the Obscuration Model and required model input parameters. The Battlefield Environment Routine (BEC) described in Secton 4.5 uses the battlefield source location and characteristics data base file generated by SORDAT and meteorological parameters generated by the Mesoscale Wind-Field Model.

4.1 MIXING-LAYER ANALYSIS ROUTINE

The Mixing-Layer Analysis Routine employs a relatively simple approach in utilizing the various types of data available from the AMSORB mass storage data base to calculate initialization parameters for the Mesoscale Wind-Field Model. The decision to use a simple approach was made so that the effects of logic decisions on the derived parameters

could be easily traced and analyzed. The Mixing-Layer Analysis Routine is thus designed to perform a modified "single-station analysis" rather than a more complex analysis of the pressure, wind and temperature fields over the entire region of interest. It should also be noted that some of the logic decisions made in accepting, rejecting and analyzing the data are somewhat arbitrary. Where possible, we have attempted to study the effects of the various decision processes. However, until the routine is used to predict dosage and concentration fields under a wide variety of meteorological conditions, the full implications of many of the decision processes cannot be determined.

Key features of the Mixing-Layer Analysis Routine (MIXLYR) are shown in the schematic logic diagram of Figure 4-1. The key features are:

- Rawinsonde data from the closest station with a radius of less than 100 kilometers from the release point and less than three-hours old at the time of request are used without modification to obtain estimates of the input parameters to the Mesoscale Wind-Field Model

- Rawinsonde data measured at the closest station less than 100 kilometers from the release point, greater than three-hours old and less than twelve-hours old are subject to modification using CWC-predicted and surface winds and temperatures

- Climatological estimates of mixing-layer depths and surface wind speeds are used as inputs if all rawinsonde data are more than twelve- hours old or if there are no stations within a 100 kilometer radius of the release point

FIGURE 4-1. Schematic diagram illustrating procedures for obtaining inputs to the Mesoscale Wind-field Model.

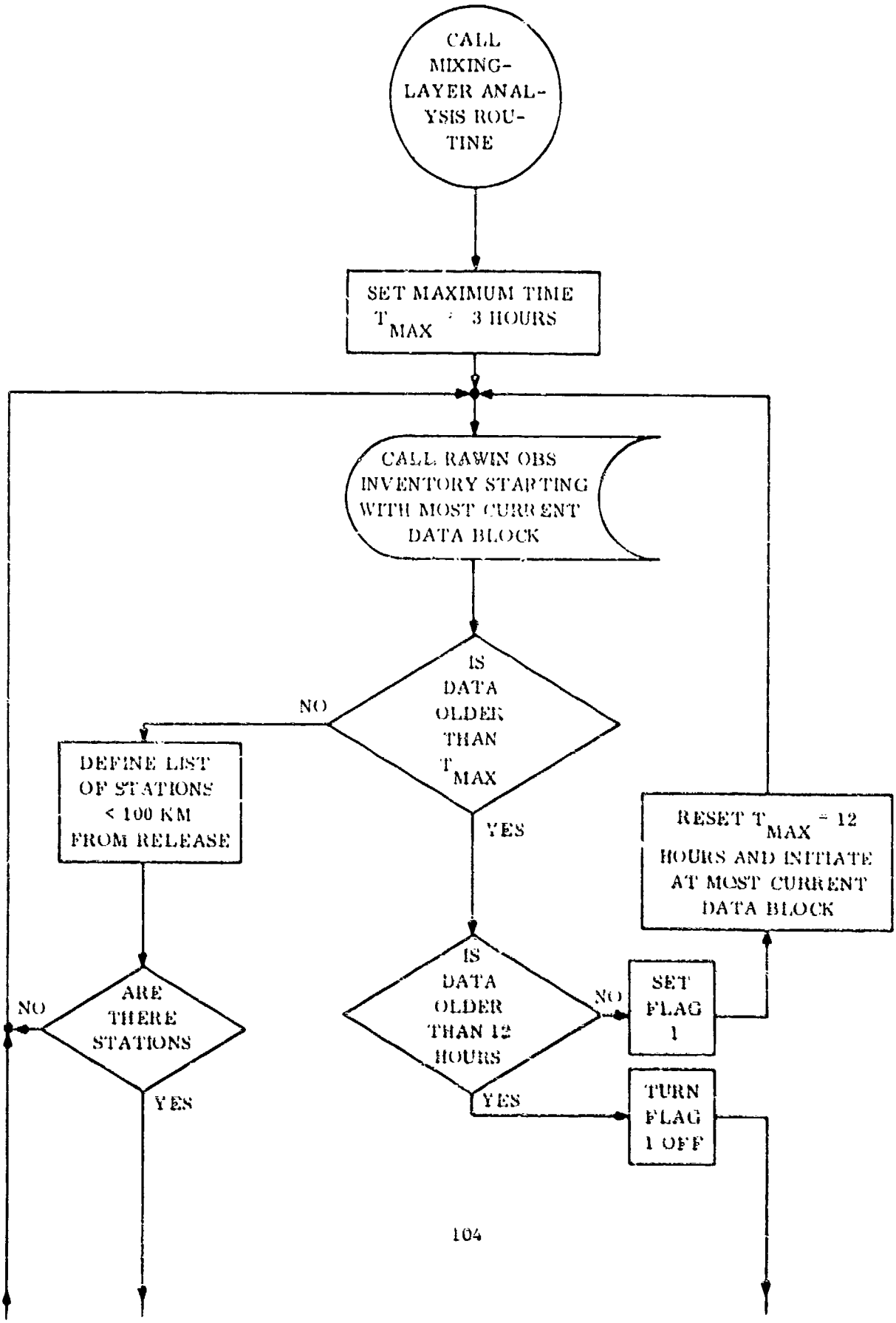

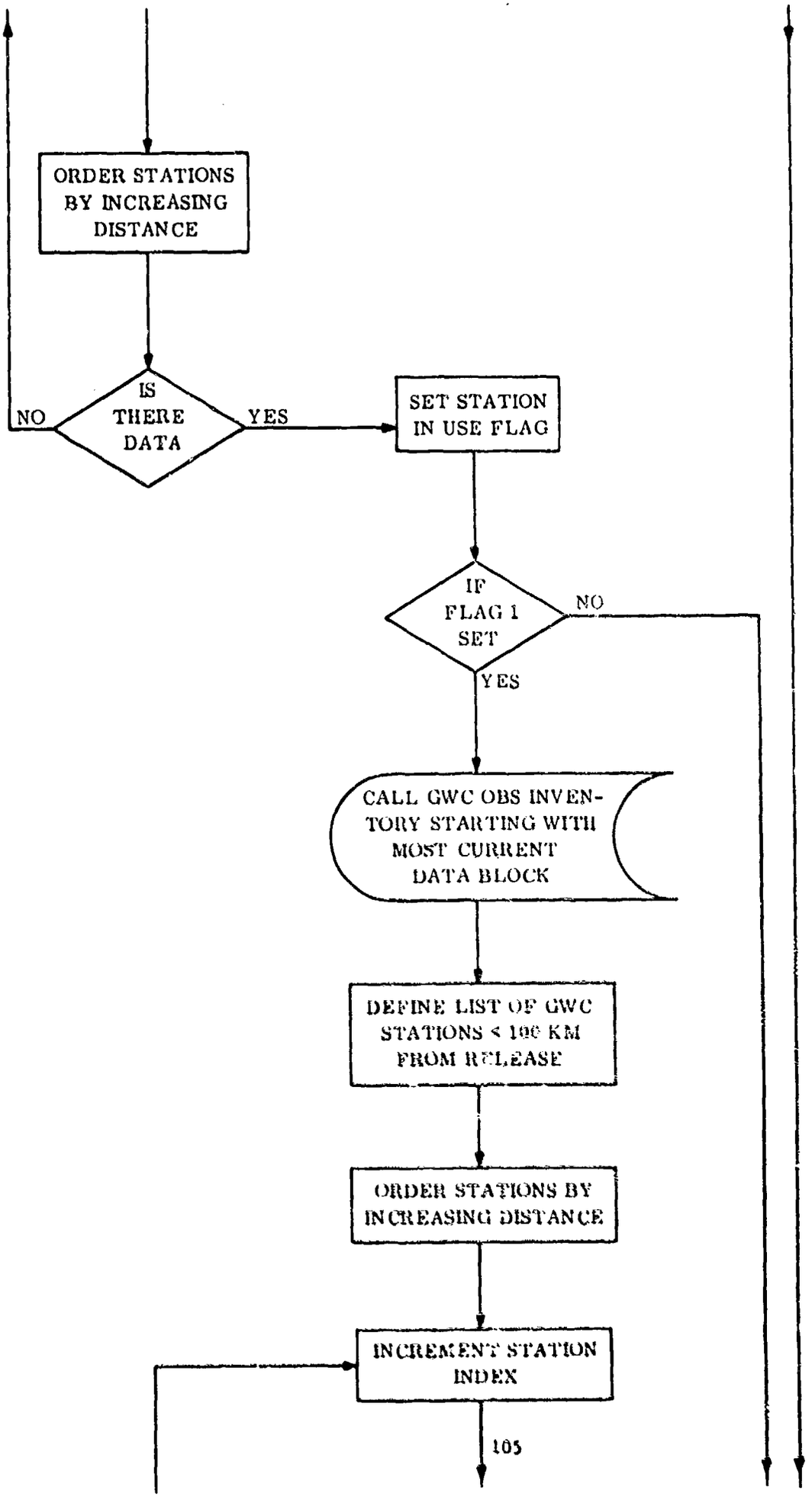
ORDER STATIONS BY INCREASING DISTANCE
IS THERE DATA
NO
YES
SET STATION IN USE FLAG
IF FLAG 1 SET
NO
YES
CALL GWC OBS INVENTORY STARTING WITH MOST CURRENT DATA BLOCK
DEFINE LIST OF GWC STATIONS < 100 KM FROM RELEASE
ORDER STATIONS BY INCREASING DISTANCE
INCREMENT STATION INDEX

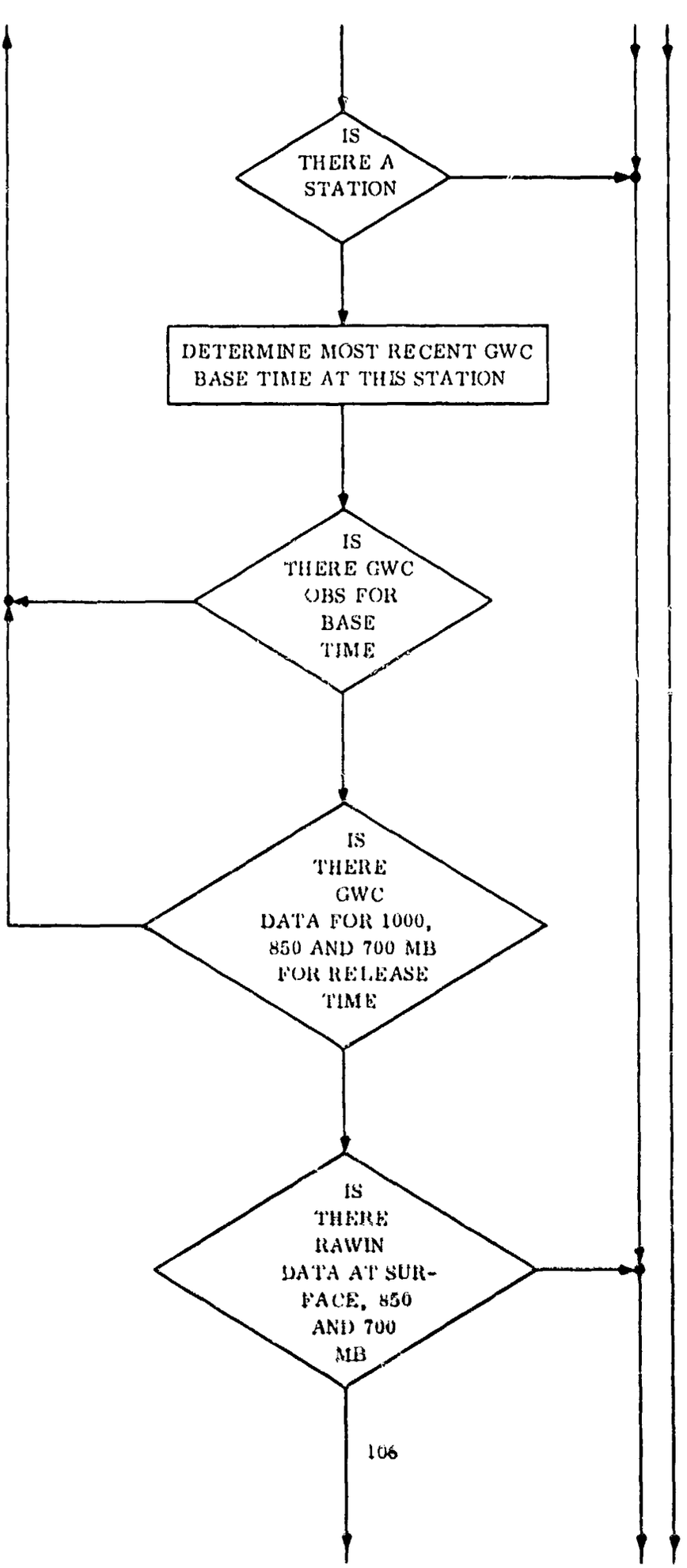
IS THERE A STATION
DETERMINE MOST RECENT GWC BASE TIME AT THIS STATION
IS THERE GWC OBS FOR BASE TIME
IS THERE GWC DATA FOR 1000, 850 AND 700 MB FOR RELEASE TIME
IS THERE RAWIN DATA AT SURFACE, 850 AND 700 MB

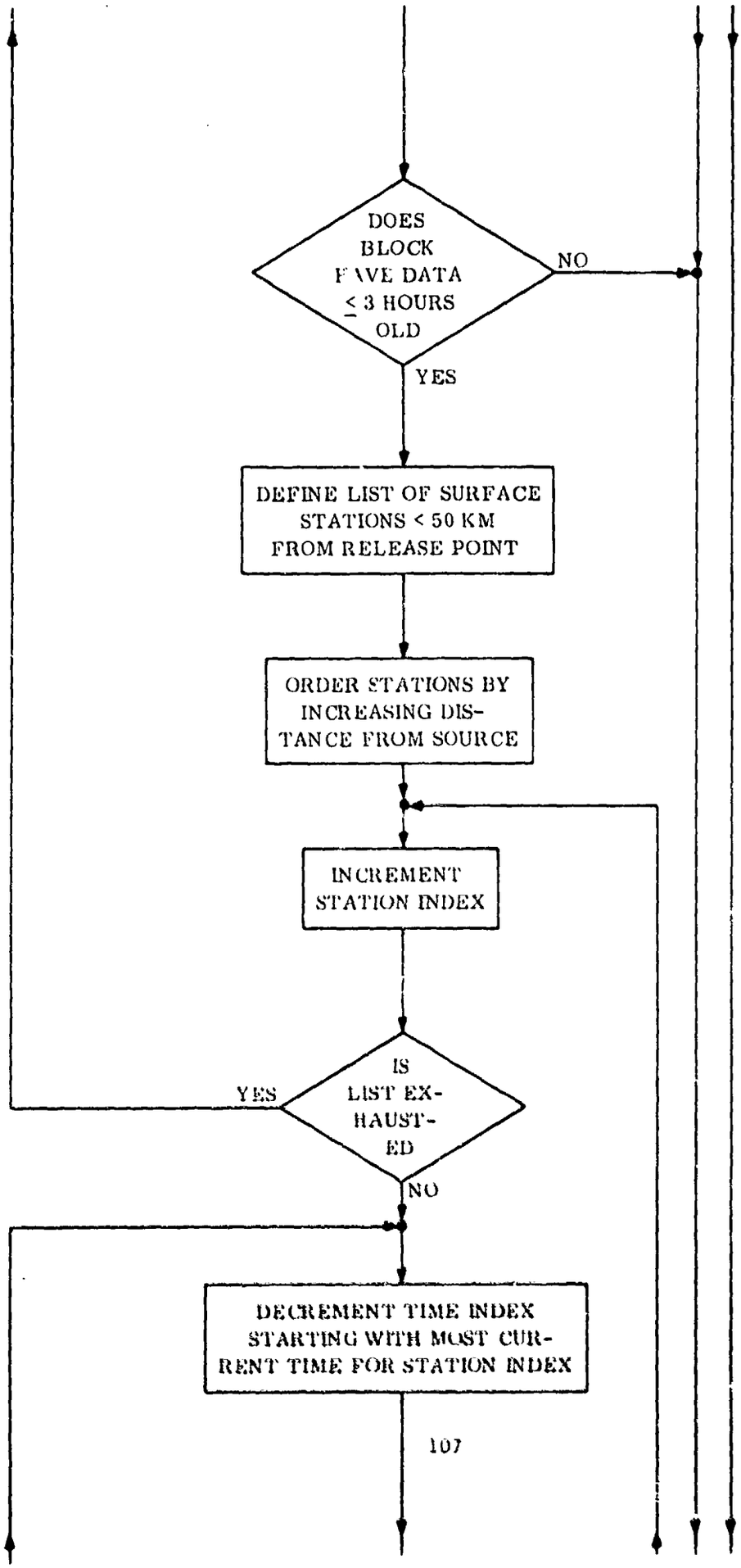
DOES BLOCK HAVE DATA ≤ 3 HOURS OLD
NO
YES
DEFINE LIST OF SURFACE STATIONS < 50 KM FROM RELEASE POINT
ORDER STATIONS BY INCREASING DISTANCE FROM SOURCE
INCREMENT STATION INDEX
IS LIST EXHAUSTED
YES
NO
DECREMENT TIME INDEX STARTING WITH MOST CURRENT TIME FOR STATION INDEX

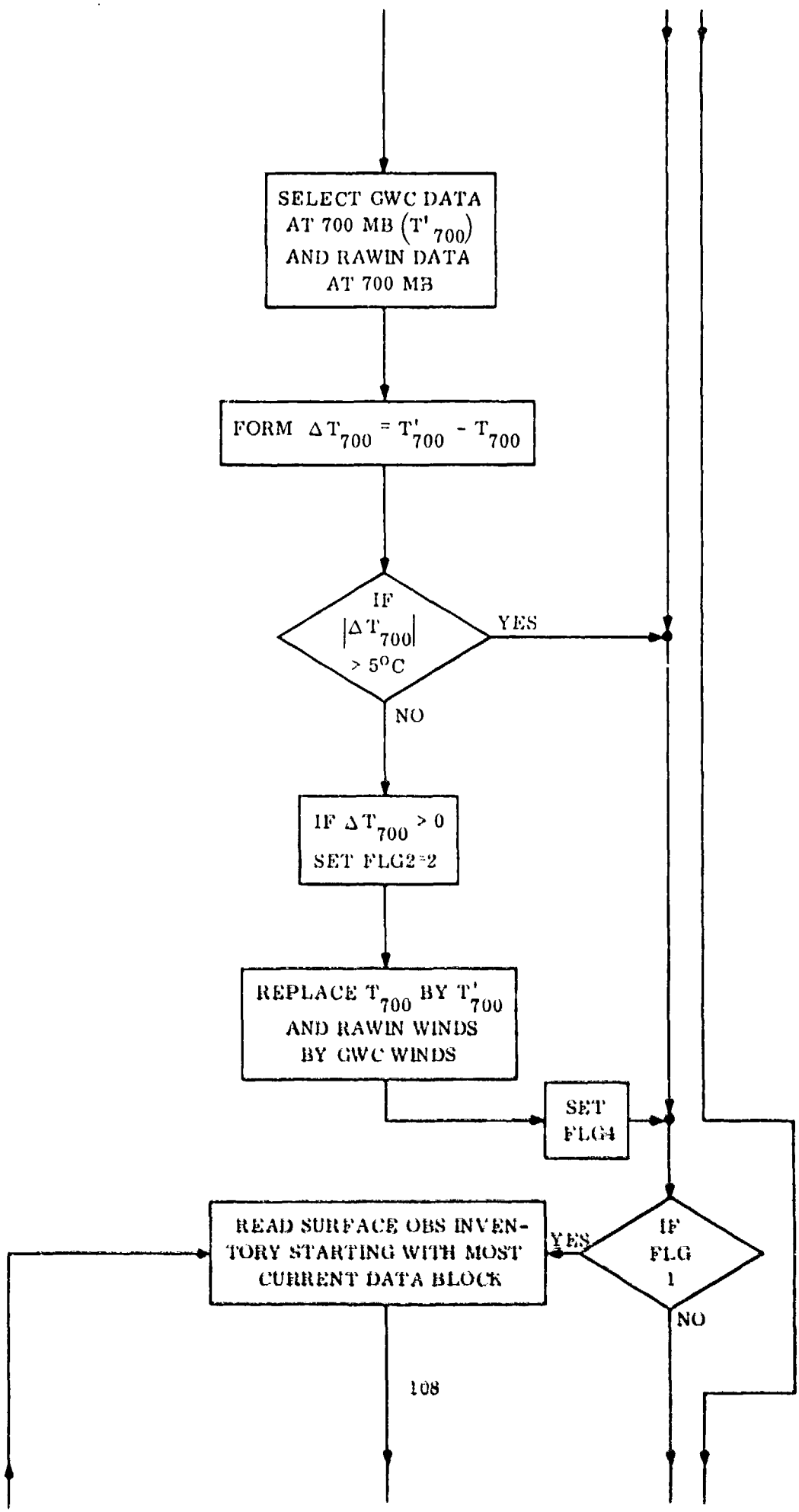
SELECT GWC DATA AT 700 MB (T'_{700}) AND RAWIN DATA AT 700 MB
FORM $\Delta T_{700} = T'_{700} - T_{700}$
IF $|\Delta T_{700}| > 5^{o}C$
YES
NO
IF $\Delta T_{700} > 0$ SET FLG2=2
REPLACE T_{700} BY T'_{700} AND RAWIN WINDS BY GWC WINDS
SET FLG4
IF FLG 1
YES
NO
READ SURFACE OBS INVENTORY STARTING WITH MOST CURRENT DATA BLOCK

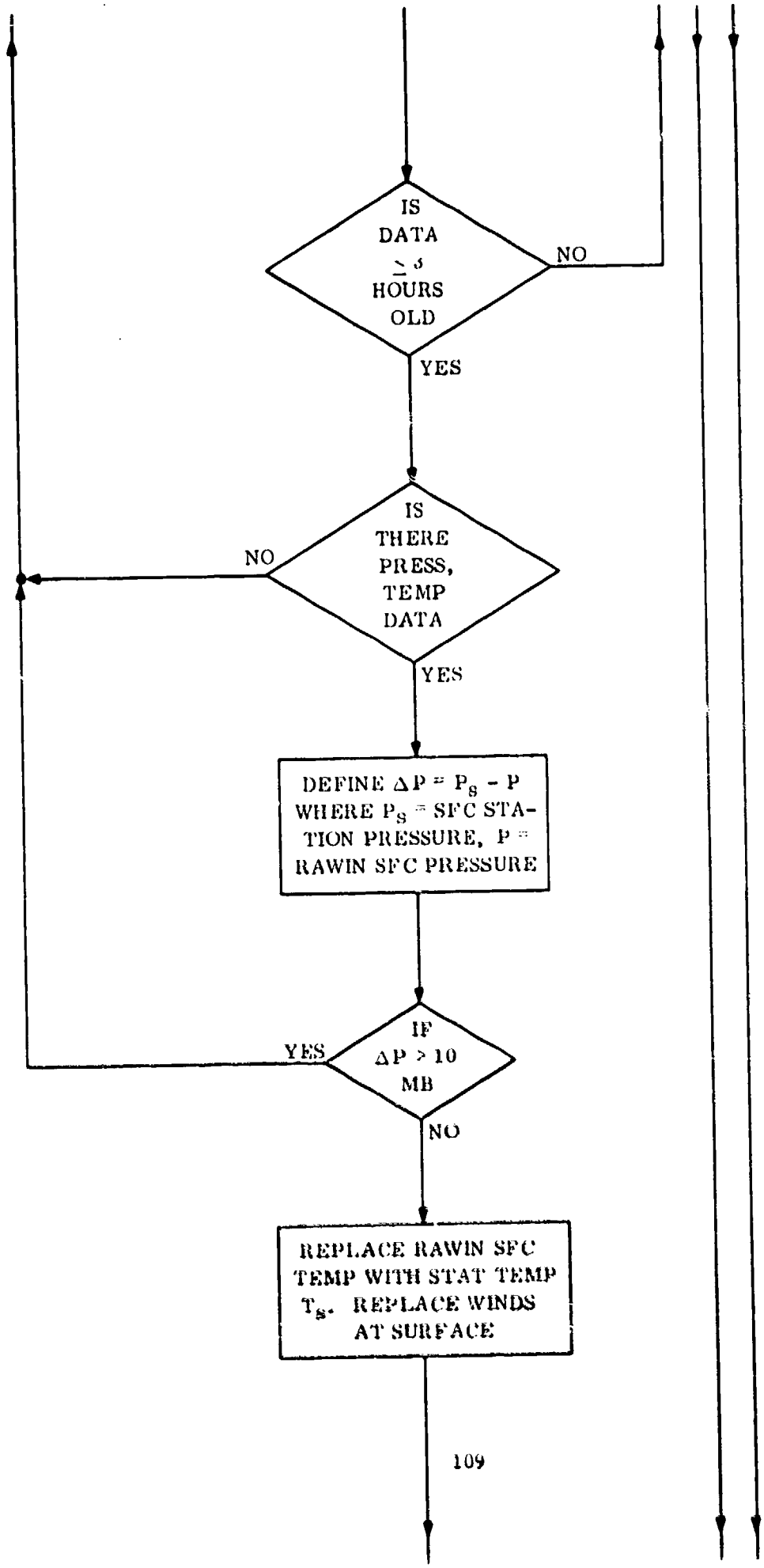
IS DATA ≥ 3 HOURS OLD
NO
YES
IS THERE PRESS, TEMP DATA
NO
YES
DEFINE ΔP = P_S - P WHERE P_S = SFC STATION PRESSURE, P = RAWIN SFC PRESSURE
IF ΔP > 10 MB
YES
NO
REPLACE RAWIN SFC TEMP WITH STAT TEMP T_s. REPLACE WINDS AT SURFACE

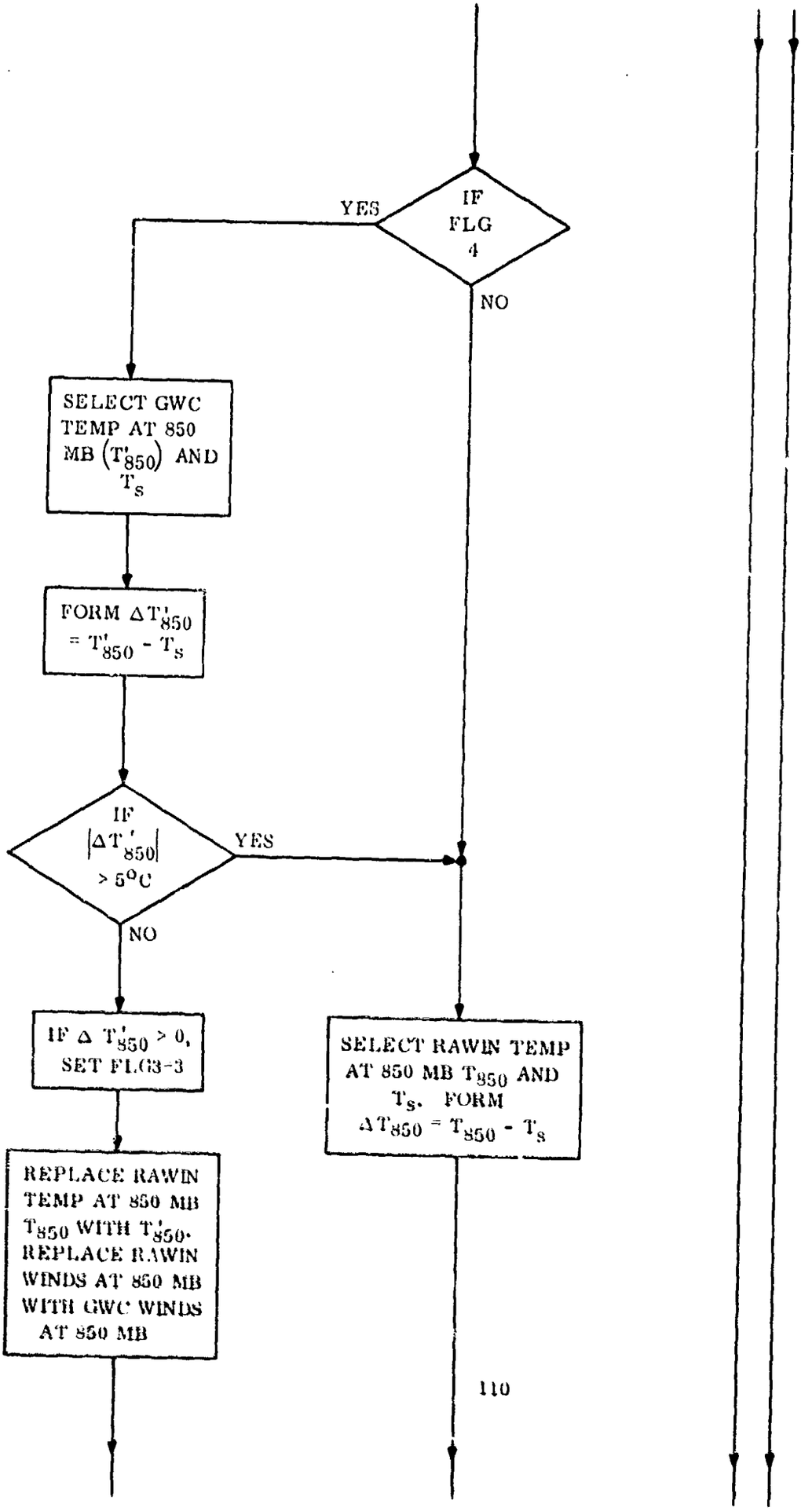
IF FLG 4
YES
NO
SELECT GWC TEMP AT 850 MB (T'_{850}) AND T_s
FORM $\Delta T'_{850} = T'_{850} - T_s$
IF $|\Delta T'_{850}| > 5^oC$
YES
NO
IF $\Delta T'_{850} > 0$, SET FLG3-3
REPLACE RAWIN TEMP AT 850 MB T_{850} WITH T'_{850}. REPLACE RAWIN WINDS AT 850 MB WITH GWC WINDS AT 850 MB
SELECT RAWIN TEMP AT 850 MB T_{850} AND T_s. FORM $\Delta T_{850} = T_{850} - T_s$

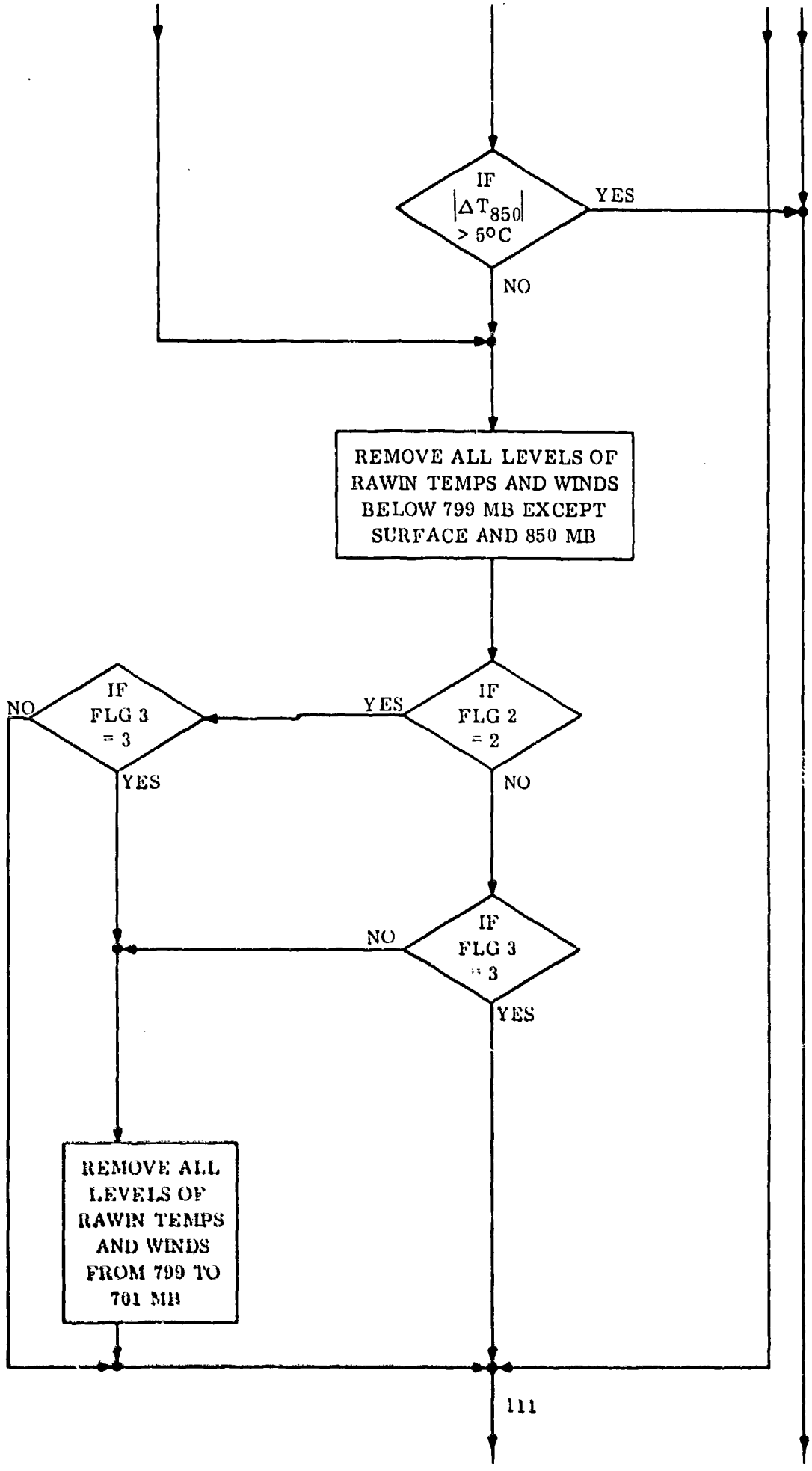
IF
$|\Delta T_{850}|$
> 5°C
YES
NO
REMOVE ALL LEVELS OF RAWIN TEMPS AND WINDS BELOW 799 MB EXCEPT SURFACE AND 850 MB
IF
FLG 2
= 2
YES
NO
IF
FLG 3
= 3
NO
YES
IF
FLG 3
= 3
NO
YES
REMOVE ALL LEVELS OF RAWIN TEMPS AND WINDS FROM 799 TO 701 MB

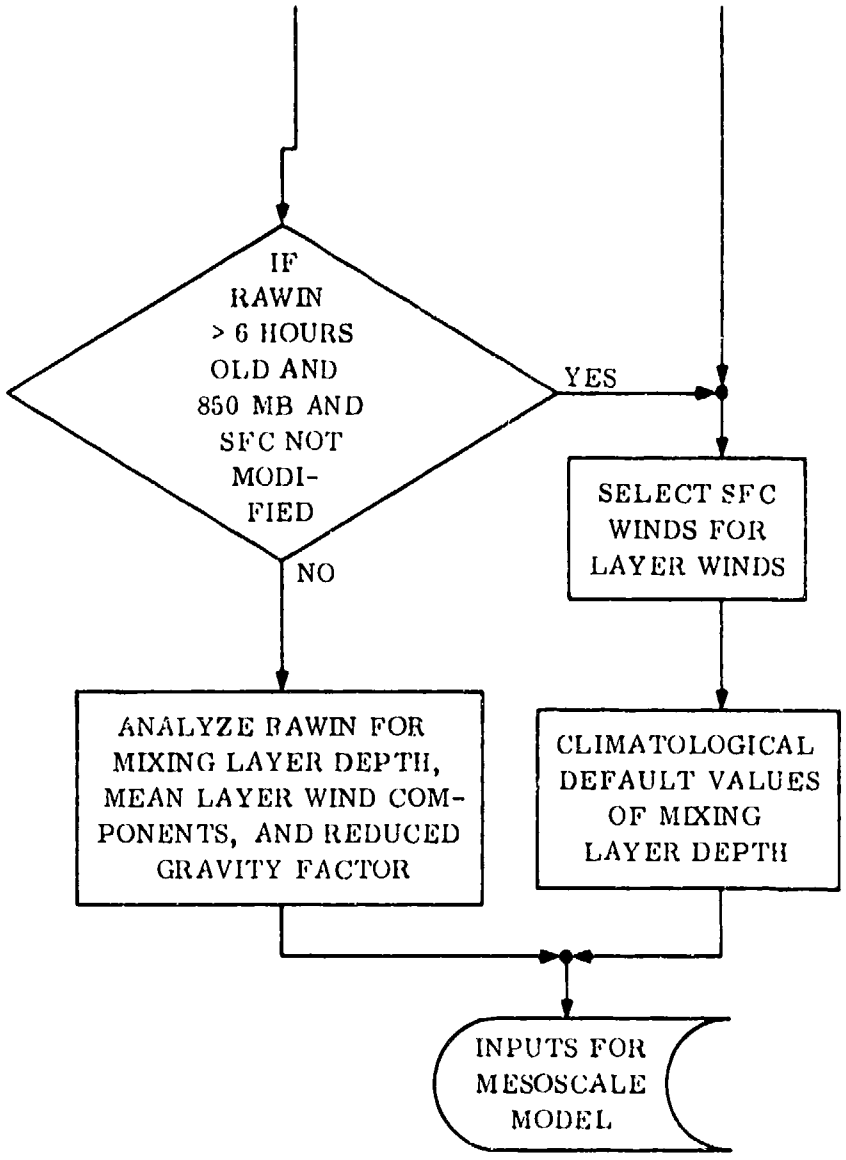
IF
RAWIN
> 6 HOURS
OLD AND
850 MB AND
SFC NOT
MODI-
FIED
YES
NO
SELECT SFC
WINDS FOR
LAYER WINDS
ANALYZE RAWIN FOR
MIXING LAYER DEPTH,
MEAN LAYER WIND COM-
PONENTS, AND REDUCED
GRAVITY FACTOR
CLIMATOLOGICAL
DEFAULT VALUES
OF MIXING
LAYER DEPTH
INPUTS FOR
MESOSCALE
MODEL

- Climatological estimates are also used if the rawinsonde data are more than six-hours old and the rawinsonde surface temperature and 850-millibar temperatures have not been modified because GWC and surface data are either unavailable or inadequate

- GWC data are used to modify the rawinsonde temperatures and winds at the 700- and 850-millibar levels; rawinsonde temperatures and winds at the 700-millibar level are replaced by the GWC-predicted temperature for that level if the GWC-predicted temperature for the hour of interest is within 5 degrees Celsius; rawinsonde temperatures and winds at 850 millibars are replaced if the temperature from the reporting surface station nearest the time and point of release is within 5 degrees Celsius of the GWC-predicted temperature at the 850 millibar level for the hours of interest

- Surface temperature and wind data from the closest station less than 50 kilometers from the release point, less than three-hours old, and with a surface pressure from the rawinsonde observation, are used to modify the surface rawinsonde observation when it is more than three-hours old

- Surface wind speeds from the closest station to the point of release are used as default values for the mean-layer wind speed if the rawinsonde data are not analyzed

Climatological estimates of the mixing-layer depth shown in Table 4-1 are used as default values where the rawinsonde data are not available or are not analyzed. These estimates of the median mixing depths as a function of month and time-of-day are based on the work of Norton and

TABLE 4-1

CLIMATOLOGICAL ESTIMATES OF THE MEDIAN SURFACE MIXING DEPTH H_m IN METERS (AFTER NORTON AND HOIDALE, 1975)

Local Time (Hour Ending)	Month											
	Jan	Feb	Mar	Apr	May	June	July	Aug	Sept	Oct	Nov	Dec
0700	30	30	30	50	30	30	30	30	30	30	30	30
0800	30	30	30	107	110	139	103	35	30	30	30	30
0900	30	30	114	326	467	403	329	238	129	89	30	30
1000	64	122	387	740	865	691	688	615	490	271	165	96
1100	232	329	632	1255	1298	1274	1034	1042	933	539	400	239
1200	434	639	1247	1761	1907	2053	1342	1431	1343	873	593	369
1300	645	1054	1518	2177	2521	2654	1868	1840	1708	1217	792	533
1400	822	1363	1804	2513	2915	2983	2388	2347	1896	1554	1025	734
1500	967	1543	2145	2872	3195	3162	2503	2749	1940	1711	1126	718
1600	753	1586	2276	2843	3292	3144	2116	2484	2038	1344	1039	435
1700	366	1148	1835	1954	2727	3065	1279	1572	1762	696	669	206
1800	102	436	946	824	1578	2606	516	816	932	280	231	102
1900	30	68	255	229	549	1466	191	398	252	181	71	35
2000	30	111	30	63	77	427	172	115	30	164	45	30
2100	30	142	30	30	30	30	153	30	30	77	30	30
2200-0600	30	30	30	30	30	30	30	30	30	30	30	30

Hoidale (1975), who analyzed 8,236 rawinsonde observations made at WSMR between 1961 and 1972 using the technique described by Holzworth (1967).

As shown in Figure 4-1, the rawinsonde data are analyzed to determine the mixing-layer depth, mean-layer wind direction and speed and reduced gravity factor. In developing an automated procedure for determining the mixing-layer depth, we evaluated four methods for establishing that a surface-based or elevated inversion was indicated by the rawinsonde observations. The simple criteria associated with the four methods for determining the base of an inversion were:

Method	Criteria
1	$\frac{\Delta\Phi}{\Delta z} > .01$
2	$\frac{\Delta T}{\Delta z} \geq 0$
3	$\frac{\Delta \theta_w}{\Delta z} \geq 0$
4	$\frac{\Delta T_v}{\Delta z} \geq -5\times10^{-4}$

where

$\frac{\Delta\Phi}{\Delta z}$ = lapse rate of potential temperature

$\frac{\Delta T}{\Delta z}$ = lapse rate of temperature

$\frac{\Delta\theta_w}{\Delta z}$ = lapse rate of wet-bulb potential temperature

$\frac{\Delta T_v}{\Delta z}$ = lapse rate of virtual temperature

The MIXLYR routine, which incorporates these criteria, was used to analyze twice-daily rawinsonde observations from Salt Lake City, Utah, for the first five days of each month during the period June 1972 through May 1973 and for all the month of January 1973. The heights of the bases of stable layers obtained from the routine were then qualitatively compared with those selected by meteorologists from the plots of the data. All the criteria produced bases of stable layers in agreement with those selected by the meteorologists for cases in which clearly-defined stable layers were present. In our view, however, the criterion based on the lapse rate of virtual temperature (Method 4) performed more consistently than the other criteria when stable layers were not as clearly defined and for all seasons of the year. For this reason, the procedure finally used in the routine is based on this criterion.

The routine accepts the raw or modified rawinsonde data and begins the selection process by checking

$$\frac{\Delta T_{v,n}}{\Delta z_n} = \frac{\Delta T_{v,n+1} - T_{v,n}}{\Delta z_{n+1} - z_n} \qquad (4\text{-}1)$$

in the first height interval above the surface. If the criterion for the base of a stable layer is met (e.g., if $\Delta T_{v,1} / \Delta z_1 \geq -5\text{x}10^{-4}$) and the height interval Δz is greater than or equal to 100 meters, the routine defines a surface-based inversion and sets, by default, the surface mixing depth to 30 meters. If Δz_1 is less than 100 meters but $\Delta T_{v,1}/\Delta z_1 \geq -5\text{x}10^{-4}$,

the routine then checks $\Delta T_{v,2}/\Delta z_2$. If $\Delta T_{v,2}/\Delta z_2 \geq -5x10^{-4}$ $(\Delta z_1 + \Delta z_2) \geq 100$ meters, the routine checks the quantity

$$\frac{\Delta T'}{\Delta z} = \frac{T_{v,n+2} - T_{v,n}}{z_{n+2} - z_n} = \frac{T_{v,3} - T_{v,1}}{z_3 - z_1} \qquad (4\text{-}2)$$

If $(\Delta T/\Delta z) \geq -5x10^{-4}$, the routine again defines a surface-based inversion. If no surface based inversion is found, the routine increments n and proceeds through the same operations until the base of an elevated inversion is found or until z_{n+1} exceeds 3000 meters AGL. If z_{n+1} exceeds 3000 meters AGL, the surface mixing depth is defaulted to 3000 meters.

After the depth of the surface mixing layer H_m is established, the routine analyzes the rawinsonde data between the surface and H_m to obtain estimates of the mean-layer wind components and the reduced gravity factor using the expressions:

$$u_{H_m} = \frac{\sum_{n=1}^{H_m} u_n (z_{n+1} - z_n)}{\sum_{n=1}^{H_m} (z_{n+1} - z_n)} \qquad (4\text{-}3)$$

$$v_{H_m} = \frac{\sum_{n=1}^{H_m} v_n (z_{n+1} - z_n)}{\sum_{n=1}^{H_m} (z_{n+1} - z_n)} \qquad (4\text{-}4)$$

$$g' = g\left[1 - \frac{\left(\sum_{n=1}^{H_m} T_n\,(z_{n+1} - z_n) \Big/ \sum_{n=1}^{H_m} (z_{n+1} - z_n)\right)}{T_{I,max}}\right] \qquad (4\text{-}5)$$

where $T_{I,max}$ is the maximum temperature in the stable layer above H_m. In the routine, g' is restricted so that if it exceeds 0.3 it is set to 0.3 and if less than 0.1 is set to 0.1.

4.2 BATTLEFIELD SOURCE CHARACTERISTICS ROUTINE

The Battlefield Source Characteristics Routine (SORDAT) is designed to develop the source characteristics for a large number of sources required to describe a battlefield environment problem. From a relatively few inputs supplied by the user, SORDAT generates all necessary source characteristics required for dispersion modeling purposes. Additionally, SORDAT saves all source data in the battlefield source location and characteristics data base for subsequent use by the Battlefield Environment Routine (BEC). Routine SORDAT generates source characteristics for any of the various types of sources discussed in Section 3. As shown in Figure 4-2, the routine reads user-provided data, which includes the source location on the battlefield, the time of day the source emission began, the type of source or source category, and other data that may be required for a particular source category. Depending on the source category, the routine then computes or retrieves the source characteristics required for dispersion modeling from data tables. These source characteristics include the initial cloud dimensions, the total source emission time, the mass rate of emission, and the cloud release height or parameters required to calculate the cloud height. Some source categories require additional characteristics; for example, the vehicle movement source category requires the direction, speed and time of travel of the vehicle movement. SORDAT then stores

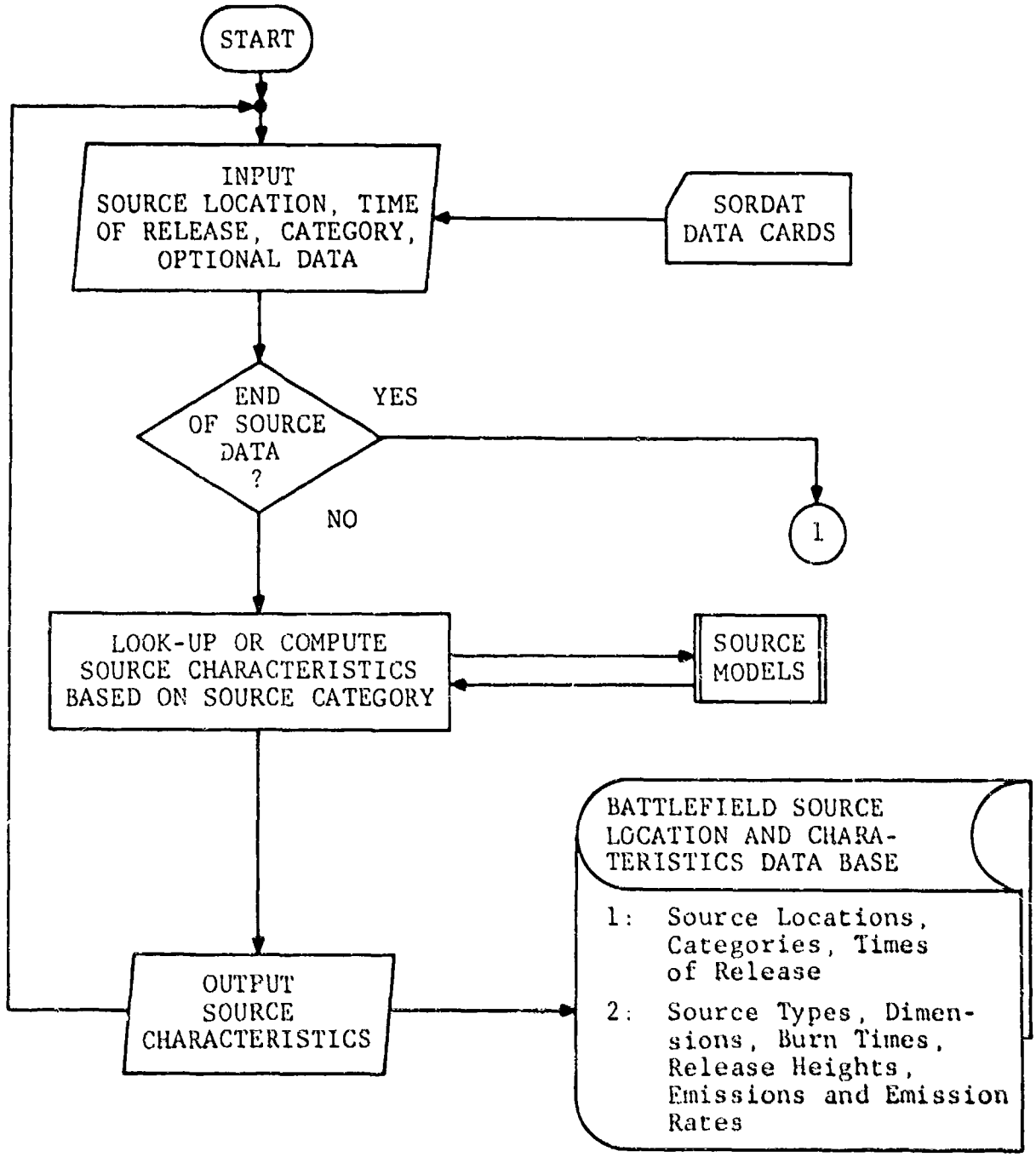

FIGURE 4-2. Battlefield Source Characteristics Routine Flow Diagram.

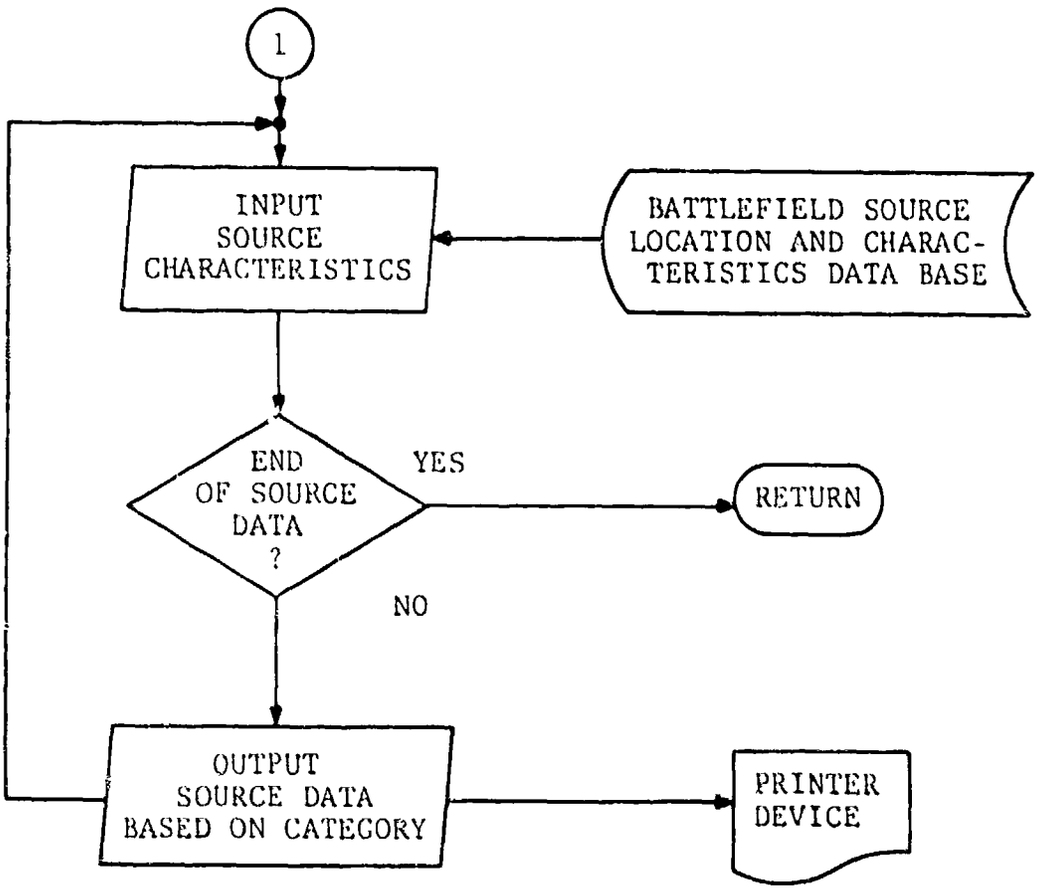

FIGURE 4-2. (Continued)

the source data into the data base and loops back to read another source data card set. After all user-provided source data have been processed, SORDAT optionally prints tables of the source characteristics data based on source category.

4.3 DISPERSION MODEL ROUTINES AND METEOROLOGICAL PARAMETERS REQUIRED BY THE DISPERSION MODELS

The meteorological parameters required by the dispersion models are given in Table 4-2. Of the meteorological parameters shown in the table, the user need only supply the program with values of r and Λ if the dispersion models in Section 2.3.2 are being used and if these parameter values respectively differ from the default values of 1 and 0. When the MS3 Routine of AMSORB is used, the subscript n equals unity and only the values of the parameters in Table 4-2 at the source location are used in the calculations.

The turbulence parameters $\sigma'_{A,n}$ and $\sigma'_{E,n}$, their power-law coefficients for height dependency m and q, and the power-law coefficient p_n are not routinely measured at meteorological stations. A means of assigning appropriate values to these meteorological parameters is therefore required. Swanson and Cramer (1965) made a comprehensive study of the height dependence of σ_A as a function of wind speed and time-of-day using measurements from a 62-meter tower at WSMR. We have used the results of this study in conjunction with a stability classification system, similar to the Pasquill definition of stability categories (Turner, 1964) used by the Environmental Protection Agency, to select and assign values to these parameters. Figure 4-3 is a schematic diagram of the logic sequence used by the routine in defining the parameters and the use of the parameters in the dispersion models.

Key features of the procedure shown in Figure 4-3 are:

TABLE 4-2

METEOROLOGICAL INPUTS FOR THE DISPERSION MODELS

Parameter	Definition
NR	Net radiation index
$H_{m,n}$	Depth of the surface mixing layer at the nth point in the trajectory (m)
$\bar{u}_n$	Mean layer wind speed in the surface mixing layer at the nth point on the trajectory ($m\ s^{-1}$)
$\sigma'_{A,n}$	Standard deviation of the wind azimuth angle at the nth point on the trajectory (radians)
m	Power-law coefficient used to describe the height dependency of $\sigma_{A,n}$ in the surface mixing layer
$\sigma'_{E,n}$	Standard deviation of the wind elevation angle at the nth point on the trajectory (radians)
q	Power-law coefficient used to describe the height dependency of $\sigma_{E,n}$ in the surface mixing layer
p_n	Power-law coefficient used to describe the height dependency of wind speed in the surface mixing layer
α	Lateral cloud expansion coefficient
β	Vertical cloud expansion coefficient
r	Fraction of material reflected at the surface
Λ	Washout coefficient or fraction of material removed by precipitation scavenging per unit time
RH	Relative humidity (percent) used to compute the yield factor (YF) for smoke munitions

FIGURE 4-3. Schematic diagram illustrating procedures for obtaining inputs to the dispersion models.

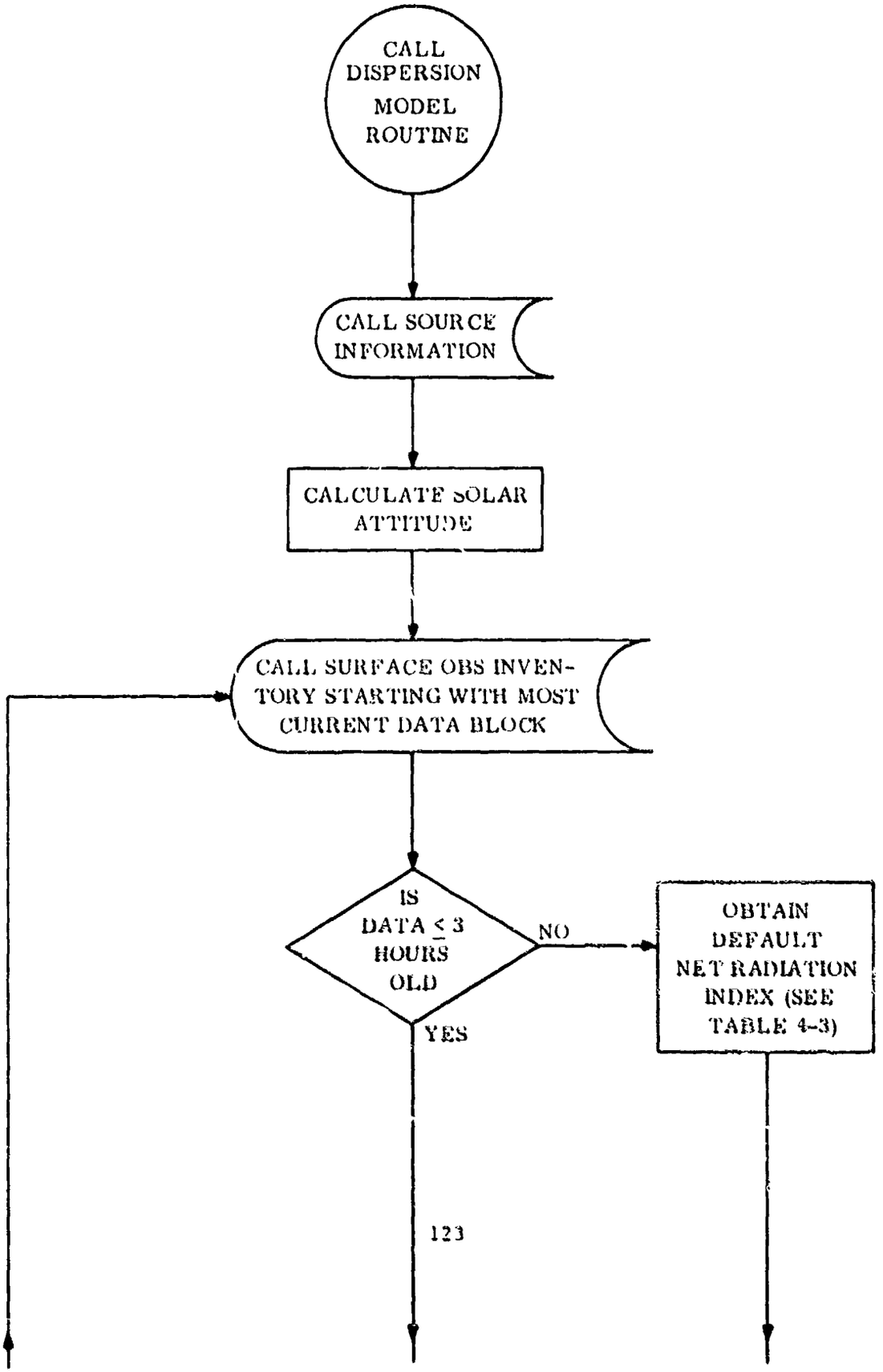

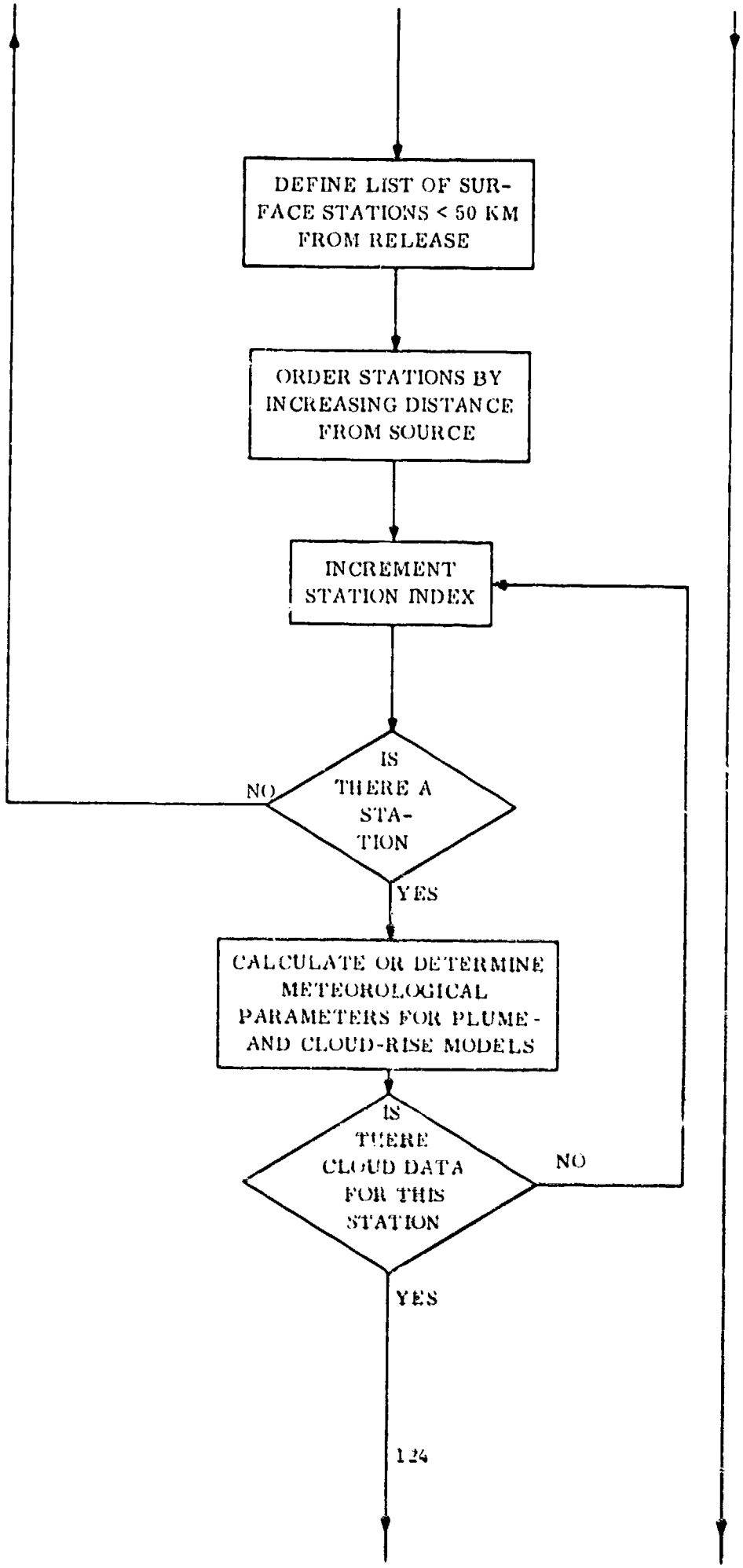
DEFINE LIST OF SURFACE STATIONS < 50 KM FROM RELEASE
ORDER STATIONS BY INCREASING DISTANCE FROM SOURCE
INCREMENT STATION INDEX
IS THERE A STATION
NO
YES
CALCULATE OR DETERMINE METEOROLOGICAL PARAMETERS FOR PLUME- AND CLOUD-RISE MODELS
IS THERE CLOUD DATA FOR THIS STATION
NO
YES

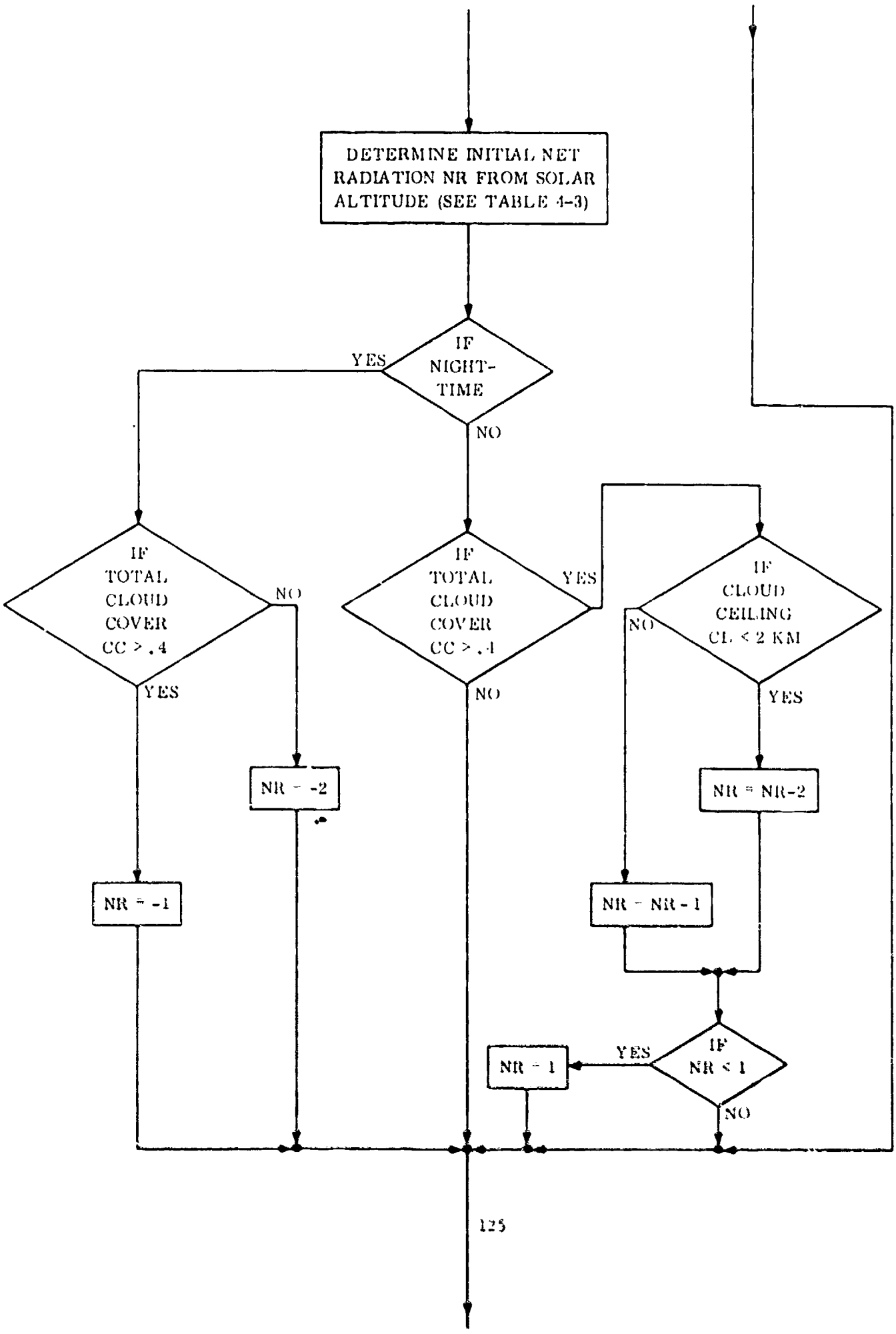
DETERMINE INITIAL NET RADIATION NR FROM SOLAR ALTITUDE (SEE TABLE 4-3)
IF NIGHT-TIME
YES
NO
IF TOTAL CLOUD COVER CC > .4
NO
YES
NR = -2
NR = -1
IF TOTAL CLOUD COVER CC > .1
YES
NO
IF CLOUD CEILING CL < 2 KM
NO
YES
NR = NR-2
NR = NR - 1
IF NR < 1
YES
NO
NR = 1

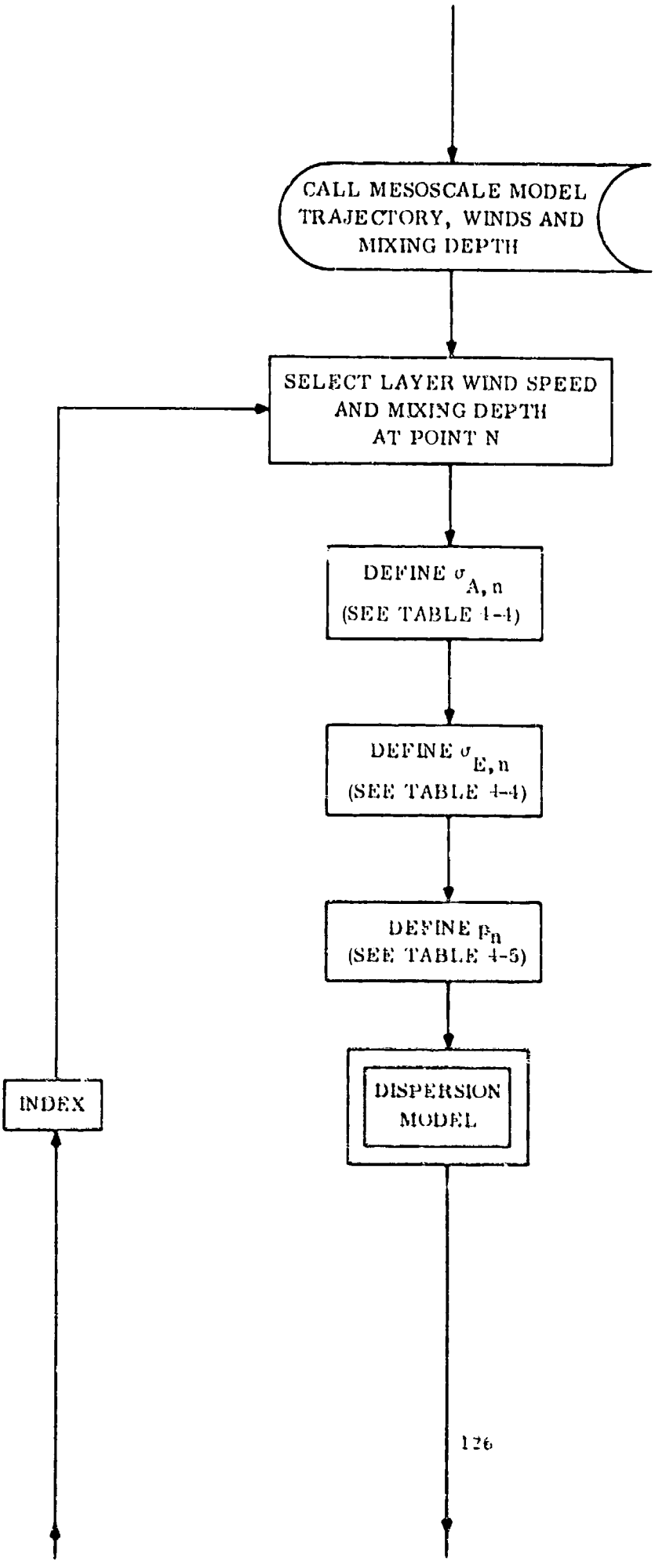
CALL MESOSCALE MODEL TRAJECTORY, WINDS AND MIXING DEPTH
SELECT LAYER WIND SPEED AND MIXING DEPTH AT POINT N
DEFINE $\sigma_{A,n}$ (SEE TABLE 4-4)
DEFINE $\sigma_{E,n}$ (SEE TABLE 4-4)
DEFINE P_n (SEE TABLE 4-5)
DISPERSION MODEL
INDEX

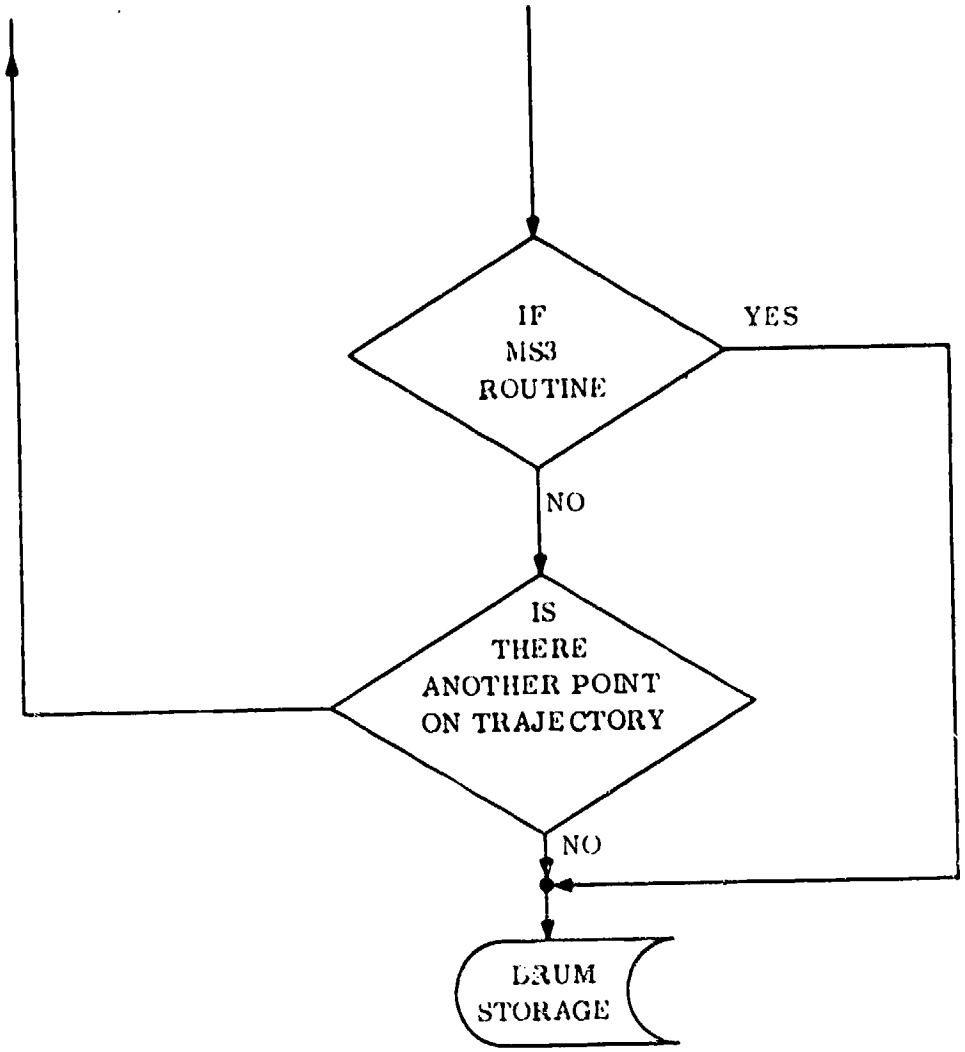
IF
MS3
ROUTINE
YES
NO
IS
THERE
ANOTHER POINT
ON TRAJECTORY
NO
DRUM
STORAGE

- Solar altitudes for the release point and time of request are calculated using an algorithm suggested by Woolf (1968)

- The routine then seeks the most recent cloud and ceiling data from the reporting station nearest to the release point

- If there are no stations reporting cloud and ceiling data within a 50-kilometer radius from the release point or the data are more than three-hours old, the routine selects a default net radiation index from Table 4-3

- When cloud data are available, the routine calculates an initial net radiation index based on solar altitude (also see Table 4-3) and adjusts the index based on the time-of-day, total cloud cover, and ceiling height

- The net radiation index and the wind speeds from the Mesoscale Wind-Field Model for the release point and points along the cloud trajectory are used to select turbulence input parameters and wind power-law coefficients for the dispersion models

- Values of the surface mixing depth $H_{m,n}$ for each nth point along the cloud trajectory are obtained from the Mesoscale Wind-Field Model solution using the interpolation procedure given by Equation (2-6)

Table 4-4(a) shows values of the ten-minute standard deviations of the wind azimuth angle in degrees $\sigma_A(t=10\ min)$ and associated values of the power-law coefficient m for describing σ_A variation with height above the surface based on the study of Swanson and Cramer.

TABLE 4-3

NET RADIATION INDICES

Solar Altitude η In Degrees	Daytime Index	Default Index
$\eta > 60$	4	3
$35 < \eta \leq 60$	3	2
$15 < \eta \leq 35$	2	1
$0 < \eta \leq 15$	1	0
Nighttime	N/A	-1

TABLE 4-4

TURBULENCE PARAMETERS FOR DISPERSION MODELS

(a) Ten-Minute Standard Deviations of the Wind Azimuth Angle in Degrees (σ_A) and Corresponding Values of the Power-Law Exponent m

Wind Speed at 5 Meters (m/sec)	Net Radiation Index													
	4		3		2		1		0		-1		-2	
	σ_A	m	σ_A	m	σ_A	m	σ_A	m	σ_A	m	σ_A	m	σ_A	m
$\bar{u} < 1$	26	-.109	26	-.109	21	-.133	15	-.112	11	-.120	8.6	-.189	8.6	-.189
$1 \leq \bar{u} < 3$	26	-.109	22	-.128	16	-.123	11	-.112	10	-.120	8.6	-.189	8.6	-.189
$3 \leq \bar{u} < 5$	19	-.122	16	-.123	13	-.103	9	-.120	9	-.134	7.8	-.207	7.8	-.189
$5 \leq \bar{u} < 7$	14	-.105	11	-.117	11	-.117	8	-.148	7	-.126	6.7	-.287	6.7	-.189
$7 \leq \bar{u}$	9	-.100	9	-.117	8	-.110	8	-.148	7	-.126	6.7	-.287	6.7	-.189

(b) Standard Deviation of the Wind Elevation Angle In Degrees (σ_E) and Corresponding Values of the Power-Law Exponent q

Wind Speed at 5 Meters (m/sec)	Net Radiation Index													
	4		3		2		1		0		-1		-2	
	σ_E	q	σ_E	q	σ_E	q	σ_E	q	σ_E	q	σ_E	q	σ_E	q
$\bar{u} < 1$	8.7	.10	8.7	.10	7.0	.07	5.0	0	3.7	0	2.9	-.20	2.9	-.30
$1 \leq \bar{u} < 3$	8.7	.10	7.4	.13	5.3	.07	3.7	0	3.3	0	2.9	-.20	2.9	-.25
$3 \leq \bar{u} < 5$	6.3	.15	5.3	.15	4.3	.13	3.0	0	3.0	0	2.6	-.20	2.6	-.20
$5 \leq \bar{u} < 7$	4.7	.20	3.7	.20	3.7	.15	2.7	0	2.7	0	2.2	-.15	2.2	-.15
$7 \leq \bar{u}$	3.0	.25	3.0	.20	2.7	.20	2.7	0	2.7	0	2.2	-.15	2.2	-.15

Values of the standard deviation of the wind elevation angle in degrees and the power-law coefficient q describing the variation of σ_E with height above the surface are shown in Figure 4-4(b). These values of σ_E were assigned under the assumption that (after Cramer, et al., 1972) turbulence is isotropic for short averaging times and that the one-fifth power law can be used as a scale factor to adjust σ_A for averaging times less than 10 minutes. Thus,

$$\sigma_E \cong \sigma_A\{\tau=10 \text{ min}\} \left(\frac{2.5}{600}\right)^{1/5} \tag{4-6}$$

$$\cong \sigma_A\{\tau=10 \text{ min}\} /2.99 \tag{4-7}$$

The values of the power-law coefficient q were assigned under the assumptions that:

- Under stable conditions (NR = -1, -2)

$$\sigma_{E,z} \sim \sigma_{E,z_R} \left(\frac{z}{z_R}\right)^{-p_n} \tag{4-8}$$

- Under near-neutral conditions (NR = 0,1)

$$\sigma_{E,z} \sim \sigma_{E,z_R} \tag{4-9}$$

- Under unstable conditions (NR = 2,3,4)

$$\sigma_{E,z} \sim \sigma_{E,z_R} \left(\frac{z}{z_R}\right)^{0.3-p_n} \tag{4-10}$$

The values of the wind power-law coefficient p_n as a function of net radiation index and mean layer wind speed used in the routine are shown in Table 4-5. These values are similar to those suggested for use at WSMR by Swanson and Hoidale (1962) and for Dugway Proving Ground by Cramer, et al. (1972).

The plume-rise models described in Section 2.3.1 and 2.3.2 above require estimates of the ambient air temperature and density and, under stable conditions, the lapse-rate of potential temperature. If surface meteorological data are available, the routine automatically selects the ambient air temperatures and densities according to the procedures shown in Figure 4-3 and the lapse-rate of potential temperature is calculated from the rawinsonde sounding established using the procedure described in Figure 4-1. If no surface data are available, the default values of surface temperature shown in Table 4-6 and a default air density of 1204.2 grams per cubic meter are used. The temperatures in the table are based on the monthly normal and maximum temperatures at El Paso extracted from the report "Climatic Atlas of the United States" published by the U. S. Department of Commerce in June 1968. The values shown for a net radiation index of -1 and -2 correspond to the normal minimum temperature for each month. Similarly, the values shown for net radiation indices of 0 and 1 and for indices of 2 and 3 respectively, correspond to the normal average and normal maximum temperatures for each month. Finally, the surface temperatures for a net radiation index of -4 were obtained by taking an average of the recorded maximum temperature and the normal maximum temperature at El Paso for each month.

If no rawinsonde data are available, the routine selects default values of the lapse rate of potential temperature from Table 4-7 based on the net radiation index and the calculated wind speed at the effective source height. A default value of 1 is always used for the vertical cloud expansion coefficient β. A default value of 1 for the

TABLE 4-5

WIND POWER-LAW EXPONENT p FOR
THE DISPERSION MODELS

Mean Layer Wind Speed $\bar{u}$ (m/sec)	Net Radiation Index						
	4	3	2	1	0	-1	-2
$\bar{u} < 1$	.2	.2	.20	.20	.20	.20	.3
$1 \leq \bar{u} < 3$	.2	.17	.20	.20	.20	.20	.25
$3 \leq \bar{u} < 5$	.15	.15	.17	.17	.20	.20	.20
$5 \leq \bar{u} < 7$	.10	.10	.15	.15	.15	.15	.15
$7 \leq \bar{u}$	.05	.10	.10	.10	.15	.15	.15

TABLE 4-6

DEFAULT VALUES OF SURFACE TEMPERATURE T_s (^oK)

Month	Net Radiation Index			
	4	3, 2	1, 0	-1, -2
Jan	292	286	279	272
Feb	296	290	282	275
Mar	300	294	286	277
Apr	303	299	290	282
May	308	304	295	287
Jun	312	308	300	292
Jul	312	308	301	294
Aug	310	307	300	293
Sep	308	304	297	289
Oct	303	299	291	283
Nov	297	292	284	275
Dec	293	287	280	272

TABLE 4-7

DEFAULT VALUES OF THE LAPSE RATE OF POTENTIAL TEMPERATURE $\bar{\Phi}$ (deg K/m)

Wind Speed $\bar{u}\{h\}$ (m sec^{-1})	Net Radiation Index			
	1	0	-1	-2
0 - 1.4	0.005	0.015	0.030	0.040
1.5 - 2.9	0.003	0.010	0.020	0.030
3.0 - 4.9	0.001	0.005	0.015	0.020

lateral cloud expansion coefficient α is used for instantaneous sources and a value of 0.9 is used for quasi-continuous and continuous sources.

The dispersion models described in Section 2.3.2 require a yield factor (YF). The factor YF is calculated as a function of relative humity (RH) by the dispersion models. If no relative humidy value is available from the Data Base, the routine selects a default value shown in Table 4-8 based on the time of day and season. The values used in Table 4-8 are for El Paso and are obtained from the "Climatic Atlas of the United States" published by the U. S. Department of Commerce in June 1968.

4.4 OBSCURATION MODEL ROUTINE AND MODEL PARAMETERS

The function of the Obscuration Model Routine is to calculate the probability of detecting a target. Figure 4-4 is a program logic flow diagram of the Obscuration Model. Before a probability of detection value can be computed, several sets of calculations must be performed, as shown in Figure 4-4. First, the line-of-sight (LOS) integrated concentration from the observer to the target is calculated for all contributing obscurant sources. The Obscuration Model Routine references the Dispersion Model Routines in order to compute integrated concentration values. Prior to performing the more time consuming calculations such as cloud brightness, the routine checks to determine if sufficient obscurants are present to reduce the transmittance through the cloud to a level at which targets displaying the largest possible contrast are always obscured. If it is determined that this condition exists, the routine indicates the target is obscured and returns control to the calling program. Otherwise, the routine continues processing and computes the brightness of the target as viewed from the observer. The Dispersion Model Routines are again referenced for computing the observer-to-background LOS integrated concentration and the brightness of the

TABLE 4-8

DEFAULT VALUES OF RELATIVE HUMIDITY (PERCENT) FOR COMPUTING THE YIELD FACTOR (YF)

Season	Time of Day (hours)			
	2200 - 0300	0400 - 1000	1100 - 1700	1800 - 2100
Winter	36	61	40	35
Spring	31	40	22	16
Summer	48	60	34	30
Fall	48	59	35	36

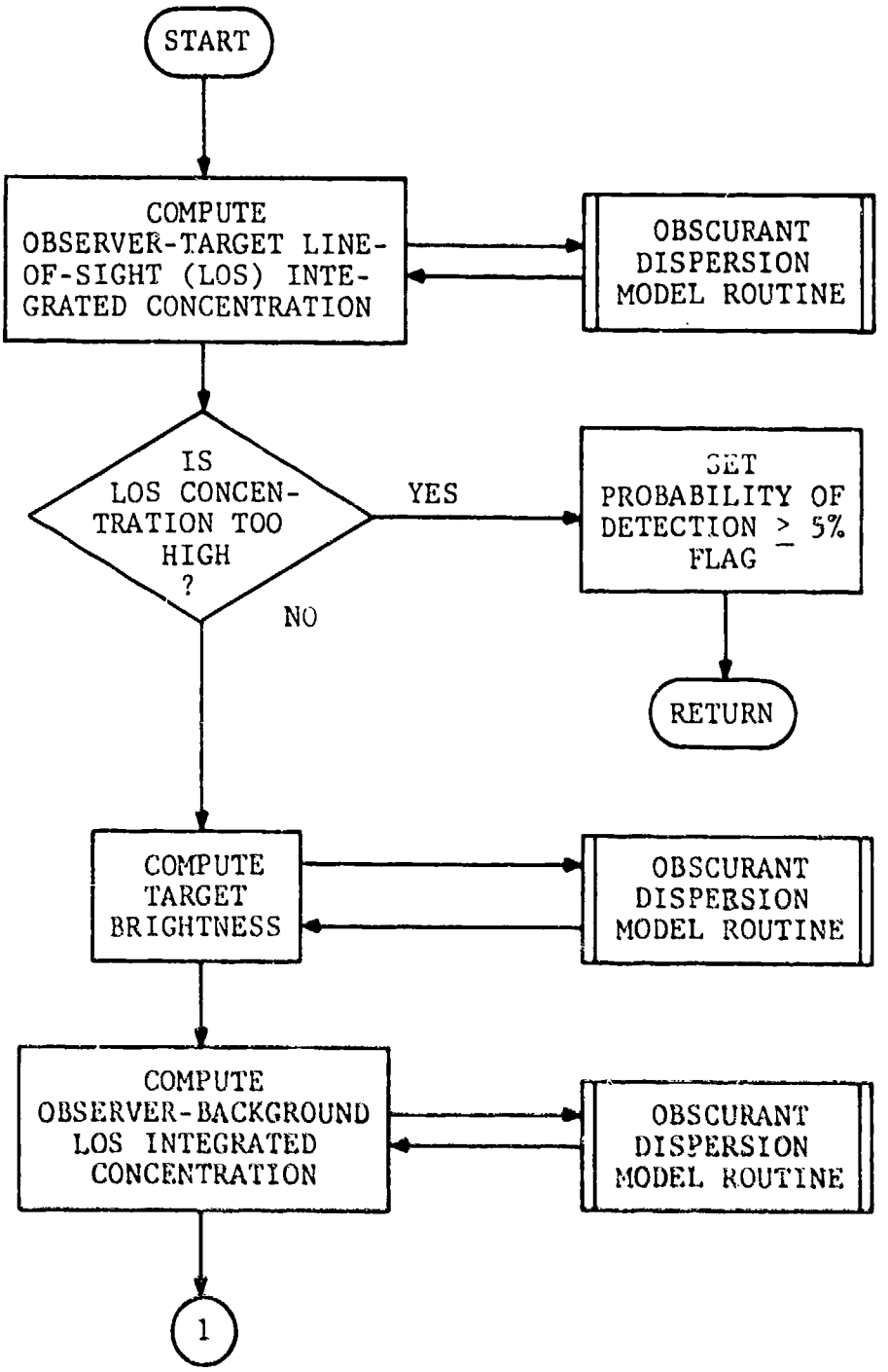

FIGURE 4-4. Obscuration Model Routine Flow Diagram.

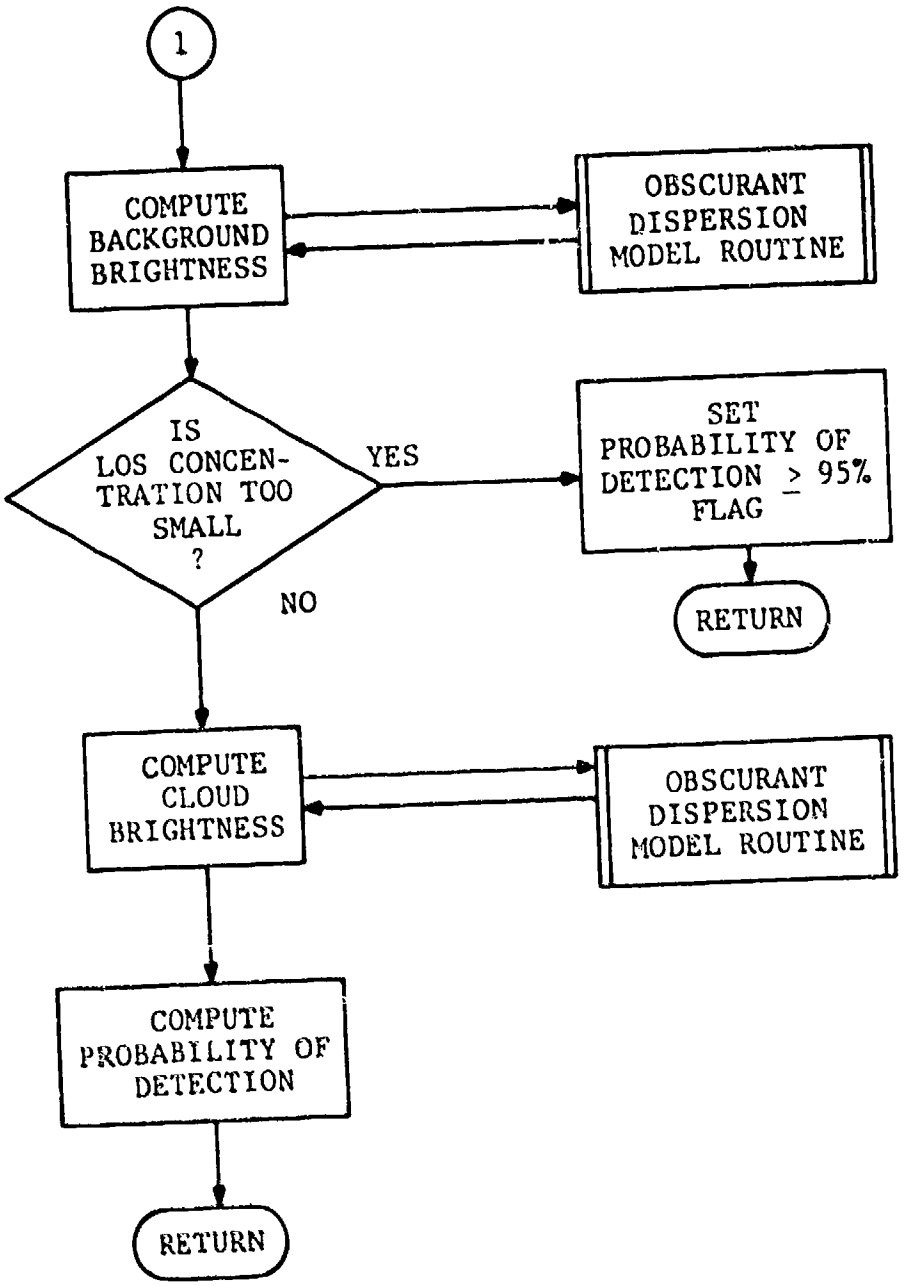

FIGURE 4-4. (Continued)

background as viewed from the observer. These calculations and the calculations of the target brightness are then used to determine if the LOS integrated concentration is sufficient to obscure the target from the observer. If not, a flag is set indicating that the observer has a 95 percent or greater probability of detecting the target and program control returns to the calling program. Should an obscuration be present, the program continues processing and calculates the brightness of the obscurant clouds along the LOS, and finally calculates the probability of detection as shown in the flow diagram. The Obscuration Model Routine then returns to the calling program.

The parameters required by the Obscuration Model described in Section 2.4 are given in Table 4-9. Of the parameters listed in the table, only the coordinates of the observer and target need be input by the user for visible scenarios unless the user has specified a source of obscurants not included in the data base. In addition, a code for the target background description must be input. As noted earlier, the inputs required by the Obscuration Model are the same as those required by the ASLSOM code for infrared, laser, and nighttime scenarios, or when adverse weather is to be considered in the calculations. Details of the inputs required by the Obscuration Model Routine for calculations under these conditions are contained in Volume II, Section A.4 of the program users' manual.

Target and background codes or target and background reflectivities for the wavelength of interest as well as the target size must be entered, as mentioned above. To assist the program user, examples of codes currently used in the model to define the type of target and background, the target size, and the target and background reflectivities for radiation in the visible spectrum are presented in Table 4-10. As an example of the use of the code to specify a scenario, assume the program user wishes to calculate the probability of detecting a vehicle with ordinary camouflage paint against a background of vegetation.

TABLE 4-9

INPUTS FOR THE OBSCURATION MODEL

Parameter	Definition
x_o, y_o, z_o	Coordinates of the observer (m)
x_t, y_t, z_t	Coordinates of the target (m)
d	Average diameter of the target (m)
R_t	Target reflectivity or a code specifying target type
R_b	Background reflectivity or a code specifying background type
B_{oi}	Brightness of the ith light source (candles m^{-2} in the visible region of the spectrum and $\mu W\ m^{-2}$ steradian $^{-1}$ in the infrared)
$\alpha\ \{\lambda\}$	Attenuation coefficient for wavelength λ ($m^2\ mg^{-1}$)
C_B	Threshold contrast
ϕ_i	Scattering angle for the ith light source (deg)
$\frac{F\ \{\phi_i,\ \lambda\}}{k^2}$	Mie scattering function divided by the square of the propagation constant
λ	Wavelength of light or a code specifying the wavelength or region of interest (μm)

TABLE 4-10

OBSCURATION ROUTINE CODE FOR TARGET AND BACKGROUND REFLECTIVITIES AND TARGET SIZES

(a) Target Information

Code	Reflectivity in the Visible Region	Average Target Diameter (m)	Target Type	Reference for Reflectivity Values
2	0.08	5	Army vehicle (ordinary camouflage paint)	Dolce (1974)
3	0.30	10	Red brick building	Handbook of Chemistry & Physics (1957,p2745)
4	0.40	10	Wood (pine) building	Handbook of Chemistry & Physics (1957,p2745)
5	0.55	5	Steel target	American Institute of Physics Handbook (1957)
6	0.69	5	Polished aluminum target	American Institute of Physics Handbook (1957)
7	0.72	1	White painted sign	Handbook of Chemistry & Physics (1957,p2745)
8	0.72	10	White painted building	Handbook of Chemistry & Physics (1957,p2745)

(b) Background Information

Code	Reflectivity in the Visible Region	Background Type	Reference for Reflectivity Values
2	0.08	Soil (damp)	Finklestein (1964)
3	0.15	Vegetation	Dolce (1974)
4	0.40	Granite	(estimated value)
5	0.93	Snow	American Institute of Physics Handbook (1957)
6	1.0	Sky	Dolce (1974, p56)

Inspection of Table 4-10 shows a code of 2 for the target and 3 for the background provide the requisite input variables describing such a scenario. The actual target and background reflectivities and target size, if known, can be entered by the program user.

Most of the remaining parameters required by the Obscuration Model are automatically obtained from data tables in the mass storage file of AMSORB. Attenuation coefficients for various types of obscurants and for five wavelengths or wavelength ranges are given in Table 4-11, as well as the type of experimental conditions (atmospheric or smoke chamber) under which the data were obtained and the reference citing the experiments. The routines automatically select the proper attenuation coefficient based on the obscurant type specified by the user (see Section 2.4).

The Obscuration Model partitions the sky, as noted in Section 2.4, into either 6 or 16 partitions depending on whether the sun is behind, or in front of, the target. For overcast skies (total sky cover greater than or equal to 0.85), the routine uses 16 sky partitions. Table 4-12 shows the azimuth and zenith angles used to represent the centroids of the sky partitions for the brightness calculations. The azimuth angles shown in Table 4-12 are based on a reference coordinate system in which 0 degrees corresponds to grid north and 90 degrees to grid east. The routine automatically translates these azimuth angles to a reference frame in which a ray with an azimuth of 0 degrees is oriented along the observer to target line-of-sight. The sun's position and the total sky cover are passed to the Obscuration Model through the data base management system from the Mixing-Layer Analysis Routine (see Section 4.1). The sun's position is also used to determine the position of the sun's partition when direct radiation is used in the calculations for clear to partly-cloudy days. Scattering angles for the sun and sky partitions are calculated under the assumption that the light sources are at very large distances from the target and observer. As shown in

TABLE 4-11

ATTENUATION COEFFICIENTS FOR VARIOUS TYPES OF OBSCURANTS

Type of Obscurant	Wavelength Range (μm)	Coefficient of Attenuation ($m^2\ mg^{-1}$)	Test Conditions	Reference
HC Smoke	.4 - .7	.0033	Atmospheric	DPG (1978b)
WP Smoke	.4 - .7	.0021	Atmospheric	DPG (1978b)
Fog Oil Smoke	.4 - .7	.0029	Smoke chamber	Allen and Simonson (1970)
FS Smoke	.4 - .7	.0047	Smoke chamber	Allen and Simonson (1970)
Explosive Munition Dust	.4 - .7	.00032	Atmospheric	DPG (1978c)
Vehicle Movement Dust	.4 - .7	.00024	Atmospheric	DPG (1978d)
Muzzle Blast Smoke and Dust	.4 - .7	.00024	(a)	DPG (1978d)
Burning Brush	.4 - .7	.0042	Atmospheric	Turner, et al., (1979), and Eccleston, et al., (1974)
Burning Building	.4 - .7	.0076	Atmospheric	Turner, et al, (1979)
Burning Vehicle	.4 - .7	.0076	(b)	-
HC Smoke	1.06	.00098	Atmospheric	DPG (1978b)
WP Smoke	1.06	.00059	Atmospheric	DPG (1978b)
Explosive Munition Dust	1.06	.00035	Atmospheric	DPG (1978c)
Vehicle Movement Dust	1.06	.00019	Atmospheric	DPG (1978d)
Muzzle Blast Smoke and Dust	1.06	.00019	(a)	DPG (1978d)
HC Smoke	3.4	.00011	Atmospheric	DPG (1978b)
WP Smoke	3.4	.00023	Atmospheric	DPG (1978b)
Explosive Munition Dust	3.4	.00027	Atmospheric	DPG (1978c)
Vehicle Movement Dust	3.4	.00016	Atmospheric	DPG (1978d)

TABLE 4-11 (Continued)

Type of Obscurant	Wavelength Range (μm)	Coefficient of Attenuation (m^2 mg^{-1})	Test Conditions	Reference
Muzzle Blast Smoke and Dust	3.4	.00016	ⓐ	DPG (1978d)
HC Smoke	9.75	.000044	Atmospheric	DPG (1978b)
WP Smoke	9.75	.00027	Atmospheric	DPG (1978b)
Explosive Munition Dust	9.75	.00021	Atmospheric	DPG (1978c)
Vehicle Movement Dust	9.75	.00013	Atmospheric	DPG (1978d)
Muzzle Blast Smoke and Dust	9.75	.00013	ⓐ	DPG (1978d)
HC Smoke	10.6	.00015	Atmospheric	DPG (1978b)
WP Smoke	10.6	.00048	Atmospheric	DPG (1978b)
Fog Oil Smoke	10.6	.00025	Smoke Chamber	Allen and Simonson (1970)
FS Smoke	10.6	.00052	Smoke Chamber	Allen and Simonson (1970)

ⓐ Assumed to be identical to the attenuation coefficient measured for dust clouds produced by surface dust generated by a moving vehicle.

ⓑ The attenuation coefficient for a burning vehicle is assumed to be approximately equal to the coefficient for a burning building.

TABLE 4-12

ANGLES REPRESENTING THE CENTROIDS OF THE SKY PARTITIONS

(a) 6 Sky Partitions (used when the sun is in front of the target)	
Azimuth ψ (deg)	Zenith θ (deg)
60.0	14.4775
180.0	14.4775
300.0	14.4775
60.0	48.5904
180.0	48.5904
300.0	48.5904

(b) 16 Sky Partitions (used when the sun is behind the target or obscured by clouds)	
Azimuth ψ (deg)	Zenith θ (deg)
22.5	14.4775
67.5	14.4775
112.5	14.4775
157.5	14.4775
202.5	14.4775
247.5	14.4775
292.5	14.4775
337.5	14.4775
22.5	48.5904
67.5	48.5904
112.5	48.5904
157.5	48.5904
202.5	48.5904
247.5	48.5904
292.5	48.5904
337.5	48.5904

Figure 4-5, the light rays arriving from each source can thus be assumed parallel, and the scattering angle ϕ_i for the ith light source is determined from the cosine law as follows:

$$\cos \phi_i = \sin \theta' \cdot \sin \theta_i + \cos \theta' \cdot \cos \theta_i \cdot \cos \psi_i \qquad (4\text{-}11)$$

where

ϕ_i = azimuth angle with respect to the observer-target line-of-sight for the ith light source

θ_i = elevation angle of the ith light source

θ' = elevation of the line-of-sight with respect to the plane of the horizon

Table 4-13 gives two sets of the Mie scattering function $F\{\phi_i, \lambda\}$ divided by the square of the propagation constant k for scattering angle increments of 2 degrees currently contained in the data base. The values for the dilute WP in the visible spectrum shown in Table 4-13 were obtained from the SOMI program (Johnson, et al, 1972) and the values for HC at the 10.6-micrometer wavelength were obtained from the ASLSOM code (Gomez, 1978). The obscuration routines use linear interpolation to determine the exact value of $F\{\phi_i,\lambda\}/k^2$ for the scattering angle calculated from Equation (4-11). In the absence of values for HC smoke in the visible, the program uses the values shown in Table 4-13 for dilute WP smoke. Should Mie fractions for other obscurants and/or other wavelengths be required, they must be entered by the user (see Section A.4 of Volume II).

The Obscurant Dispersion Model routine is called when concentrations or line-of-sight integrated concentrations are to be calculated for use in the transmission and brightness calculations. At this point, the obscuration routine also performs the tests described in Section 2.4

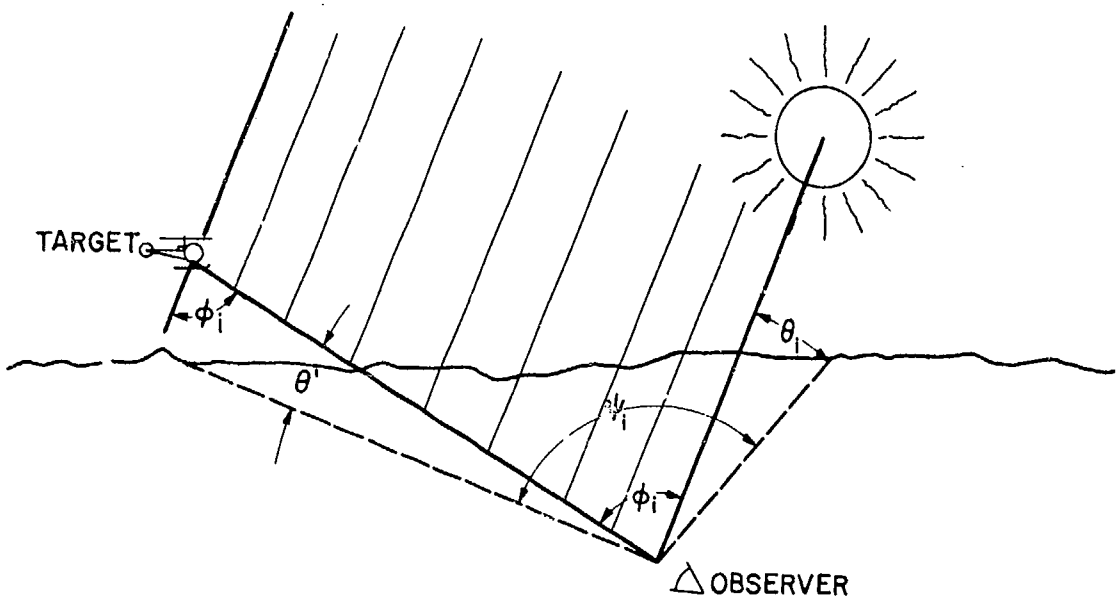

FIGURE 4-5. Sketch showing the angular relationship of the observer, target and a light source.

TABLE 4-13

VALUES OF $F\{\phi_i,\lambda\}/k^2$ FOR DILUTE WHITE PHOSPHORUS AND HEXACHLOROETHANE SMOKES

Scattering Angle (deg)	Scattering Fraction	Scattering Angle (deg)	Scattering Fraction	Scattering Angle (deg)	Scattering Fraction
(a) Dilute White Phosphorous (WP) in the visible					
0.0	1.17889×10^{-2}	62.0	1.32288×10^{-4}	124.0	4.19813×10^{-5}
2.0	1.15003×10^{-2}	64.0	1.17992×10^{-4}	126.0	4.42084×10^{-5}
4.0	1.06873×10^{-2}	66.0	1.05331×10^{-5}	128.0	4.65831×10^{-5}
6.0	9.49033×10^{-3}	68.0	9.41838×10^{-5}	130.0	4.91241×10^{-5}
8.0	8.09441×10^{-3}	70.0	8.43939×10^{-5}	132.0	5.18116×10^{-5}
10.0	6.67796×10^{-3}	72.0	7.57852×10^{-5}	134.0	5.45844×10^{-5}
12.0	5.37472×10^{-3}	74.0	6.82063×10^{-5}	136.0	5.73895×10^{-5}
14.0	4.25876×10^{-3}	76.0	6.15570×10^{-5}	138.0	6.02246×10^{-5}
16.0	3.35111×10^{-3}	78.0	5.57700×10^{-5}	140.0	6.31207×10^{-5}
18.0	2.63791×10^{-3}	80.0	5.07699×10^{-5}	142.0	6.60882×10^{-5}
20.0	2.08918×10^{-3}	82.0	4.64580×10^{-5}	144.0	6.91061×10^{-5}
22.0	1.67184×10^{-3}	84.0	4.27384×10^{-5}	146.0	7.21815×10^{-5}
24.0	1.35602×10^{-3}	86.0	3.95518×10^{-5}	148.0	7.53955×10^{-5}
26.0	1.11700×10^{-4}	88.0	3.68754×10^{-5}	150.0	7.88504×10^{-5}
28.0	9.35254×10^{-4}	90.0	3.46875×10^{-5}	152.0	8.25509×10^{-5}
30.0	7.95836×10^{-4}	92.0	3.29384×10^{-5}	154.0	8.63627×10^{-5}
32.0	6.87646×10^{-4}	94.0	3.15606×10^{-5}	156.0	9.01061×10^{-5}
34.0	6.02473×10^{-4}	96.0	3.05042×10^{-5}	158.0	9.36426×10^{-5}
36.0	5.34125×10^{-4}	98.0	2.97533×10^{-5}	160.0	9.67548×10^{-5}
38.0	4.77872×10^{-4}	100.0	2.93072×10^{-5}	162.0	9.88716×10^{-5}
40.0	4.30176×10^{-4}	102.0	2.91520×10^{-5}	164.0	9.90212×10^{-5}
42.0	3.88561×10^{-4}	104.0	2.92579×10^{-5}	166.0	9.63625×10^{-5}
44.0	3.51418×10^{-4}	106.0	2.96015×10^{-5}	168.0	9.10971×10^{-5}
46.0	3.17742×10^{-4}	108.0	3.01796×10^{-5}	170.0	8.49746×10^{-5}
48.0	2.86893×10^{-4}	110.0	3.09933×10^{-5}	172.0	8.06542×10^{-5}
50.0	2.58465×10^{-4}	112.0	3.20259×10^{-5}	174.0	8.00654×10^{-5}
52.0	2.32238×10^{-4}	114.0	3.32457×10^{-5}	176.0	8.29279×10^{-5}
54.0	2.08134×10^{-4}	116.0	3.46332×10^{-5}	178.0	8.67358×10^{-5}
56.0	1.86144×10^{-4}	118.0	3.61965×10^{-5}	180.0	8.84540×10^{-5}
58.0	1.66238×10^{-4}	120.0	3.79510×10^{-5}		
60.0	1.48329×10^{-4}	122.0	3.98892×10^{-5}		

TABLE 4-13 (Continued)

VALUES OF $F\{\phi_i,\lambda\}/k^2$ FOR DILUTE WHITE PHOSPHORUS AND HEXACHLOROETHANE SMOKES

Scattering Angle (deg)	Scattering Fraction	Scattering Angle (deg)	Scattering Fraction	Scattering Angle (deg)	Scattering Fraction
(b) Hexachloroethane (HC) in the Infrared (10.6 μm)					
0.0	1.45197×10^{-4}	62.0	1.32705×10^{-5}	124.0	1.73621×10^{-6}
2.0	1.44700×10^{-4}	64.0	1.19637×10^{-5}	126.0	1.71047×10^{-6}
4.0	1.43221×10^{-4}	66.0	1.08002×10^{-6}	128.0	1.68992×10^{-6}
6.0	1.40794×10^{-4}	68.0	9.76416×10^{-6}	130.0	1.67422×10^{-6}
8.0	1.37476×10^{-4}	70.0	8.84154×10^{-6}	132.0	1.66315×10^{-6}
10.0	1.33343×10^{-4}	72.0	8.01987×10^{-6}	134.0	1.65651×10^{-6}
12.0	1.28485×10^{-4}	74.0	7.28812×10^{-6}	136.0	1.65417×10^{-6}
14.0	1.23007×10^{-4}	76.0	6.63652×10^{-6}	138.0	1.65602×10^{-6}
16.0	1.17022×10^{-4}	78.0	6.05637×10^{-6}	140.0	1.66200×10^{-6}
18.0	1.10648×10^{-4}	80.0	5.53996×10^{-6}	142.0	1.67204×10^{-6}
20.0	1.04004×10^{-5}	82.0	5.08040×10^{-6}	144.0	1.68605×10^{-6}
22.0	9.72039×10^{-5}	84.0	4.67152×10^{-6}	146.0	1.70393×10^{-6}
24.0	9.03570×10^{-5}	86.0	4.30779×10^{-6}	148.0	1.72551×10^{-6}
26.0	8.35627×10^{-5}	88.0	3.98427×10^{-6}	150.0	1.75057×10^{-6}
28.0	7.69090×10^{-5}	90.0	3.69652×10^{-6}	152.0	1.77878×10^{-6}
30.0	7.04710×10^{-5}	92.0	3.44060×10^{-6}	154.0	1.80974×10^{-6}
32.0	6.43100×10^{-5}	94.0	3.21297×10^{-6}	156.0	1.84294×10^{-6}
34.0	5.84734×10^{-5}	96.0	3.01051×10^{-6}	158.0	1.87779×10^{-6}
36.0	5.29951×10^{-5}	98.0	2.83046×10^{-6}	160.0	1.91359×10^{-6}
38.0	4.78963×10^{-5}	100.0	2.67037×10^{-6}	162.0	1.94956×10^{-6}
40.0	4.31870×10^{-5}	102.0	2.52811×10^{-6}	164.0	1.98490×10^{-6}
42.0	3.88673×10^{-5}	104.0	2.40180×10^{-6}	166.0	2.01874×10^{-6}
44.0	3.49290×10^{-5}	106.0	2.28981×10^{-6}	168.0	2.05022×10^{-6}
46.0	3.13576×10^{-5}	108.0	2.19069×10^{-6}	170.0	2.07852×10^{-6}
48.0	2.81337×10^{-5}	110.0	2.10318×10^{-6}	172.0	2.10285×10^{-6}
50.0	2.52346×10^{-5}	112.0	2.02615×10^{-6}	174.0	2.12255×10^{-6}
52.0	2.26356×10^{-5}	114.0	1.95864×10^{-6}	176.0	2.13704×10^{-6}
54.0	2.03113×10^{-5}	116.0	1.89975×10^{-6}	178.0	2.14591×10^{-6}
56.0	1.82363×10^{-5}	118.0	1.84872×10^{-6}	180.0	2.14889×10
58.0	1.638×10^{-5}	120.0	1.80484×10^{-6}		
60.0	1.47382×10^{-5}	122.0	1.76752×10^{-6}		

to determine if any obscurant is required to obscure the target or if there is too little obscurant present to affect the probability of detection. The amount of direct and diffuse illumination of the scenario is an important parameter in the calculation of the target and background brightness, cloud brightness and in determining the threshold contrast. The present version of the obscuration routines provides for three levels of sky luminance: a clear to partly cloudy day (total cloud cover less than 0.85) with the sun near its meridian, a mostly overcast day (total sky cover equal to or greater than 0.85) and a clear to partly-cloudy day at sunrise or sunset. Luminance levels for these sky conditions used in the routines are shown in Table 4-14 (Handbook of Chemistry and Physics, 1957). The direct sun luminance of 6×10^6 candles per square meter for sunrise and sunset under clear to partly cloudy sky conditions is considered to occur, for calculation purposes, between one half-hour prior to and one half-hour after sunset and sunrise, respectively. The diffuse sky luminance of 8000 candles per square meter is an average brightness for the sky according to the Handbook of Chemistry and Physics, (1957). The brightness for each sky partition B_{oi} is obtained by dividing the indirect radiation value given in Table 4-14 by 6 or 16, depending on the number of sky partitions used in the calculation. For clear to partly-cloudy skies, when direct radiation is present, the sun's partition is assigned the brightness of 1.6×10^9 candles per square meter. For infrared scenarios the sky brightness is not input. Instead, as described in Section A.4 of Volume II, radiance values for the target, sky and terrain in microwatts per square meter per steradian must be input by the user.

The threshold contrasts for a 50-percent probability of detection used in the routines, and shown in Table 4-15 as a function of illumination level and target size, are compiled from data presented by Blackwell (1946). It should be noted that these threshold contrasts are for viewing in the visible spectrum by the human eye. Two sets of threshold contrast values are given, the first for use when the brightness of the target has been calculated to be more than the background brightness and the second set when the target brightness is less than the background brightness. In the test to determine if smoke is required to obscure the target, the

TABLE 4-14

LUMINANCE LEVELS FOR VARIOUS SKY CONDITIONS

Direct Radiation, (candles/m^2)	Indirect Radiation, (candles/m^2)	Sky Condition
1.6×10^9	8000	Clear to Partly Cloudy (TSC* < 0.85)
0	8000	Mostly Overcast (TSC ≥ 0.85)
6.0×10^6	8000	Clear to Partly Cloudy Sunrise & Sunset (TSC < 0.85)

* TSC is the total sky cover or fraction of the sky covered by clouds.

TABLE 4-15

THRESHOLD CONTRAST VALUES

Target Size (minutes of arc)	Total Available Luminance (candles/m^2)				
	$\geq 10^4$	10^3	10^2	10	1
(a) Threshold Contrasts for Targets Brighter than the Background					
150	0.0027	0.0027	0.0027	0.0030	0.0038
100	0.0027	0.0027	0.0028	0.0032	0.0044
50	0.0028	0.0028	0.0030	0.0034	0.0050
20	0.0031	0.0033	0.0036	0.0042	0.0073
15	0.0034	0.0038	0.0044	0.0051	0.0095
10	0.0042	0.0050	0.0064	0.0073	0.0150
8	0.0052	0.0062	0.0081	0.0096	0.020
6	0.0068	0.0083	0.012	0.014	0.030
4	0.011	0.0135	0.021	0.025	0.055
2	0.025	0.036	0.062	0.082	0.190
1	0.072	0.130	0.230	0.340	0.800
(b) Threshold Contrasts for Targets Darker than the Background					
150	0.0070	0.0070	0.0072	0.0073	0.0092
100	0.0074	0.0074	0.0077	0.0079	0.0102
50	0.0087	0.0087	0.0094	0.0100	0.0138
20	0.0130	0.0130	0.014	0.0160	0.025
15	0.0155	0.0155	0.017	0.0195	0.031
10	0.021	0.021	0.023	0.027	0.045
8	0.026	0.026	0.029	0.034	0.059
6	0.035	0.034	0.040	0.047	0.085
4	0.056	0.054	0.065	0.082	0.150
2	0.150	0.140	0.175	0.220	0.410
1	0.470	0.450	0.520	0.660	1.00

target and background reflectivities are compared to determine which set to use in selecting the threshold contrast for comparison with the contrast calculated from Equation (2-150). The angular size of the target in minutes of arc β is determined from the expression

$$\beta = 120 \tan^{-1} (d/2D) \qquad (4\text{-}12)$$

where d is the diameter of the target obtained either from Table 4-13 when a code is used to specify the scenario, or from input specified by the user. The distance D between the target and observer is given by

$$D = \sqrt{(x_o - x_t)^2 + (y_o - y_t)^2 + (z_o - z_t)^2} \qquad (4\text{-}13)$$

For target sizes intermediate between the tabulated values shown in Table 4-15, the routines use linear interpolation to obtain the requisite threshold contrasts. Although Blackwell's data show that the threshold contrast is not linear with target size, the errors introduced by linear interpolation between the target sizes in Table 4-15 do not greatly affect the probability-of-detection calculation.

Finally, as shown in Figure 4-4, the cloud brightness is calculated, if necessary, and the probability of detection is calculated for the first time step. After the time profile of probability-of-detection has been completed, the results are stored in AMSORB's data files.

4.5 BATTLEFIELD ENVIRONMENT ROUTINE

The first function of the AMSORB Battlefield Environment Routine (BEC) is to determine sources on the battlefield that most

likely contribute to the observer-target LOS concentration, and to the obscuration of the target. BEC then references the Trajectory/Transport Routine, Obscurant Dispersion Model and Obscuration Model Routine to perform the concentration and obscuration calculations for these selected battlefield sources. Figure 4-6 is a schematic diagram showing the flow logic of BEC.

As shown in the first two boxes of the BEC schematic diagram (Figure 4-6), the routine reads user-provided input data discussed in Section A.4 of Volume II and reads the mesoscale analysis meteorological data base created from the Analysis Phase routines of AMSORB. From these input data, the routine computes parameters remaining constant throughout the calculations. Due to the size of the battlefield grid and the need to conserve calculation time, a closed boundary is defined using the Trajectory/Transport Routine discussed in Section 2.2 to eliminate sources which can not possibly affect the observer-target LOS concentration or probability of detection calculation. As shown on the second page of Figure 4-6, BEC loops over all battlefield source locations to determine sources within the closed boundary, reading the source locations from the battlefield source location and characteristics data base previously created by the SORDAT Routine discussed in Section 4.2. The BEC Routine sets a flag (eligible source flag) for those sources within the boundary, effectively eliminating sources outside the boundary from further consideration, and references the Trajectory/Transport Routine to calculate an average wind speed, travel distance and travel time between the grid point closest to each source and the LOS.

As shown on pages 3 and 4 of Figure 4-6, BEC makes a second loop over all battlefield sources and again references the battlefield source location and characteristics data base created by SORDAT. Although processing battlefield source data would be more efficient if the data were initially transferred from the mass storage data base to core

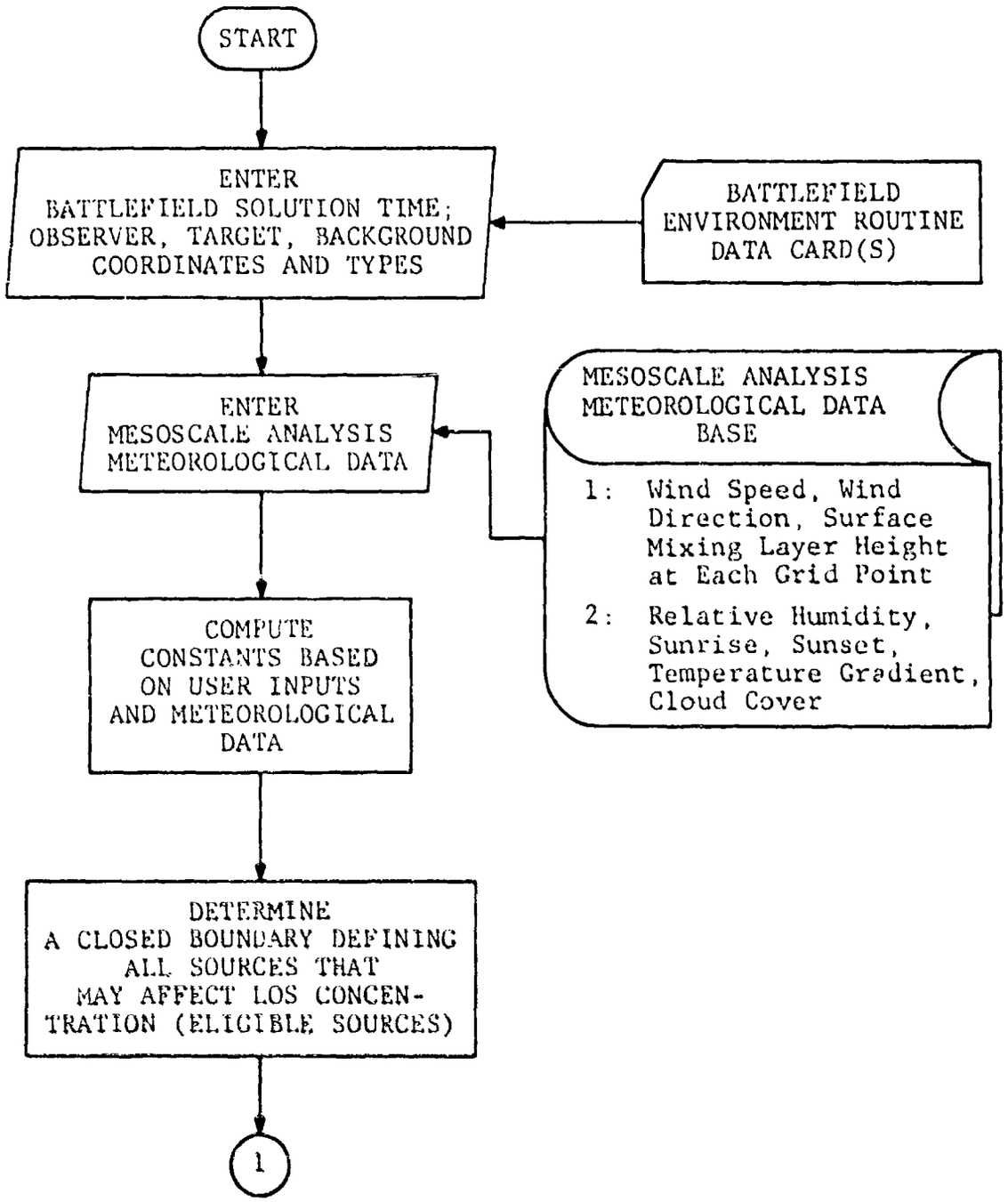

FIGURE 4-5. Battlefield Environment Routine (BEC) Schematic Diagram.

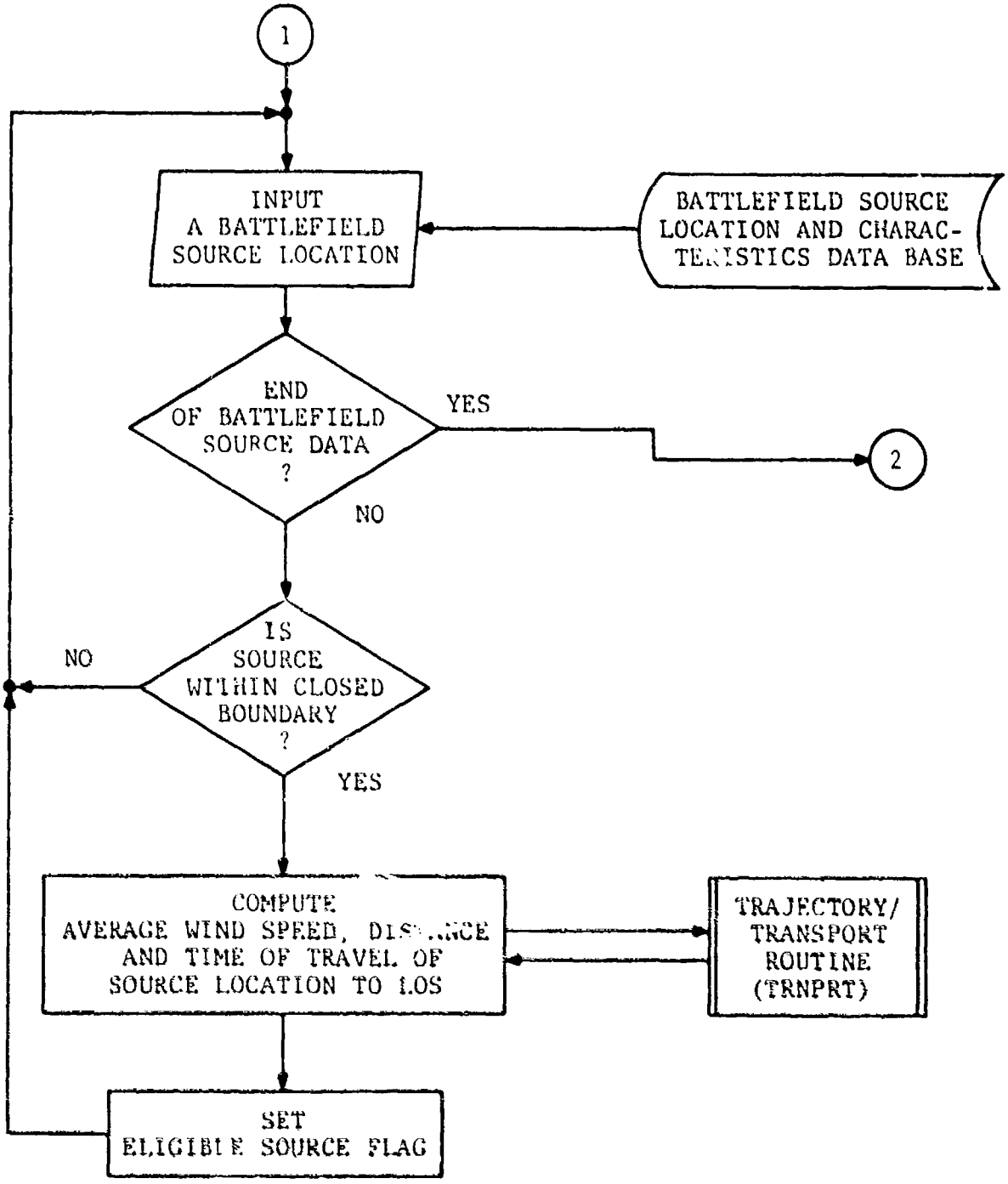

FIGURE 4-6. (Continued)

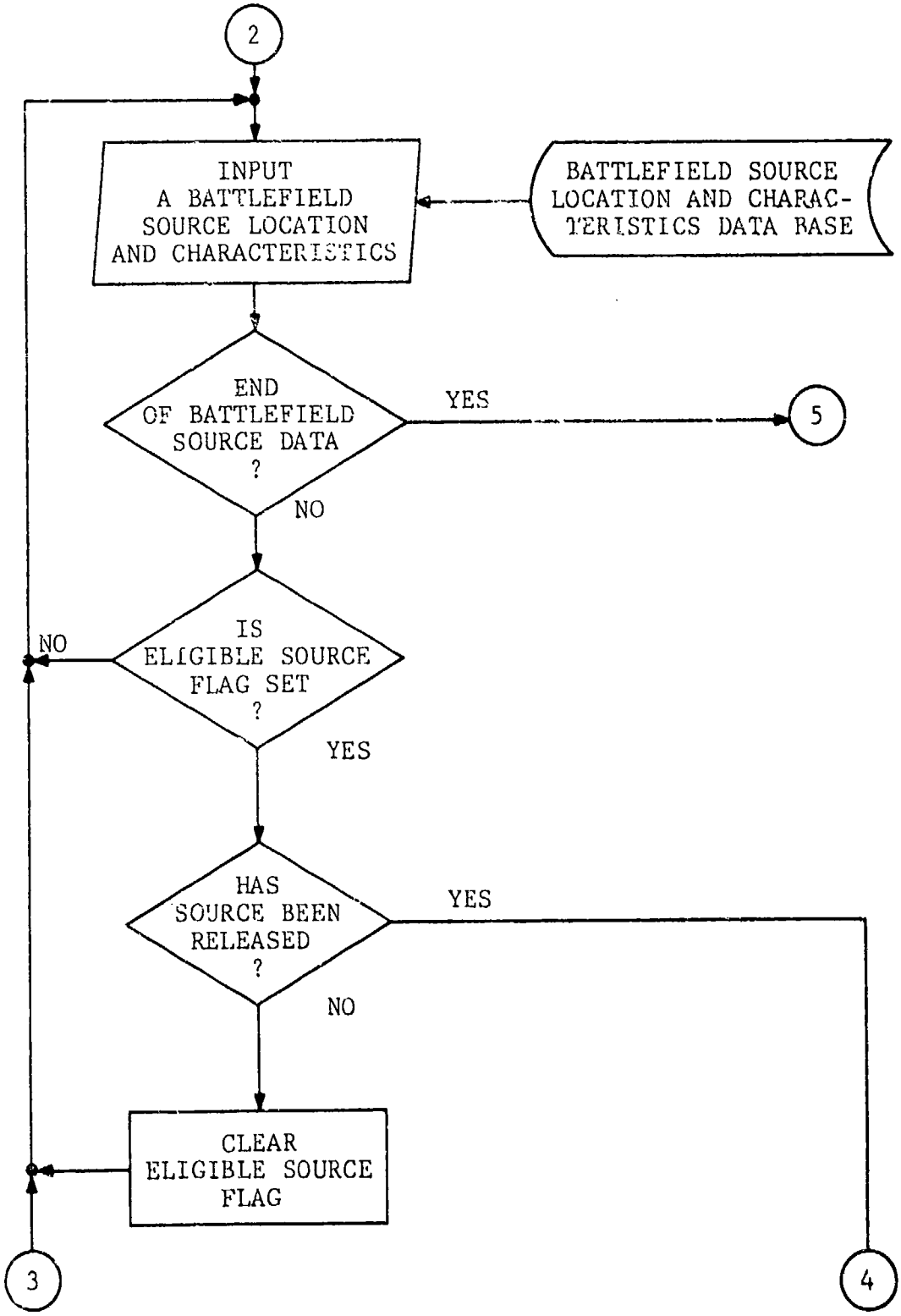

FIGURE 4-6. (Continued)

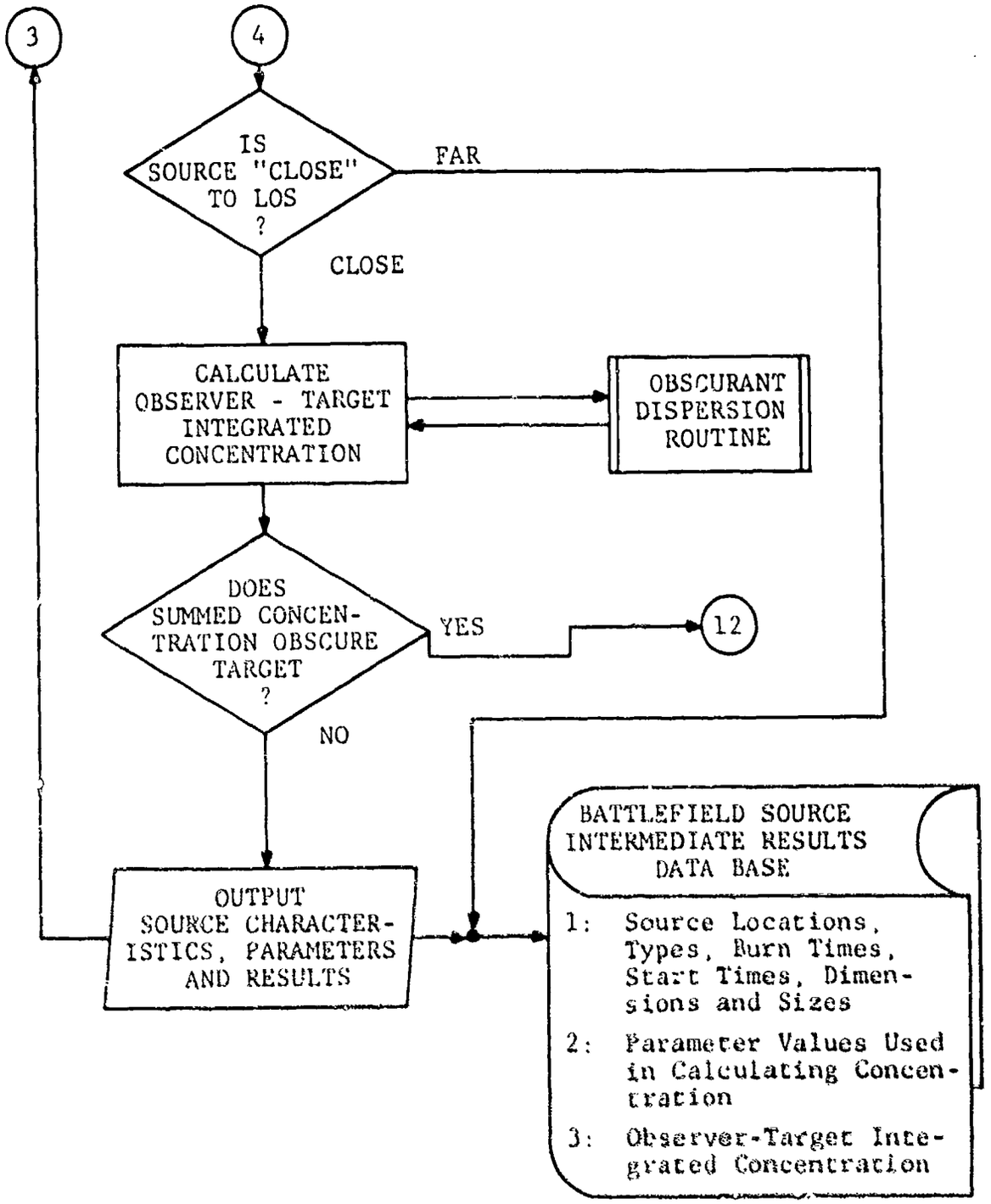

FIGURE 4-6. (Continued)

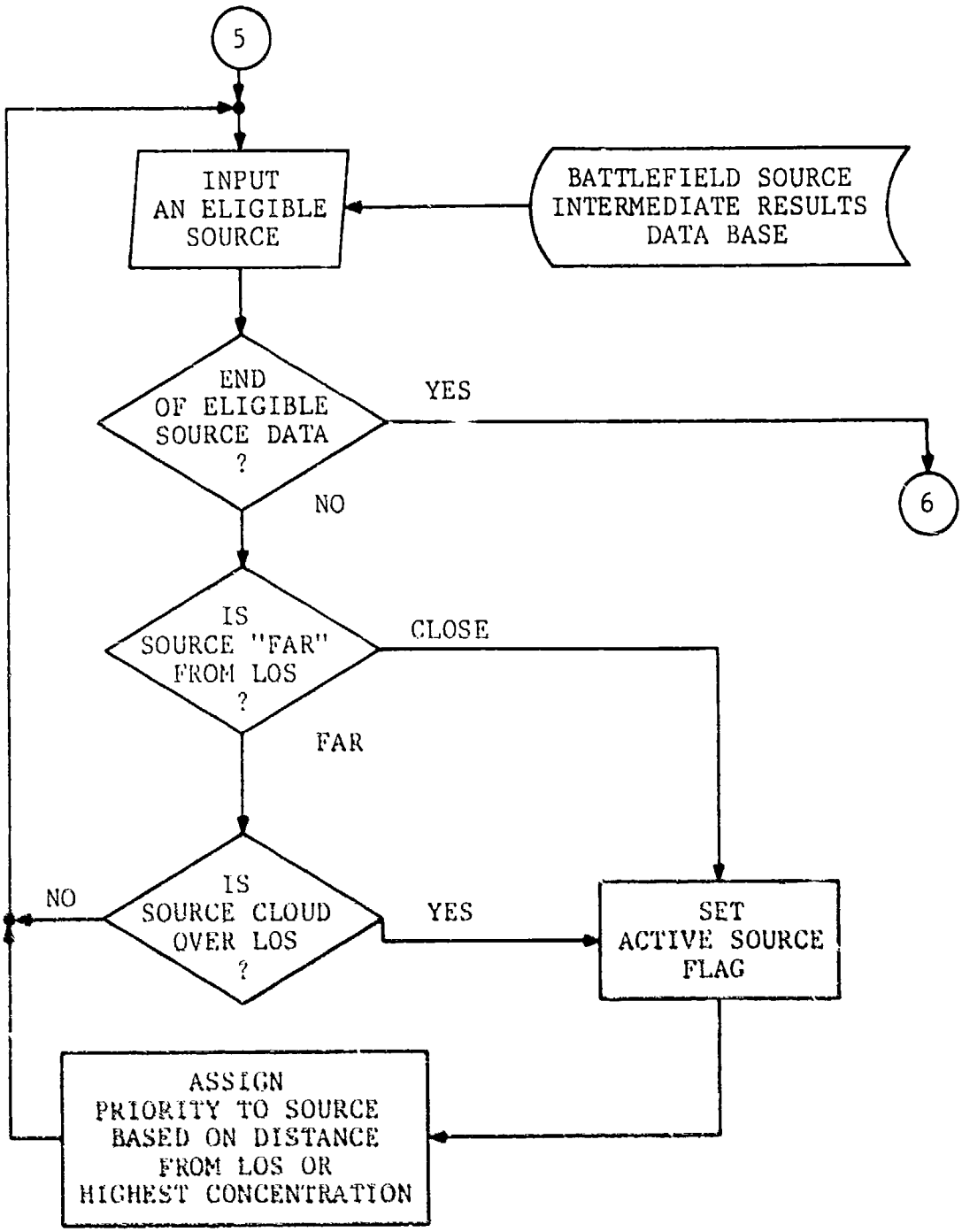

FIGURE 4-6. (Continued)

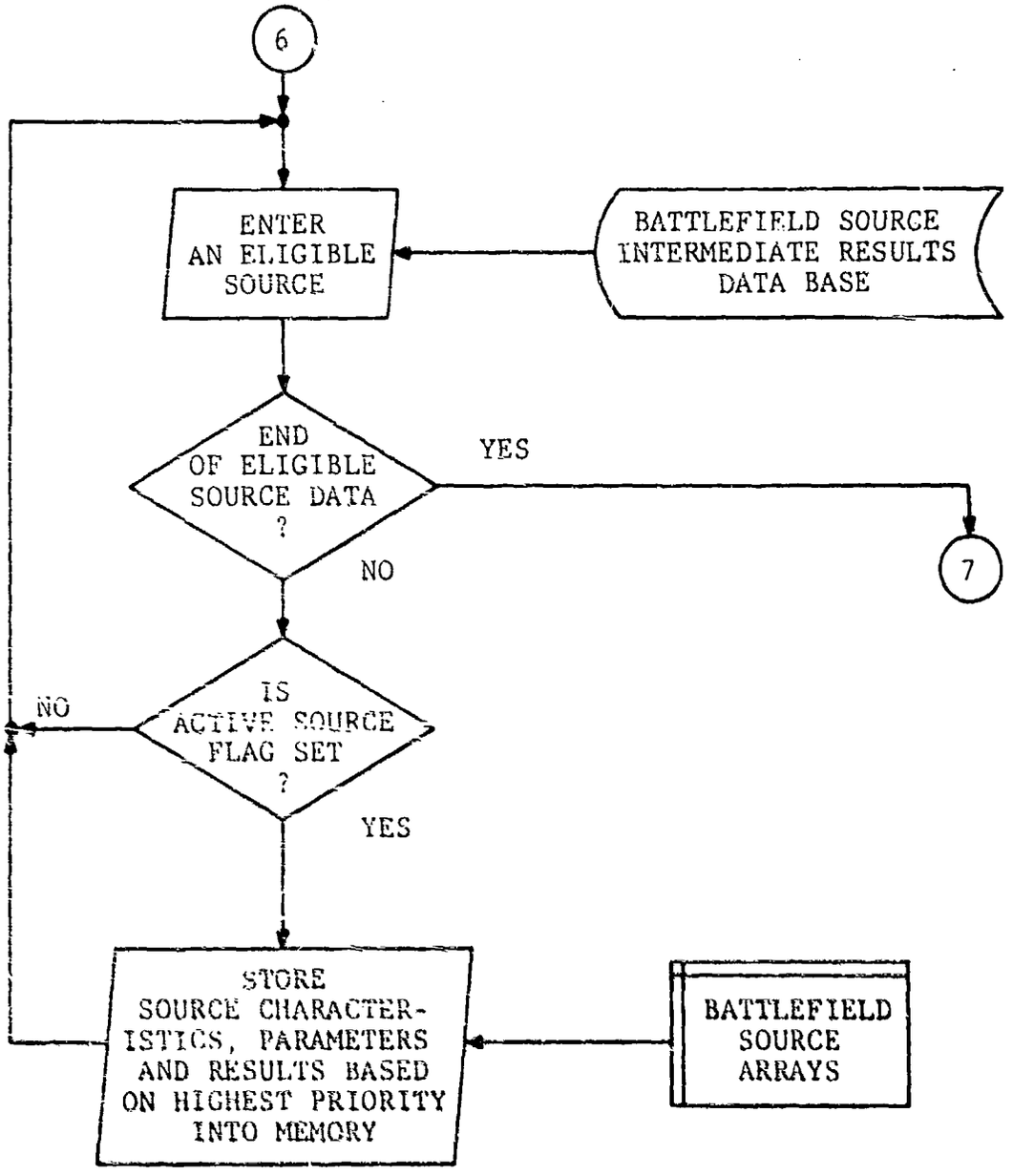

FIGURE 4-6. (Continued)

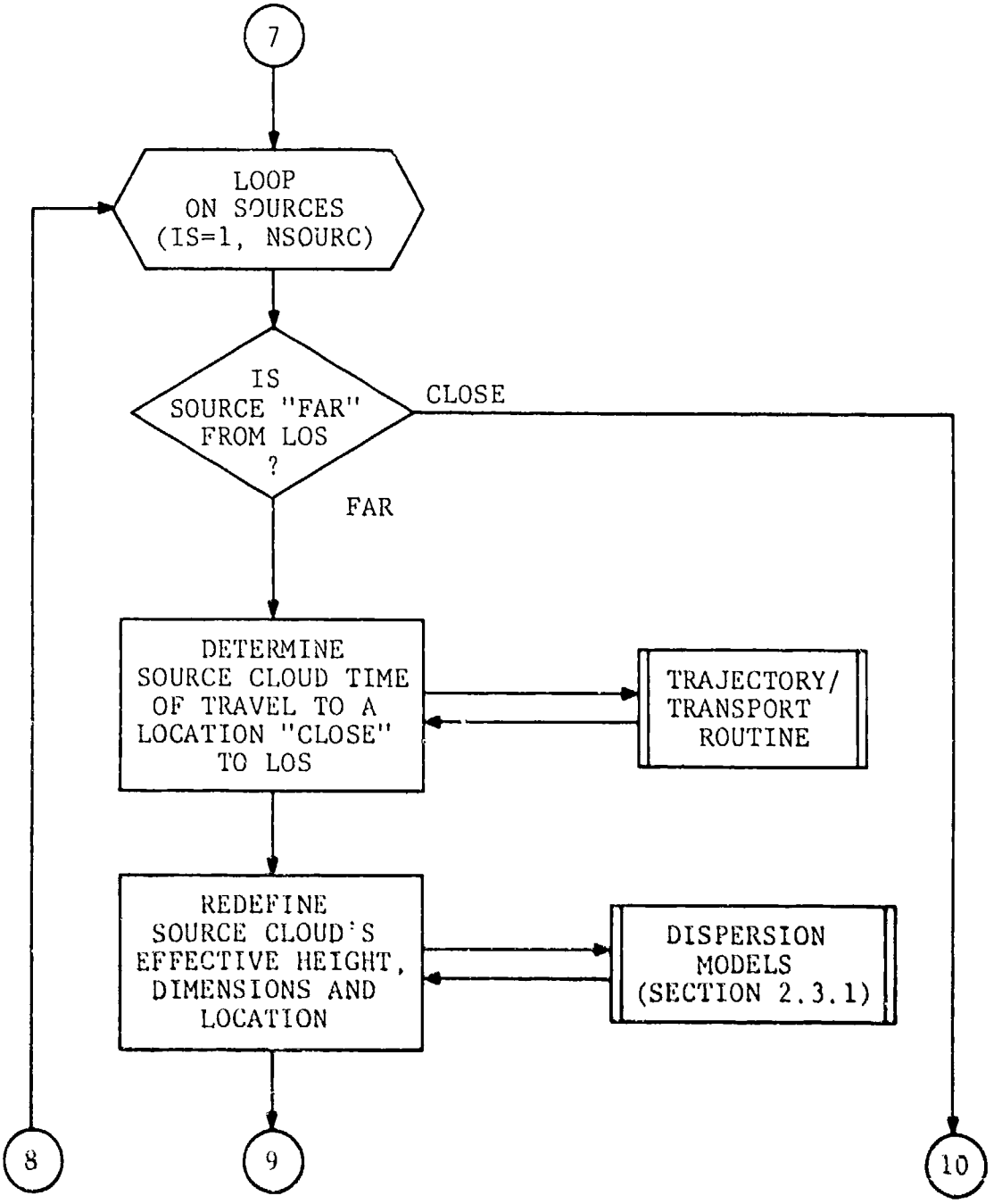

FIGURE 4-6. (Continued)

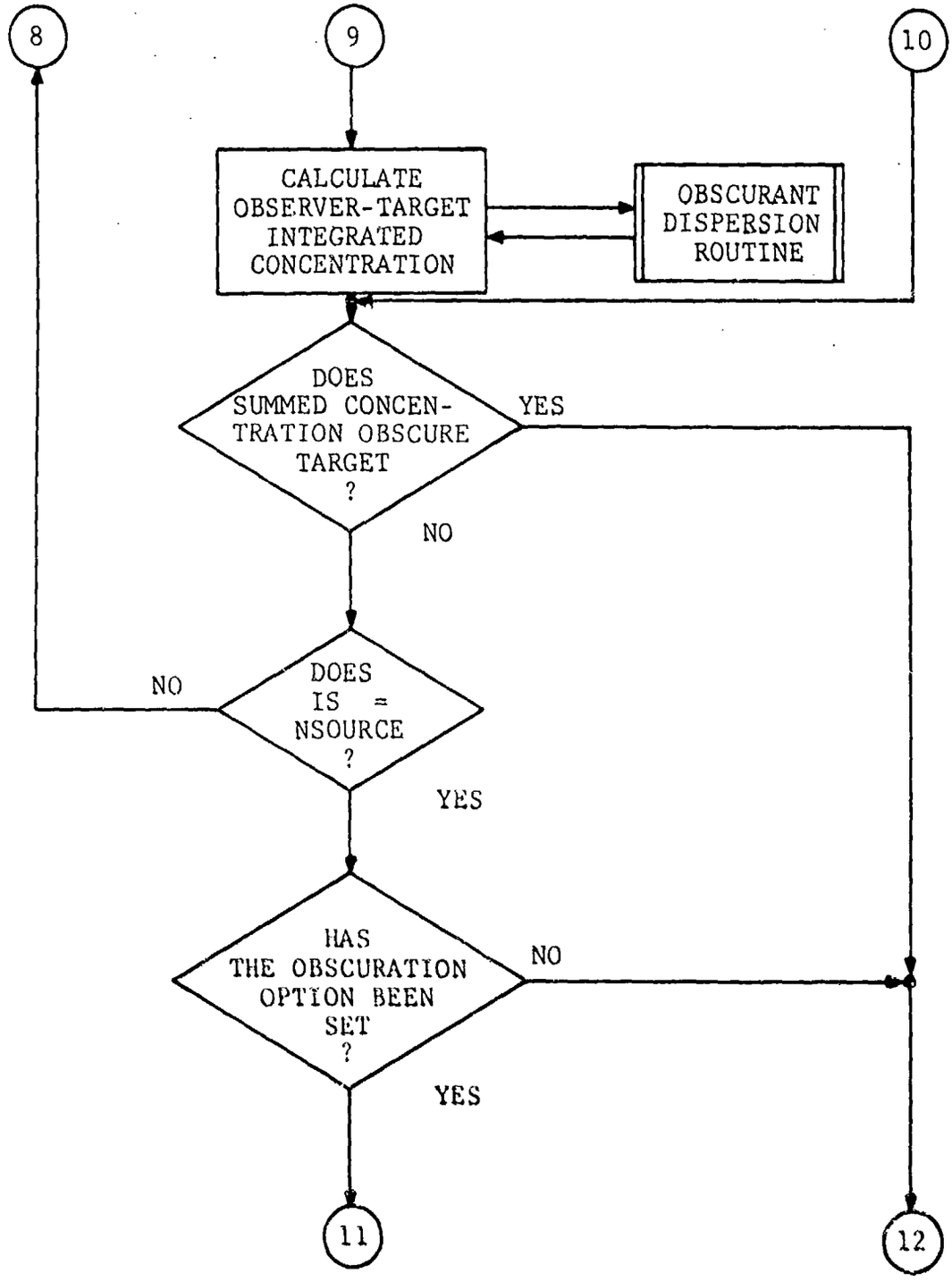

FIGURE 4-6. (Continued)

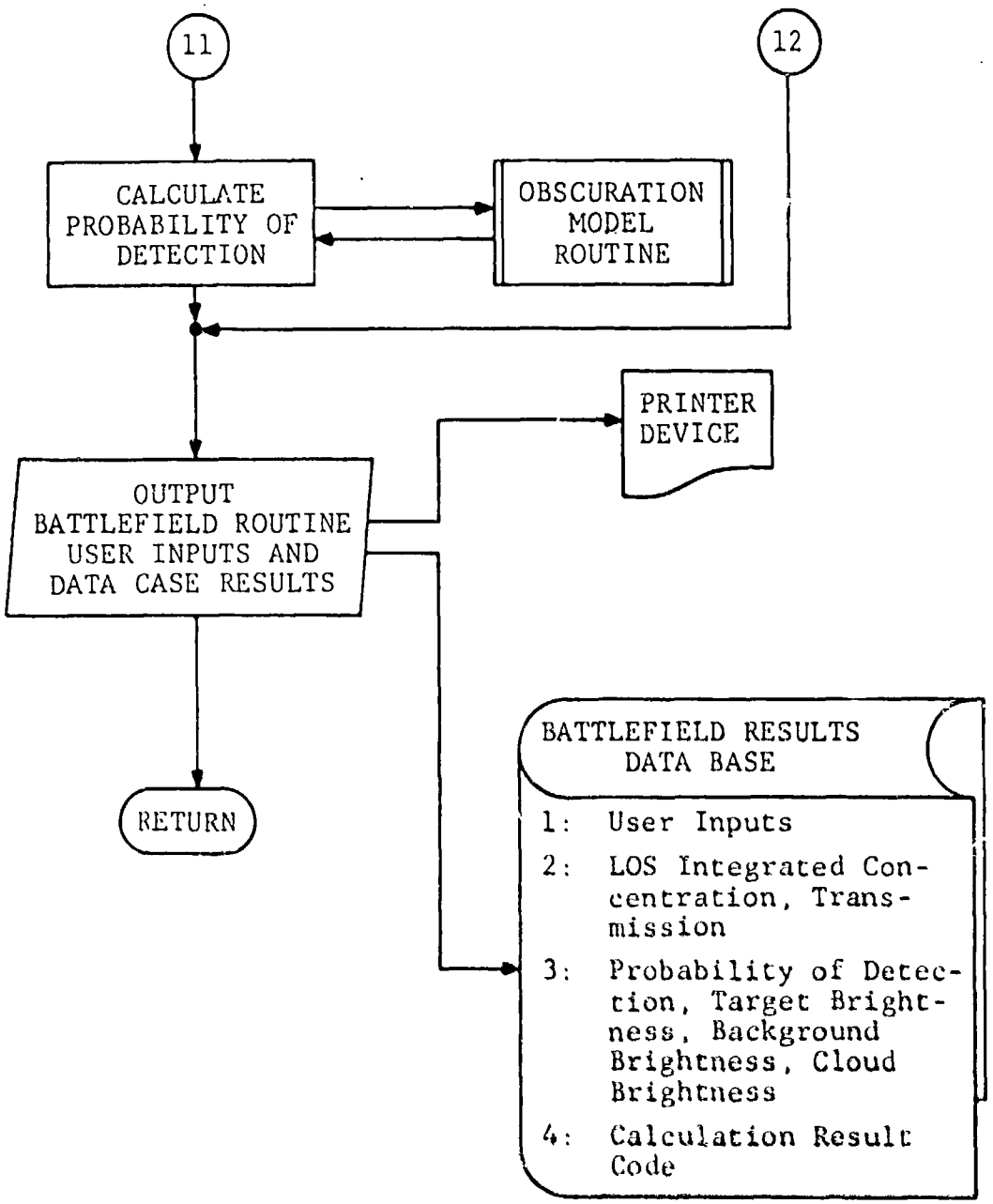

FIGURE 4-5. (Continued)

memory, BEC assumes that the initial number of battlefield sources can exceed BEC's core memory array allocation. The purpose of this second and successive loops over the battlefield source data from a mass storage data base is to select the sources most likely to contribute to the LOS concentration and the obscuration of the target. For "eligible" sources, BEC determines if the source has been released prior to the user-input calculation time. If the source has been released, BEC determines if the source is within one mesoscale grid spacing from the line-of-sight. In our diagram, we have called this source a "close" source and all other more distant sources are called "far" sources. If the source is "close", BEC references the appropriate obscurant dispersion model and computes its contribution to the observer-target LOS integrated concentration. The computed concentration is then summed with the contributions from other "close" sources. If BEC determines that the summed contributions are sufficient to obscure the target, all processing is terminated and the user is notified that the target is obscured.

If no obscuration exists at this point, BEC has recognized all sources which have been released prior to the user-specified calculation time and has calculated LOS integrated concentrations for "close" sources. The BEC logic shown on page 5 of Figure 4-6 is designed to determine if the clouds from the "far" sources are in the vicinity of the LOS at the specified time, defines the "close" sources and the "far" sources whose clouds are in the vicinity of the LOS at the user specified time as "active" sources, and assigns a priority to these active sources based on distance from the LOS ("far" sources) and concentration ("close" sources). Up to this point, BEC has retrieved and stored all battlefield source data from and to mass storage data bases. To increase the speed of subsequent processing, BEC stores all information for the active sources with highest priority into the program's core memory arrays as shown on page 6 of Figure 4-6. It should be noted that the number of active sources could exceed the routine's core memory array limits (currently equal to 200). If this occurs, the routine prints a warning message and processes the 200 highest priority sources.

The primary purpose of the BEC logic shown on page 7 of Figure 4-6 is to effectively use the Trajectory/Transport Routine described in Section 2.2 and the Dispersion Models described in Section 2.3.1 in moving and dispersing clouds from a point of origin "far" from the LOS to a distance not greater than one mesoscale grid spacing from the LOS. In effect, the models are used to redefine a "new" source close to the LOS with dimensions equivalent to those predicted to occur for cloud travel over a trajectory from the source far from the LOS. The "new" source has a release time equivalent to the original time of release plus the predicted travel time along the trajectory from the point of origin to the location of the "new" source. The appropriate cloud-rise equations described in Section 2.3.1 are also used to define the cloud rise from buoyant sources and thus the effective height of the "new" source. As shown on page 8 of Figure 4-6, the contribution of the "new" source to the LOS integrated concentration is then calculated and added to the sum of concentrations from the sources originally "close" to the line of sight and all previously processed "new" sources whose origin was closer in distance to the LOS. If the summed concentration clearly exceeds the concentration required to form an obscuration, the program ceases to process sources and informs the user the target is obscured. Otherwise, sources are processed until there are no more active sources to consider. At this point, the program calculates the probability of detecting the target, if the obscuration option has been selected by the user, using the Obscuration Model Routine described in Section 2.4. The Obscuration Model Routine also computes the target, background and cloud brightness, and the target-background contrast.

When all model processing is completed, BEC outputs the input data and the results to a printer device and to a battlefield results data base as shown on the final page of Figure 4-6. BEC outputs to the printer device some of the user-provided input data, the observer-target line-of-sight integrated concentration and the observer-target transmittance. For the obscuration option, the Obscuration Model calculation

results are also printed. Finally, a brief message is listed indicating what portions of BEC were utilized. The messages may also indicate diagnostics or errors that occurred during program execution. Refer to Section 6 for an example print output produced by BEC. Upon completion of all model processing, the battlefield results data base contains all user-provided data and meteorological constants used in the data case and all calculated results. The data base also contains a calculation result code which indicates the portions of BEC utilized in the processing and is analogous to the messages listed on the printer device.

SECTION 5

STRUCTURE OF THE COMPUTER PROGRAM: ANALYSIS, DATA PROCESSOR, APPLICATION AND GRAPHICS PHASES OF AMSORB

Figure 5-1 shows the executive components, in the form of a block diagram, of the AMSORB system. The AMSORB executive system manager, labeled XECAMS in Figure 5-1, is where all processing begins and ends. The executive systems manager on option passes control to the Supervisors' labeled ANALIZ, DATPRO, APPLY and PLTPRG.

The Analysis Supervisor ANALIZ controls all processing in the Analysis Phase of AMSORB and passes control to the Mixing-Layer Analysis and Mesoscale Wind-Field Models foreman MIXLYR or to other meteorological analysis model routines. The operational elements of MIXLYR are described in Section 5.1 below.

The Data Processor Supervisor DATPRO controls all processing in the Data Processor Phase of AMSORB and passes control to the Battlefield Source Characteristics Routine foreman SORDAT. Section 5.2 contains a discussion of the operational elements of SORDAT. The Application Supervisor APPLY passes control on option to the Trajectory/Transport Dispersion Model application foreman TRYDIF, to the MS3 Obscurant Dispersion and Obscuration Models application foreman MS3, to the Battlefield Environment Routine (BEC) Obscurant Dispersion and Obscuration Models application foreman BEC, or to other application routines. The operational elements of TRYDIF, MS3 and BEC are described in Section 5.3.1, 5.3.2 and 5.3.3, respectively. At the completion of any of these phases, program control is returned to XECAMS. The executive systems manager can address, on option, the Graphics Supervisor PLTPRG to obtain either printed or plotted solutions developed in the application routines. Further details of the Graphics Supervisor PLTPRG are described in Section 5.4 below.

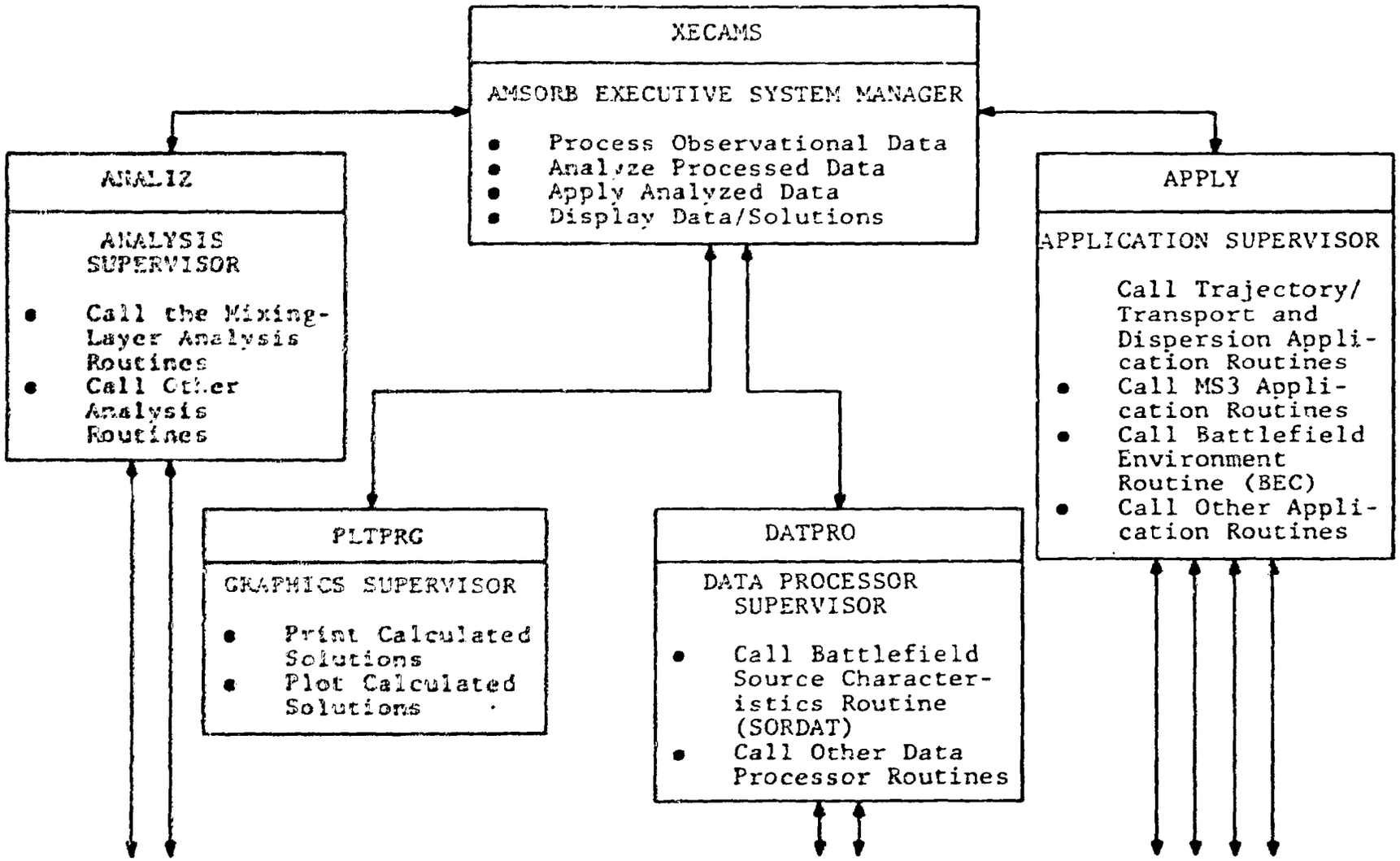

FIGURE 5-1. Executive System and Supervisors of the Analysis, Data Processor, Application and Graphics Phases of AMSORB.

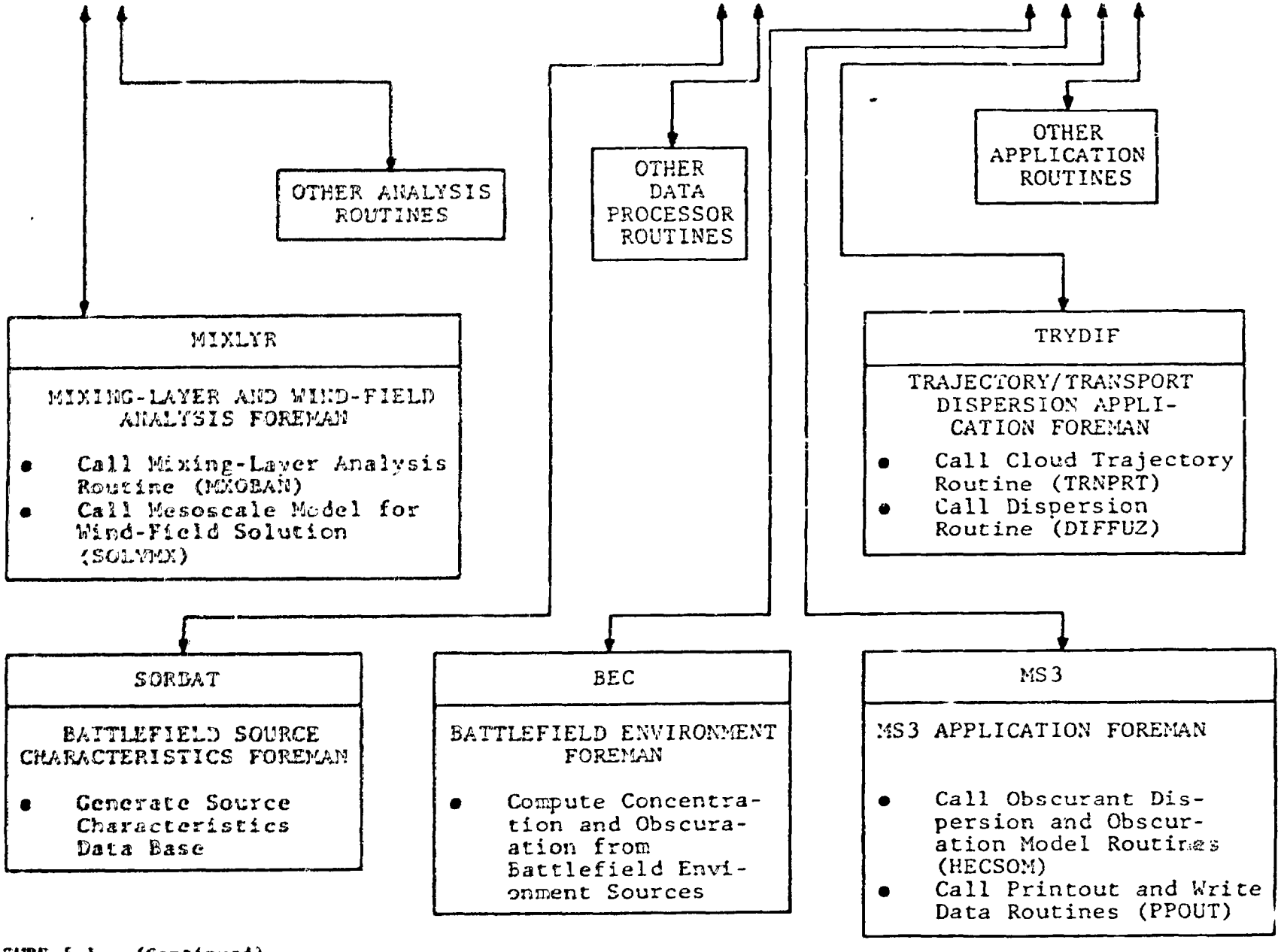

FIGURE 5-1. (Continued)

5.1 ANALYSIS PHASE OF AMSORB

As shown in Figure 5-1, the foreman MIXLYR of the Analysis Phase of AMSORB is comprised of the two operational elements MXOBAN and SOLVMX. The operational subroutines of MXOBAN are shown in the block diagram in Figure 5-2. The operational element MXOBAN controls the analysis of all meteorological data and passes the results of the data analysis to the subroutine SOLVMX at the completion of execution. The AMSORB System user requests transport and dispersion information for a given time and source, which is then passed to MXOBAN via XECAMS. The MXOBAN Mixing-Layer Analysis Model routine then proceeds to analyze rawinsonde, GWC and surface meteorological data according to the logic process described in Section 4.1. The subroutine MXUADT obtains rawinsonde data from the AMSORB data base for the desired solution time and source location. GWC prediction data and surface weather observations for use in the analysis are obtained from the data base via the subroutines MXGWDT and MXSFDT. These subroutines also use the GWC and surface data to modify the rawinsonde data if appropriate. The subroutine MXSFDT also calculates the net-radiation index for the surface meteorological station using information obtained from the LONLAT and DAYNIT subroutines. The rawinsonde data are then used in the subroutine LYRDHM to calculate the depth of the surface mixing layer and the mean wind components in the layer as described in Section 4.1. If insufficient data are available for calculating the mixing-layer depth or wind components, default data are supplied via the LYRDHM and MXSFDT subroutines. Control is then returned to the operational element MIXLYR and processing continues by branching to the subroutine SOLVMX.

A block diagram showing operational subelements of SOLVMX is given in Figure 5-3. Processing begins through examination of the Mesoscale Wind-Field Model routine input parameters passed to SOLVMX from MIXLYR to determine which of two procedures are to be used in initializing the Mesoscale Wind-Field Model routine. Thus, the input parameters from MIXLYR are compared in the subroutine MXSTAT with the input

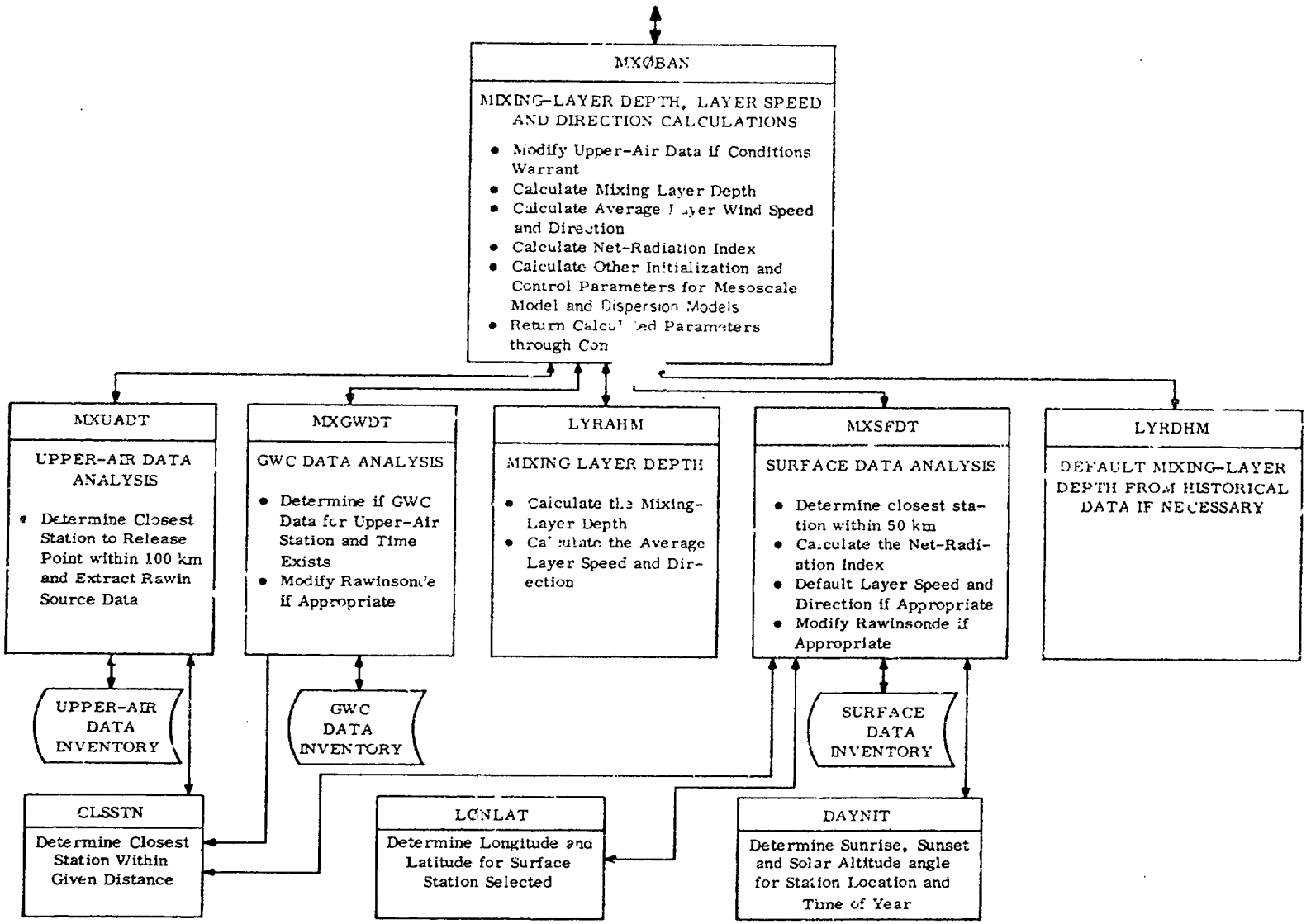

Figure 5-2. Operational Elements of MXØBAN Analysis Phase.

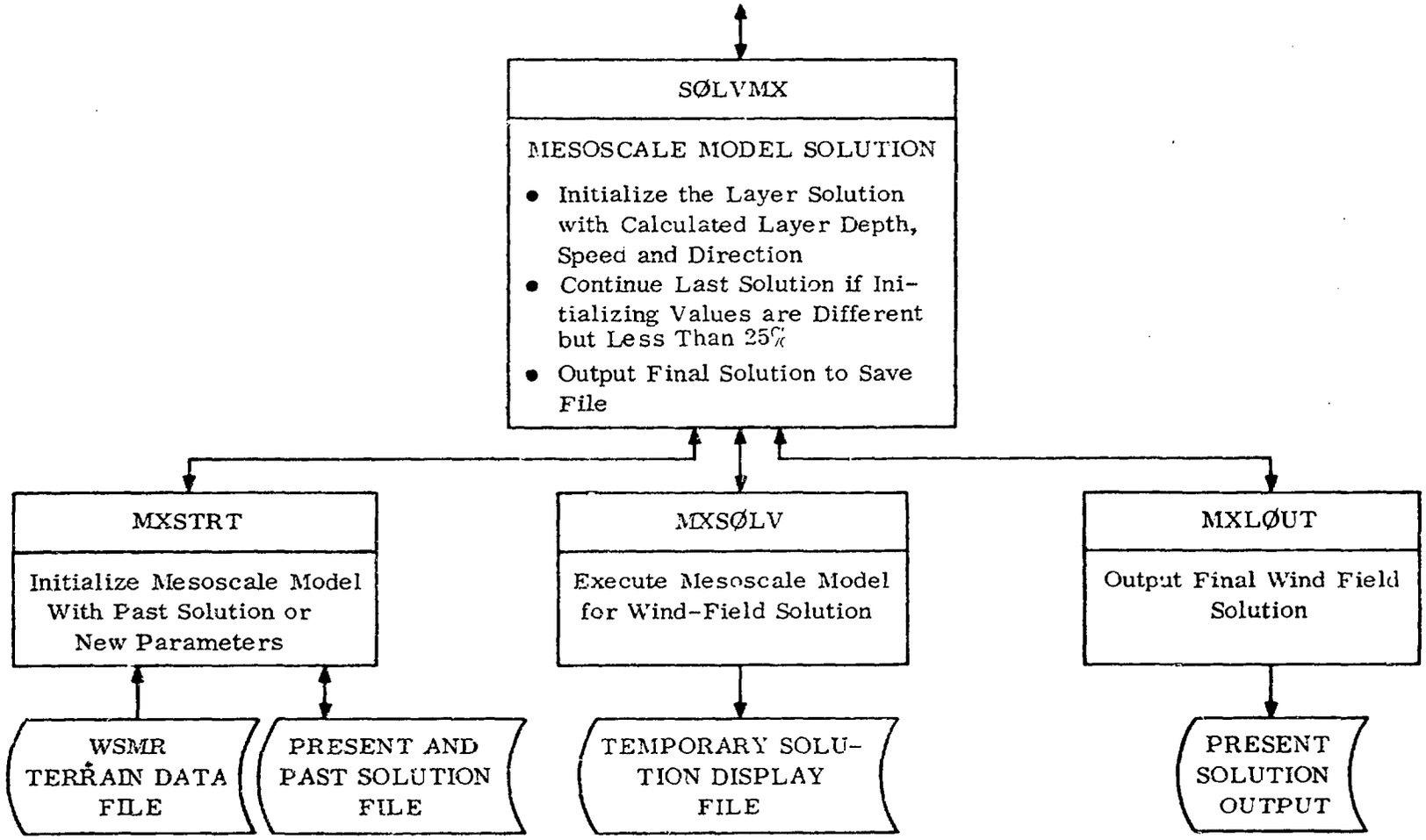

Figure 5-3. Operational Elements of SØLVMX Analysis Phase.

parameters used to generate the last solution of the mesoscale routine resident in the AMSORB data base. The mesoscale routine is initialized with the new inputs from MXOBAN if the mean layer wind speeds and elevation of the mixing depth above mean sea level (MSL) differ by more than twenty-five percent and the mean wind directions differ by more than ten degrees (cold start). The initial layer depth and momentum components for a cold start are given by the expressions

$$H_{m;i,j} = H'_{n,j} \tag{5-1}$$

$$M_{i,j} = U_n \left(H'_n - h'_{min}\right) \tag{5-2}$$

$$N_{i,j} = V_n \left(H'_n - h'_{min}\right) \tag{5-3}$$

where

H'_n = mixing depth (MSL) calculated for the present hour

U_n = easterly component of the mean layer wind for the present hour

h'_{min} = minimum terrain elevation (MSL) in the solution matrix

V_n = northerly component of the mean layer wind for the present hour

If the differences are less than those specified above, subroutine MXSTRT calculates initialization parameters for a "hot" start from the expressions

$$H_{m;i,j} = \left(H'_{i,j} - h'_{i,j}\right) + H'_n - H'_o \tag{5-4}$$

$$M_{i,j} = \left(H'_{i,j} - h'_{i,j}\right) U_{i,j} + \left(H'_o - h'_{min}\right)\left(U_n - U_o\right) + U_n \left(H'_n - H'_o\right) \tag{5-5}$$

$$N_{i,j} = \left(H'_{i,j} - h'_{i,j}\right) V_{i,j} + \left(H'_o - h'_{min}\right)\left(V_n - V_o\right) + V_n \left(H'_n - H'_o\right) \tag{5-6}$$

where

$H'_{i,j}$ = mixing depth (MSL) at each solution matrix grid point for the previous wind-field solution

$h'_{i,j}$ = terrain elevation (MSL) at each solution matrix grid point

H'_o = mixing depth (MSL) used to initialize the previous wind-field solution

$U_{i,j}$ = easterly component of the mean layer wind at each solution matrix grid point for the previous wind-field solution

U_o = easterly component of the mean layer wind used to initialize the previous wind-field solution

$V_{i,j}$ = northerly component of the mean layer wind at each solution matrix grid point for the previous wind-field solution

V_o = northerly component of the mean layer wind used to initialize the previous wind-field solution

After the initialization procedure has been completed, the input parameters are passed to the subroutine MXSOLV via SOLVMX for execution of the Mesoscale Wind-Field Model described in Section 2.1.

Subroutine MXSOLV will allow the mesoscale routine to execute for a maximum model time of approximately 7200 seconds for a cold start and 1800 seconds for a hot start or until the solution converges, whichever occurs first. The subroutine begins to check convergence criteria after 1200 seconds model time has elapsed for a cold start or 600 seconds for a hot start. The convergence criteria are then checked after every application of the nine-point filter (after every seventh time-step if the default value is used). Subroutine MXSOLV begins the convergence check by calculating the relative variance of the change in mixing layer depth $V_R(\Delta H_m)$ over the solution matrix according to the expression

$$V_R(\Delta H_m) = \left\{ \sum_{i=1}^{n} \sum_{j=1}^{m} \left(H'_{m;i,j} - H_{m;i,j}\right)^2 - n \cdot m \left[\sum_{i=1}^{n} \sum_{j=1}^{m} \left(H'_{m;i,j} - H_{m;i,j}\right) \right]^2 \right\} \Bigg/ \left\{ \sum_{i=1}^{n} \sum_{j=1}^{m} \left(H'_{m;i,j}\right)^2 - n \cdot m \left[\sum_{i=1}^{n} \sum_{j=1}^{m} \left(H'_{m;i,j}\right) \right]^2 \right\} \quad (5\text{-}7)$$

where

H'_m = layer depth calculated for the present time step at each point in the n by m matrix

H_m = layer depth for the previous time step at each point in the n by m matrix

The subroutine determines the slope of the curve describing $V_R(\Delta H_m)$ as a function of time and the difference between $V_R(\Delta H_m)$ at the present and previous application of the filter. The solution is assumed to have converged if the

- Slope of the curve describing $V_R(\Delta H_m)$ as a function of time is equal to or less than zero
- Present value of $V_R(\Delta H_m)$ is less than the previous value and the difference between the values is less than or equal to 1×10^{-5}

The Analysis Phase saves the converged Mesoscale Wind-Field Model solution and other parameters calculated in the Mixing-Layer Analysis Model routines by passing them to the AMSORB data base. At this point MIXLYR is terminated and control is returned to XECAMS.

5.2 DATA PROCESSOR PHASE OF AMSORB

The AMSORB executive XECAMS accesses the Data Processor Phase by calling Supervisor DATPRO. Supervisor DATPRO passes program control to the Battlefield Source Characteristics Routine foreman SORDAT, or passes program control to other data processor foreman routines.

Figure 5-4 shows a block diagram of the Data Processor Phase of AMSORB after program control is passed from Supervisor DATPRO. Foreman SORDAT, which is also the main routine of the source characteristics program, reads the first data card and calls one of the following source type or category subroutines: RDSMK, BRNBR, BRNBL, EXPMUN, MUZZLE, or VHMOVE, to read the remaining input data cards for the source category specified in the first data card. These specific subroutines provide default values and/or compute the source input parameters particular to each type source category. The default values and source model used for a particular source category are based on the values and source models discussed in the corresponding source category subsection in Section 3. These routines write all model input parameters to a mass storage data base that is in turn referenced by the Battlefield Environment Routine (BEC) discussed in Section 5.3.3. After the processing of data for one source is completed, a return is made by the category subroutine to SORDAT to read the next set of source cards until an end-of-file card is encountered.

At the users option, SORDAT calls DRVPRT to print source characteristics tables containing input values and model input parameters. DRVPRT utilizes the following subroutines in creating these tables: PRTSOR, PRTSMK, PRTINS, PRTQC, PRTBBR, PRTBBL, PRTBVH, PRTEXP, PRTMUZ and PRTVHM. Program control is then returned from SORDAT to the Data Processor Supervisor DATPRO which in turn passes control to XECAMS.

5.3 APPLICATION PHASE OF AMSORB

5.3.1 Foreman TRYDIF

Inspection of Figure 5-1 above shows the foreman TRYDIF of the Applications Phase of AMSORB is comprised of the two operational elements TRNPRT and DIFFUZ. These operational elements perform the

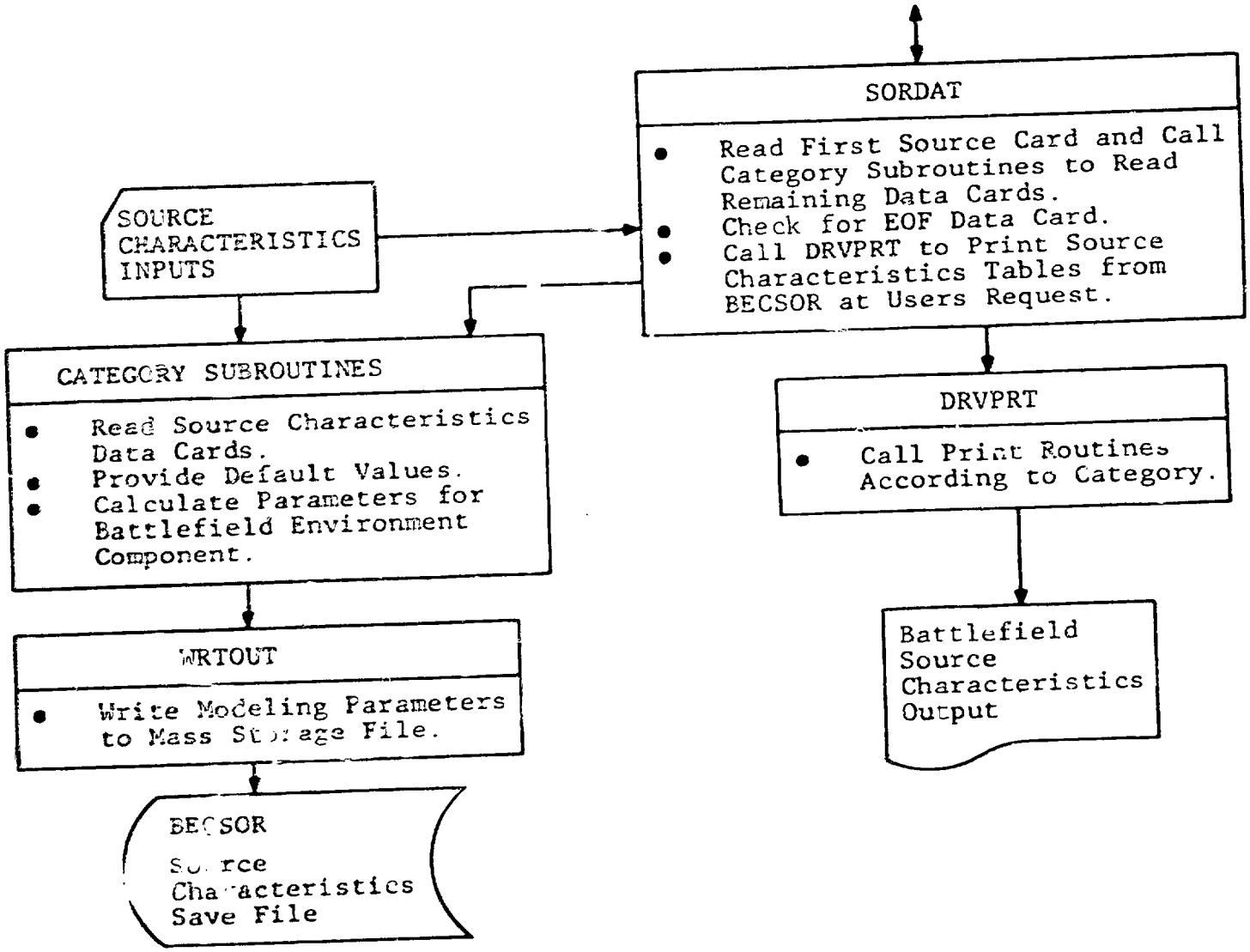

FIGURE 5-4. Routines Controlled by the Data Processor Phase Foreman of AMSORB.

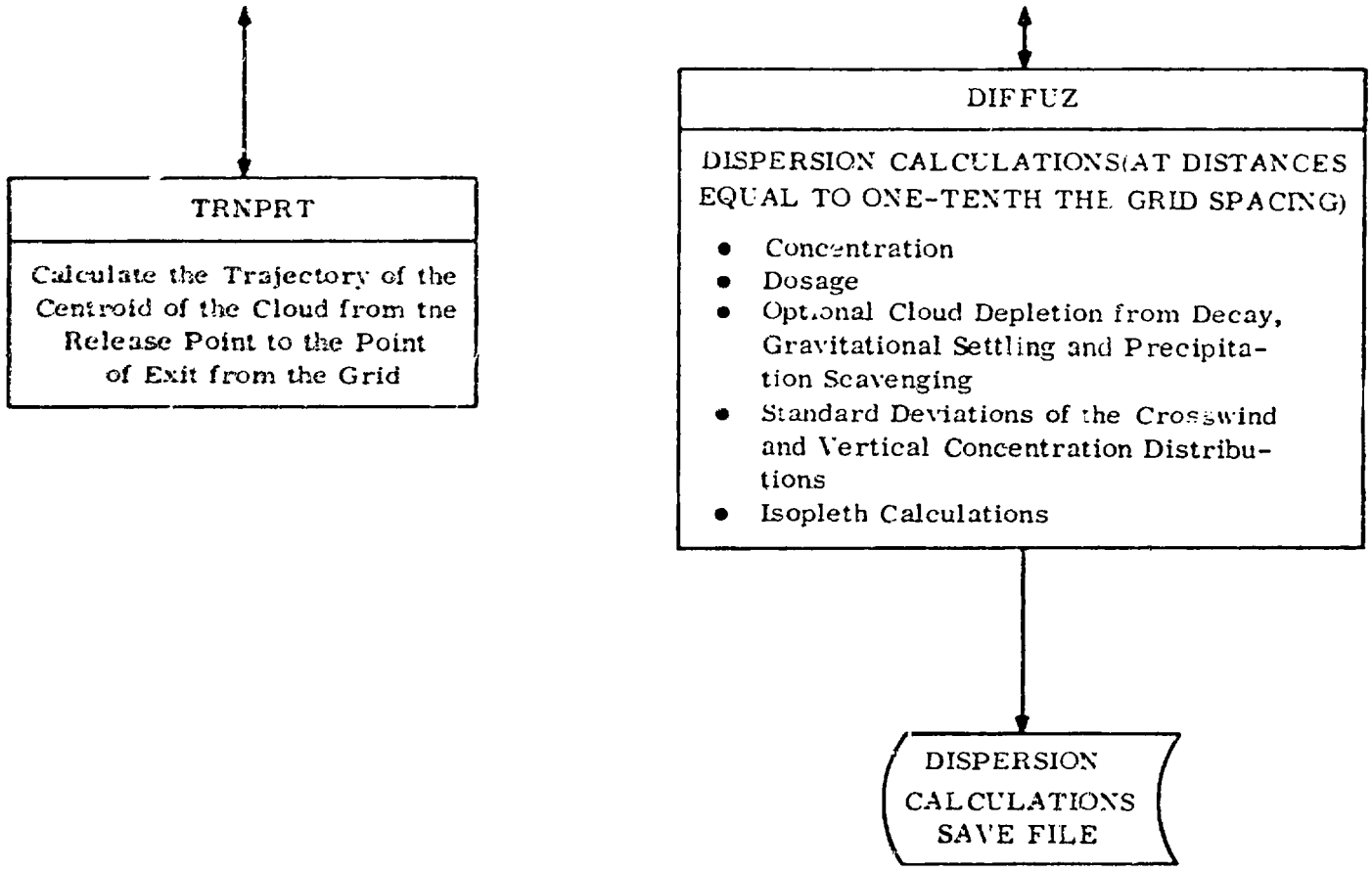

FIGURE 5-5. Routines controlled by the Application Phase TRYDIF Foreman of AMSORB.

calculations outlined in the block diagram shown in Figure 5-5 after receiving program control through the foreman TRYDIF from XECAMS and Supervisor APPLY.

The subroutine TRNPRT calculates the trajectory of the cloud centroid downwind from the source location using the output from the Mesoscale Wind-Field Model routine and the procedures outlined in Section 2.2 above. Subroutine TRNPRT calculates a point on the trajectory at intervals equal to one-tenth the spacing of the solution matrix of the Mesoscale Wind-Field Model routine (default value is 500 meters). At each of the calculated points on the trajectory, the subroutine also determines the appropriate mixing-layer depth and wind speed for use in the dispersion models, using the interpolation techniques described in Section 2.2. After completion of the calculations, program control is passed to subroutine DIFFUZ via TRYDIF.

The subroutine DIFFUZ calculates concentration and dosage with optional cloud depletion due to decay and either deposition losses from gravitational settling or precipitation scavenging, using the instantaneous and continuous-source dispersion models described in Section 2.3 above. At the user's option, the program also calculates concentration and/or dosage isopleth half-widths at each point along the trajectory for instantaneous sources and concentration isopleth half-widths for continuous sources. At the completion of the dispersion model calculations, the program writes the solution to the AMSORB print file and returns control to XECAMS.

5.3.2 Foreman MS3

Figure 5-1 shows that the Foreman MS3 of the applications phase of AMSORB consists of the two primary operational elements HECSOM and PPOUT. Figure 5-6 is a block diagram showing the function of these primary operational elements after receiving program control through

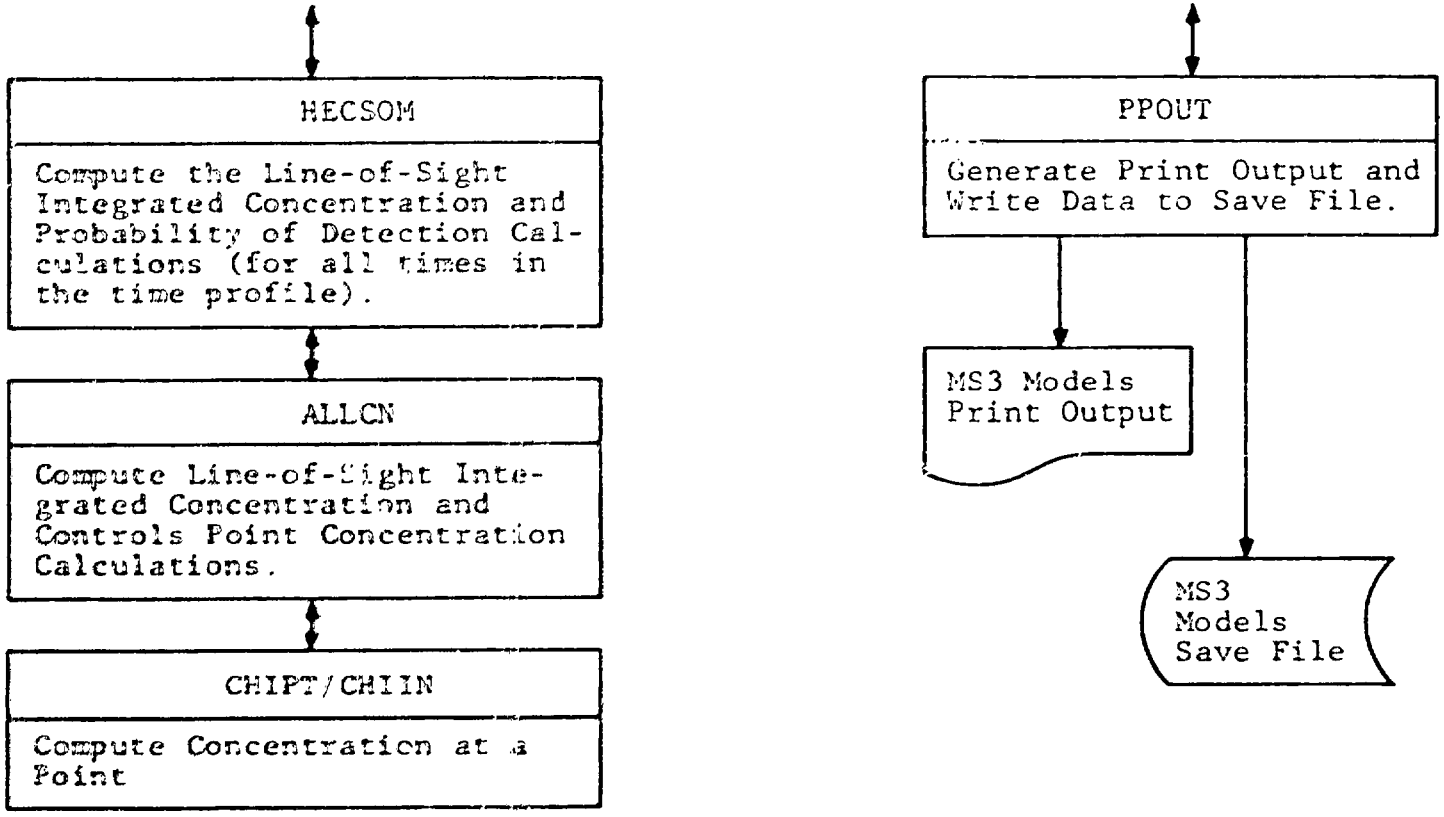

FIGURE 5-6. Routines controlled by the Application Phase MS3 foreman of AMSORB.

foreman MS3 from XECAMS and the Supervisor APPLY. Figure 5-6 also shows the relationship between these primary operational elements and subordinate elements.

Subroutine HECSOM supervises the number of times to be processed in the time profiles, controls concentration calculations and contains the MS3 Obscuration Model described in Section 2.4.1. For each time in the time profile, this subroutine calculates the target, background and cloud brightnesses which are then used to compute the time profiles of probability-of-detection and transmittance. This subroutine also passes program control to the subordinate routine ALLCN when a line-integrated concentration is required, or when the number of smoke cloud elements and the concentration at each element are required. Program control is passed back to foreman MS3 after completion of all calculations performed by subroutine HECSOM.

The MS3 Dispersion Model described in Section 2.3.2 is contained within routines ALLCN, CHIPT and CHIIN. Subroutine HECSOM passes the observer and target locations (as end points of the line-of-sight) to ALLCN. ALLCN controls the integration of concentration along the line-of-sight between the observer and target and also performs the calculation of line integrated concentrations between light sources and the target, background and cloud elements. ALLCN also calculates the number and position of cloud elements required to obtain an accurate description of the cloud for use in the cloud brightness calculations performed by the MS3 Obscuration Model resident in HECSOM. When concentrations at points along the observer-target line-of-sight are required, subroutine ALLCN passes control to CHIPT or CHIIN where the concentrations at the points are calculated using Equation (2-40) or (2-64) after which control is returned to ALLCN. Program control is passed back to the calling routine HECSOM after completion of the calculations performed in routine ALLCN.

Subroutine PPOUT controls the print output and writes all calculations to a save file for later use by the Graphics Phase of AMSORB. This routine serves the MS3 Obscurant Dispersion and Obscuration Models for print output and for saving all calculations in a data file. Program control is returned to foreman MS3 upon completion of the routine.

5.3.3 Foreman BEC

As shown in Figure 5-1, program control is passed to foreman BEC from Supervisor APPLY. Subroutine BEC contains most of the program logic of the Battlefield Environment Routine. This subroutine reads the user input data, determines which battlefield sources may contribute to the observer-target LOS concentration, computes the probability of detecting the target, and prints and saves the calculation results. Subroutines TRNPRT, DIFFUZ and ALLCN are called by subroutine BEC. Figure 5-7 shows the relationship of these subroutines and foreman BEC.

Subroutine TRNPRT has the same program logic as described in Section 5.3.1. It is used by subroutine BEC to determine the boundary of active battlefield sources located within the battlefield grid and to compute the trajectory of clouds from battlefield sources.

Subroutine DIFFUZ has the same logic as described in Section 5.3.1. It is used by subroutine BEC to account for dispersion from sources distant from the line-of-sight (see Section 4.5).

Subroutine ALLCN has the same program logic as described in Section 5.3.2. It is called by subroutine BEC when an integrated concentration calculation along a line is required. When subroutine BEC is computing the cloud brightness in the probability of detection calculation, ALLCN is also called to compute the number, position and concentration of the cloud elements required to approximate the cloud. For

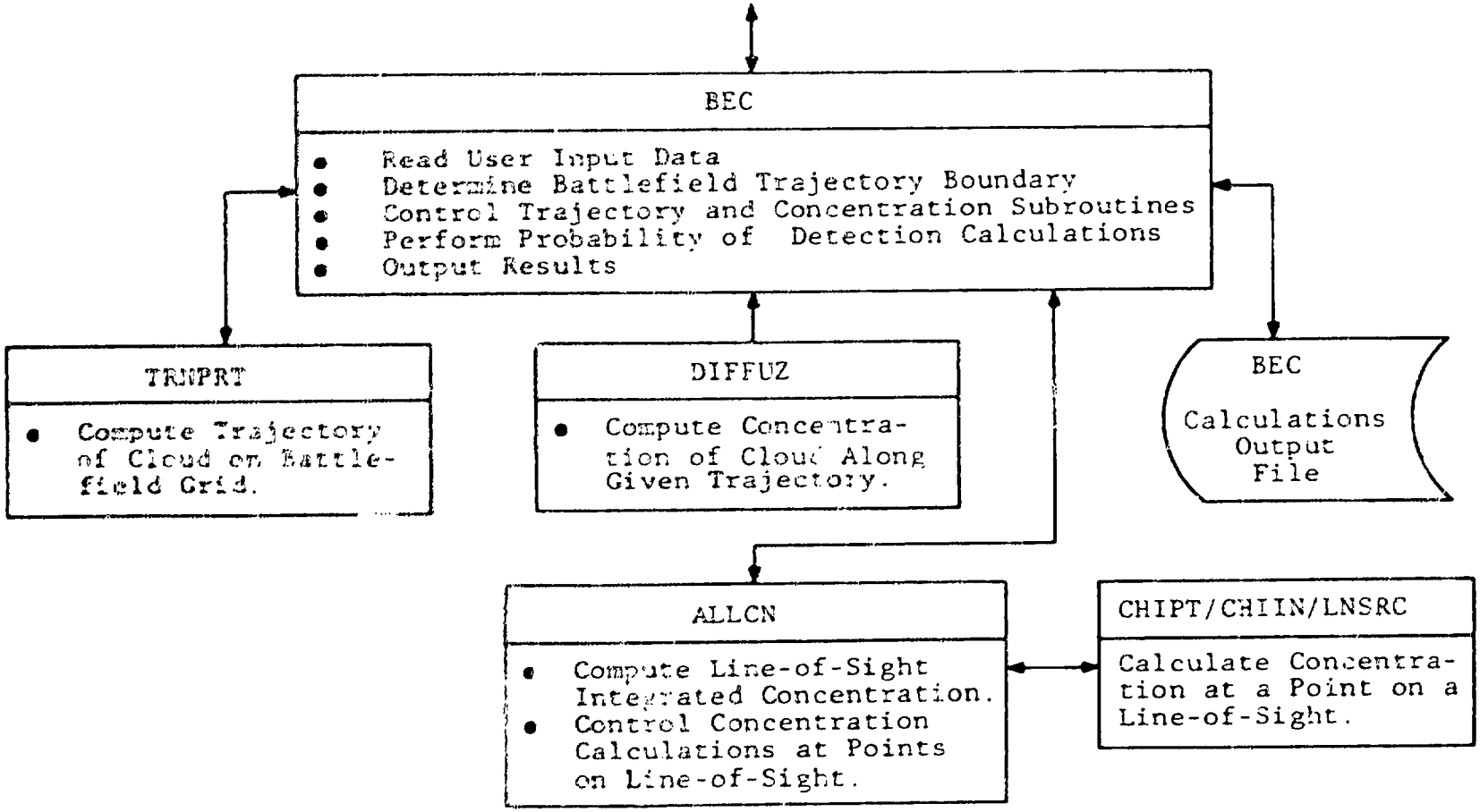

FIGURE 5-1. Relationship of Application Phase foreman BEC and its supporting subroutines.

quasi-continuous sources, ALLCN calls subroutine CHIPT to calculate the concentration at a point on the line-of-sight. CHIPT has the same logic as discussed in Section 5.3.2. CHIIN and LNSRC are similar in purpose to subroutine CHIPT.

5.4 GRAPHICS PHASE OF AMSORB

Figures 5-8 and 5-9 show block diagrams of the Graphics Phase of AMSORB. The program routine PLTPRG is the Supervisor that controls all graphics output.

For the outputs from the Mixing-Layer Analysis Model routine and the Trajectory/Transport Dispersion Model application routine, PLTPRG retrieves the solutions from the data files and prints and/or plots the solutions on option as directed by the user through XECAMS, as shown in Figure 5-8. Options include the printing and plotting of intermediate and final wind-field patterns produced by the mesoscale model, isopleths of concentration and dosage, cloud trajectories and mixing-layer depth contours. The plotted solutions are shown on a base map of the solution matrix grid with a background of terrain-height contours. The subroutine labeled HEC004 in Figure 5-8 plots and labels the axes of each plot and the terrain height contours are added to the plot by subroutines HEC005 and HEC009. Wind vectors are calculated and plotted by subroutine HEC006. The program can, in subroutine HEC008, recalculate (at the user's option) additional cloud trajectories for other source locations using the wind-field solution in the AMSORB data base. The supervisor PLTPRG can also calculate and display concentration and dosage isopleths for additional levels at the user's option. This feature is useful if the initially-requested levels do not show details in which the user is interested or if the initial levels are either so large or so small that they do not occur in the solution matrix. It should be noted that PLTPRG or its subroutines do not recalculate the wind-field nor the

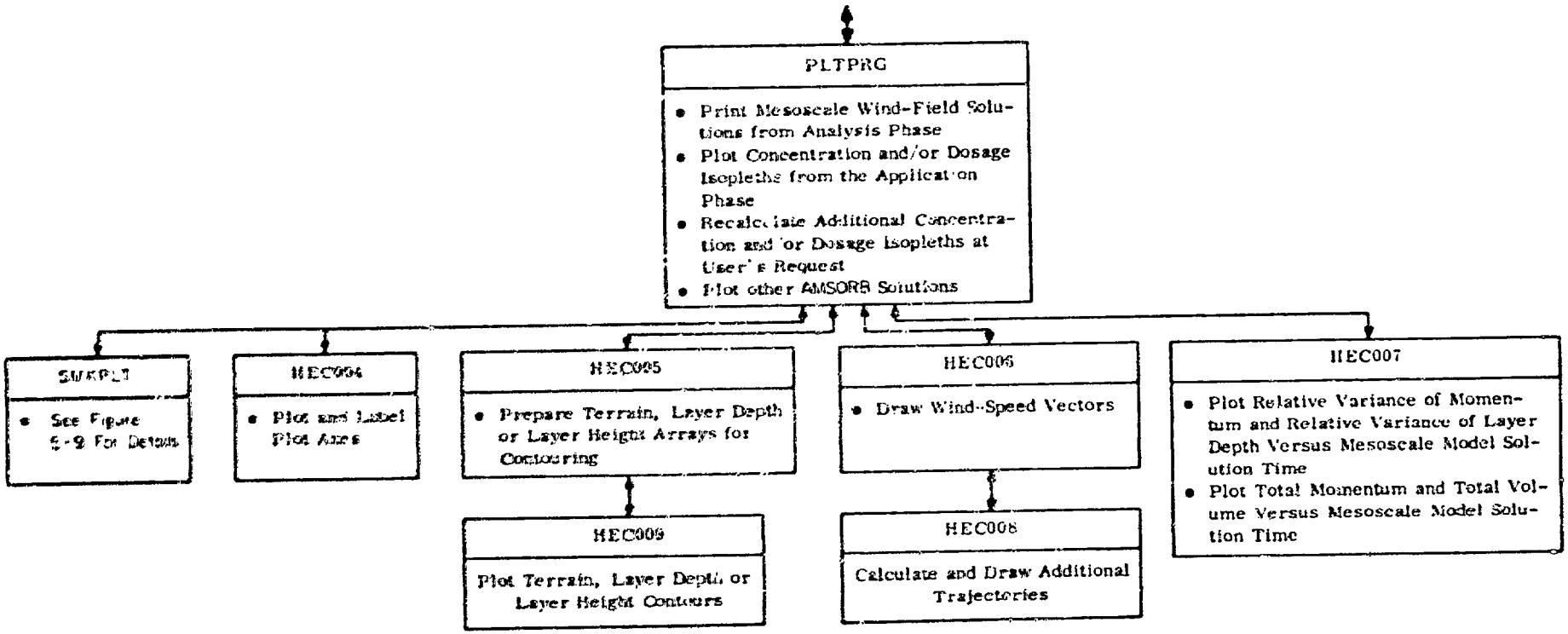

FIGURE 5-8. Operational elements of PLTPRC Graphics Phase for Mixing-Layer Analysis Model Data Output and Trajectory/Transport Diffusion Model Application Data Output.

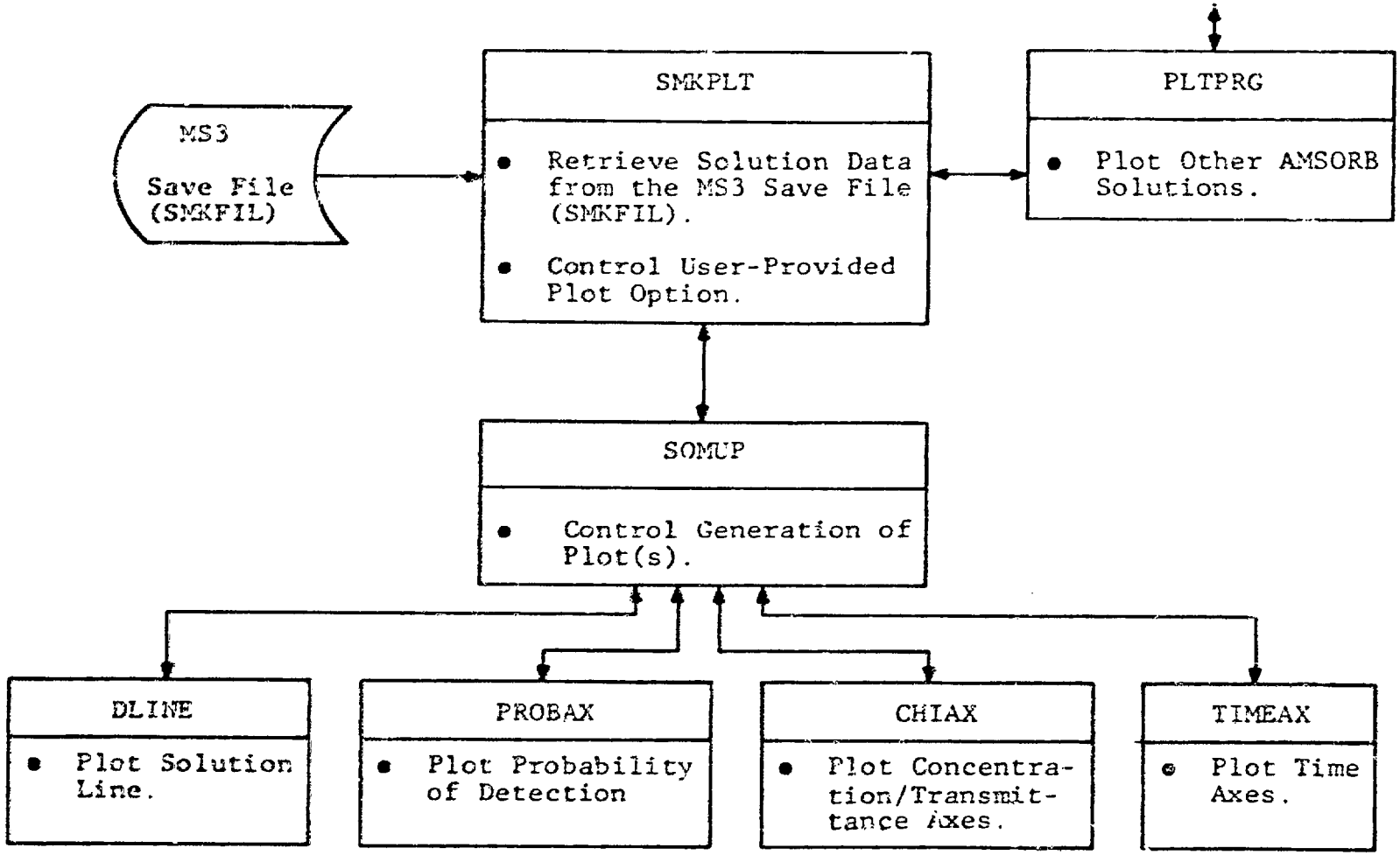

FIGURE 5-9. Operational Elements of PLTPRG Graphics Phase for the MS3 Routine Data Output.

dispersion parameters, but use information from the last solutions to recalculate additional trajectories and isopleths. The subroutine HEC007 controls the plotting of the relative variance of the change in layer depth, the relative variance of the change in momentum, and the total mass and total momentum as a function of model solution time. As noted in Section 5.1, the relative variance of the change in layer depth is used as criteria for establishing that the Mesoscale Wind-Field Model solution has converged. Since the Mesoscale Wind-Field Model theoretically conserves mass and momentum, the plots of total mass and momentum versus model time are useful in monitoring the effects of numerical approximations in calculations of the wind-field solutions.

For the MS3 Routine output, PLTPRG passes program control to subroutine SMKPLT. Details of subroutine SMKPLT are shown in Figure 5-9. Subroutine SMKPLT retrieves the output data from data file SMKFIL and passes program control to subroutine SOMUP along with the plot option chosen by the user through PLTPRG. Depending on the plot option chosen, subroutine SOMUP passes program control to subordinate routines when necessary. As shown in Figure 5-9, subroutine DLINE plots the solution line which represents either line-of-sight integrated concentration, probability of detection or transmittance. Subroutine PROBAX plots the probability-of-detection axes, subroutine CHIAX plots the line-of-sight integrated concentration/transmittance axes and subroutine TIMEAX plots the time axes. Program control is passed from subroutine SOMUP back to subroutine SMKPLT, and then from SMKPLT to routine PLTPRG when all plot output has been accomplished.

At the completion of the plotting and print operations from the Graphics Phase, program control is returned from routine PLTPRG to XECAMS.

SECTION 6
EXAMPLE CALCULATIONS

The Analysis and Application Phases of AMSORB are used to illustrate the capability of the battlefield environment components (BEC) of AMSORB to calculate line-of-sight integrated concentrations and probability of detection for meteorological conditions that occurred in the vicinity of WSMR during 14 November, 1974. These meteorological conditions have previously been used, for example, to illustrate the capabilities of the Mesoscale Wind-Field Model (Dumbauld and Bjorklund, 1977) and the MS3 component (Dumbauld, Saterlie and Cheney, 1979).

The surface weather pattern in the western United States on the 12th of November was characterized by a high-pressure ridge extending from the Pacific Northwest southeastward to Texas. The high-pressure ridge began to break down on the 13th of November with the rapid approach of a low-pressure system moving into the central U. S. from western Canada. The cold front associated with this system tended to remain east of the Rocky Mountains as it pushed south and east during the day. By the morning of the 14th, the low-pressure cell had moved into the northeast and the cold front extended southwestward through the eastern U. S., into Texas and northeast Mexico, then abruptly northward along the eastern slopes of the Rockies. The cold front had actually passed El Paso during the night from the "back-door," or moving from east to west. The passage was not accompanied by significant weather at WSMR, but broken middle and high clouds were reported. The high-pressure system behind the cold front had moved over WSMR by the morning of the 15th of November and calm winds were reported at many surface stations in the area.

The temperature profiles from rawinsonde observations made at El Paso during the period are shown in Figure 6-1. Inspection of Figure 6-1 shows that the cold front had not reached El Paso by 1700 L on the

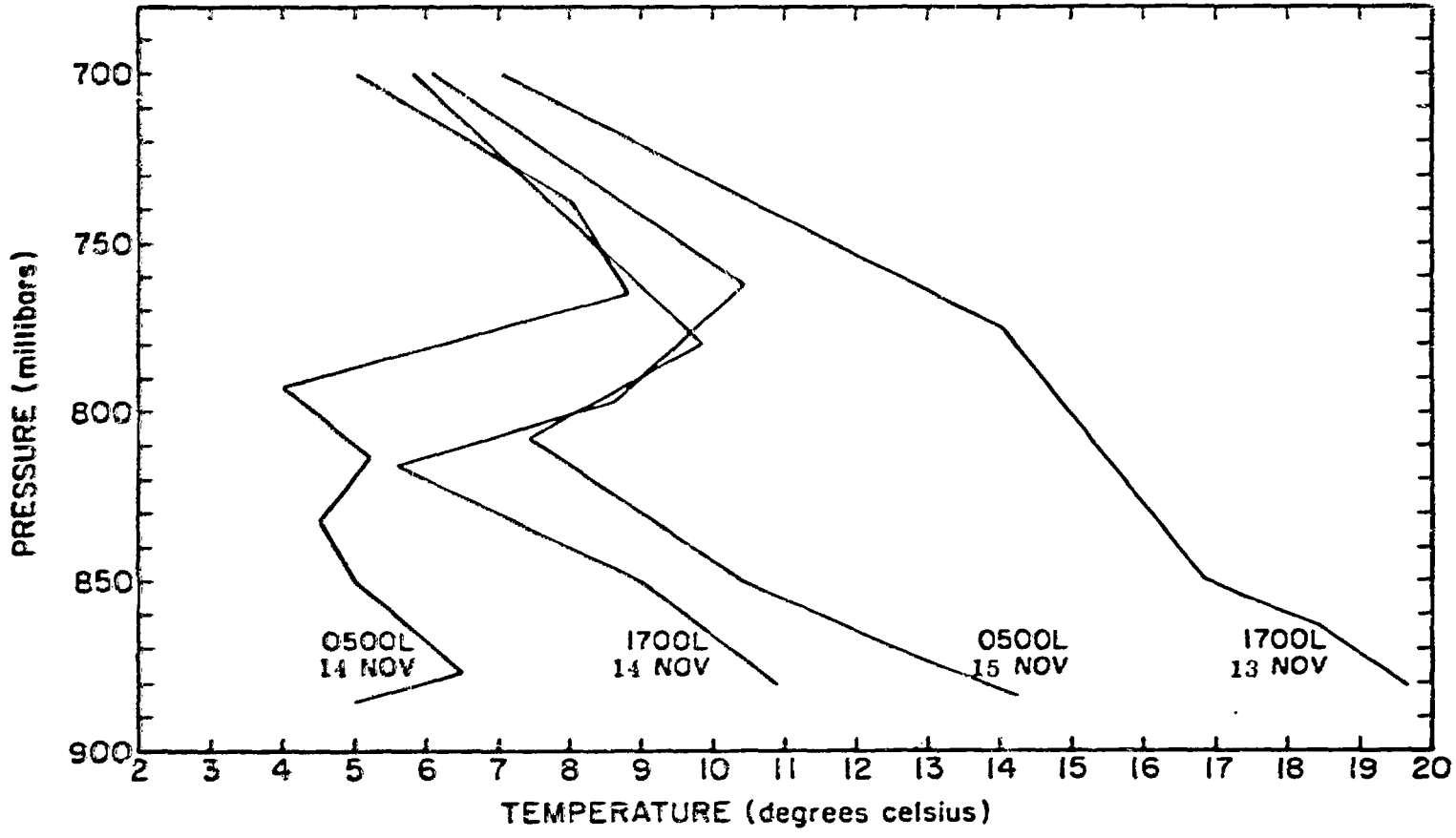

FIGURE 6-1. Temperature profiles from El Paso, Texas rawinsonde observations for 13, 14 and 15 November 1974.

13th of November. By 0500 L on the 14th, the cold front had passed El Paso and the temperature inversion at about 800 millibars associated with the frontal surface persisted in the rawinsonde observations made at 1700 L on the 14th and 0500 L on the 15th of November. Surface observations made at El Paso indicate that relatively shallow surface-based inversions formed during the nighttime and were eliminated by surface heating during the early morning hours. The mesoscale wind-field solution for 0700 L on the 14th of November is shown in Figure 6-2. Southeasterly winds dominate the flow pattern in the southern portions of the Tularosa Valley and the Valley Jornada Del Muerto west of the Organ Mountains. The San Andres, Organ and Sacremento Mountains extend above the depth of the surface mixing layer and form an effective barrier to the southeasterly flow, diverting the wind flow in the surface layer northward in the northern portion of the Tularosa Valley.

Section 6.1 below illustrates the use of the Battlefield Source Characteristics Routine (SORDAT) to define a battlefield scenario. Example calculations of obscuration information for this battlefield scenario are described in Section 6.2.

6.1 EXAMPLE BATTLEFIELD SCENARIO

The Battlefield Source Characteristics Routine (SORDAT) described in Section 4.2 is used to generate the battlefield scenario in the form of a battlefield source location and characteristics data base file. For illustration purposes, we have used the smoke and dust sources shown in Table 6-1 for our calculations. As indicated in Table 6-1, we have used 4 smoke munitions, 3 dust clouds from exploding munitions, burning brush/vegetation, a burning building and 6 muzzle blasts from a 155-mm artillery piece. The last source in the table, labeled with a source identification number of 204, is used with the other sources in a second problem described in Section 6.2. The loca-

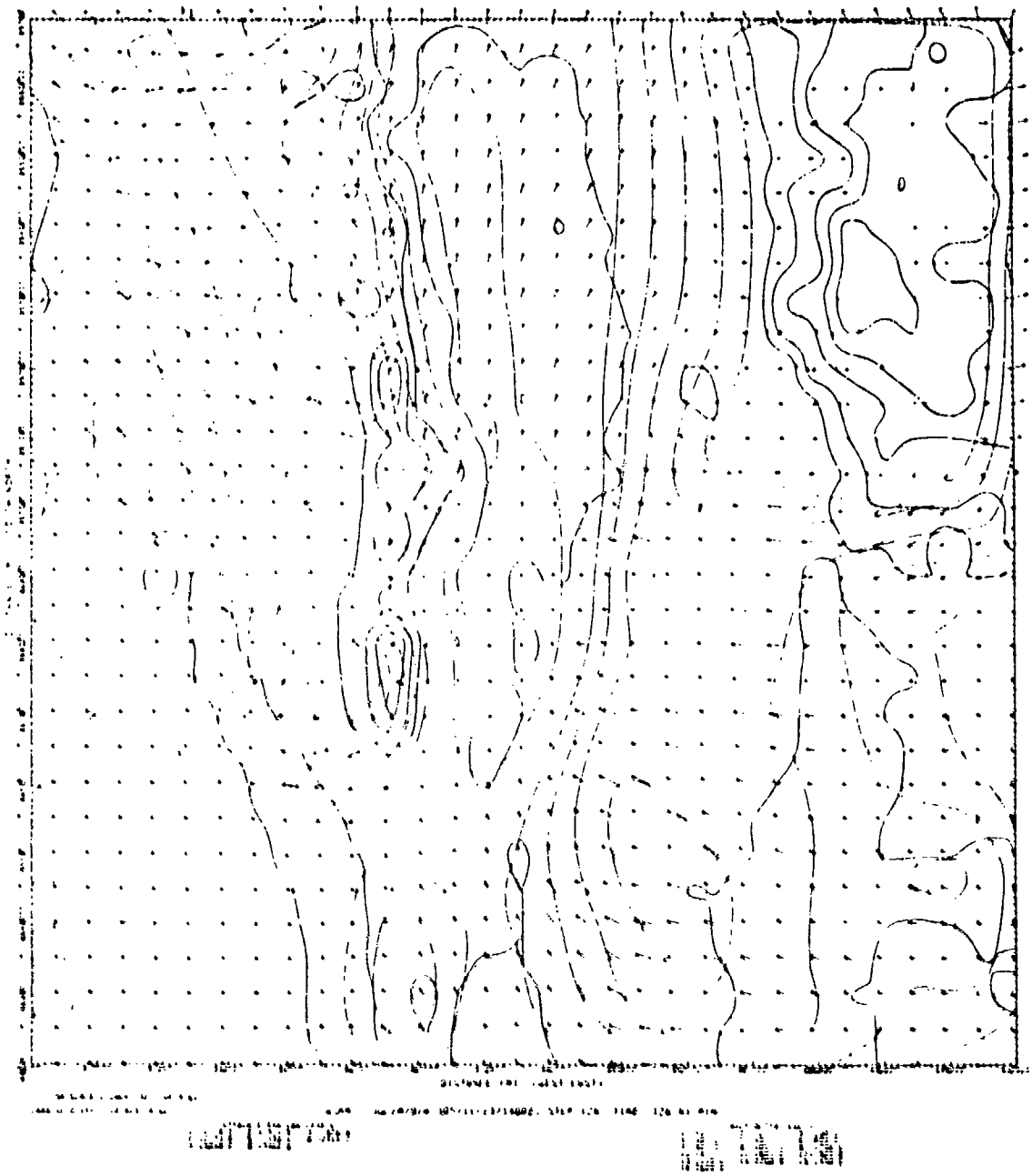

FIGURE 6-2. Mesoscale wind-field model solution for 0700L, 14 November 1974.

TABLE 6-1

SOURCES USED IN THE EXAMPLE CALCULATIONS

Source Identification Number	Source Category	Source Description	Time of Release (hr,min,s)	Source coordinates* x, y, z (m)
101	Smoke Munition	155 mm HC	9:37:10	380000,3636000,0
102	Smoke Munition	105 mm HC	9:37:15	374000,3639000,0
103	Smoke Munition	155 mm XM825 WP wedge	8:40:00	376000,3613000,0
104	Smoke Munition	155 mm M110E2 bulk WP	8:30:00	412000,3582000,0
201	Explosive Munition	155 mm artillery	9:39:00	376000,3639000,0
202	Explosive Munition	155 mm artillery	9:34:18	377000,3643000,0
203	Explosive Munition	8 in artillery	9:21:46	373000,3621000,0
301	Burning Brush Vegetation	User Entered Burning Brush	8:53:00	374000,3621000,0
401	Burning Building	Burning Building	9:38:00	378000,3643000,3
501	Muzzle Blast	155 mm artillery	9:14:45	386000,3632400,2
502	Muzzle Blast	155 mm artillery	9:37:19	386000,3632395,2
503	Muzzle Blast	155 mm artillery	9:37:17	386000,3632390,2
504	Muzzle Blast	155 mm artillery	9:37:15	386000,3632385,2
505	Muzzle Blast	155 mm artillery	9:37:13	386000,3632380,2
506	Muzzle Blast	155 mm artillery	9:37:11	386000,3632375,2
204	Explosive Munition	155 mm artillery	9:39:19	380300,3636300,0

* coordinates of the centroid

tion of these sources with respect to the line-of-sight between the observer, target and background is shown by the "X" marks in Figure 6-3.

Figure 6-4 shows the card input data to SORDAT. The user instructions for completing this card input are given in Section A.3 of Volume II. The first data card directs the AMSORB executive routine XECAMS to call SORDAT. Because the executive variable TYPE3 (column 9 of the first data card) is greater than zero, SORDAT expects FORTRAN NAMELIST input data using name QLST4. The QLST4 input data are shown in the second data card. The remaining input data cards, except the last card, describe the source types, locations, release times and other required information. For example, input data cards 3 through 5 in Figure 6-4 describe source number 101 in Table 6-1, the 155 mm HC smoke munition. The number 101 is arbitrarily assigned as the source identification number. Following the instructions for smoke munitions in Section A.3.1 of Volume II, the number in column 7 identifies this card as the first card for this munition. The number 1 in column 11 signifies HC smoke. The value of 0 in column 14 signifies a 155 mm HC munition. Columns 16 through 20 contain the number 93710 indicating the munitions bursts at 0937 hours and 10 seconds in local time. Finally, the UTM x and y location of the burst and the burst height are given in the required columns of card number 1. The second card for the 155 mm HC smoke projectile shows the number 2 in column 7, indicating this is the second data card for this source. The rest of the columns on this card are blank because we will use the program default data for the 155 mm HC munition. The third card for this source is also blank except for the 3 in column 7 indicating the third data card for this source and the value 45 appearing in columns 39 and 40. The value 45 indicates the smoke projectile approached the burst location with an angle of 45 degrees from grid north (towards the northeast). The remaining data cards are completed in a similar manner following the user instructions given in Section A.3 of Volume II. The last input data card indicates an end of data to the computer program. The SORDAT routine also requires the mass

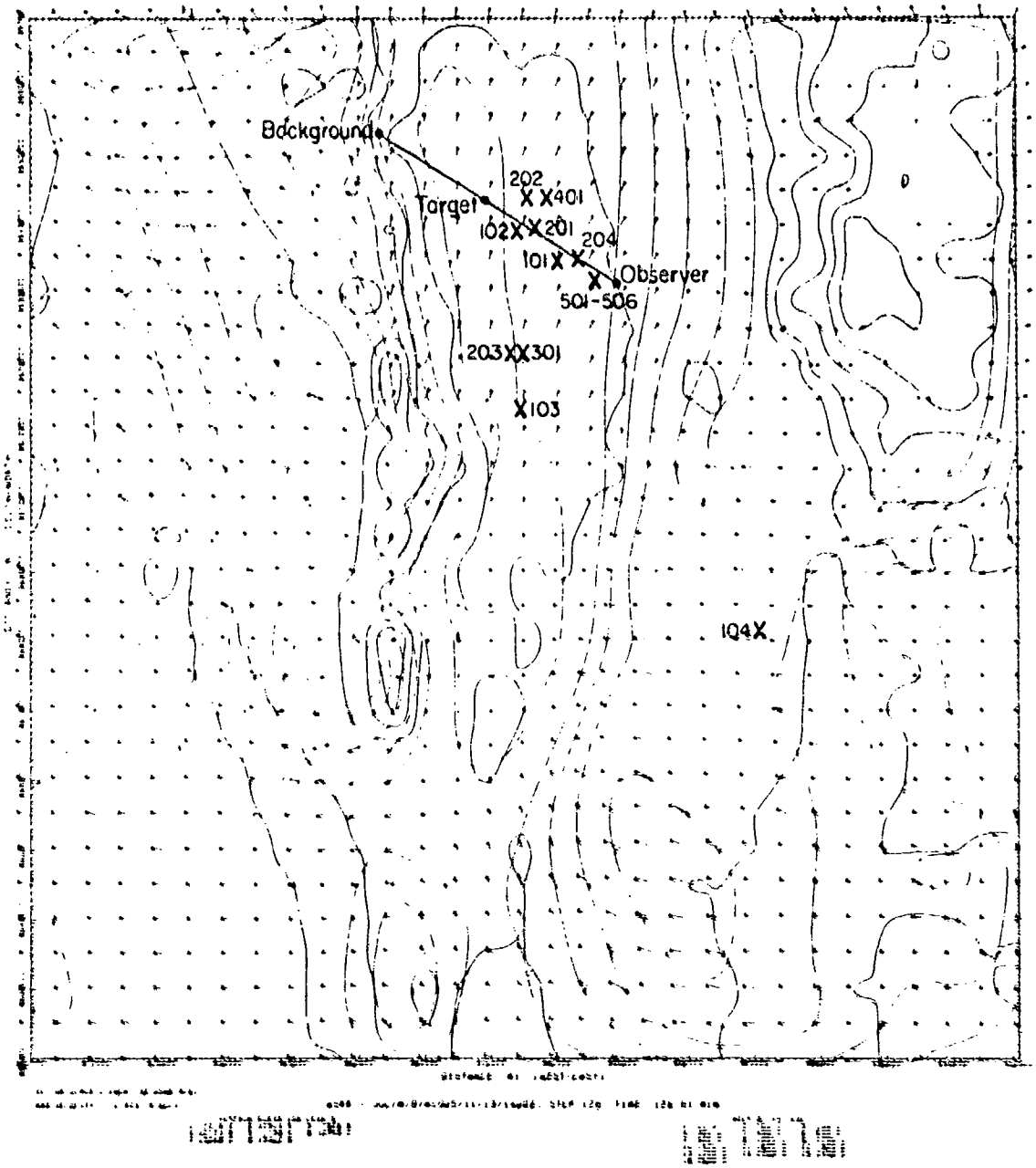

FIGURE 6-3. Location of the smoke and dust sources and the observer-target-background line-of-sight used in the example calculations.

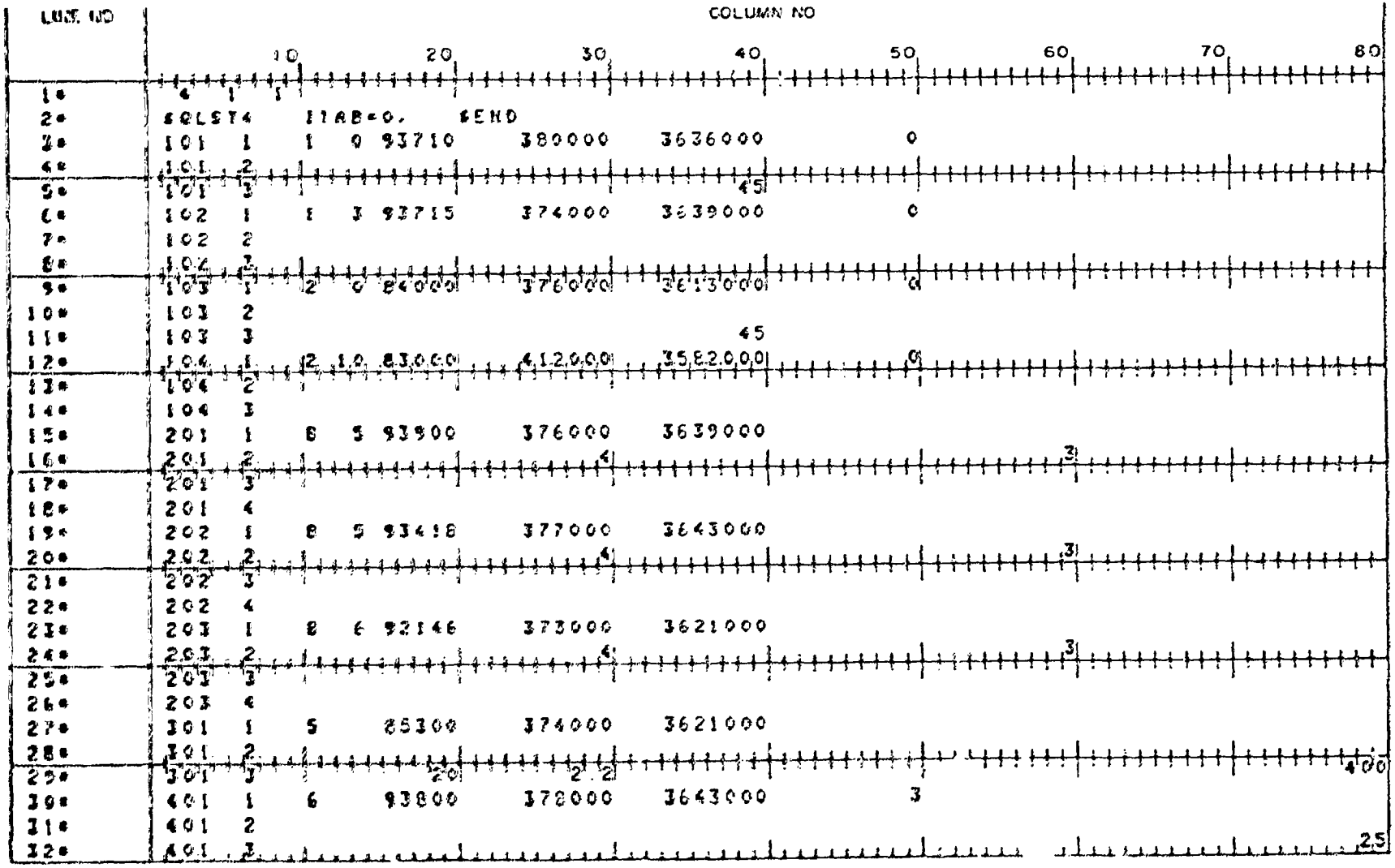

FIGURE C-4. Example card input data to SORDAT.

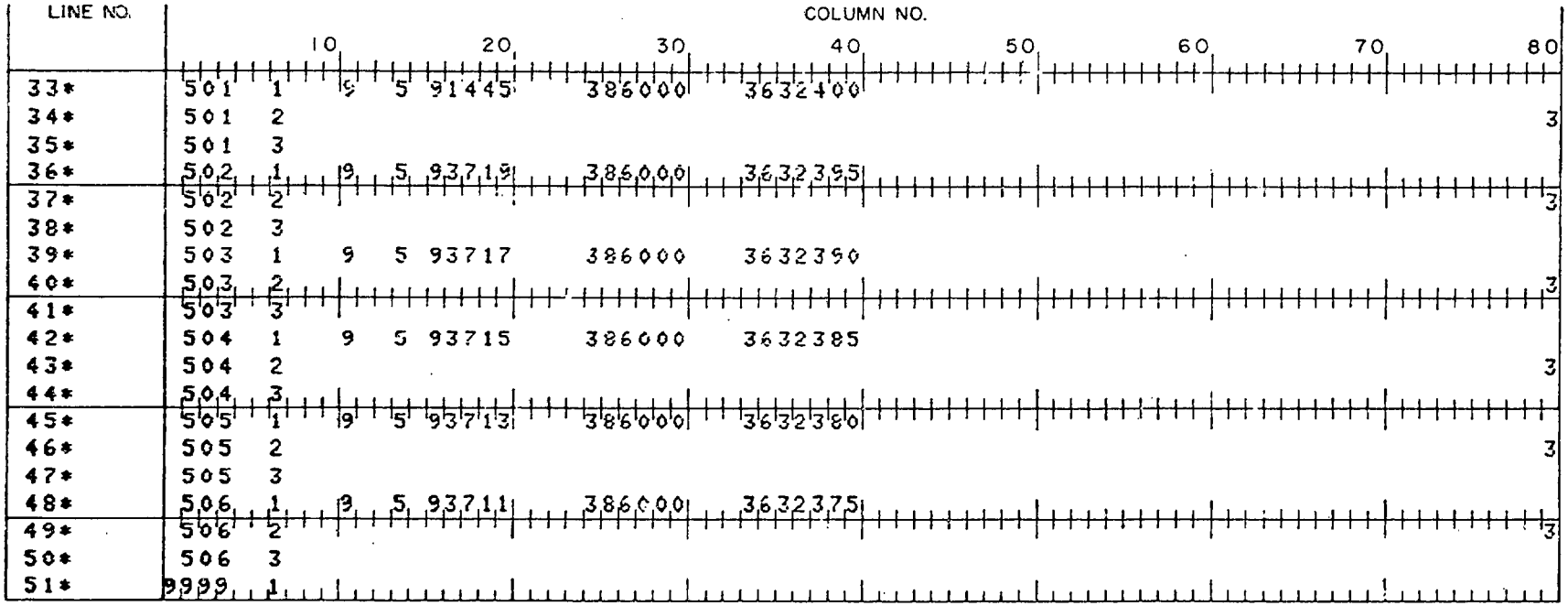

FIGURE 6-4. (Continued)

storage data base file SMKDAT described in Section A.8 of Volume II. The data input example in Section A.7 of Volume II ensures that SMKDAT is assigned in the runstream.

The optional print output produced by SORDAT is shown in Figures 6-5 and 6-6. These output tables contain all the source input information required by the dispersion and plume rise models. For example, the exact position of the 4 canisters comprising the 155 mm HC smoke munition labeled with source identification number 101, the mass of each submunition, the burn coefficients, source dimensions (sigmas) and heat content of each submunition are shown in Figure 6-5. Figure 6-6 contains additional information for the same submunitions. Two output tables are presented because not all information could be included in a single output table. Some information is repeated in the output tables for user convenience. Also, for user convenience, the output tables are partitioned into different categories of battlefield sources, i.e., smoke munition sources, burning brush/vegetation sources, burning building sources, etc.

The appropriate dispersion model and plume-rise model input data are also written to the battlefield source location and characteristics data base file BECSOR (described in Section A.8 of Volume II) for subsequent use in the transport and dispersion model calculations.

6.2 BATTLEFIELD ENVIRONMENT ROUTINE (BEC) CALCULATIONS

Two solutions of BEC are described. The first solution is for all the sources shown in Table 6-1 except the source identified as 204 and the second solution includes 204. Figure 6-7 shows the card input data to BEC. The first data card directs the AMSORB executive routine XECAMS to call BEC in the Applications Phase of AMSORB and the remaining cards are read by BEC. As discussed in Section A.4 of Volume II, BEC

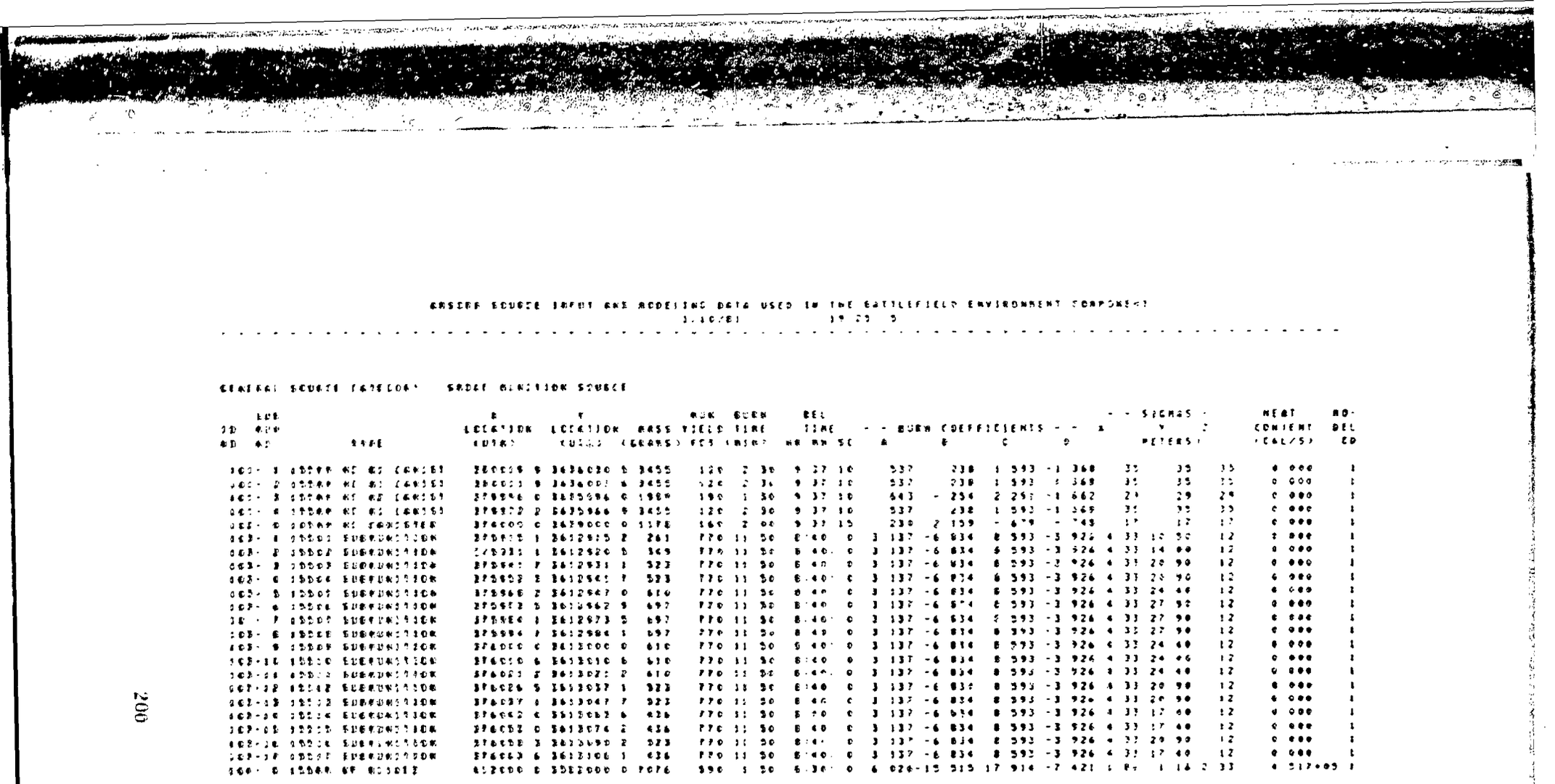

GENERAL SOURCE INPUT AND MODELING DATA USED IN THE BATTLEFIELD ENVIRONMENT COMPONENT

3.10/81 19 23 9

GENERAL SOURCE CATEGORY: SMOKE GENERATION SOURCE

ID	SUB ID	TYPE	X LOCATION (UTM)	Y LOCATION (UTM)	MASS (GRAMS)	RUN YIELD PCT	BURN TIME (MIN)	REL TIME HR:MN:SC	BURN COEFFICIENTS A	B	C	D	SIGMAS X (METERS)	Y	Z	HEAT CONTENT (CAL/S)	RO-DEL ID
101	1	SMOKE WI #1 (GRID)	3800010	3636030	3455	120	30	9 37 10	537	238	1 593 -1	368	35	35	35	0 000	1
102	2	SMOKE WI #1 (GRID)	3800010	3636000	3455	120	30	9 37 10	537	238	1 593 -1	368	35	35	35	0 000	1
401	3	SMOKE WI #2 (GRID)	3789996	3635996	1980	100	30	9 37 10	643	-254	2 253 -1	662	29	29	29	0 000	1
041	4	SMOKE WI #1 (GRID)	3789972	3635966	3455	120	30	9 37 10	537	238	1 593 -1	369	35	35	35	0 000	1
051	5	SMOKE SCREEN	3796000	3629000	1178	100	00	9 37 15	230	2 159	-679	-748	17	17	17	0 000	1
053	1	SUBMUNITION	3790015	3612915	281	770	11 50	8 40 0	3 137 -6	834	8 593 -3	926	4 33	15 90	12	0 000	1
054	2	SUBMUNITION	3790031	3612920	369	770	11 50	8 40 0	3 137 -6	834	8 593 -3	926	4 33	14 00	12	0 000	1
055	3	SUBMUNITION	3790047	3612931	323	770	11 50	8 40 0	3 137 -6	834	8 593 -3	926	4 33	20 90	12	0 000	1
056	4	SUBMUNITION	3790063	3612941	323	770	11 50	8.40 0	3 137 -6	834	8 593 -3	926	4 33	20 90	12	0 000	1
057	5	SUBMUNITION	3790079	3612947	610	770	11 50	8 40 0	3 137 -6	834	8 593 -3	926	4 33	24 40	12	0 000	1
058	6	SUBMUNITION	3790095	3612962	697	770	11 50	8 40 0	3 137 -6	834	8 593 -3	926	4 33	27 90	12	0 000	1
059	7	SUBMUNITION	3790111	3612973	697	770	11 50	8.40 0	3 137 -6	834	8 593 -3	926	4 33	27 90	12	0 000	1
060	8	SUBMUNITION	3790096	3612984	697	770	11 50	8 40 0	3 137 -6	834	8 593 -3	926	4 33	27 90	12	0 000	1
061	9	SUBMUNITION	3790080	3613000	610	770	11 50	8 40 0	3 137 -6	834	8 593 -3	926	4 33	24 40	12	0 000	1
062	10	SUBMUNITION	3790064	3613010	610	770	11 50	8 40 0	3 137 -6	834	8 593 -3	926	4 33	24 40	12	0 000	1
063	11	SUBMUNITION	3790048	3613021	610	770	11 50	8 40 0	3 137 -6	834	8 593 -3	926	4 33	24 40	12	0 000	1
064	12	SUBMUNITION	3790032	3613037	323	770	11 50	8 40 0	3 137 -6	834	8 593 -3	926	4 33	20 90	12	0 000	1
065	13	SUBMUNITION	3790017	3613047	323	770	11 50	8 40 0	3 137 -6	834	8 593 -3	926	4 33	20 90	12	0 000	1
066	14	SUBMUNITION	3790062	3613062	426	770	11 50	8 40 0	3 137 -6	834	8 593 -3	926	4 33	17 40	12	0 000	1
067	15	SUBMUNITION	3790078	3613074	426	770	11 50	8 40 0	3 137 -6	834	8 593 -3	926	4 33	17 40	12	0 000	1
068	16	SUBMUNITION	3790094	3613090	323	770	11 50	8 40 0	3 137 -6	834	8 593 -3	926	4 33	20 90	12	0 000	1
069	17	SUBMUNITION	3790063	3613106	426	770	11 50	8 40 0	3 137 -6	834	8 593 -3	926	4 33	17 40	12	0 000	1
100	0	SMOKE WI #1 GRID	4120000	3562000	7076	990	1 50	6 30 0	6 026-15	515 17	914 -7	421	1 84	1 14	2 33	0 517+09	1

GENERAL SOURCE CATEGORY: BURNING BELEM/VEGETATION SOURCE

ID	X LOCATION (UTM)	Y LOCATION (UTM)	MASS (GRAMS)	RUN YIELD PCT	BURN TIME (MIN)	REL TIME HR:MN:SC	BURN COEFFICIENTS A	B	C	D	SIGMAS X (METERS)	Y	Z	HEAT CONTENT (CAL/S)	RO-DEL ID
3W1	3796000	3623000	13960	1 000	7 00	6 53 0	1 000	000	000	000	5 77	5 77	5 77	7 280+06	1

GENERAL SOURCE CATEGORY: BURNING BUILDING SOURCE

ID	X LOCATION (UTM)	Y LOCATION (UTM)	MASS (GRAMS)	RUN YIELD PCT	BURN TIME (MIN)	REL TIME HR:MN:SC	BURN COEFFICIENTS A	B	C	D	SIGMAS X (METERS)	Y	Z	HEAT CONTENT (CAL/S)	RO-DEL ID
001	3796000	3661000	9000	1 000	4 46	9 38 0	1 000	000	000	000	1 63	1 63	1 73	7 280+06	1

FIGURE 6-5. Example optional print output by SORDAT of the general source tables.

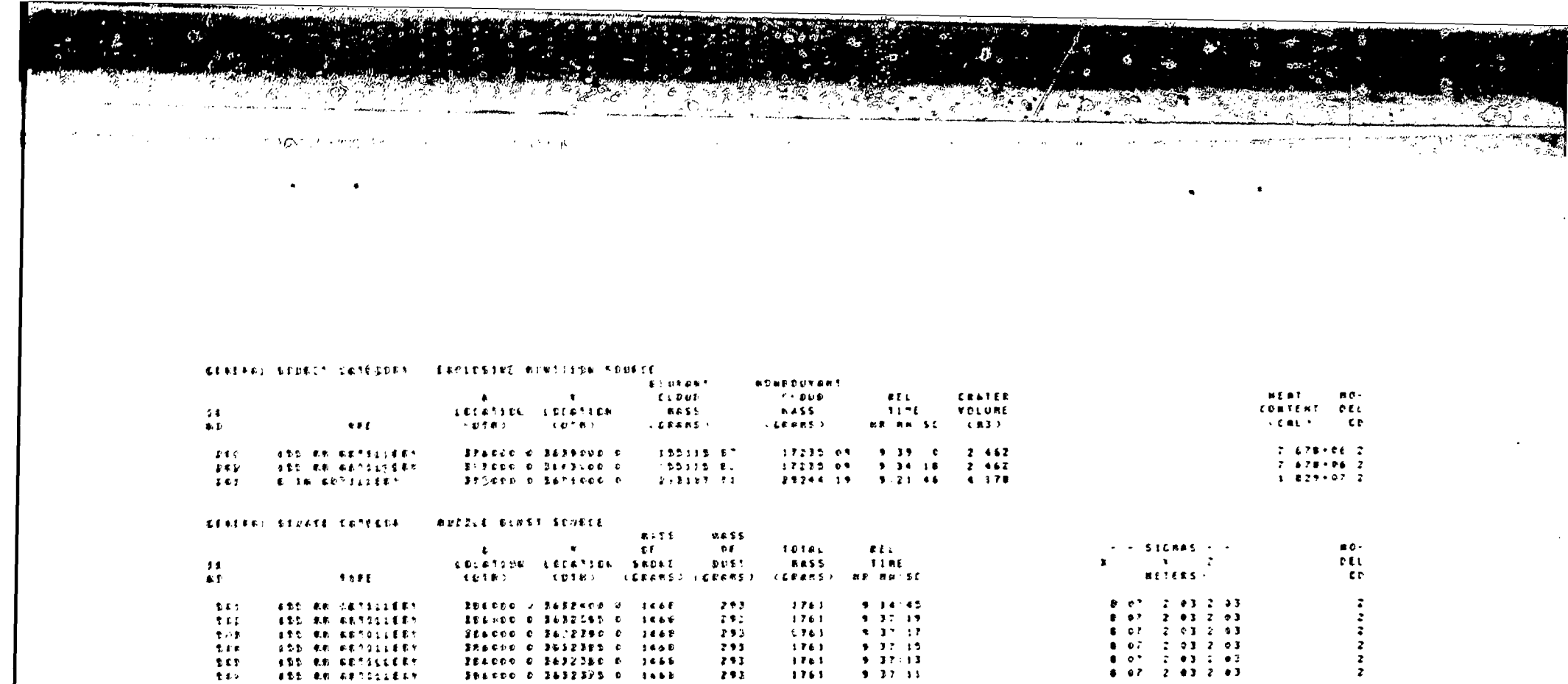

FIGURE 6-5. (Continued)

GRIDDED SOURCE INPUT AND MODELING DATA USED IN THE BATTLEFIELD ENVIRONMENT COMPONENT
1/10/81 19 25 5

SOURCE PARAMETERS SMOKE MUNITION SOURCE

ID NO	SUB MUN NO	TYPE	X LOCATION (UTM)	Y LOCATION (UTM)	RELEASE HEIGHT	DIRECTION OF FLIGHT WRT GRD NO FOR THOSE MUNITIONS COMPOSED OF SUBMUNITIONS	CANISTER CENTROID FROM WHICH SUBMUNITION GENERATED X LOCATION	Y LOCATION
101-	1	155MM HC M1 CANIST	380019 9	3636030 5	0	45 0000	380000 0	3636000 0
101-	2	155MM HC M1 CANIST	380011 9	3636006 6	0	45 0000	380000 0	3636000 0
101-	3	155MM HC M2 CANIST	379996 0	3635996 0	0	45 0000	380000 0	3636000 0
101-	4	155MM HC M1 CANIST	379972 2	3635966 9	0	45 0000	380000 0	3636000 0
102-	0	155MM HC CANISTER	376000 0	3639000 0	0	0000	0	.
103-	1	155S1 SUBMUNITION	375915 1	3612915 2	0	45 0000	376000 0	3613000 0
103-	2	155S2 SUBMUNITION	375931 1	3612920 5	0	45 0000	376000 0	3613000 0
103-	3	155S3 SUBMUNITION	375941 7	3612931 1	0	45 0000	376000 0	3613000 0
103-	4	155S4 SUBMUNITION	375952 3	3612941 7	0	45 0000	376000 0	3613000 0
103-	5	155S5 SUBMUNITION	375964 2	3612947 0	0	45 0000	376000 0	3613000 0
103-	6	155S6 SUBMUNITION	375973 5	3612961 9	0	45 0000	376000 0	3613000 0
103-	7	155S7 SUBMUNITION	375984 1	3612973 5	0	45 0000	376000 0	3613000 0
103-	8	155S8 SUBMUNITION	375994 7	3612984 1	0	45 0000	376000 0	3613000 0
103-	9	155S9 SUBMUNITION	376000 0	3613000 0	0	45 0000	376000 0	3613000 0
103-10		155S10 SUBMUNITION	376010 6	3613010 6	0	45 0000	376000 0	3613000 0
103-11		155S11 SUBMUNITION	376021 2	3613021 2	0	45 0000	376000 0	3613000 0
103-12		155S12 SUBMUNITION	376026 5	3613037 1	0	45 0000	376000 0	3613000 0
103-13		155S13 SUBMUNITION	376037 1	3613047 7	0	45 0000	376000 0	3613000 0
103-14		155S14 SUBMUNITION	376042 4	3613063 6	0	45 0000	376000 0	3613000 0
103-15		155S15 SUBMUNITION	376053 0	3613074 2	0	45 0000	376000 0	3613000 0
103-16		155S16 SUBMUNITION	376058 3	3613090 2	0	45 0000	376000 0	3613000 0
103-17		155S17 SUBMUNITION	376063 6	3613106 1	0	45 0000	376000 0	3613000 0
104-	0	155MM WP MILDEX	412000 0	3582000 0	0	0000	0	0

SOURCE PARAMETERS BURNING BRUSH/VEGETATION SOURCE

ID NO	X LOCATION (UTM)	Y LOCATION (UTM)	AREA (M**2)	VEG CODE	FUEL LOADING (KG/M**2)	BURN RATE (M**2/MIN)	BASE FUEL LOADING (KG/M**2)	PARTICULATE EMISSION (G/KG)	HEAT RELEASE (CAL/KG)
301	376000 0	3621000 0	400 000	20	2 200	50 900	800	18 000	3 900+06

SOURCE PARAMETERS BURNING BUILDING SOURCE

ID NO	X LOCATION (UTM)	Y LOCATION (UTM)	AREA (M**2)	HEIGHT OF BLD (M)	FUEL LOADING (KG/M**2)	BURN RATE (M**2/MIN)	BASE FUEL LOADING (KG/M**2)	PARTICULATE EMISSION (G/KG)	HEAT RELEASE (CAL/KG)
401	378000 0	3643000 0	25 000	3 0	20 000	5 600	.800	18 000	3 900+06

FIGURE 6-6. Example optional print output by SORDAT of the source parameter tables.

SOURCE PARAMETERS EXPLOSIVE MUNITION SOURCE

ID		X LOCATION	Y LOCATION	SOIL TYPE	SOIL DENSITY	CHARGE WEIGHT	SOB DEPTH	DET TYP	DET DEPTH	FRAC ENERGY	FRAC MASS IN BOUYANT	EMPIRICAL CRATER COEFFICIENTS				
NO	TYPE	(UTM)	(UTM)	CD	(X10**6) (G/M**3)	(KG of TNT-EQ)	(M)	CD	(M)	AVL	CLOUD	B0	B1	B2	B3	B4
201	155 MM ARTILLERY	376000 E	3639000 N	3	7	6.95	00	4	- 6	1.0	90	386 - 849 189 - 840	367 447.3	993 300.2	100	
202	155 MM ARTILLERY	377000 E	3643000 N	3	7	6.98	00	4	- 6	1.0	90	386 - 849 189 - 840	367 447.3	993 300.2	100	
203	8 IN ARTILLERY	373000 E	3621000 N	3	7	16.63	00	4	- 6	1.0	90	386 - 849 189 - 840	367 447.3	993 300.2	100	

SOURCE PARAMETERS MUZZLE BLAST SOURCE

ID		X LOCATION	Y LOCATION	WEIGHT OF MUZZLE	SOIL TYPE	SOIL DENSITY	LOSS OF SMOKE	FLASH DIAMETER
NO	TYPE	(UTM)	(UTM)	(KG)	CD	(X10**6) (G/M**3)	(GRAMS)	(M)
201	155 MM ARTILLERY	386000 E	3632400 N	2.0	3	7	1468.0	12.18
202	155 MM ARTILLERY	386000 E	3632399 N	2.0	3	7	1468.0	12.18
203	155 MM ARTILLERY	386000 E	3632398 N	2.0	3	7	1468.0	12.18
204	155 MM ARTILLERY	386000 E	3632382 N	2.0	3	7	1468.0	12.18
205	155 MM ARTILLERY	386000 E	3632380 N	2.0	3	7	1468.0	12.18
206	155 MM ARTILLERY	386000 E	3632378 N	2.0	3	7	1468.0	12.18

FIGURE 6-6. (Continued)

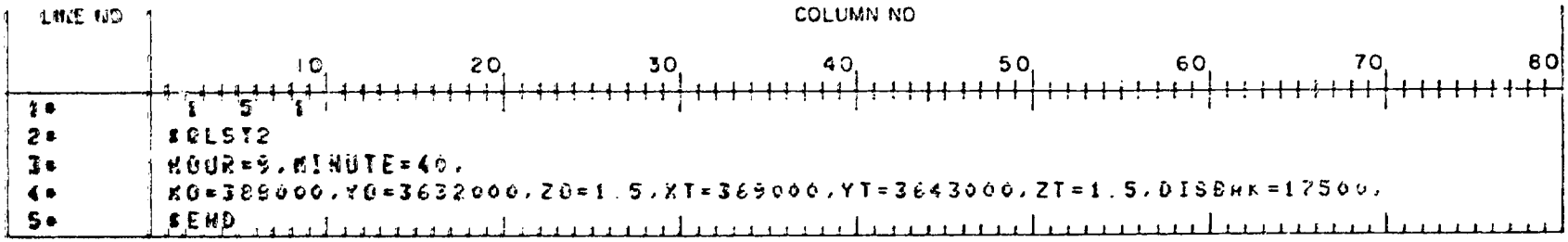

FIGURE 6-7. Example card input data to BEC.

uses the FORTRAN NAMELIST method of card input associated with NAMELIST name QLST2. The third card in the sequence specifies the time the user desires to obtain the solution, either in terms of line-of-sight integrated concentration or obscuration information. Figure 6-7 shows that a solution is desired for 0940 local time. The fourth card in the sequence defines the coordinates of the observer (X_o, Y_o, Z_o) and target (X_t, Y_t, Z_t) and the distance DISBAK between the target and background along the line of sight. The values in card 4 of the sequence correspond to the locations of the observer, target and background shown in Figure 6-3. Besides card input data, BEC requires mass storage data base files as input. In this case, the mesoscale wind-field solution shown in Figure 6-3 (from file MXLYRF), along with file BECSOR, SMKDAT and WSTRRN were used in the calculations. These files are discussed in Section A.8 of Volume II and the example runstream for assigning these files is given in Section A.7 of Volume II.

Figure 6-8 shows the print output produced by BEC for the first data case (source 204 omitted). The data base identifiers are output first to show the user the time and date of the computer run, the solution time, the time and date of the mesoscale wind-field solution, and the date and time the battlefield source location and characteristics data base file was generated using SORDAT. The user generated input for the observer, target, and background locations are listed next, followed by the calculation results.

As shown in Figure 6-8, BEC has calculated a line-of-sight integrated concentration (combined dust and smoke) of 1.41×10^3 milligrams per square meter and a transmittance in the visible (.4 - .7 μm) of 0.108. For our example problem, 29 of the total of 34 individual sources were considered in the concentration and obscuration calculations. That is, 6 sources were excluded from the calculation either because they were not released at a time that allowed them to be in the vicinity of the line-of-sight at the calculation time or because the sources are

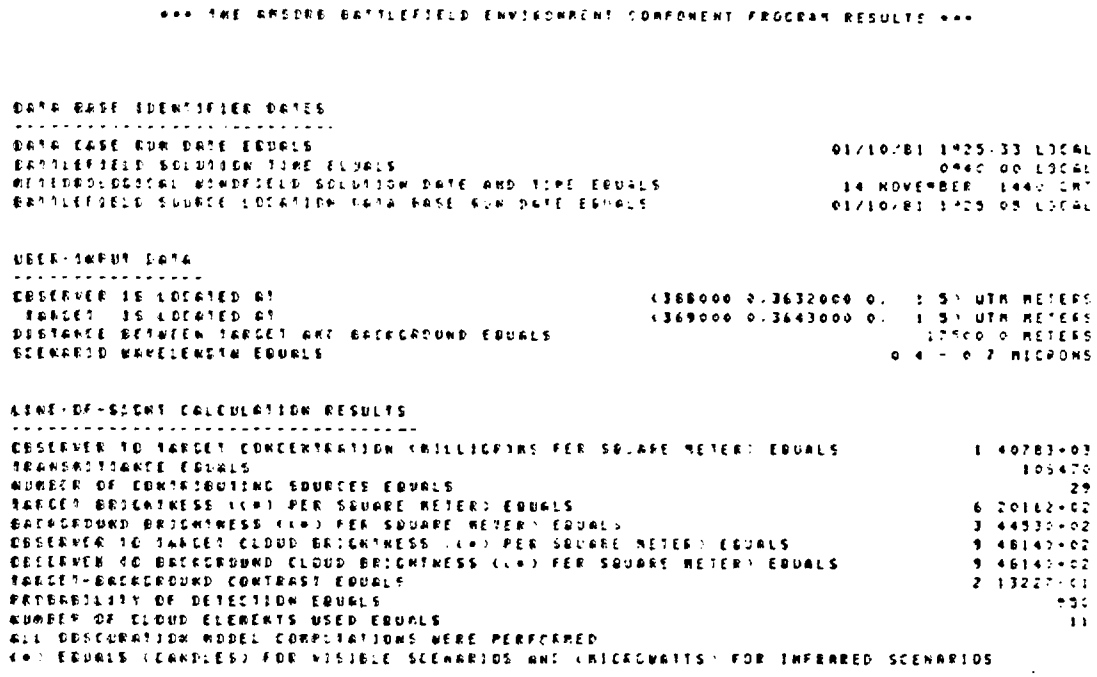

```
*** THE AMSDRB BATTLEFIELD ENVIRONMENT COMPONENT PROGRAM RESULTS ***

DATA BASE IDENTIFIER DATES
--------------------------
DATA CASE RUN DATE EQUALS                                          01/10/81 1925.33 LOCAL
BATTLEFIELD SOLUTION TIME EQUALS                                          0940.00 LOCAL
METEOROLOGICAL WINDFIELD SOLUTION DATE AND TIME EQUALS              14 NOVEMBER  1440 GMT
BATTLEFIELD SOURCE LOCATION DATA BASE RUN DATE EQUALS              01/10/81 1925.05 LOCAL

USER-INPUT DATA
---------------
OBSERVER IS LOCATED AT                          (368000 0.3632000 0.   1.5) UTM METERS
 TARGET  IS LOCATED AT                          (369000 0.3643000 0.   1.5) UTM METERS
DISTANCE BETWEEN TARGET AND BACKGROUND EQUALS                            17500.0 METERS
SCENARIO WAVELENGTH EQUALS                                          0.4 - 0.7 MICRONS

LINE-OF-SIGHT CALCULATION RESULTS
---------------------------------
OBSERVER TO TARGET CONCENTRATION (MILLIGRAMS PER SQUARE METER) EQUALS          1.40783+03
TRANSMITTANCE EQUALS                                                             105470
NUMBER OF CONTRIBUTING SOURCES EQUALS                                                 29
TARGET BRIGHTNESS ((*) PER SQUARE METER) EQUALS                                6.20162+02
BACKGROUND BRIGHTNESS ((*) PER SQUARE METER) EQUALS                            3.44530+02
OBSERVER TO TARGET CLOUD BRIGHTNESS ((*) PER SQUARE METER) EQUALS              9.48140+02
OBSERVER TO BACKGROUND CLOUD BRIGHTNESS ((*) PER SQUARE METER) EQUALS          9.48140+02
TARGET-BACKGROUND CONTRAST EQUALS                                              2.13227+01
PROBABILITY OF DETECTION EQUALS                                                      950
NUMBER OF CLOUD ELEMENTS USED EQUALS                                                  11
ALL OBSCURATION MODEL COMPUTATIONS WERE PERFORMED
(*) EQUALS (CANDLES) FOR VISIBLE SCENARIOS AND (MICROWATTS) FOR INFRARED SCENARIOS
```

FIGURE 6-8. Example print output produced by BEC for the first data case (source 204 omitted).

located in regions where winds will not carry the material through the line-of-sight (for example, sources 202 and 401 in Figure 6-3). Figure 6-8 shows that the calculated target brightness is 620 candles per square meter (cd m^{-2}), the background brightness is 345 cd m^{-2}, and the observer to target and observer to background brightness of the obscurant cloud are 948 cd m^{-2}. The calculated target-background contrast is 0.21 for our example calculation, which yields a probability of detection equal to or greater than 95 percent. The output also indicates that all visibility model computations were performed and that there were 11 cloud elements along the line-of-sight used in the obscuration calculations. In addition to the printed output, BEC outputs results of the calculations and model inputs to the mass storage data base file BECSOL, discussed in more detail in Section A.8 of Volume II. For this data case, the BEC calculations required 290 seconds of UNIVAC time.

Figure 6-9 shows the results of calculations made for all the sources described in Table 6-1, including the source identified by the number 204. In this case the line-of-sight integrated concentration is 4.7×10^5 milligram per square meter. Since the sum of the products of the line-of-sight integrated concentration of each pollutant and its' respective coefficient of attenuation in the visible (.4 - .7 μm) is greater than 11 (see Section 2.4.2) for the user specified calculation time with the addition of the source identified as 204, AMSORB does not make the time consuming brightness calculations. Instead the transmittance is automatically set to zero and the probability of detection is less than 5 percent. For this data case, the computation time is a little greater than 2 seconds, or more than a factor of 10 less than the calculation time required when the brightness calculations had to be made when the source identified by 204 was omitted from the scenario.

```
*** THE AMSAA BATTLEFIELD ENVIRONMENT COMPONENT PROGRAM RESULTS ***


DATA BASE IDENTIFIER DATES:
---------------------------
DATA CASE RUN DATE EQUALS                                        01/10/81 2030:40 LOCAL
BATTLEFIELD SOLUTION TIME EQUALS                                          0940:00 LOCAL
METEOROLOGICAL WINDFIELD SOLUTION DATE AND TIME EQUALS             14 NOVEMBER  1440 GMT
BATTLEFIELD SOURCE LOCATION DATA BASE RUN DATE EQUALS            01/10/81 2029:41 LOCAL


USER-INPUT DATA:
----------------
OBSERVER IS LOCATED AT                    (388000 0.3632000 0.   1 5  UTM METERS
 TARGET  IS LOCATED AT                    (369000 0.3643000 0.   1 5  UTM METERS
DISTANCE BETWEEN TARGET AND BACKGROUND EQUALS                          17500 0 METERS
SPECTRAL WAVELENGTH EQUALS                                      0 4 - 0 7 MICRONS


LINE-OF-SIGHT CALCULATION RESULTS:
----------------------------------
OBSERVER TO TARGET CONCENTRATION (MILLIGRAMS PER SQUARE METER) EQUALS      4 70892+03
TRANSMITTANCE EQUALS                                                         000000
NUMBER OF CONTRIBUTING SOURCES EQUALS                                            12
THE PROGRAM HAS DETERMINED THAT THE INTEGRATED CONCENTRATION OF THE
SOURCES IS HIGH ENOUGH TO OBSCURE THE TARGET
PROBABILITY OF DETECTION IS LESS THAN 5 PERCENT
```

FIGURE 6-9. Example print output produced by BEC for the second data case (source 204 included).

REFERENCES

Abramowitz, M. and J. A. Stegun (ed.), 1964: Handbook of Mathematical Functions with Formulas, Graphs and Mathematical Tables. NBS Applied Mathematics, Series 55, U. S. Government Printing Office, 1046.

Allen, G. and B. E. Simonson, 1970: Attenuation of infrared laser radiation by HC, FS, WP and fog-oil smokes. Edgewood Arsenal Technical Report EATR 4405, Edgewood Arsenal, Maryland 21010.

American Institute of Physics Handbook, McGraw-Hill, New York, NY, 1957, p. 6-43.

Ammunition Handbook, Headquarters Department of the Army, FM 9-13, March 1973, pp 7-24-7-39.

Blackwell, H. R., 1946: Contrast thresholds of the human eye. Journ. of Opt. Soc. of Amer., 36, pp. 624-643.

Briggs, G. A., 1971: Some recent analyses of plume rise observations. In Proceedings of the Second International Clean Air Congress, Academic Press, New York.

Briggs, G. A., 1972: Chimney plumes in neutral and stable surroundings. Atm. Env., 6(7), 507-510.

Carnahan, Luther and Wilkes, 1969: Applied Numerical Methods. Wiley and Sons, Inc., New York, New York.

Carter, F. L., R. K. Dumbauld and J. E. Rafferty, 1979: Validation of a transport and dispersion model for smoke. Dugway Proving Ground, Report No. DPG-FR-702. U. S. Army Dugway Proving Ground, Dugway, Utah 80442.

Cheney, C. S. and R. K. Dumbauld, 1979: User's instruction manual for the smoke model computer program (HECSMOKE-1), H. E. Cramer Company FR-79-307-01, prepared under Contract No. DAAB-09-77-C-0005 with U. S. Army Dugway Proving Ground, Dugway, Utah 84022.

Climatic Atlas of the United States, U. S. Department of Commerce, Washington, D. C., 1968, p. 62.

Cowherd, Jr., C. and R. V. Hendriks, 1977: Fugitive emissions from integrated iron and steel plants - open dust sources, Paper No. 77-6.2 presented at the 70th annual meeting of the Air Pollution Control Association, Toronto, Ontario, Canada, Inc. 20-24, 1977.

Cramer, H. E., et al., 1972: Development of dosage models and concepts. Technical Report, Contract No. DAADO9-67-6-6-0020(R), Deseret Test Center, Fort Douglas, Utah.

Daniels, A. W. Bach and K. How, 1975: Prediction of air pollution concentrations from agricultural burning, Paper 75-26.4 presented at the 68th annual meeting of the Air Pollution Control Association, Boston, Massachusetts, June 15-20, 1975.

Dolce, T. J., 1974: User's Guide to the Smoke Obscuration Program Package, prepared for Joint Technical Coordinating Group for Munitions Effectiveness, Edgewood Arsenal, Maryland 21010, p. 94.

Dugway Proving Ground, 1978a: Smoke test of the grenade, RP, 1.8A1 (Phase 11b), Final Test Report, TECOM Project No. 7-CO-RD7-DPI-003, U. S. Army Dugway Proving Ground, Dugway, Utah 84022.

Dugway Proving Ground, 1978b: Inventory smoke munition test (Phase IIa), Final Test Report, TECOM Project No. 7-CO-RD7-DPI-002, U. S. Army Dugway Proving Ground, Dugway, Utah 84022.

Dugway Proving Ground, 1978c: Dust trial phase of inventory smoke munition test (Phase IIa), Final Test Report, TECOM Project No 7-CO-RD7-DPI-002, U. S. Army Dugway Proving Ground, Dugway, Utah 84022.

Dugway Proving Ground, 1978d: Dust/debris test conducted at Fort Sill, Oklahoma by Dugway Proving Ground, Final Test Report, TECOM Project No. 7-CO-RD8-DPI-005, U. S. Army Dugway Proving Ground, Dugway, Utah 84022.

Dumbauld, R. K., et al., 1970: Handbook for estimating toxic fuel hazards. Final Report under Contract No. NAS8-21453, NASA Report No. CR-61326.

Dumbauld, R. K., J. R. Bjorklund and J. F. Bowers, 1973: NASA/MSFC multilayer diffusion models and computer program for operational prediction of toxic fuel hazards. NASA Contractor Report NASA CR-129006. H. E. Cramer Company Technical Report prepared for National Aeronautics and Space Administration, George C. Marshall Space Flight Center, Alabama 35812.

Dumbauld, R. K. and J. R. Bjorklund, 1977: Mixing-layer analysis and transport/diffusion application routine for EPAMS. Research and Development Technical Report ECOM-77-2, Atmospheric Sciences Laboratory, White Sands Missile Range, New Mexico 88002.

Dumbauld, R. K., S. F. Saterlie and C. S. Cheney, 1979: Smoke obscuration routine for EPAMS, H. E. Cramer Company TR-79-307-01, prepared under Contract No. DAEA 18-77-C-0060, Atmospheric Sciences Laboratory, White Sands Missile Range, New Mexico 88002.

REFERENCES (Continued)

Duncan, L. D., et al., 1979: The electro-optical systems atmospheric effects library, Vol. 1: technical documentation. Atmospheric Sciences Laboratory Report No. ASL-TR-0047, Atmospheric Sciences Laboratory, White Sands Missile Range, New Mexico 88002.

Eccleston, A. J., N. K. King and D. R. Packham, 1974: The scattering coefficient and mass concentration of smoke from some Australian forest fires, J. Air Poll. Control Assoc., 24, pp 1047-1050.

Ebersole, J. F., R. Vaglio-Laurin and D. S. Dvore, 1979: Optical and fluid dynamic properties of explosion-produced dust clouds, Aerodyne Research, Inc. Final Technical Report ARI-RR-181.1, prepared under Contract No. DAAK20-79-Q-0043 with Atmospheric Sciences Laboratory, White Sands Missile Range, New Mexico 88002.

Finklestein, L., 1964: History of R & D of the Chemical Warfare Service in WWII. Screening Smokes; Part II, Edgewood Arsenal, Maryland.

Gibson, B., 1978: 105 mm tank gun dust and smoke model, Technical Note LMSC-HREC TN-D568453, prepared by Lockheed, Huntsville Research and Engineering Center under Contract DAAK40-77-A-0010, Huntsville, Alabama.

Gomez, R. B., 1978: Personal communication.

Gomez, R. B. and L. D. Duncan, 1978: Description of the Atmospheric Sciences Smoke Obscuration Model (ASLSOM). Paper presented at the Symposium on Smoke and Adverse Weather Effects on Electro-Optical Systems, Royal Signals and Research Establishment, Malbern, England, 22-24 May 1978.

Gomez, R. B., R. A. Sutherland, L. S. Levitt and E. A. Olivas, 1979: Products of vehicle and grass fires affecting electro-optical system performance, Technical Note 219-05, prepared for U. S. Army Atmospheric Sciences Laboratory, Electronics Research and Development Command, White Sands Missile Range, New Mexico 88022.

Handbook of Chemistry and Physics, 39th Edition, Chemical Rubber Publishing Co., Cleveland, Ohio 1957.

Holzworth, G. C., 1967: Estimates of mean maximum mixing depths in the contiguous United States. Mon. Wea. Rev., 92, 235-242.

Johnson, M. D., P. D. Forney and T. J. Dolce, 1972: The effectiveness of obscuring smokes. Report prepared for the Joint Technical Coordinating Group for Munitions Effectiveness, Operations Research Group, Edgewood Arsenal, Maryland 21010.

Lavoie, R. L., 1972: A mesoscale numerical model of lake-effect storms. J. Atm. Sci., 29(6), 1025-1040.

Lindberg, J. D., 1979: Measured effects of battlefield dust and smoke on visible infrared and millimeter wavelength propagation: A preliminary report on Dusty Infrared Test-1 (DIRT-1), Technical Report ASL-TR-0021, Atmospheric Sciences Laboratory, White Sands Missile Range, New Mexico 88002.

Lundien, J., 1979: Graf II realistic battlefield sensor trials, Technical Report, U. S. Army Engineer Waterways Experiment Station, Vicksburg, Mississippi.

Mann, C. O. and C. C. Cowherd, Jr., 1977: Fugitive dust sources in Supplement No. 8 for compilation of air pollutant emission factors, Office of Air Programs Publication No. AP 42 (third edition), December 1977, pp 11.2.1-1-11.2.1-5.

Middleton, W. E. Knowles, 1968: Vision through the Atmosphere, University of Toronto Press, Copyright Canada, 1952. Reprinted with correction, 1958, Reprinted 1963, 1968 in the United Sates of America.

Miller, C. A., 1979: Terrain characteristics at DIRT-1 test site White Sands Missile Range, New Mexico, Report No. ASL-IAO-79-8146-1, prepared by Environmental Laboratory, U. S. Army Engineer Waterways Experiment Station for Atmospheric Sciences Laboratory, White Sands Missile Range, New Mexico 88002.

Norton C. and G. Hoidale, 1975: The diurnal variation of mixing depth by month over White Sands Missile Range, N. M. Research and Development Technical Report ECOM-5579, Atmospheric Sciences laboratory, U. S. Army Electronics Command, White Sands Missile Range, New Mexico 88002.

Pasquill, F., 1962: Atmospheric Diffusion. D. Van Nostrand Co., Ltd. London, 297.

Peterson, E. G., 1978: Basic smoke characterization test, final report. Final Report TECOM Project No. 7-CO-RD7-DPI-001. U. S. Army Dugway Proving Ground, Dugway, Utah 84022.

Salomon, et al., 1978: Characterization of obscuring clouds in the field. Army Science Conference Proceedings, West Point, New York.

Shapiro, R., 1970: Smoothing, filtering and boundary effects. Reviews of Geophysics and Space Physics, 8 (2), 359-387.

REFERENCES (Continued)

Stuebing, E. W., F. D. Verderame, R. W. Doherty, J. J. Pinto, E. A. Lucia and G. Vinansky: The nature of gun smoke and dust obscuration due to canon firing, Pitman-Dunn Laboratory Technical Report, Frankford Arsenal.

Swanson, R. N. and M. M. Hoidale, 1962: Low-level wind profile prediction techniques. Progress Report 4, SMSA, White Sands Missile Range, New Mexico.

Swanson, R. N. and H. E. Cramer, 1965: A study of lateral and longitudinal intensities of turbulence. J. Appl. Met., 4, 409-417.

Thompson, J. H., 1979: Models for munition dust clouds, Technical Report ASL-CR-79-0005-2, prepared by General Electric Company Center for Advanced Studies under Contract DAAD07-78-C-0005 for Atmospheric Sciences Laboratory, White Sands Missile Range, New Mexico 88002.

Tingle, A. G. and J. R. Bjorklund, 1973: Study and investigation of computer algorithms for the solution of the shallow-fluid equations as a means of computing terrain influences on wind fields. H. E. Cramer Company Technical Report TR-73-302-01 prepared under Contract No. DAA07-73-C-0309 with ASL, ECOM, White Sands Missile Range, New Mexico 88002.

Turner, D. B., 1964: A diffusion model for an urban area. J. Appl, Meteor., 3(1), 83-91.

Turner, R. E., P. G. Eitner and J. L. Manning, 1979: Analysis of battlefield-induced contaminants for E-O SAEL Vol I, Science Applications, Inc. Final Report SAI-79-005-AA-I, prepared under Contract No. DAAD07-79-C-0032 with Atmospheric Sciences Laboratory, White Sands, New Mexico 88002.

Vatavuk, W. M. and G. Yamate, 1975: Forest wildfires in compilation of air pollutant emission factors, Office of Air Programs Publication No. AP 42 (third edition), January 1975, pp 11.1-1-11.1-5.

Woolf, H. M., 1968: On the computation of solar elevation angles and the determination of sunrise and sunset times. NASA TMS-1646. National Meteorological Center, ESSA, Hillcrest Heights, Maryland.

Zirkind, R., 1979: A battlefield obscuration model (smoke and dust), Final Report 524-02-79-CR, prepared by General Research Corporation for U. S. Army Night Vision and Electro-optical Laboratory: Fort Belvoir, Virginia.